



University of Salerno

Department of Chemistry and Biology "A. Zambelli"

XXXII Doctoral Cycle in Chemistry

Ph.D. thesis in:

Chiral Bioactive Cyclopeptides: Concepts and Purposes

Supervisors:

Prof. F. De Riccardis

Prof. A. Casapullo

(DIFARMA, University of Salerno)

Dr. L. Arista

(Ridgeline Therapeutics, Basel, Switzerland)

Coordinator:

Prof. R. Zanasi

Ph.D. student:

Assunta D'Amato

Matr. 8800100029

Academic year: 2018/2019

The Butterfly Effect



If the single flap of a butterfly's wings can be instrumental in generating a tornado, so also can all the previous and subsequent flaps of its wings, as can the flaps of the wings of millions of other butterflies, not to mention the activities of innumerable more powerful creatures, including our own species.

E. N. Lorentz, *Am. Ass. Adv. Sci.*,
139th meeting, **1972**

Index

Abbreviations	9
1 Introduction	15
1.1 Tackling biological imitation	15
1.2 Nature's recipe for success: <i>N</i> -substitution plus <i>cyclization</i>	19
1.3 The advent of peptoids	23
1.4 Cyclic peptoids: state of the art	27
1.5 Aim of the project	34
2 Cyclic peptoids as mimics of natural depsipeptides	39
2.1 Introduction	39
2.1.1 Fungal cyclooligomer depsipeptides: a survey	39
2.1.2 Cyclohexadepsipeptides mycotoxins: enniatins and beauvericin	40
2.1.3 Cyclooctadepsipeptides mycotoxins: bassianolide, verticilide and PF1022 congeners	45
2.1.4 Purpose of the research	49
2.2 Cyclohexapeptoids as mimics of enniatins and beauvericin mycotoxins	52
2.2.1 Results and discussion	52
2.2.1.1 Synthesis and structural analysis of cyclohexapeptoids 47-51	52
2.2.1.2 Conformational chirality in conformationally stable cyclohexapeptoids	58
2.2.1.3 Sodium binding studies for cyclohexapeptoids 47-52	60
2.2.1.4 Ionophoric activity: transmembrane carrier capability of cyclohexapeptoids 47- 52	65
2.2.1.5 Cytotoxicity of cyclopeptoids 47-52 against human cancer cell lines	71
2.2.2 Conclusions	72
2.2.3 Experimental section	73
2.2.3.1 General methods	73
2.2.3.2 General methods for the sub-monomeric solid-phase oligomerization. Synthesis of the linear peptoids 58-62	74
2.2.3.3 General methods for the head-to-tail cyclization reaction. Synthesis of the cyclic peptoids 47-51	76
2.2.3.4 General procedure for the monometallic complexes formation and evaluation of the apparent K_{at} . Preparation of the complexes [47-52·Na]⁺TFPB⁻	77

2.2.3.5	General procedure for the bimetallic complexes formation. Preparation of the complexes $[48-52 \cdot 2Na]^{2+} \cdot 2TFPB^-$	80
2.2.3.6	Procedure for the evaluation of the apparent K_{a2} in $[51 \cdot 2Na]^{2+} \cdot 2TFPB^-$	82
2.2.3.7	General procedure for the 1H -NMR VT (variable temperature) experiments and ΔG^\ddagger evaluation	82
2.2.3.8	General procedure for the Pirkle's alcohol addition to racemic mixtures of cyclic peptoids	82
2.3	Cyclopeptoids as mimics of bassianolide, verticilide and PF1022s congeners	83
2.3.1	Results and discussion	83
2.3.1.1	Synthesis and structural analysis of cyclopeptoids 53-57	83
2.3.1.2	Complexation studies for cyclopeptoids 53-57	87
2.3.1.3	Biological activity of cyclopeptoids 53-57	90
2.3.2	Conclusions	91
2.3.3	Experimental section	91
2.3.3.1	General methods	91
2.3.3.2	Synthesis of linear peptoids 65-69	92
2.3.3.3	Synthesis of the cyclic peptoids 53-57	92
2.3.3.4	Preparation of the monometallic complex $[55 \cdot Na]^+ \cdot TFPB^-$	95
2.3.3.5	General procedure for the bimetallic complexes formation and evaluation of the apparent association constant K_{aTOT} . Preparation of the disodium complexes $[53- 54, 56- 57 \cdot 2Na]^{2+} \cdot 2TFPB^-$	96
3	Conformational chirality in cyclic peptoids and its control	101
3.1	Introduction	101
3.1.1	Foldamers: a synthetic approach	101
3.1.2	Definition <i>conformational chirality</i> and its application to macrocyclic systems	102
3.1.3	Conformational control and secondary assembly in linear peptoids	107
3.1.4	Early studies on cyclic peptoids' conformational control	111
3.1.5	Purpose of the research	112
3.2	Conformational chirality in cyclic peptoids and its specification	114
3.2.1	Results and discussion	114
3.2.2	Experimental section	121
3.2.2.1	General methods	121

3.2.2.2	Synthesis of linear peptoids 82-83	122
3.2.2.3	Synthesis of cyclic peptoids 80-81	122
3.3	Central-to-conformational chirality transfer. Stereogenic centre present in the backbone	123
3.3.1	Results and discussion	123
3.3.1.1	Cyclic trimers	123
3.3.1.2	Cyclic tetramers	128
3.3.1.3	Cyclic hexamers	129
3.3.2	Conclusions	132
3.3.3	Experimental section	132
3.3.3.1	General methods	132
3.3.3.2	Synthesis of <i>N</i> -Fmoc- <i>N</i> -benzyl-alanine (87)	133
3.3.3.3	General methods for the sub-monomeric/monomeric solid-phase oligomerization. Synthesis of the linear peptoids 84, 88, 90, 93, 96, 99, 101	134
3.3.3.4	Synthesis of the cyclic peptoids 85, 89, 91, 94/95, 98b, 100, 102	137
3.3.3.5	Preparation of the monometallic complexes $[\mathbf{100}, \mathbf{102} \cdot \text{Na}]^+ \text{TFPB}^-$ and apparent K_{a1} evaluation	141
3.3.3.6	Synthesis of benzylammonium tetrakis(3,5-bis(trifluoromethyl)phenyl)borate $[\text{BnNH}_3]^+ [\text{TFPB}]^-$	142
3.3.3.7	General procedure for the evaluation of the apparent K_{aTOT} in $[\mathbf{100} \cdot (\text{BnNH}_3)_2]^{2+} 2[\text{TFPB}]^-$	142
3.3.3.8	UV-Vis spectroscopy	143
3.3.3.9	Circular dichroism (CD) spectroscopy	143
3.4	Central-to-conformational chirality transfer. Stereogenic centre(s) present in the side-chain(s)	144
3.4.1	Results and discussion	144
3.4.1.1	Cyclic trimers	144
3.4.1.2	Cyclic tetramers	149
3.4.1.3	Cyclic hexamers	154
3.4.1.4	Cyclic octamers	158
3.4.1.5	Metal complexes	160
3.4.2	Conclusions	168
3.4.3	Experimental section	168
3.4.3.1	General methods	168

3.4.3.2	Synthesis of linear peptoids 103, 110, 111, 117, 119, 120, 125, 126, 130-132, 134-136, 140-141	169
3.4.3.3	Synthesis of the cyclic derivatives 104, 108, 109, 118, 121, 122a/b, 123, 127, 128a/b, 129, 137, 138, 139a/b	173
3.4.3.4	Preparation of the monometallic complexes [127, 128, 129 ·Na] ⁺ TFPB ⁻ , [139 ·Na] ⁺ PF ₆ ⁻ and apparent K_{a1} evaluation	180
3.4.3.5	Preparation of the bimetallic complexes [128, 129, 137-139 ·2Na] ²⁺ 2TFPB ⁻ and apparent K_{aTOT} evaluation for [137-139 ·2Na] ²⁺ 2TFPB ⁻	181
4	Cyclic tripeptoids as mimics of natural siderophores	185
4.1	Introduction	185
4.1.1	Catecholamide-based natural siderophores	185
4.1.2	Purpose of the research	190
4.2	Catechol-based cyclotripeptoids as transition metal chelators	191
4.2.1	Results and discussion	191
4.2.1.1	Synthesis and structural analysis of cyclotripeptoids 147a-c	191
4.2.1.2	Transition metal complexation studies	192
4.2.2	Conclusions	195
4.2.3	Experimental section	195
4.2.3.1	General methods	195
4.2.3.2	Synthesis of 2,3-bis(benzyloxy)benzoic acid (148)	195
4.2.3.3	Synthesis of <i>tert</i> -butyl (2-aminoethyl)carbamate (149a)	196
4.2.3.4	General methods for the preparation of the amines 152a-c	197
4.2.3.5	Synthesis of the linear peptoids 153a-c	199
4.2.3.6	Synthesis of the cyclic peptoids 154a-c	200
4.2.3.7	Catalytic hydrogenation procedure. Synthesis of the cyclic peptoids 147a-c	202
5	Cyclic tripeptoids as mimics for natural DNA bis-intercalators	207
5.1	Introduction	207
5.1.1	Natural DNA bis-intercalators: a survey	207
5.1.2	Purpose of the research	211
5.2	Results and discussion	212
5.2.1	Synthesis of the first generation of DNA-intercalators	212
5.2.2	Synthesis of the second generation of DNA-intercalators	215
5.2.3	Conclusions	216

5.2.4	Experimental section	217
5.2.4.1	General methods	217
5.2.4.2	Synthesis of the linear peptoids 167, 170, 173	217
5.2.4.3	Synthesis of the cyclic peptoids 168, 171, 174	218
5.2.4.4	<i>t</i> -Butoxycarbonyl deprotection procedure. Synthesis of the cyclic peptoids, trifluoroacetate salts 169, 172, 175	219
5.2.4.5	Anion exchange procedure. Synthesis of the cyclic peptoid, chloride salt 166	220
5.2.4.6	General procedure for the acylation with quinaldoyl chloride. Synthesis of cyclic peptoids 163, 165, 176	220
5.2.4.7	Dde deprotection procedure. Synthesis of the cyclic peptoid 164	222
5.2.4.8	General procedure for the acylation with carboxylic acids. Synthesis of cyclic peptoids 177-180	222
	Appendix. Cyclopeptoids as catalysts for ROP (Ring Opening Polymerization)	227
	A.1 Introduction: route to sustainable polymers	227
	A.2 Results and discussion: Cyclopeptoid Na⁺ complexes as catalysts for L-lactide ROP	230
A.2.1	Synthesis of the cyclic peptoids 185-186 and their complexes	230
A.2.2	Experimental section	232
A.2.2.1	General methods	232
A.2.2.2	Synthesis of the linear peptoids 187 and 188	232
A.2.2.3	Synthesis of the cyclic peptoids 185 and 186	232
A.2.2.4	General procedure for the formation of complexes [185-186 -Na] ⁺ [TFPB] ⁻ and [185-186 -2Na] ²⁺ 2[TFPB] ⁻	234

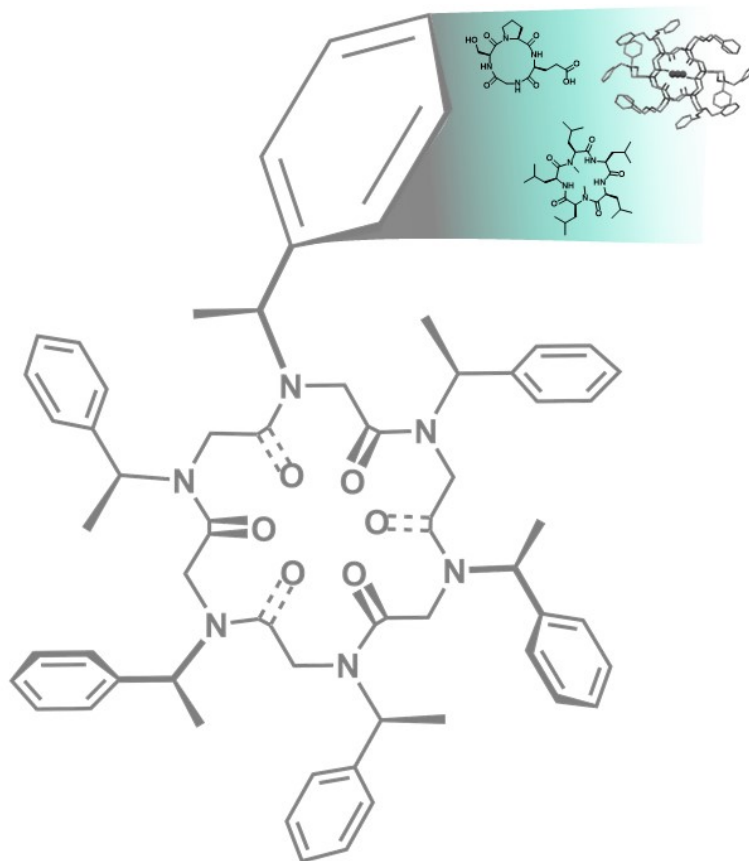
Abbreviations

aa: Amino acid
AcOEt: Ethyl acetate
AcOH: Acetic acid
Ar: Aryl
Bn: Benzyl
Boc: *tert*-Butoxycarbonyl
CCCP: Carbonyl cyanide 3-chlorophenylhydrazone
CD: Circular dichroism
CODs: Cyclooligomer depsipeptides
COSY: Correlation spectroscopy
CP: Cyclic peptoid
Cyt c: Cytochrome c
DBU: 1,8-Diazabicyclo[5.4.0]undec-7-ene
DCM: Dichloromethane
Dde: 2-Acetyl-5,5-dimethyl-1,3-cyclohexanedione
DFT: Density functional theory
DIAD: Diisopropyl azodicarboxylate
DIC: *N,N'*-Diisopropylcarbodiimide
DIPEA: *N,N*-Diisopropylethylamine
DKP: Diketopiperazine
DMAP: 4-Dimethylaminopyridine
DMF: *N,N*-Dimethylformamide
DMSO: Dimethyl sulfoxide
DNA: Deoxyribonucleic acid
DNJ: Deoxynojirimycin
ED: Effective dose
EDC: *N*-(3-Dimethylaminopropyl)-*N'*-ethylcarbodiimide hydrochloride
EDTA: Ethylenediaminetetraacetic acid
EtOAc: Ethyl acetate
EtOH: Ethanol
EYPC: Egg yolk phosphatidylcholine
EYPG: Egg yolk phosphatidylglycerol
FI: Fluorescence intensity
Fmoc: 9-Fluorenylmethoxycarbonyl
G: Guest
GPC: Gel permeation chromatography
H: Host
HATU: 1-[Bis(dimethylamino)methylene]-1H-1,2,3-triazolo[4,5-b]pyridinium 3-oxid hexafluorophosphate
HEPES: 4-(2-Hydroxyethyl)piperazine-1-ethanesulfonic acid
HFIP: 1,1,1,3,3,3-Hexafluoroisopropanol

HIV: Immunodeficiency virus
HMBC: Heteronuclear multiple bond correlation
HMQC: Heteronuclear multiple quantum coherence
HOBt: 1-Hydroxybenzotriazole hydrate
HPLC: High-performance liquid chromatography
***i*PrOH:** *i*sopropanol
L-LA: L-Lactide
LUV: Large unilamellar vesicle
MeOH: Methanol
MIC: Minimal inhibitory concentration
 M_n : Number average molecular weight
 M_n^{th} : Theoretical average molecular weight
MRI: Magnetic Resonance Imaging
MTBE: Methyl *tert*-butyl ether
MTT: 3-(4,5-Dimethyl-2-thiazolyl)-2,5-diphenyl-2H-tetrazolium bromide
***N*am:** *N*-(Pentyl)glycine
***n*Am:** *n*-Amyl
***N*ap:** *N*-(Aminopropyl)glycine
***N*be:** *N*-(Benzyloxyethyl)glycine
NBS: *N*-Bromosuccinimide
***N*me:** *N*-(Methoxyethyl)glycine
NMP: *N*-Methyl-2-pyrrolidone
***N*mpm:** *N*-(1-Naphtylmethyl)glycine
***N*pa:** *N*-(Propargyl)glycine
***Nr*1npe:** *N*-((*R*)-1-Naphtylethyl)glycine
***Nr*pe:** *N*-((*R*)-1-Phenylethyl)glycine
***N*sce:** *N*-((*S*)-(1-Carboxyethyl)glycine
***N*sch:** *N*-((*S*)-(1-Cyclohexylethyl)glycine
***N*spe:** *N*-((*S*)-1-Phenylethyl)glycine
***N*ssb:** *N*-((*S*)-(2-Butyl)glycine
PC: Phosphatidylcholine
PDB: Protein data bank
PDI: Polydispersity index
PG: Phosphatidylglycerol
Ph: Phenyl
Pic: Picrate
PLA: Polylactide
PPI: Polyproline helix of type I
PPII: Polyproline helix of type II
PyBOP: (Benzotriazol-1-yloxy)tripyrrolidinophosphonium hexafluorophosphate
Pyr: Pyrene
RNA: Ribonucleic acid
ROE: Rotating Overhauser effect

ROESY: Rotating-frame nuclear Overhauser effect correlation spectroscopy
ROP: Ring-opening polymerization
RP-HPLC: Reverse-phase HPLC
Sar: Sarcosine
SAR: Structure-activity relationship
TCDE: Tetrachlorodideoethane
TEA: Triethylamine
TFA: Trifluoroacetic acid
TFPB: Tetrakis[3,5-bis(trifluoromethyl)phenyl]borate
THF: Tetrahydrofuran
TLC: Thin layer chromatography
TsOH: *p*-Toluenesulfonic acid

Chapter 1



1 Introduction

1.1 Tackling biological imitation

“Bioinspiration” is the *art* – or rather the *science* – of observing the Nature as the scientist’s main muse. Taking inspiration from complex biological systems led to most of the discoveries and the inventions of the last few centuries. Understanding on a molecular level the functions of complex living systems could be rather challenging, but the main aim of *biomimicry* is to understand and imitate them on a molecular level, using a simplified and/or a different mechanism.¹

Peptides are an endless source of inspiration for medicinal chemistry, as these biomacromolecules regulate a number of biological activities, acting as hormones, neurotransmitters, signalling molecules in the immune response, and so on; they show high affinity towards therapeutic targets and a known mechanism of action, thus are easy to identify and present few side-effects. Moreover, peptides are often secreted as secondary metabolites in many bacterial and fungal species, possessing several interesting characteristics.² However, peptides have their drawbacks due to their extreme metabolic instability and low bioavailability.^{3a} The high hydrogen-bonding potential combined with the low lipophilicity, result in scarce cell permeability, while the low oral bioavailability of peptides is mostly due to enzymatic- and pH-mediated hydrolysis in the gastrointestinal tract and in the liver.^{3b} In fact, *in vivo*, proteins and peptides often display a plasma half-life within a few minutes or hours, which are not effective in delivering a sufficient amount of drug to the target tissue. This rather short half-life is mainly due to the cleavage by *exo*- or *endo*-peptidases; orally administered drugs are transported through the intestine and the venae portae to the liver before entering the blood system; parenteral administered drugs have to pass liver and kidneys as well, which contain a copious amount of proteolytic enzymes.⁴ The *exo*-peptidases can cleave the peptide or the protein at the *N*-termini or at the *C*-termini. Because of their cleavage specificity, it is possible to protect amine and carboxyl end groups, as *N*-acetyl and *C*-amide, respectively. Protection towards the *endo*-peptidases is quite more challenging.

¹ Whitesides G. M., *Interface Focus* **2015**, *5*, 20150031.

² Räder A. F. B., Reichart F., Weinmüller M., Kessler H., *Bioorg. Med. Chem.* **2018**, *26*, 2766-2773.

³ a) Di L., *AAPS J.* **2015**, *17*, 1, 134-143; b) Erak M., Bellmann-Sickert K., Els-Heindl S., Beck-Sickingler A. G., *Bioorg. Med. Chem.* **2018**, *26*, 2759-2765.

⁴ Werle M., Bernkop-Schürch A., *Amino Acids* **2006**, *30*, 351-367.

To address the various methods known to improve the oral availability of a peptide drug, we take account of the case of somatostatin 14, a natural endogen hormone discovered in the 70s (Figure 1.1, **1**).⁵ The cyclic tetradecapeptide showed to be a potent inhibitor for the release of growth hormone factor from pituitary cells. In the effort to synthesize a valid analogue, with improved bioavailability, it was discovered that small changes could affect substantially the biological activity.

First, the so-called *Veber-Hirschmann* peptide, *cyclo*(-PFwKTF) introduced to the scientific community in 1981,⁶ a cyclic hexapeptide with switched configuration from L to D at the Trp position, and a reduced scaffold (Figure 1.1, **2**).

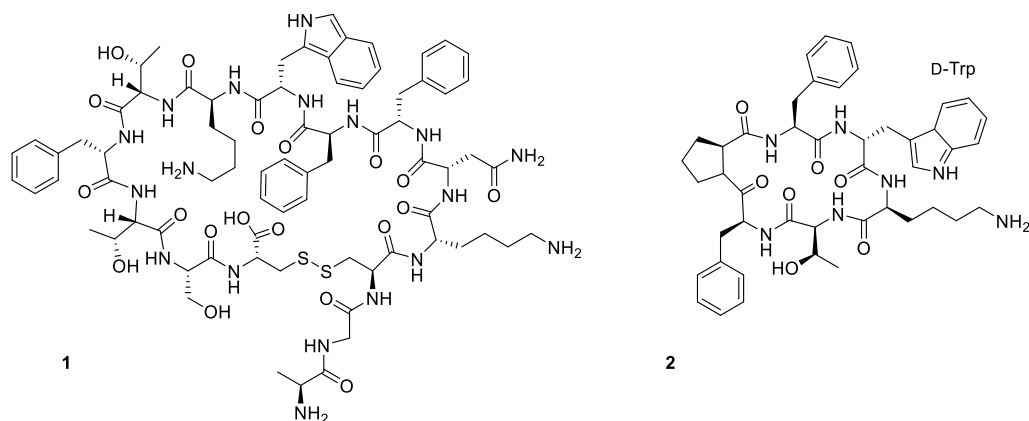


Figure 1.1. somatostatin 14 (**1**); *cyclo*(-PFwKTF) (**2**).

Switching from L- to D-amino acids and shortening the amino acid sequence has proven to be crucial in improving the *in vivo* potency by 20 times; another more recent example is ocreotide (Sandostatin), an 8 amino acid synthetic peptide drug for intestinal endocrine tumors, whose half-life was extended from a few minutes up to 1.5 hours by retaining the pharmacophore sequence Phe-Trp-Lys-Thr while shortening the rest of the peptide sequence.⁷

However, in many cases, these measures are still insufficient to assure the synthetic drug sufficient half-life to be administered orally. As a matter of fact, Sandostatin itself is administered parentally, due to its low oral bioavailability.

⁵ Brazeau P., Vale W., Burgus R., Ling N., Butcher M., Rivier J., Guillemin R., *Science* **1973**, *178*, 77-79.

⁶ Veber D. F., Freidinger R. M., Schwenk Perlow D., Paleveda W. J. Jr., Holly F. W., Strachan R. G., Nutt R. F., Arison B. H., Homnick C., Randall W. C., Glitzer M. S., Saperstein R., Hirschmann R., *Nature* **1981**, *292*, 55-58.

⁷ Harris A. G., *Gut* **1994**, *35*, 1-4.

In 2008, another crucial characteristic emerged: *N*-substitution. In an outstanding research,⁸ Kessler and co-workers disclosed the first somatostatin analogue capable to give a complete pharmacokinetic profile when administered orally. The active analogue presented *N*-methylation at the D-Trp⁸, Lys⁹ and Phe¹¹ residues; as hypothesized by the authors, the combination of the cyclization *and* the *N*-alkylation was decisive into inducing a strained conformation, which hampered the activity of the *endo*-peptidases, resulting in metabolic stability in the intestinal wall. Moreover, the enhanced lipophilicity, gained by means of the multiple *N*-substitutions, caused the shift from a passive paracellular pathway type of absorption to a passive transcellular absorption, thus providing an extensive flux into the intestinal walls. In fact, the paracellular pathway is preferred for hydrophilic molecules with a low molecular weight, but is not convenient as it occurs only in the gaps between the epithelial cells (the tight junctions, TJs), which are only a small fraction of the total area of the intestine. On the contrary, the transcellular diffusion occurs in lipophilic small drugs, with good membrane permeability, allowing a massive intake of the molecule through the vast intestinal epithelial monolayer surface (Figure 1.2).⁹

⁸ Biron E., Chatterjee J., Ovadia O., Langenegger D., Brueggen J., Hoyer D., Schmid H. A., Jelinek R., Gilon C., Hoffmann A., Kessler H., *Angew. Chem. Int. Ed.* **2008**, *47*, 2595-2599.

⁹ Räder A. F. B., Weinmüller M., Reichart F., Schumacher-Klinger A., Merzbach S., Gilon C., Hoffman A., Kessler H., *Angew. Chem. Int. Ed.* **2018**, *57*, 14414-14438.

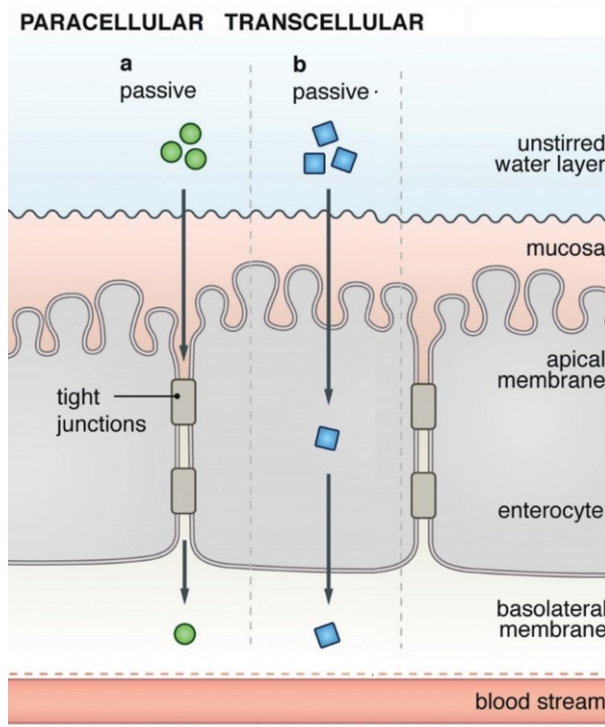


Figure 1.2. Paracellular vs. transcellular intestinal uptake pathways.

1.2 Nature's recipe for success: N-substitution plus cyclization

Taking a closer look into natural compounds, cyclic, N-alkylated peptides are quite common; these are found very often in marine organisms and display antimicrobial and/or cytotoxic activity against a wide range of cancer cells.

Cyclization is crucial in enhancing cell permeability;¹⁰ this guarantees the presence of a preferred conformation, stable in the solution state. In this way, the entropic penalties in the course of a peptide-ligand interaction are diminished (compared to the linear counterpart). Moreover, the proteolytic degradation is fairly reduced; cyclic peptides cannot fit into *endo*-peptidases catalytic pockets, which recognize β -sheets in linear segments that involve a sequence of 4-5 amino acids. Both pharmacodynamic and pharmacokinetic properties are improved, if the system itself is cyclic and shows a reduced scaffold (namely, a reduced molecular weight), taking account of the Lipinski rule of five.¹¹

Cyclo(Gly-L-Ser-L-Pro-L-Glu) (Figure 1.3, **3**) was first isolated from the *Rugeria* strain of marine bacteria, showing antimicrobial activity against *Bacillus subtilis*. In a recent paper,¹² a few derivatives of the cyclic tetrapeptide were synthesized, displaying antibacterial activity against *S. aureus*. Nonetheless, two out of four derivatives displayed also antitumor activity against 4 human cancer cell lines, in an MTT (3-(4,5-dimethylthiazol-2-yl)-2,5-diphenyltetrazolium bromide) assay. Galaxamide (Figure 1.3, **4**) is a cyclic pentapeptide obtained first from marine algae *Galaxaura filamentosa*, later on reproduced synthetically. Galaxamide structure displays all Leu residues and two N-methylations; the compound exhibits potent cytotoxic activity against pancreatic cell lines. Again, many (26) biologically active artificial variations of the original structure were proposed,¹³ differentiated by the number and the position of the N-methylations, the side-chains, and the absolute configuration of the amino acid residues.

¹⁰ a) Ahlbach C. L., Lexa K. W., Bockus A. T., Chen V., Crews P., Jacobson M. P., Lokey R. S., *Future Med. Chem.* **2015**, *7*, 16, 2121-2130; b) Yudin A. K., *Chem. Sci.* **2015**, *6*, 30-49; c) Walport L. J., Obexer R., Suga H., *Curr. Opin. Biotech.* **2017**, *48*, 242-250; d) Bock J. E., Gavenonis J., Kritzer J. A., *ACS Chem. Biol.* **2013**, *8*, 488-499.

¹¹ Lipinski C. A., Lombardo F., Dominy B. W., Feeney P. J., *Adv. Drug Deliv. Rev.* **1997**, *46*, 3-25.

¹² Chakraborty S., Tai D., Lin Y., Chiou T., *Mar. Drugs* **2015**, *13*, 3029-3045.

¹³ Lunagariya J., Zhong S., Chen J., Bai D., Bhadja P., Long W., Liao X., Tang X., Xu S., *Mar. Drugs* **2016**, *14*, 161-183.

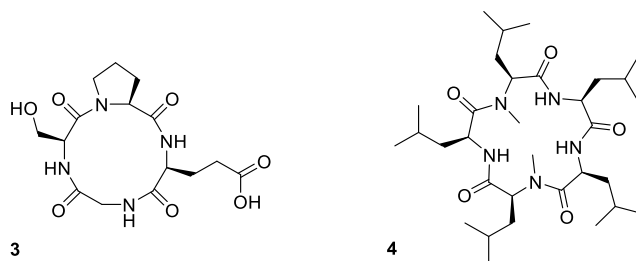


Figure 1.3. Cyclo(Gly-L-Ser-L-Pro-L-Glu) (**3**); galaxamide (**4**).

Proline-rich cyclic peptides are also very common; L-Pro, in fact, provides both an enhancement in lipophilicity, as the prolyl cycle acts as a mimic for *N*-substitution, and as geometric constraint, which favours the macrocyclization. *Phakellistatins* are a family of cyclohepta- and decapeptides isolated from a number of marine sponges, mainly of *Axinella* sp. (class *Demospongiae*, order *Axinellida*), *Stylotella aurantium* (class *Demospongiae*, order *Halichondrida*) and from *Phakellia* sp. (class *Demospongiae*, order *Axinellida*). *Phakellistatin 1* (**5**, Figure 1.4) shows three residues of L-Pro, and a potent cell growth inhibitory activity (P388 murine leukemia, ED₅₀ 7.5 µg/mL); the *cis* geometry of the Xaa-Pro amide bond, as we will examine in depth later, is crucial in determining a favoured, stable, biologically active conformation.¹⁴

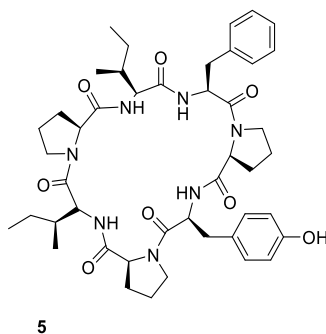


Figure 1.4. *Phakellistatin 1* (**5**).

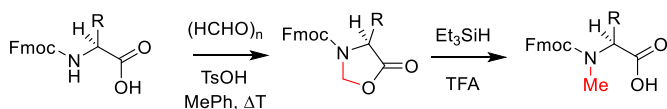
Although the *N*-substitution, as well as the cyclization, is crucial to modulate the biological function of a peptide system, the former is not always easy to accomplish. Natural peptides are modified enzymatically to induce specific physical properties, related

¹⁴ Meli A., Tedesco C., Della Sala G., Schettini R., Albericio F., De Riccardis F., Izzo I., *Mar. Drugs* **2017**, *15*, 78-94.

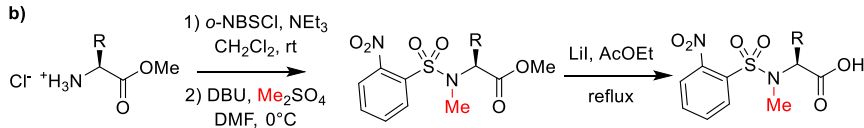
to a determined target, such as the cell membrane, DNA, protein phosphatases, and so on.^{2,15}

Replicating this kind of synthesis on an artificial level is a challenging task for two reasons: first, addressing the preparation of the *N*-methylated or, in general, the *N*-substituted amino acids; second, tackling the oligomerization of the bulky monomers. Despite the plethora of synthetic strategies developed from the 60s on, *N*-methylated amino acids are still very expensive and not always commercially available. *N*-methylation can be accomplished in solution, according to a wide range of procedures, using, for instance, the Fmoc-protected amino acid (Freidinger's method,^{16a} Scheme 1.1, a), for unfunctionalized aas), which is coupled with *p*-formaldehyde to obtain an oxazolidinone, further opened to gain the final product. Alternatively, for functionalized aas, the methylation is accomplished using *N*-sulfonamidoamino acid esters^{16b,c} derivatives (Scheme 1.1, b)). Further development of the latter strategy involves the use of a solid support, which improved the yields as well as reduced the entity of side-reactions for functionalized amino acids (Scheme 1.1, c)).^{16b,d}

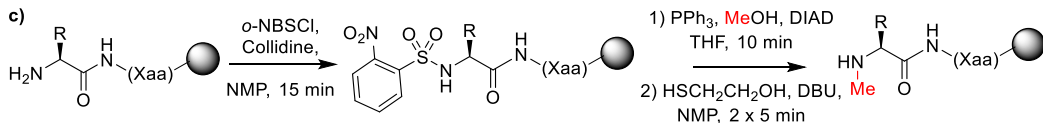
a)



b)



c)



Scheme 1.1. Synthetic pathways to *N*-methyl amino acids.

Low yields constitute main drawback for all the procedures, especially for amino acids with functionalized side-chains (*i.e.* Lys, Arg, Ser, Thr and so on), together with the labour-intensive procedures. Moreover, the solid-phase assisted coupling between the

¹⁵ Chatterjee J., Rechenmacher F., Kessler H., *Angew. Chem. Int. Ed.* **2013**, *52*, 254-269.

¹⁶ a) Freidinger R. M., Hinkle J. S., Perlow D. S., Arison B. H., *J. Org. Chem.* **1983**, *48*, 77-81; b) Sharma A., Kumar A., Abdel Monaim S. A. H., Jad Y. E., El-Faham A., de la Torre B. G., Albericio F., *Biopolymers* **2018**, *109*, e23110; c) Chatterjee J., Gilon C., Hoffman A., Kessler H., *Acc. Chem. Res.* **2008**, *41*, 10, 1331-1342; d) Aurelio L., Brownlee R. T. C., Hughes A. B., *Chem. Rev.* **2004**, *104*, 5823-5846.

steric hindered *N*-methyl- or *N*-alkyl-L-amino acids is hampered starting from the third residue, resulting in a number of side-reactions, such as deletion of fragments, over-incorporation of amino acids, acetylation of *N*-methylamino acid, fragmentation or formation of DKP (diketopiperazine) during the cleavage.¹⁷

¹⁷ Teixidó M., Albericio F., Giralt E., *J. Pept. Res.* **2005**, *65*, 153-166.

1.3 The advent of peptoids

In the vast realm of the peptidomimetics,¹⁸ peptoids emerge as compounds able to overcome most of the peptides' synthetic drawbacks discussed before, while providing the enormous therapeutic and pharmaceutical potential. α -Peptoids, oligomers of *N*-alkyl glycines, were described for the first time in 1992, in a research paper by P. A. Bartlett, who envisioned that “*such libraries, and the individual peptoids that are identified through screening them, will provide exciting leads for drug design. By virtue of their resistance to enzymatic degradation, these lead compounds will be well along the way toward new pharmaceuticals*”.¹⁹

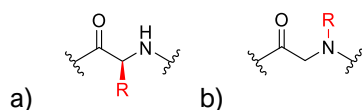
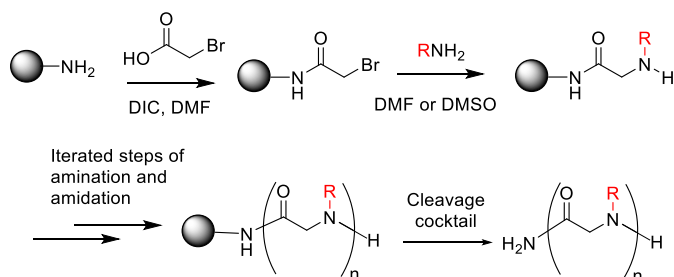


Figure 1.5. Generic structure of a) a peptide and b) a peptoid.

A few months later, the same research group published for the first time the “sub-monomeric” solid-phase protocol still used for the synthesis of these oligomers (Scheme 1.2).²⁰



Scheme 1.2. Solid-phase assisted synthesis of a peptoid.

The targeted oligomer is easily accomplished using standard SPPS (solid-phase peptide synthesis), proceeding from the carboxy to the amino direction. The solid support is constituted by a polystyrene/divinylbenzene type resin, functionalized with trityl, amine or amide groups, to which the first sub-monomer, an α -haloacetic acid, is anchored. The

¹⁸ a) Ariëns E. J., *TIPS* **1979**, *1*, 11-15; b) Farmer P. S., Ariëns E. J., *TIPS* **1982**, 362-365.

¹⁹ Simon R. J., Kania R. S., Zuckermann R. N., Huebner V. D., Jewell D. A., Banville S., Ng S., Wang L., Rosenberg S., Marlowe C. K., Spellmeyer D. C., Tans R., Frankel A. D., Santi D. V., Cohen F. E., Bartlett P. A., *Proc. Natl. Acad. Sci. USA* **1992**, *89*, 9367-9371.

²⁰ a) Zuckermann R. N., Kerr J. M., Kent S. B. H., Moos W. H., *J. Am. Chem. Soc.* **1992**, *114*, 10646-10647; b) Culf A. S., Ouellette R. J., *Molecules* **2010**, *15*, 5282-5335.

complete monomer is then obtained through an S_N2 displacement using a primary amine; this allows the use of an infinite range of commercially available primary amines and the complete freedom to mix and match the side-chains throughout the oligomer. This cycle of reactions is performed to the desired chain, which is finally detached from the resin, usually using a protic acid. Besides the availability of a large number of side-chains and the ease of synthesis, the main advantage are the high yields, almost quantitative for every step, even for 20-mers and more. Generally, peptoid nomenclature follows a 3 letter code indicating the side-chain residue; for example, *N*-(4-aminobutyl)glycine is indicated as *N*Lys, mimic for the amino acid Lys. However, not all amino acidic type monomers follow this abbreviation: *N*-substituted phenylalanine can be alternatively indicated as *N*Phe or *N*pm, which stands for *N*-(phenylmethyl)glycine.

In the course of almost thirty years, peptoids were discovered to be a wide pool of inspiration and applications. Linear peptoids were used for drug delivery, molecular recognition, as inhibitors of RNA-protein interactions, inhibitors of protein-protein interactions, antimicrobial agents, protein mimics and so on, just to cite the biological pertinency.²¹ Besides the ease of synthesis, the main advantage of a peptoid backbone, over a peptide one, is the extremely enhanced proteolytic stability.²²

The reduced H-bond potential, given by the tertiary amide, rather than the secondary, present in peptides, combined with the extreme flexibility of the peptoid backbone, due to the lack of the $C\alpha$ stereogenic centre, suggested the possible improved ADME (absorption, distribution, metabolism, excretion) pharmaceutical properties since the early days (1994). In a qualitative assessment, linear oligopeptides were compared with the homologous oligopeptoids in a stability study against a series of common proteases, including serine-proteases, cysteine-proteases and metallo-proteases.^{22a} While, as expected, all the hexapeptides were efficiently cleaved by the respective peptidases, no cleavage whatsoever was observed for the peptoid counterpart. As far as the metabolism and absorption are concerned, later studies *in vivo* proved the durability of peptoid systems in the body, with improved metabolic stability, compared to the peptide homologous.^{22b}

²¹ a) Patch J. A., Kirshenbaum K., Seuryneck S. L., Zuckermann R. N., Barron A. E., in *Pseudopeptides in Drug Development*, ed. Nielsen P. E., Wiley-VCH, Weinheim, Germany, **2004**, pp. 1-31; b) Fowler S. A., Blackwell H. E., *Org. Biomol. Chem.* **2009**, *7*, 1508-1524; c) Gangloff N., Ulbricht J., Lorson T., Schlaad H., Luxenhofer R., *Chem. Rev.* **2016**, *116*, 1753-1802.

²² a) Miller S. M., Simon R. J., Ng S., Zuckermann R. N., Kerr J. M., Moos W. H., *Bioorg. Med. Chem. Lett.* **1994**, *4*, 22, 2657-2662; b) Wang Y., Lin H., Tullman R., Jewell C. F. Jr., Weetall M. L., Tse F. L. S., *Biopharm. Drug Dispos.* **1999**, *20*, 69-75; c) Kwon Y.-U., Kodadek T., *J. Am. Chem. Soc.* **2007**, *129*, 1508-1509.

Thanks to the characteristics discussed above, the cell permeability of an *N*-alkyl glycol oligomer is enhanced, compared to the parent oligopeptide, up to 20 times; the relative peptide/peptoid permeability has been assessed employing different protocols, involving, for example, the use of a fluorescence-labelled functional group attached to the oligomer, such as SDex-COOH (Dexamethasone-21-thiopropionic acid).^{22c}

As far as the conformational order is concerned, the lack of the C α stereogenic centre, combined with the already mentioned absence of N-H...C=O hydrogen bonding, causes a faster *cis/trans* amide bond isomerization for the tertiary amide bonds, compared to the secondary peptide counterpart. The energy barrier between the *cis* and *trans* conformations is assessed at around 18-20 kcal/mol, close to the proline isomerization (Figure 1.6).²³

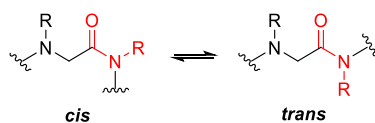


Figure 1.6. Peptoid *cis/trans* amide bond isomerization.

The high flexibility of the achiral peptoid backbone, however, hampers the stabilization of a single conformer in the solution state. This complicates the formation of stable secondary structures reducing, at the same time, possible biological applications (a ligand-substrate interaction is favoured for a single, defined, rigid secondary motif, according to the common concept that “structure *is* function”).²⁴

Researchers have developed all kinds of expedients to induce the formation of peptide-like patterns, resembling peptides’ helix, turn and loop structures.^{21b} As we will discuss in Chapter 3, backbone-to-backbone and backbone-to-side-chain non-covalent interactions are crucial in inducing the folding of the peptoid chain in a specific conformation. For instance, the introduction of an α -chiral or an α -branched side-chain (1-phenylethyl or 1-naphtylethyl)^{25a} in *cis*-amide can induce the formation of right- or left-handed helical structures (similar to polyproline helix type I, PPI, helices).^{25b,c}

²³ Sui Q., Borchardt D., Rabenstein D. L., *J. Am. Chem. Soc.* **2007**, *129*, 12042-12048.

²⁴ Gopalakrishnan R., Frolov A. I., Knerr L., Drury W. J., Valeur E., *J. Med. Chem.* **2016**, *59*, 9599-9621.

²⁵ a) Kirshenbaum K., Barron A. E., Goldsmith R. A., Armand P., Bradley E. K., Truong K. T. V., Dill K. A., Cohen F. E., Zuckermann R. N., *Proc. Natl. Acad. Sci. USA* **1998**, *95*, 4303-4308; b) Wu C. W., Sanborn T. J., Huang K., Zuckermann R. N., Barron A. E., *J. Am. Chem. Soc.* **2001**, *123*, 6778-6784; c) Armand P., Kirshenbaum K., Falicov A., Dunbrack R. L. Jr., Dill K. A., Zuckermann R. N., Cohen F. E., *Folding Des.* **1997**, *2*, 6, 369-375.

On the other side, *trans*-amide bonds (induced by *N*-aryl monomers) form polyproline helix type II (PPII).

The evaluation of the secondary structures is usually obtained by means of computational methods, circular dichroism (CD) spectroscopy, NMR and X-ray. In Figure 1.7 a) is reported the first peptoid helix: a right-handed *Nspe*₈ sequence containing *cis* amide bonds and about three residues per turn.^{25c}

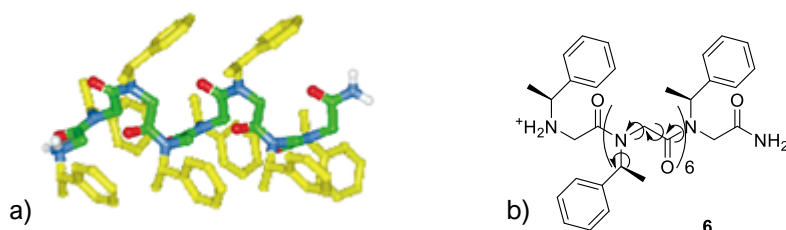


Figure 1.7. a) Stereo diagram of the predicted structure of *Nspe*₈ (**6**) and b) its structure. Mainchain C, green; sidechain C, yellow; N, blue; O, red.

Later studies on a series of nonameric sequences^{26,27} demonstrated the importance of the hydrogen bonding for the formation of folded structures clarifying the relevance of intramolecular interactions, solvents and pH.

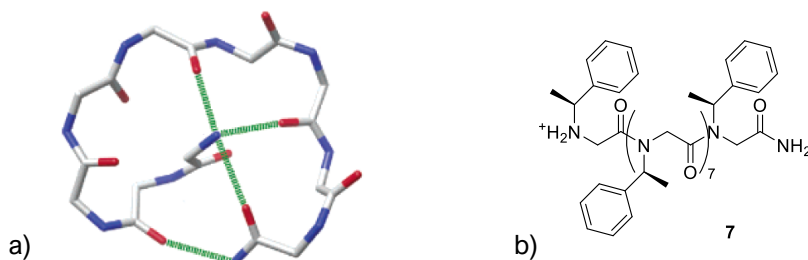


Figure 1.8. Solution backbone structure and hydrogen bonding in *Nspe*₉ (**7**). Dashed green lines denote hydrogen bonding; C, silver; N, blue; O, red.

²⁶ Huang K., Wu C. W., Sanborn T. J., Patch J. A., Kirshenbaum K., Zuckermann R. N., Barron A. E., Radhakrishnan I., *J. Am. Chem. Soc.* **2006**, *128*, 1733-1738.

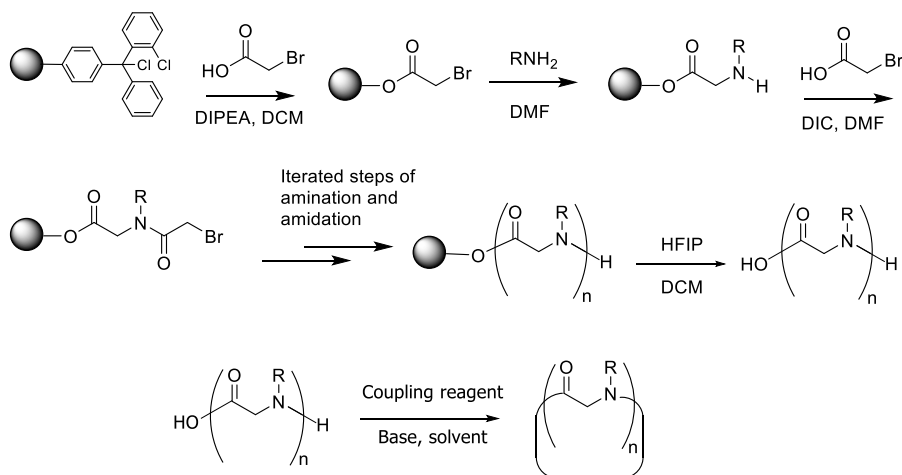
²⁷ Butterfoss G. L., Yoo B., Jaworski J. N., Chorny I., Dill K. A., Zuckermann R. N., Bonneau R., Kirshenbaum K., Voelz V. A., *Proc. Natl. Acad. Sci. USA* **2012**, *109*, 36, 14320-14325.

1.4 Cyclic peptoids: state of the art

There is actually another powerful tool meant to induce the folding of a peptoid backbone into a defined, repetitive amide bond geometry pattern: macrocyclization.

Cyclic peptoids were introduced in 2007 by Kirshenbaum and co-workers²⁸ with the idea to discover novel stable secondary structures. As expected, the introduction of a covalent constraint, in the form of a head-to-tail coupling, disclosed a whole new scenario.

The most common method to accomplish macrocyclization involves the preparation of a linear oligomer with a C-terminus linked to a 2-chlorotrityl chloride resin; detachment of the linear oligomer from the resin is achieved with mild acid conditions, leaving side-chain protecting groups unaltered. The cyclization reaction occurs in solution with standard coupling reagents, such as carbodiimides, phosphonium, and uronium salts, at concentrations up to 70 mM with good yields for model sequences ranging from 5-20 mers (Scheme 1.3).²⁹



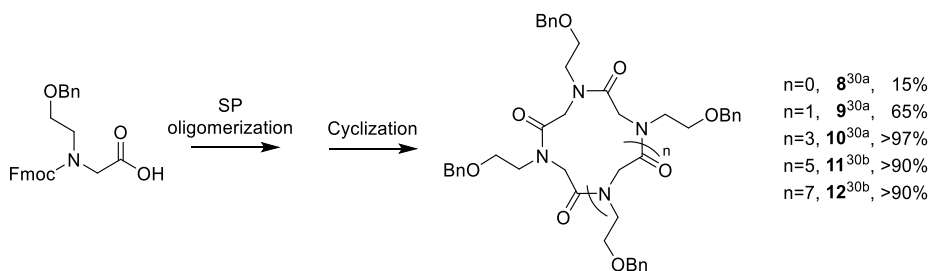
Scheme 1.3. General synthesis of a head-to-tail cyclopeptoid.

De Riccardis and co-workers disclosed in two papers³⁰ the “monomeric” synthesis of five cyclic tri-, tetra-, hexa-, octa- and decamer homooligomeric derivatives, using Fmoc-protected *N*-(benzyloxyethyl)glycine (Scheme 1.4).

²⁸ Shin S. B. Y., Yoo B., Todaro L. J., Kirshenbaum K., *J. Am. Chem. Soc.* **2007**, *129*, 3218-3225.

²⁹ a) Yoo B., Shin S. B. Y., Huang M. L., Kirshenbaum K., *Chem. Eur. J.* **2010**, *16*, 5528-5537; b) Webster A. M., Cobb S. L., *Chem. Eur. J.* **2018**, *24*, 7560-7573.

³⁰ a) Maulucci N., Izzo I., Bifulco G., Aliberti A., De Cola C., Comegna D., Gaeta C., Napolitano A., Pizza C., Tedesco C., Flot C. De Riccardis F., *Chem. Commun.* **2008**, 3927-3929; b) De Cola C., Licen S., Comegna D., Cafaro E., Bifulco G., Izzo I., Tecilla P., De Riccardis F., *Org. Biomol. Chem.* **2009**, *7*, 2851-2854.



Scheme 1.4. Synthesis of *N*-benzyloxyethyl cyclopeptoids.

In the reported papers both conformation and stability of the synthesized cyclic peptoids were reported (¹H-NMR analysis in a 9:1 mixture of CD₃CN:CDCl₃ and help of computational data). The following general considerations were made:

- cyclic trimers show *C*₃ symmetry (all-*cis* “crown” conformation);
- cyclic tetramers display *S*₂ symmetry, with *cis/trans* alternated amide bonds (*ctct* “chair” conformation);
- cyclic hexa-, octa- and decapeptoids often show multiple conformations in slow equilibrium on the NMR time scale.

However, a single, all-*trans* species emerges for both cyclic hexamers and octamers, *via* complexation with picrate salts of alkali metals. The sodium complexation takes place through the carbonyl oxygens, blocking macrocycle **10** in an *S*₆-symmetry species, as revealed by NMR, computational studies and X-ray diffraction studies; the structural analysis was accomplished using needle-like crystals of **10** as a 2:3 complex with strontium picrate.

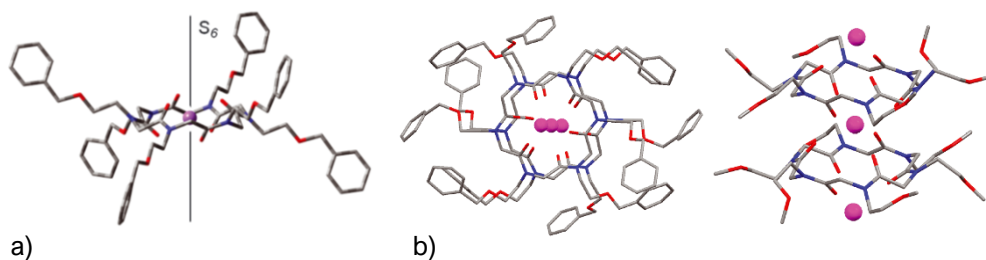


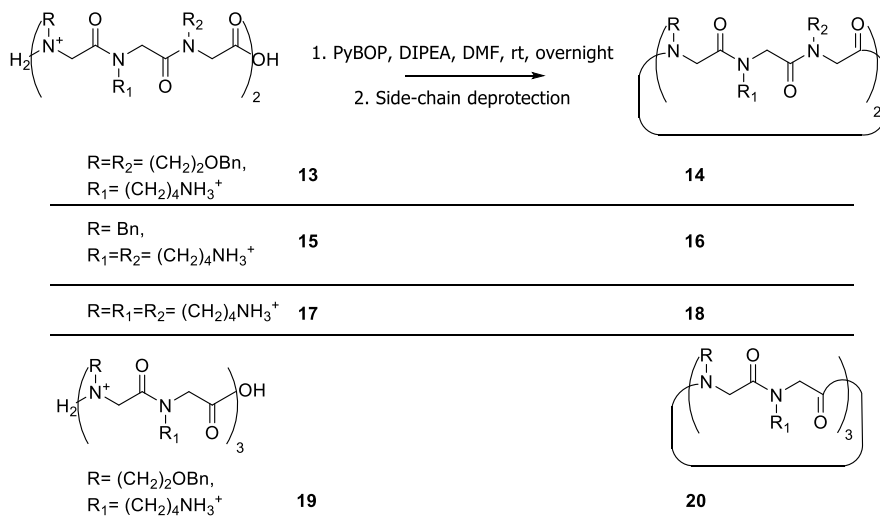
Figure 1.9. a) Predicted lowest conformation for the [**10**-Na]⁺ complex and b) X-ray crystal structure of **10**:2:[Sr(Picr)₂]₃ complex. C, silver; N, blue; O, red; Na, magenta.

A similar all-*trans* conformation was observed for complexed cyclic octamer **11**, while for **12** no preferred conformation was assessed *via* NMR, probably due to the

emerging of multiple folded conformations. Taking advantage of the Cram's method,³¹ the association constants of the various complexes were calculated, reflecting a strict correlation between the cation radius and the size of the macrocycle's cavity. For instance, a good selectivity for sodium was discovered in the case of **10**, caesium for **11**, and a slight preference for potassium for **12**. What's notable is the extent of the K_a s, of the order of 10^6 M^{-1} , comparable with most of the best complexing agents known in the literature, such as crown ethers.

This property led to the first biological application of these molecules as ionophores; in fact, peptoids' macrocycles proved to be able to carry alkali metals ions through a phospholipidic membrane; this was investigated using the pH-sensitive fluorescent dye HPTS (8-Hydroxypyrene-1,3,6-trisulfonic acid).

The direct follow-up regarded the test of cyclic peptoid **10** as antimicrobial agent against several pathogenic fungi, Gram-positive and Gram-negative bacteria strains, as it is known that most of the antimicrobial peptides act as disruptors of the bacteria lipidic membrane.³² Evaluation of MIC (minimal inhibitory concentration) on few derivatives with alternating *N*-benzyloxyethyl/*N*-benzyl and *N*-(4-aminobutyl) side-chains (Scheme 1.5) showed interesting results.



Scheme 1.5. Synthesis of antimicrobial peptoids and their cyclic counterparts.

³¹ Koenig K. E., Lein G. M., Stuckler P., Kaneda T., Cram D. J., *J. Am. Chem. Soc.* **1979**, *101*, 3553-3566.

³² Comegna D., Benincasa M., Gennaro R., Izzo I., De Riccardis F., *Bioorg. Med. Chem.* **2010**, *18*, 2010-2018.

In all cases the cyclic system proved to be more active than the respective linear one against 5 pathogenic fungi and 3 bacteria species, *E. coli*, *Salmonella typhimurium* and *S. aureus*, up to 80 times fold (cpd **15** vs. **16**), confirming that the macrocyclization is crucial for the activity. Cyclohexapeptoid **16** showed the best results, thanks to the optimal *N*-benzyloxyethyl/*N*Lys ratio, with MICs values lower than 100 μM for all the fungi species. Another important feature of an antimicrobial agent is the low haemolytic activity. In all cases, the cyclopeptoids showed no haemolytic activity up to 100 μM , encouraging their development as antimicrobial effectors.

Further studies by Kirshenbaum and co-workers³³ evidenced that it is crucial to introduce *alternating* cationic and hydrophobic moieties as side-chains of the macrocycle. In fact, macrocyclization induces the placement of such groups onto opposite faces of the planar macrocycle, resulting in an amphiphilic molecule (Figure 1.10).

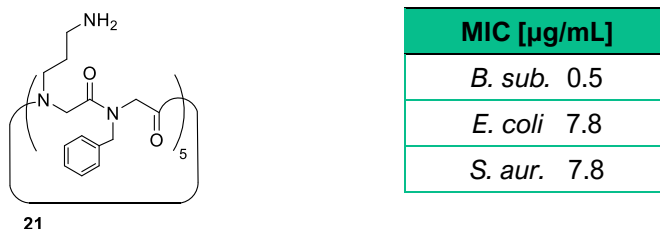


Figure 1.10. $c[\text{Nap/Npm}]_5$ and its antimicrobial activity.

Compound **21** displayed remarkable MIC values and a strong antimicrobial activity vs. haemolytic activity; what's more interesting, for all the tested compounds, cyclization improved the activity, as testified by the decrease of the MICs. As expected, the constraint cyclic structure enhanced the activity, as already stated in an earlier research paper for linear oligomers;³⁴ in general, enforcing the secondary structure results in a stronger, more selective biological activity.

Lastly, the mechanism of action was investigated using SEM (scanning electron microscopy), observing the changes of the bacterial wall before and after the administration of the antimicrobial cyclic peptoid. Healthy *S. aureus* cell surfaces appear smooth, with cell diameter in the range of 500-800 nm; upon administration of **21** in sub-MIC, MIC and supra-MIC concentrations, the cell wall collapsed or underwent the formation of pores or craters. This is consistent with the assumption that the main

³³ a) Huang M. L., Shin S. B. Y., Benson M. A., Torres V. J., Kirshenbaum K., *ChemMedChem* **2012**, *7*, 114-122; b) Huang M. L., Benson M. A., Shin S. B. Y., Torres V. J., Kirshenbaum K., *Eur. J. Org. Chem.* **2013**, *17*, 3560-3566.

³⁴ Patch J. A., Barron A. E., *J. Am. Chem. Soc.* **2003**, *125*, 12092-12093.

antimicrobial action involves an interaction with the negatively charged lipids in the bacteria membrane (similarly to antimicrobial peptides).

The other two pharmacological applications of cyclic peptoids known in the literature were recently reported by our research group.

The first one exploited the already-mentioned excellent ability of cyclic hexamers to act as macrocyclic hosts for metal cations; two molecules were prepared as Gd^{3+} chelators, bearing carboxylic pending moieties for optimal water solubility (Figure 1.11).³⁵

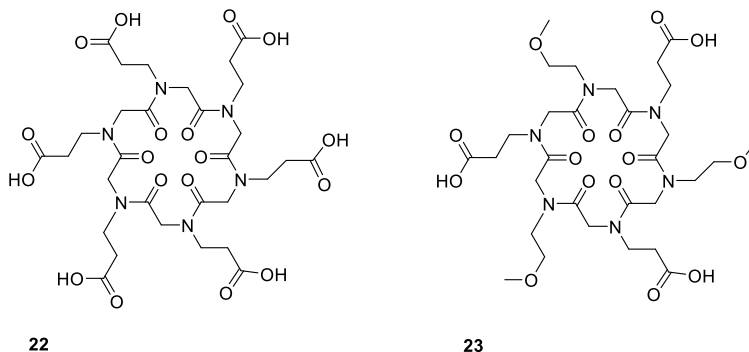


Figure 1.11. Gd^{3+} binding cyclohexapeptoids.

Paramagnetic gadolinium(III) complexes are the most common MRI contrast agents used nowadays, with macrocyclic hosts preferred over linear ones, thanks to the enhanced kinetic and thermodynamic stabilities. The complexation is accomplished through the six carboxyl amide oxygens, leaving three coordination sites available for water molecules, which are crucial for the imaging process (Figure 1.12).

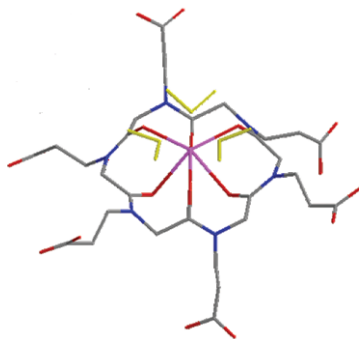


Figure 1.12. 3D model of $[22 \cdot Gd]^{3+}$ complex; the coordination sphere includes three water molecules. C, silver; N, blue; O, red; Gd, magenta; H_2O , yellow.

³⁵ De Cola C., Fiorillo G., Meli A., Aime S., Gianolio E., Izzo I., De Riccardis F., *Org. Biomol. Chem.* **2014**, *12*, 424-431.

Taking advantage of the paramagnetic relaxation theory, it was possible to determinate the thermodynamic stability for the [22-Gd]³⁺ complex, estimated ca 10¹⁶; this remarkable result opened a new route for cyclopeptoids as macrocyclic hosts for MRI applications.

The latter application involves the preparation of multi-valent cyclopeptoid cores as functionalized inhibitors for glycosidases. These enzymes are catalysts for the hydrolysis of the glycoside bond; such reaction is widespread in many biological systems, which is why it is crucial to better understand its mechanism.

1-deoxynojirimycin (1-DNJ) is a known iminosugar glycosidase inhibitor; using an inhibitor as molecular probe helps to estimate the glycosidase action mechanism as well as the design of drugs candidates. Such inhibitor, conveniently spaced with an oligo(ethyleneglycol) unit and bearing an azido moiety, can be inserted onto propargyl units *via* click-chemistry.³⁶ The functionalization involves a copper(I) catalysed azide-alkyne cycloaddition (CuAAC). The main advantage of using a macrocyclic nucleus is the possibility to exploit the so-called multi-valent effect: statistically, the spatial proximity of multiple ligands to a single-site binding unit, enhances the affinity of the ligand itself.

A series of iminosugar-cyclopeptoid based clusters was synthesized, the first generation bearing single DNJ pending moieties (Figure 1.13, a)),^{37a} the second one presenting trivalent iminosugar clusters (Figure 1.13, b)).^{37b}

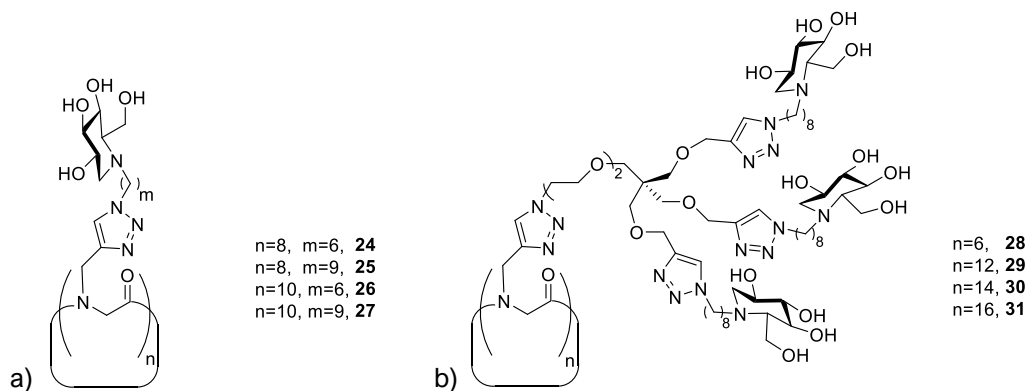


Figure 1.13. Cyclopeptoid-based glycosidase inhibitors.

³⁶ Compain P., *Chem. Rec.* **2019**, *19*, 1-14.

³⁷ a) Lepage M. L., Meli A., Bodlener A., Tarnus C., De Riccardis F., Izzo I., Compain P., *Beilstein J. Org. Chem.* **2014**, *10*, 1406-1412; b) Lepage M. L., Schneider J. P., Bodlener A., Meli A., De Riccardis F., Schmitt M., Tarnus C., Nguyen-Huynh N.-T., Francois Y.-N., Leize-Wagner E., Birk C., Cousido-Siah A., Podjarny A., Izzo I., Compain P., *Chem. Eur. J.* **2016**, *22*, 5151-5155.

The first study evidenced how both the macrocycle's cavity and the spacer length play a role in improving the inhibition activity; the relative inhibition potency (rp), defined as K_i (monovalent reference)/ K_i (glycocluster) (K_i being the inhibitory activity [μM] against jack bean α -mannosidase), were found to be 15 for cpd **24**, 23 for **25**, 21 for **26** and 38 for **27**. These results were modest when compared to 7-valent β -cyclodextrin-based DNJ clusters already known in the literature, showing rp values 2 to 31 time higher.

Exploiting the same CuAAC synthetic strategy, a second generation of compounds was then prepared (cpds **28-31**), bearing trivalent clusters. In this way, the authors systematically investigated the relationship between the number of DNJ units and the inhibition activity, estimating rp/n (rp /total number of DNJs). Adding only 8 units (from **27** to **28**) resulted in a 20-fold increase of rp/n . Moreover, for **29** rp/n was assessed as 4747, the highest value so far in the literature for glycosidase inhibition; following an exponential relation, the value decreased for cpds **30** and **31**, leading to a *plateau* in the K_i values.

Overall, as in the comparison between linear and cyclic peptides, also for peptoids macrocyclization is a powerful tool able to enhance conformational stability and, consequently, proteolytic stability and biological activity. Along with the already mentioned comparisons between the biological activity of linear peptoids vs. the cyclic ones, recently a systematic study about the relative cellular uptake of such scaffolds was presented.³⁸

Using a cell permeability assay, the authors analysed two series of corresponding linear and cyclic molecules, tagged with a chloroalkane moiety, reactive in the cytosol with expressed HaloTag, a modified haloalkane dehalogenase enzyme. The variation of the chain length and the use of diverse (functionalized or unfunctionalized) side-chains did not affect the cellular uptake, up to 70% more effective for the cyclic systems.

³⁸ Shin M., Hyun Y., Lee J. H., Lim H., *ACS Comb. Sci.* **2018**, *20*, 237-242.

1.5 Aim of the project

Given the outstanding potential of cyclic peptoids, regarding both their structural features *and* their capability of acting as hosts for biologically relevant metal cations, ionophores, antimicrobial, cytotoxic agents and so on, the main topic of this research project was answering the question “*can cyclopeptoids actually reproduce, both structurally and functionally, natural effectors?*”.

First of all, we investigated the capability of a series of cyclic hexapeptoid and a series of cyclic octapeptoids of mimicking some interesting natural cyclodepsipeptides; our molecules were found to show cytotoxic and anthelmintic activity (Chapter 2).

Moreover, the structural rigidity of most of the synthesized macrocycles led to a crucial observation: cyclic peptoids possess the property of conformational chirality. This is quite interesting, considering that natural effectors are present in enantiopure form. We, therefore, investigated the central-to-conformational chirality transfer in cyclic peptoids, with the aim to produce single, rigid conformational enantiomers. The introduction of a single or multiple stereogenic centres either on the backbone or on the side-chain(s) caused the rigidification of tri-, tetra-, hexa- and octapeptoids into preferred conformational enantiomers. The conformational properties of these chiral cyclic peptoids and, above all, the emerging turn or loop structures, will be described in Chapter 3.

Given the intrinsic rigidity of cyclic trimers, we hypothesized that this molecular platform was ideal to generate small libraries of possible biological effectors. We therefore prepared a series of catechol-based siderophores, obtaining interesting results in terms of selectivity towards iron(III) (Chapter 4).

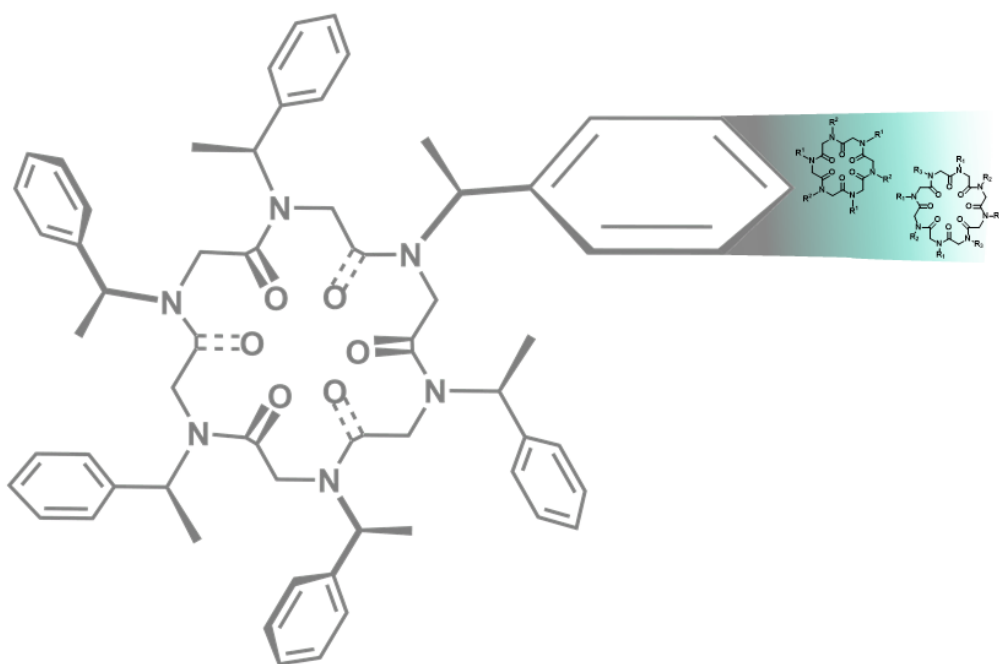
We also focused our attention on the most potent DNA bis-intercalators and, using a cyclotrimeric scaffold, we prepared two series of compounds functionalized with polyaromatic units, capable to act as cytotoxic agents towards human cancer cell lines (Chapter 5).

Finally, sensitive to environmental topics, we exploited the well-known capability of alkali metals complexes of cyclic peptoids to act as catalysts. In particular, we studied the macroring opening polymerization of lactides leading to polylactides, an emerging class of biodegradable polymers (Appendix).

Overall, the results herein presented show how this novel class of peptidomimetics possesses the potential to fully reproduce natural molecules, constituting

a small but significant step towards cyclic peptoid breaching into the realm of drug candidates.

Chapter 2



2 Cyclic peptoids as mimics of natural depsipeptides

2.1 Introduction

2.1.1 Fungal cyclooligomer depsipeptides: a survey

Depsipeptides belong to the macro class of the nonribosomal peptides (NRPs); these small molecules are often secreted as secondary metabolites of many fungal species and bacteria strains. Cyclooligomer depsipeptides (CODs) are a peculiar class of depsipeptides and are extremely common in a number of marine species, including algae, plants and cyanobacteria.

These molecules possess all sorts of interesting activities, such as anticancer, antimicrobial, anthelmintic, insecticide, immunosuppressant, and so on; for example, cryptophycins (Figure 2.1), secreted from cyanobacteria, possess outstanding cytotoxic activity against solid tumours *in vivo*, acting as inhibitors of microtubule assembly.³⁹

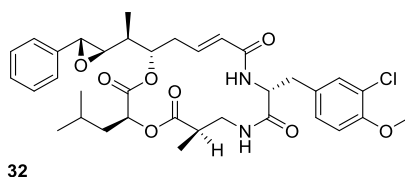


Figure 2.1. General structure of cryptophycin-1 (**32**).

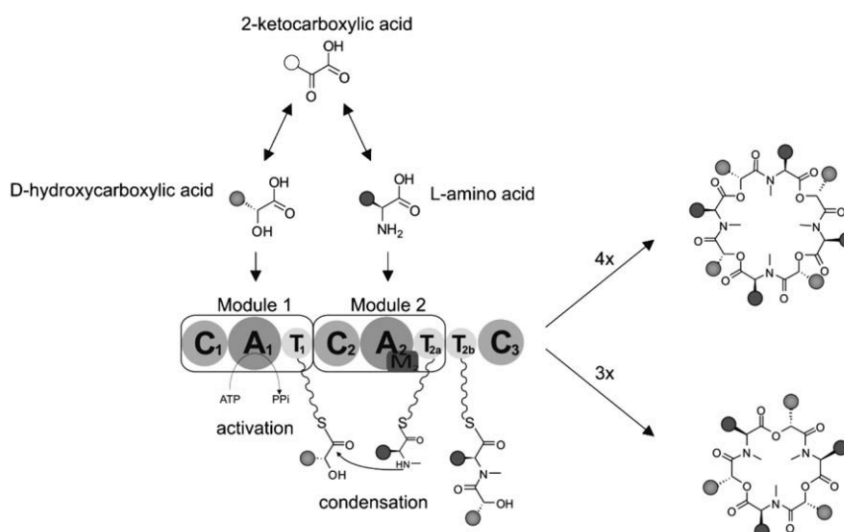
CODs present an enormous structural variety; they are constituted by a combination of α -amino acids (proteinogenic or not, D or L configuration) and α -hydroxycarboxylic acids, which can be bound either from the main functional groups or the side-chains. There are many possible variations due to the action of the “decorating enzymes”: the macrocycle can be enriched with main-chain heterocycles, lipid or glycosyl side-chains, or intramolecular bridges.⁴⁰

The two biggest families of CODs comprise cyclic hexamers and cyclic octamers. These molecules are biosynthesized following the same pathway, although with some variations from fungi to bacteria. The common precursor is an α -ketocarboxylic acid,

³⁹ Weiss C., Sammet B., Sewald N., *Nat. Prod. Rep.* **2013**, *30*, 924-940.

⁴⁰ a) Süßmuth R., Müller J., von Döhren H., Molnár I., *Nat. Prod. Rep.* **2011**, *28*, 99-124; b) Bills G., Li Y., Chen L., Yue Q., Niu X.-M., An Z., *Nat. Prod. Rep.* **2014**, *31*, 1348-1375; c) Sivanathan S., Scherckenbeck J., *Molecules* **2014**, *19*, 12368-12420; d) Wang X., Gong X., Li P., Lai D., Zhou L., *Molecules* **2018**, *23*, 169-218.

which is converted into an L- α -amino acid or a D- α -hydroxycarboxylic acid. The two monomers are bound to the respective adenylation domains to be activated, then converted to the respective thioesters (in the thiolation domain); if necessary, the amino acid is *N*-methylated. The two substrates are then coupled, to give the dimer building block, and this process is iterated three or four times to obtain the necessary oligomer, which is finally cyclized and released to give the COD (Scheme 2.1).

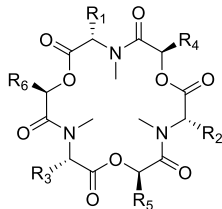


Scheme 2.1. Biosynthesis of CODs.

2.1.2 Cyclohexadepsipeptides mycotoxins: enniatins and beauvericin

Enniatins are a family of cyclohexadepsipeptides produced by *Fusarium* species, *Verticillium hemipterigenum* and *Halosarpheia* species. So far, 29 enniatins have been isolated, 18 of which isolated as single compounds, the other 11 as an inseparable mixture of homologs. The generic structure (Figure 2.2) involves the regular alternation of ester and amide bond, where the peptidol monomer is constituted by D-hydroxyisovaleric acid (D-Hiv) and an *N*-alkylated aliphatic L-amino acid, mainly *N*(Me)Ile, *N*(Me)Val, *N*(Me)Leu. In a few cases (enniatsins H, I, MK1688, L, M, N, O) the D- α -hydroxycarboxylic acid can be modified with a *sec*-butyl side-chain or with an additional hydroxyl moiety. In other cases (enniatsins J, K₁, P) the canonical amino acids can be replaced at one or more positions by

N(Me)Ala, *N*(Me) α -aminobutyric acid, *N*(Me)Thr.⁴¹ In Figure 2.2 are displayed a few of the main variants, crucial to the following discussion.



Enniatin	R ₁	R ₂	R ₃	R ₄	R ₅	R ₆
A (33)	sBu	sBu	sBu	<i>i</i> Pr	<i>i</i> Pr	<i>i</i> Pr
B (34)	<i>i</i> Pr	<i>i</i> Pr	<i>i</i> Pr	<i>i</i> Pr	<i>i</i> Pr	<i>i</i> Pr
C (35)	<i>i</i> Bu	<i>i</i> Bu	<i>i</i> Bu	<i>i</i> Pr	<i>i</i> Pr	<i>i</i> Pr
D (36)	<i>i</i> Pr	<i>i</i> Pr	<i>i</i> Bu	<i>i</i> Pr	<i>i</i> Pr	<i>i</i> Pr
E ₁ (37)	<i>i</i> Pr	<i>i</i> Bu	sBu	<i>i</i> Pr	<i>i</i> Pr	<i>i</i> Pr
F (38)	<i>i</i> Bu	sBu	sBu	<i>i</i> Pr	<i>i</i> Pr	<i>i</i> Pr
G (39)	<i>i</i> Bu	<i>i</i> Bu	<i>i</i> Pr	<i>i</i> Pr	<i>i</i> Pr	<i>i</i> Pr

Figure 2.2. Enniatins structure and peptidol composition.

The first systematic description of enniatins A, B and C, regarding their structure and properties, dates back to the early 70s.⁴²

The overall biological activity regards enniatins' capability to act as antibiotics, insecticidal, anthelmintic and herbicidal. The antimicrobial activity against *Staphylococcus* spp., *Bacillus* spp., *Mycobacterium* spp., *E. coli* and *Pseudomonas aeruginosa* was the earliest described. The pharmacological applications were discovered later; enniatins A-F can act as enzyme inhibitors, particularly towards acyl-CoA:cholesterol acyltransferase, which is significant in the treatment of atherosclerosis and hypercholesterolemia.⁴¹

Moreover, enniatins were recently used in cancer research.⁴³ Enniatins B (**34**) and B₁ (not displayed) were discovered to exert remarkable cytostatic/cytotoxic activity with IC₅₀ below 2 μ M towards human melanoma, osteosarcoma, lung cancer and leukaemia. Further investigations about apoptosis mechanism revealed a strict correlation with the inner mitochondrial membrane depolarization, directly dependent on the enniatin concentration.^{43c} Similarly, enniatin A₁ resulted a good anticancer agent against rat hepatoma, acting with the same apoptosis mechanism.

⁴¹ Sy-Cordero A. A., Pearce C. J., Oberlies N. H., *J. Antibiot.* **2012**, *65*, 541-549.

⁴² Yu Ovchinnikov A., Ivanov V. T., Evstratov A. V., Mikhaleva I. I., Bystrov V. F., Portnova S. L., Balashova T. A., Meshcheryakova E. N., Tulchinsky V. M., *Int. J. Pept. Prot. Res.* **1974**, *6*, 465-498.

⁴³ a) Dornetshuber R., Heffeter P., Kamyar M.-R., Peterbauer T., Berger W., Lemmens-Gruber R., *Chem. Res. Toxicol.* **2007**, *20*, 465-473; b) Wätjen W., Debbab A., Hohlfeld A., Chovolou Y., Kampkter A., Edrada R. A., Ebel R., Hakiki A., Mosaddak M., Totzke F., Kubbutat M. H. G., Proksch P., *Mol. Nutr. Food Res.* **2009**, *53*, 431-440; c) Tonshin A. A., Teplova V. V., Andersson M. A., Salkinoja-Salonen M. S., *Toxicol.* **2010**, *276*, 49-57.

The structure-function relationship is crucial and is dictated by three parameters that contribute to the overall exceptional rigidity; the cyclic scaffold, the configuration of the stereogenic centres, and the *N*-methylations.

Underlying the action mechanism, in all cases the capability to induce the transmembrane cation transport is fundamental; all enniatins are ionophores. The host preorganization in the solution state, stated by sharp $^1\text{H-NMR}$ signals in polar as well as nonpolar solvents, is crucial to induce the capture of the cation. The association constant (K_a) of the enniatin B potassium complex in ethanol is assessed at 6500 M^{-1} .

Employing the carbonyl oxygens, belonging either to the amide or the ester units, the macrocycle's cavity can host alkali metal cations, such as Na^+ , K^+ , Rb^+ and Cs^+ , as well as alkaline earth metals like Ca^{2+} or Mg^{2+} . The complexation occurs through a 1:1 stoichiometry, although sandwich-like complexes have been observed, displaying a 1:2 host:guest ratio, in the case of cations with a smaller radius, such as Na^+ and Ca^{2+} .⁴²

The structure of the enniatin B-KSCN was largely investigated, both *via* computational study and X-ray. In $[\mathbf{34}\cdot\text{K}]^+$ the complexation is computed involving all six oxygen atoms of the macrocycle, and the cation is placed right above the plane described by the host (Figure 2.3). The internal energy ($E(\text{int})$) of the complex is estimated at 715.3 kcal/mol .⁴⁴

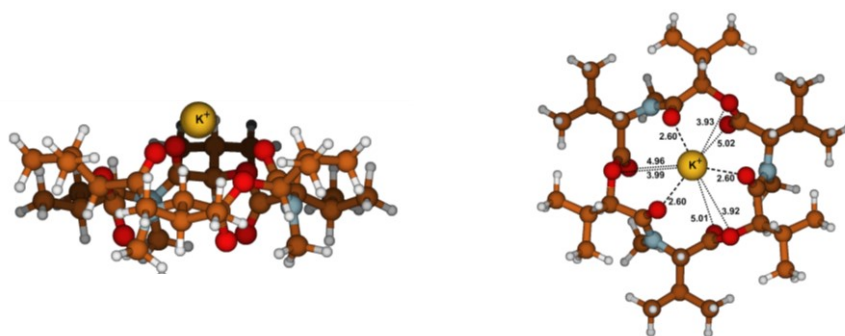


Figure 2.3. $[\mathbf{34}\cdot\text{K}]^+$ computed model in side and top projections.

This assembly has been encountered also in crystal structures of the $[\mathbf{34}\cdot\text{K}]^+\text{SCN}^-$ complex, grown from methanol. The cell unit is trigonal and contains 12 independent enniatin molecules, having three crystallographic three-fold axes. The

⁴⁴ Makrlík E., Böhm S., Vaňura P., *Monatsh Chem.* **2016**, *147*, 1687-1692.

enniatin molecules, spaced by the K^+ cations, are disposed in stacks and the complexation occurs through the carbonyl oxygen atoms (Figure 2.4).⁴⁵

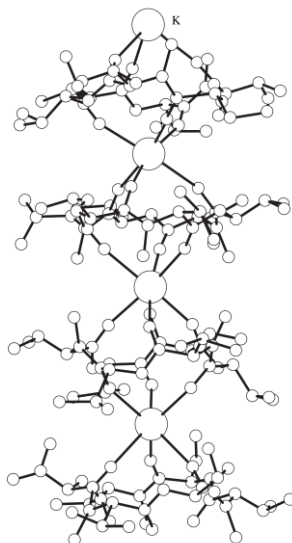


Figure 2.4. A portion of the crystal structure of $[34 \cdot K]^+SCN^-$.

Further investigations of the cation transport mode of action revealed that enniatins act as a passive membrane channel.⁴⁶ First, the lipophilic macrocycle incorporates into the cell membrane; then, according to the selectivity dictated by the cavity, acts as a pore, allowing the indiscriminate influx and efflux of K^+ , Na^+ and Ca^{2+} . In this way, the ionic gradient of the cell is disrupted, resulting in the cytostatic/cytotoxic effect.

Beauvericin (Figure 2.5) is the last member of the enniatins' family, although usually is not comprised, as it differs in the nature of the amino acid, L-N(Me)Phe.

⁴⁵ Zhukhlistova N. E., *Crystallogr. Rep.* **2002**, 47, 3, 433-442.

⁴⁶ Kamyar M., Rawnduzi P., Studenik C. R., Kouri K., Lemmens-Gruber R., *Arch. Biochem. Biophys.* **2004**, 429, 215-223.

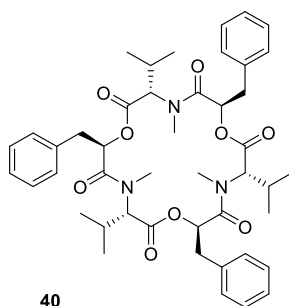
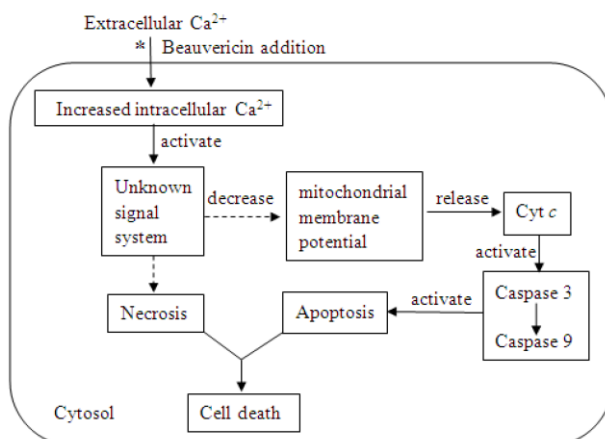


Figure 2.5. Beauvericin structure.

Beauvericin is mainly produced by *Beauveria bassiana*, but also by *Fusarium* spp., together with enniatins. The slight structural difference confers to beauvericin enhanced pharmacological properties, again related to its capability to act as ionophore. The antitumor activity of beauvericin has been largely investigated, being the most active compound of the cyclohexadepsipeptides family. The cytotoxicity against human leukaemia cells has been reported several times (IC_{50} 2.46 μ M). The mechanism of action involves the disruption of the Ca^{2+} concentration gradient in the cell.⁴⁷ Once incorporated in the cellular membrane, like in the case of enniatins, beauvericin presence induces the selective passive movement of extracellular Ca^{2+} into the cytosol. The resulting high concentration of calcium(II) causes a cascade of signals (unknown) that finally result in the release of Cyt *c* from the mitochondria. Lastly, the caspase, activated from Cyt *c*, triggers the apoptosis (Scheme 2.2). Reports of cytotoxicity of beauvericin against other cell lines suggest that also in these cases the concentration of Ca^{2+} plays a crucial role, although the signalling system is still unknown.⁴⁸

⁴⁷ Jow G.-M., Chou C.-J., Chen B.-F., Tsai J.-H., *Cancer Lett.* **2004**, *216*, 165-173.

⁴⁸ Wang Q., Xu L., *Molecules* **2012**, *17*, 2367-2377.



Scheme 2.2. Beauvericin cytotoxicity mechanism against leukaemia cells.

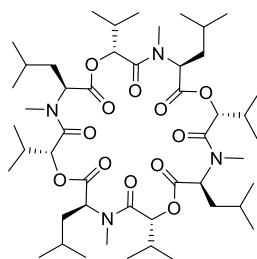
Besides the cytotoxic effect, beauvericin also displays a strong, broad-spectrum antibacterial activity against several strains, belonging to Gram-positive and Gram-negative families, with no particular selectivity.

Lastly, beauvericin showed to be a strong inhibitor of HIV-1 (immunodeficiency virus type-1) for its ability to repress HIV-1 integrase (IC₅₀ 1.9 μM) *in vitro*. This strong inhibitory activity could be related to the capability of beauvericin to hamper the oligomerization of the enzyme crucial to the catalytic activity. In fact, one of the two main tasks of HIV-1 integrase is the 3'-processing reaction, which is the removal of the terminal dinucleotide from the 3'-end of each strand of the viral cDNA (complementary DNA).⁴⁹

2.1.3 Cyclooctadepsipeptides mycotoxins: bassianolide, verticilide and PF1022 congeners

Fungal cyclooctadepsipeptides constitute a quite large family of compounds, just like the hexameric one. The first compound to be isolated and the most studied is bassianolide (Figure 2.6), obtained mainly from *Beauveria bassiana*, but also from *Lecanicilium* spp. and from *Xylaria* spp..

⁴⁹ Shin C.-G., An D.-G., Song H.-H., Lee C., *J. Antibiot.* **2009**, 62, 687-690.



41

Figure 2.6. Bassianolide structure.

The elucidation of the structure, composed by alternating D-Hiv and L-N(Me)Leu residues, was disclosed in 1978.⁵⁰ Resembling the case of the parent cyclohexadepsipeptides, the ¹H-NMR analysis revealed the presence of two rigid conformations, slowly interconverting on the NMR time scale (CDCl₃). The first conformational isomer presented a C₄ symmetry, while the other a C₂ symmetry. The biological activity of bassianolide is profoundly different from beauvericin, although isolated from the same strain. The ionophoric activity in the case of the octameric macrocycle has a different kind of cation selectivity, due to the larger cavity.

Bassianolide displays potent anthelmintic activity; its oral administration to silkworm larvae at 4 ppm concentration causes atony, which is the muscular relaxation resulting in the paralysis of the organism. Higher doses (8 ppm) lead to the death of the worms.

Verticilide, or verticilide A1, like bassianolide, is a highly symmetric molecule, produced by the hypocrelean fungus *Verticillium* spp.. The cyclic octameric structure is composed of four L-N(Me)Ala residues and four D-2-hydroxyheptanoic acid units, whose absolute stereochemistry was elucidated only in 2006.⁵¹ Like bassianolide, verticilide A1 is highly stable in solution, and presents two slowly interchanging conformers, in 3:4 ratio (CDCl₃).

⁵⁰ Kanaoka M., Isogai A., Urakoshi S. M., Ichinoe M., Suzuki A., Tamura S., *Agric. Biol. Chem.* **1978**, *42*, 3, 629-635.

⁵¹ Monma S., Sunazuka T., Nagai K., Arai T., Shiomi K., Matsui R., Ōmura S., *Org. Lett.* **2006**, *8*, 5601-5604.

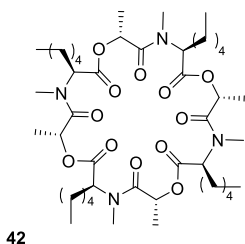


Figure 2.7. Verticilide A1 structure.

Three related molecules, verticilides A2, A3 and the cyclohexadepsipeptide verticilide B1, were discovered only in 2012 from the fungal strain FKI-2679.⁵² Despite its hexameric structure, verticilide B1 is reported here as being the direct congener of verticilide A1. However, verticilide A1 is far more biologically active than its congeners. The peculiar composition of the side-chains confers a unique biological activity. Compared to the already mentioned bassianolide, beauvericin and enniatins, verticilide A1 shows no antitumor or antimicrobial/antifungal action.

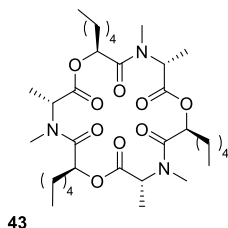


Figure 2.8. Verticilide B1 structure.

The main biological activity of verticilide A1 regards its insecticidal activity. The metabolite selectively binds ryanodine receptors, a common target for commercially available insecticides. Ryanodine receptors (RyRs) are ion-selective channels that regulate the Ca^{2+} intracellular release, in skeletal and cardiac muscle; the presence of the macrocycle hampers the correct functioning of the RyR channels, involving the capture of Ca^{2+} ions. This results in a cockroach RyR ryanodine-binding inhibition IC_{50} in the low micromolar range ($4.2 \mu\text{M}$).⁵³

The only other pharmacological activity reported regards verticilide ability to inhibit acyl-CoA:cholesterol acyltransferase (ACAC), as reported in a recent research

⁵² Ohshiro T., Matsudo D., Kazuhiro T., Uchida R., Nonaka K., Masuma R., Tomada H., *J. Antibiot.* **2012**, *65*, 255-262.

⁵³ Shiomi K., Matsui R., Kakei A., Yamaguchi Y., Masuma R., Hatano H., Arai N., Isozaki M., Tanaka H., Kobayashi S., Turberg A., Ōmura S., *J. Antibiot.* **2010**, *63*, 77-82.

paper.⁵² All four verticilides showed good IC_{50} values against two ACAC types, the best result for verticilide A1 (IC_{50} 0.23 μ M against ACAC type 2); this is remarkable considering that up to date there are no commercially available inhibitors.

PF1022A (Figure 2.9) is a potent anthelmintic against a broad spectrum of gastrointestinal nematodes and is the parent of the most recently discovered family of cyclooctadepsipeptides. It was isolated in 1992 from the strain *Mycelia sterilia* and it consists of four L-N(Me)Leu, two D-phenyllactic acids (D-PheLac) and two D-lactic acids (D-Lac). So far, PF1022s A-H have been isolated, presenting variations at the lactic acid side-chains.^{40c}

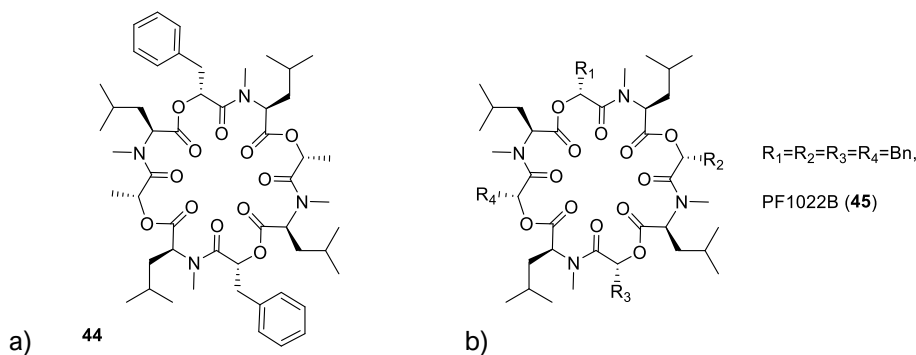


Figure 2.9. a) PF1022A structure and b) generic PF1022 scaffold; for all-Bn side-chains, PF1022B.

PF1022A, like the other cyclooctamers described so far, shows a relative conformational rigidity in the solution state. The NMR spectrum, CD₃OD, evidences two conformational isomers in 4:1 ratio, the major one completely asymmetrical (C_1), the minor showing a C_2 symmetry axis.⁵⁴

With the aim to increase the biological activity, many studies tried to chemically modify the octameric scaffold, in order to obtain a single, rigid conformation. Derivatives with the replacement of the N(Me)Leu-Lac moiety with the constrained D-Pro-L-Pro,^{55a} a Leu-Lac carbon bridge, or the replacement of one residue of Leu with a nitrogen heterocycle,^{55b} caused a strong increase of the anthelmintic activity, thanks to the presence of a single backbone conformation. The bis-[(R)-(para-morpholino-phenyl)-lactic acid] derivative of PF1022A, named emodepside (Figure 2.10), was introduced on the

⁵⁴ Sasaki T., Takagi M., Yaguchi T., Miyadoh S., Okada T., Koyama M., *J. Antibiot.* **1992**, *45*, 692-697.

⁵⁵ a) Dyker H., Harder A., Scherckenbeck J., *Bioorg. Med. Chem. Lett.* **2004**, *14*, 6129-6132; b) Dutton F. E., Lee B. H., Johnson S. S., Coscarelli E. M., Lee P. H., *J. Med. Chem.* **2003**, *46*, 2057-2073.

market in 2005 and it is currently comprised in the formulation of many veterinary anthelmintics, thanks to its enhanced efficacy.

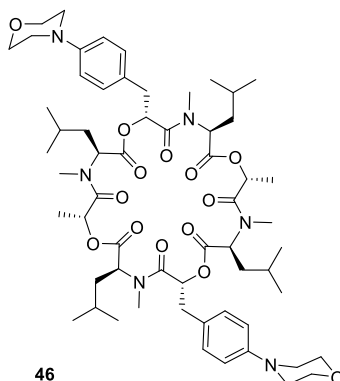


Figure 2.10. Emodepside structure.

PF1022s target the ion channels, like the other cyclooctadepsipeptides,⁵⁶ although showing a strict selectivity towards SLO-1. These ion-channels are important in the regulation of muscle and neuronal cells, and are calcium-activated channels, indicating once again the stringent correlation between the inhibition mechanism and the Ca^{2+} concentration.⁵⁷

Unfortunately, the chemical synthesis of these fascinating compounds is quite challenging; first of all, the synthesis of the peptidol monomers suffers low yields, due to the inefficient amide-ester coupling. Secondly, racemization has often been observed; lastly, as we already mentioned in Chapter 1, the coupling efficiency of *N*-Me amino acids is often reduced. These synthetic drawbacks considerably limit the possible application of both cyclohexa- and cyclooctadepsipeptides as novel drug candidates.

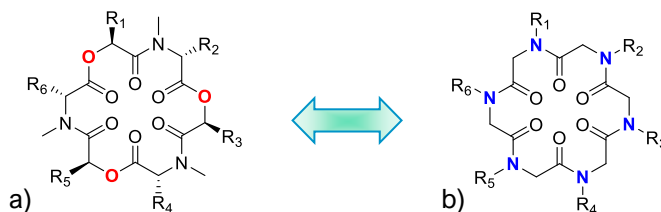
2.1.4 Purpose of the research

Our idea was the substitution of a depsipeptide scaffold with a peptoid one; we wished to validate the capability of such molecules to act as mimics for the natural counterparts, exploiting the well-established capability to act as ionophores. Moreover, we

⁵⁶ Greenberg R. M., *Curr. Clin. Micro Rpt.* **2014**, *1*, 51-60.

⁵⁷ a) Harder A., Schmitt-Wrede H.-P., Krücken J., Marinovski P., Wunderlich F., Willson J., Amliwala K., Holden-Dye L., Walker R., *Int. J. Antimicrob. Agents* **2003**, *22*, 318-331; b) Krücken J., Harder A., Jeschke P., Holden-Dye L., O'Connor V., Welz C., von Samson-Himmelstjerna G., *Trends Parasitol.* **2012**, *28*, 385-393.

aimed to test the biological activity of our synthons, mainly their cytotoxic and their anthelmintic action.



Scheme 2.3. Resemblance between a a) depsipeptide and a b) peptoid hexameric scaffolds.

In Paragraph 2.2, the syntheses, ionophoric properties and cytotoxic activity of six cyclohexapeptoids (Figure 2.11) will be described; the side-chains of these molecules were chosen on the basis of the most common enniatins' and beauvericin features.

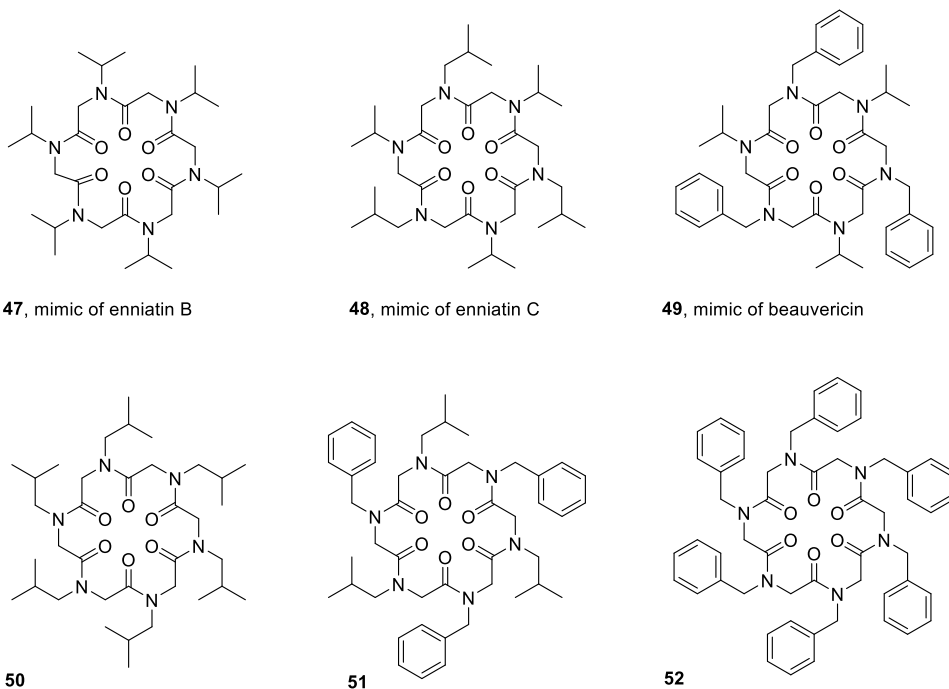
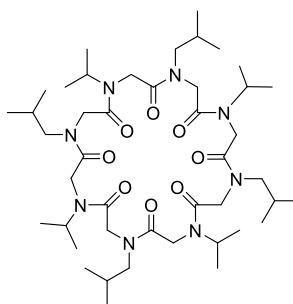
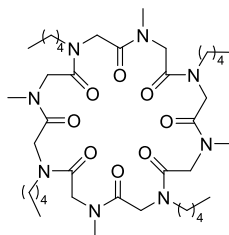


Figure 2.11. Cyclohexapeptoids mimics of enniatins and beauvericin.

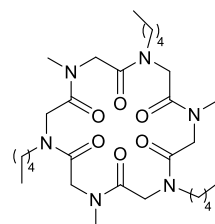
In the following Paragraph, 2.3, I will describe the synthesis of four derivatives of the cyclooctadepsipeptides family (plus the mimic for verticilide B1). For these compounds the anthelmintic properties will be reported.



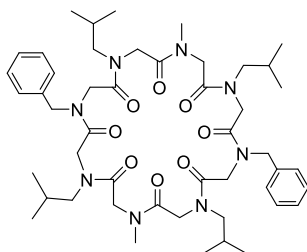
53, mimic of bassianolide



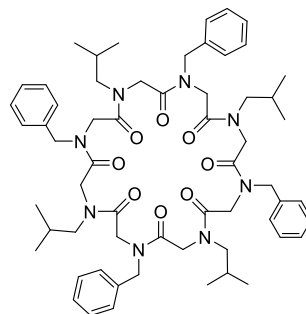
54, mimic of verticilide A1



55, mimic of verticilide B1



56, mimic of PF1022A



57, mimic of PF1022B

Figure 2.12. Cyclopeptoids mimics of cyclodepsipeptides.

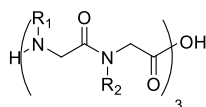
For both of the series, the conformational properties of the macrocycles will be thoroughly discussed; in most of the cases, the ionophoric activity will be shown to be in total accordance with the spatial preorganization of the peptoid host, resulting also in enhanced biological activity.

2.2 Cyclohexapeptoids as mimics of enniatins and beauvericin mycotoxins⁵⁸

2.2.1 Results and discussion

2.2.1.1 Synthesis and structural analysis of cyclohexapeptoids 47-51

The linear precursors were efficiently synthesized exploiting the already described sub-monomeric method (Paragraph 1.4), using 2-chlorotrityl chloride resin, bromoacetic acid as acyl synthon and the commercially available isopropylamine, isobutylamine and benzylamine. The linear oligomers were detached from the resin using the mild acidic 1,1,1,3,3,3-hexafluoroisopropanol (HFIP), providing linear oligomers **58-62** in decent yields.^{20,59}



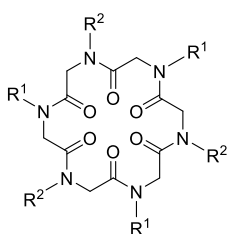
Oligomer	R ₁	R ₂	Sequence	Yield
58	<i>i</i> Pr	<i>i</i> Pr	H-[NVal] ₆ -OH	100%
59	<i>i</i> Bu	<i>i</i> Pr	H-[NLeu-NVal] ₃ -OH	92%
60	Bn	<i>i</i> Pr	H-[NPhe-NVal] ₃ -OH	87%
61	<i>i</i> Bu	<i>i</i> Bu	H-[NLeu] ₆ -OH	76%
62	Bn	<i>i</i> Bu	H-[NPhe-NLeu] ₃ -OH	78%

Figure 2.13. Linear oligomers **58-62** and their yields.

The cyclization of the linear precursors was accomplished according to our established protocol,³⁵ using HATU as condensing agent, in the presence of DIPEA as base, at 3 mM as the maximum concentration of the linear oligomer in DMF. The crude products were purified either by precipitation from slow cooling of an acetonitrile solution (**47**, **49-51**) or *via* reverse-phase chromatographic column (**48**) to yield the cyclopeptoids in high purity (>95%). Compound **52** was synthesized according the procedure reported in De Riccardis *et al.*³²

⁵⁸ D'Amato A., Volpe R., Vaccaro M. C., Terracciano S., Bruno I., Tosolini M., Tedesco C., Pierri G., Tecilla P., Costabile C., Della Sala G., Izzo I., De Riccardis F., *Cyclic Peptoids as Mycotoxins Mimics: an Exploration of Their Structural and Biological Properties*. *J. Org. Chem.* **2017**, *82*, 8848-8863.

⁵⁹ Della Sala G., Nardone B., De Riccardis F., Izzo I., *Org. Biomol. Chem.* **2013**, *11*, 726-731.



Cyclic peptoid	R ₁	R ₂	Yield
47 (enB)	<i>i</i> Pr	<i>i</i> Pr	36%
48 (enC)	<i>i</i> Bu	<i>i</i> Pr	65%
49 (bv)	Bn	<i>i</i> Pr	45%
50	<i>i</i> Bu	<i>i</i> Bu	60%
51	Bn	<i>i</i> Bu	48%

Figure 2.14. Cyclohexapeptoids' structures and their yields. In parentheses are reported the natural congeners. enB = enniatin B; enC = enniatin C; bv = beauvericin.

The conversion of the depsipeptide backbone to a lactam core caused increased flexibility of the overall structure, which resulted in the presence of multiple conformers, in slow exchange on the NMR time scale, for compound **48** and for the macrocycles **50-52**. To our delight, two of the novel compounds presented a constrained structure, thanks to the presence of the relatively bulky α -branched isopropyl side-chain(s), which resulted for **47**, in the presence of three main conformational isomers, in slow equilibrium on the NMR time scale; for **49**, congener of beauvericin, decorated with alternating *N-i*Pr/*N*-Bn, in the emerging of a single prevalent conformational isomer ($\sim 85\%$, based on the $^1\text{H-NMR}$ analysis).⁶⁰

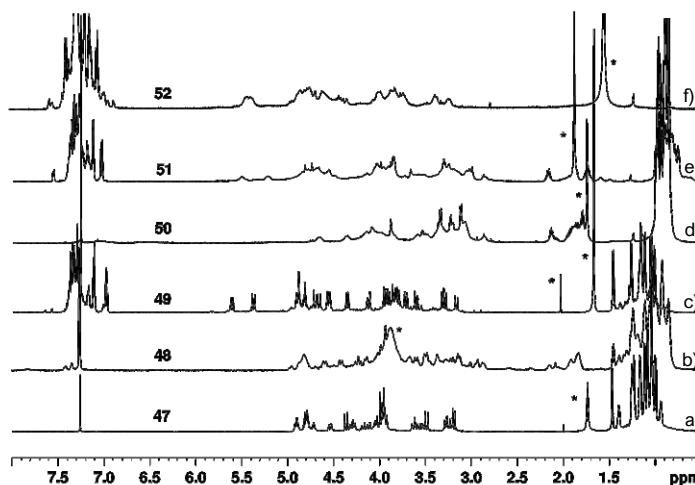


Figure 2.15. $^1\text{H-NMR}$ spectra of cyclic peptoids **47-52** (600 MHz, CDCl_3 , 5.0 mM). Water or solvent impurities are labelled with a black asterisk.

⁶⁰ Despite our efforts, we were not able to increase this integral value, using different deuterated solvents or mixtures ($\text{C}_5\text{D}_5\text{N}$, C_6D_6 , $\text{CD}_3\text{CN}:\text{CDCl}_3$ (9:1)).

It is remarkable that this is the first case of a conformationally stable⁶¹ cyclic hexapeptoid, excluding the *N*-arylated ones. In fact, in the literature cyclohexapeptoids are known to show multiple conformations in slow exchange on the NMR time scale, since the 60s.⁶²

Exploiting 2D NMR techniques, homonuclear (COSY) and heteronuclear (HSQC, HMBC), we were able to assign the resonances of the **49** major isomer. First of all, we assigned the relative *cis/trans* amide bond geometry; for the *N*Val residues, we based the assignment on the ¹H-NMR *N*-CaH chemical shift values, as previously reported for the case of (*S*)-phenylethyl side-chains.⁶³ In particular, higher chemical shift values (δ 4.87 and 4.78 ppm) indicated *cis* amide bond geometries (side-chains *syn* to the deshielding carbonyl groups); a lower chemical shift value (δ 3.81 ppm) implied a *trans* amide bond geometry. For the *N*Phe residues, the diastereotopic benzyl CH₂ $\Delta\delta$ were observed: high $\Delta\delta$ values (>1.0) implied a *cis* peptoid bond, due to a *syn* relationship with the deshielding carbonyl unit (respectively 1.82 and 1.59 ppm). On the contrary, a small $\Delta\delta$ (0.19 ppm) pointed towards a *trans* peptoid bond. Thanks to the long-range connections we were able to assign the structure as *cyclo*-[*cis*-*N*Val¹-*cis*-*N*Phe¹-*trans*-*N*Val²-*cis*-*N*Phe²-*cis*-*N*Val³-*trans*-*N*Phe³] (*i.e.*: *cyclo*-[*cctcct*]) (**49a**) (Figure 2.15). This arrangement in the solution state resembled the *cctcct* peptoid bond geometry reported for the solid-state structures of hexameric cyclic peptoids,⁶⁴ while, as already mentioned, for the complexes an all-*trans* geometry is usually observed (*cf.* Paragraph 1.4 and ref. 30a). Table 2.1 reports the full assignment of the ¹H- and ¹³C-NMR resonances and the structure of **49a**.

⁶¹ The conformational stability is assessed through a variable temperature (VT) NMR experiment. The coalescence value was calculated $\Delta G^\ddagger = 14.4$ kcal/mol (coalescence temperature (T_c) 323 K, C₂D₂Cl₄ solution, 300 MHz), according to Kurland R. J., Rubin M. B., Wise M. B., *J. Chem. Phys.* **1964**, *40*, 2426-2427.

⁶² Dale J., Titlestad K., *J. Chem. Soc. D* **1969**, 656-659.

⁶³ a) De Santis E., Edwards A. A., Alexander B. D., Holder S. J., Biesse-Martin A. S., Nielsen B. V., Mistry D., Waters L., Siligardi G., Hussain R., Faure S., Taillefumier C., *Org. Biomol. Chem.* **2016**, *14*, 11371-11380; b) Armand P., Kirshenbaum K., Goldsmith R. A., Farr-Jones S., Barron A. E., Truong K. T. V., Dill K. A., Mierke D. F., Cohen F. E., Zuckermann R. N., Bradley E. K., *Proc. Natl. Acad. Sci. USA* **1998**, *95*, 4309-4314.

⁶⁴ Tedesco C., Erra L., Izzo I., De Riccardis F., *Cryst. Eng. Comm.* **2014**, *16*, 3667-3687.

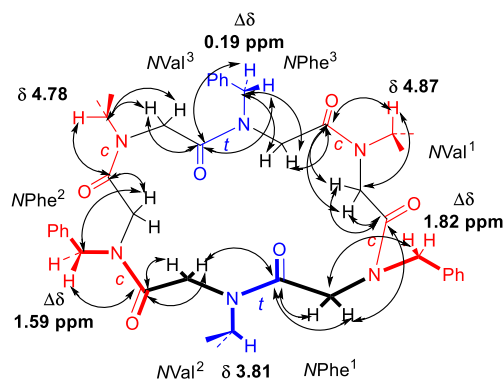
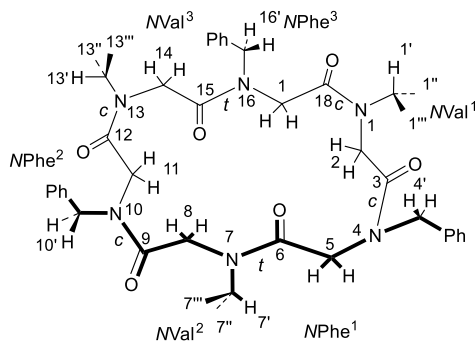


Figure 2.16. Structure of **49a** and relevant long-range ^1H - ^{13}C cross-correlations (from HMBC). *Cis* peptoid residues are depicted in red, *trans* peptoid residues are depicted in blue.



C/H number	C	H	<i>N</i> -Aa
1'	44.8	4.87 (1H, d, <i>J</i> 7 Hz)	<i>cis</i> -NVal ¹
1''	20.2	1.08 (3H, d, <i>J</i> 7 Hz)	
1'''	19.6	1.13 (3H, d, <i>J</i> 7 Hz)	
2	44.2	4.53, 3.70 (2H, d, <i>J</i> 17 Hz)	
3	169.9	-	
4'	51.3	5.60, 3.78 (2H, d, <i>J</i> 15 Hz)	<i>cis</i> -NPhe ¹
5	47.6	4.11, 3.92 (2H, d, <i>J</i> 17 Hz)	
6	167.1	-	
Ar	136.2 ^a 128.8 128.4 127.6	7.40-7.25 (5H, overlapping signals)	
7'	48.0	3.81 (1H, d, <i>J</i> 7 Hz)	<i>trans</i> -NVal ²
7''	21.5	1.41 (3H, d, <i>J</i> 7 Hz)	
7'''	21.2	1.23 (3H, d, <i>J</i> 7 Hz)	
8	42.7	4.34, 3.29 (2H, d, <i>J</i> 17 Hz)	

9	171.9	-	
10'	51.9	5.37, 3.90 (2H, d, <i>J</i> 15 Hz)	<i>cis</i> -NPhe ²
11	50.8	4.67, 3.27 (2H, d, <i>J</i> 17 Hz)	
12	168.8	-	
Ar	137.3 ^a 128.8 127.7 127.6	7.40-7.25 (5H, overlapping signals)	
13'	45.7	4.78 (1H, d, <i>J</i> 7 Hz)	<i>cis</i> -NVal ³
13''	20.4	0.98 (3H, d, <i>J</i> 7 Hz)	
13'''	19.5	1.01 (3H, d, <i>J</i> 7 Hz)	
14	43.2	3.85, 3.59 (2H, d, <i>J</i> 17 Hz)	
15	168.7	-	
16'	53.1	4.90, 4.71 (2H, d, <i>J</i> 15 Hz)	<i>trans</i> -NPhe ³
17	50.3	4.54, 3.14 (2H, d, <i>J</i> 17 Hz)	
18	170.9	-	
Ar	135.5 ^a 129.1 127.5 125.6	6.98 (2H, t, <i>J</i> 7.5 Hz, Ar- <i>m</i> - <i>H</i>), 7.40-7.25 (3H, overlapping signals)	

^a Phenyl quaternary carbon.

Table 2.1. Full ¹H- and ¹³C-NMR signals assignment for **49a**; major isomer assignment based on COSY, HSQC and HMBC experiments (¹H at 600 MHz, ¹³C at 150 MHz, CDCl₃).

The macrocyclization of the linear H-[NPhe-NVal]₃-OH **60** could, theoretically, have led to other two *cyclo*-[*cctcct*] conformational diastereoisomers, *cyclo*-[*cis*-NVal-*cis*-NPhe-*trans*-NVal-*trans*-NPhe-*cis*-NVal-*cis*-NPhe]-**49b** and *cyclo*-[*cis*-NPhe-*cis*-NVal-*trans*-NPhe-*trans*-NVal-*cis*-NPhe-*cis*-NVal]-**49c** (Figure 2.17). With the help of theoretical Density Functional Theory (DFT) calculations, we were able to determine the minimum energy structures and relative internal energies **49a** (*E* = 0 kcal/mol) < **49c** (ΔE = 11.6 kcal/mol) < **49b** (ΔE = 17.2 kcal/mol),⁶⁵ confirming the ¹H-NMR results.

⁶⁵ DFT calculations performed in CHCl₃ by prof. C. Costabile.

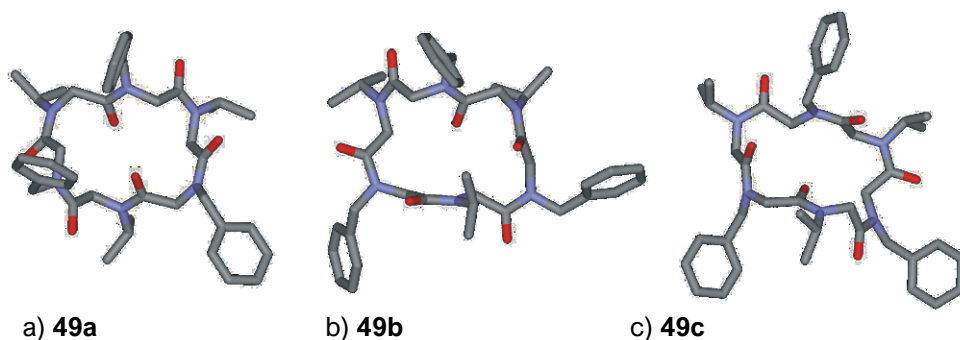


Figure 2.17. Minimum energy structures for conformational diastereoisomers a) **49a**; b) **49b**; c) **49c**. C, silver; N, blue; O, red.

The assigned structure was also corroborated by single-crystal X-ray diffraction. We obtained single crystals of **49a**, suitable for the analysis, by slow diffusion of hexane vapours into a chloroform solution. Cyclopeptoid **49a** crystallized as a chloroform solvate with a 1:2 ratio between cyclopeptoid and chloroform molecules. The molecules form ribbons parallel to the diagonal of the *ac* plane by means of side-by-side CO \cdots HC hydrogen bonds involving carbonyl oxygen atoms and side-chains methylene hydrogen atoms of the *trans* residues. The side-by-side assembly typically involves the same type of *trans* residue (e.g.: *i*Pr side-chains are alongside *i*Pr side-chains and benzyl side-chains are alongside benzyl side-chains).

Both crystallographically independent chloroform molecules interact with carbonyl oxygen atoms by CH \cdots O hydrogen bonds. As already reported in the literature,^{28,64} the alternating isopropyl and benzyl side-chains are disposed onto opposite faces of the plane described by the macrocyclic backbone.

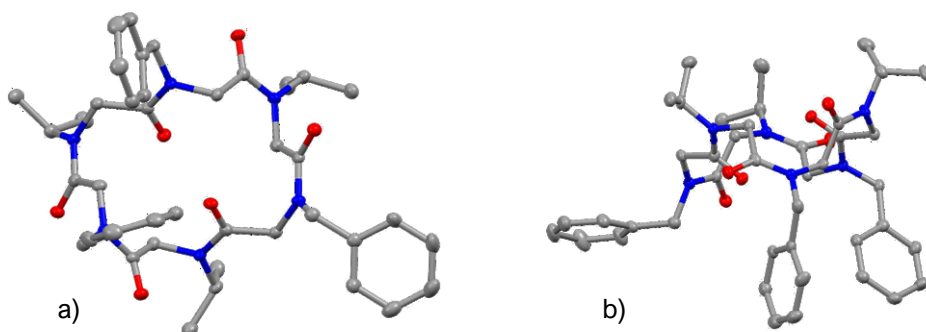


Figure 2.18. X-ray molecular structure of the cyclic peptoid beauvericin mimic **49a** a) top view and b) side view. Hydrogen atoms have been omitted for clarity. C, silver; N, blue; O, red. Thermal ellipsoids are drawn at 30% probability level.

The *cyclo-[cctcct]* arrangement was also observed for compound **47**, which crystallized by slow evaporation from a solution of 1:1 chloroform/methanol. Solvent-free crystals of **47** presented ribbons along the shortest cell axis (*a* axis) by means of side-by-side CO \cdots H₂C hydrogen bonds involving carbonyl oxygen atoms and backbone methylene hydrogen atoms.

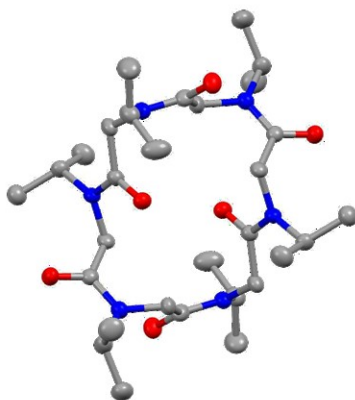


Figure 2.19. X-ray molecular structure of the cyclic peptoid enniatin B mimic **47**. Hydrogen atoms have been omitted for clarity. C, silver; N, blue; O, red. Thermal ellipsoids are drawn at 30% probability level.

2.2.1.2 Conformational chirality in conformationally stable cyclohexapeptoids

The careful observation of **49a** strained conformation revealed another peculiar characteristic of rigid cyclopeptoids, which is their conformational chirality. In fact, in the solution state, **49a** is constituted by a racemic mixture of two equivalent, non-superimposable, forms, displaying opposite directionality of the amide bond units.

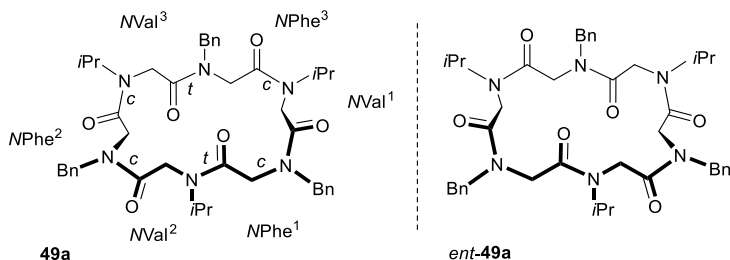


Figure 2.20. Backbone structure of **49a** and its enantiomeric form.

Cyclic peptoids show a form of “inherent chirality”, which is dictated, in absence of stereogenic centres, planes and axes of chirality,⁶⁶ by the presence of directional bonds in a conformationally rigid cyclic structure. A detailed survey, including the nomenclature definition of the planar chirality in cyclic peptoids, will be given in Chapter 3.

A proof of the chirality was given by the splitting of the ¹H-NMR resonances by stepwise addition of the chiral shift reagent known as Pirkle’s alcohol, the (*R*)-(-)-1-(9-anthryl)-2,2,2-trifluoroethanol (**63**), to a chloroform solution of **49a**. The interaction with the chiral Pirkle’s alcohol caused the formation of two diastereomeric supramolecular adducts and the splitting of the resonances close to the interaction site.⁶⁷

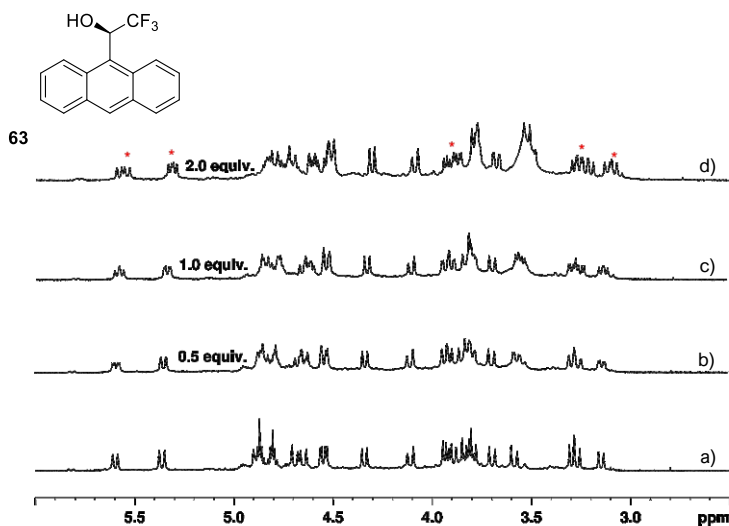


Figure 2.21. Quantitative step-wise addition of Pirkle’s alcohol to **49a**. ¹H-NMR (600 MHz, CDCl₃, 298 K, 12.0 mM solution). 6.0-2.5 ppm expansion. Split signals are denoted with a red asterisk.

As further confirmation, it is noteworthy that in the crystal packing both **49a** and *ent*-**49a** are present.

The presence of a racemic mixture of conformational enantiomers is not deleterious for the biological activity. In fact, the cellular membrane, target for the

⁶⁶ a) Dodziuk H., *Tetrahedron: Asymmetry* **1992**, *3*, 43-50; b) McIldowie M. J., Mocerino M., Ogden M. I., *Supramol. Chem.* **2010**, *22*, 13-39; c) Testa B., *Helv. Chim. Acta* **2013**, *96*, 351-372; d) Eliel E. L., Wilen S. H., Mander L. N., *Stereochemistry of Organic Compounds*, John Wiley & Sons, **1994**, pp. 1119-1190; e) Cahn R. S., Ingold, C. Prelog V., *Angew. Chem. Int. Ed. Engl.* **1966**, *5*, 385-415; f) Prelog V., Helmchen G., *Angew. Chem. Int. Ed. Engl.* **1982**, *21*, 567-583.

⁶⁷ Pirkle W. H., Beare S. D., *J. Am. Chem. Soc.* **1969**, *91*, 5150-5155.

ionophoric activity, is not chiroselective. It has been proven⁶⁸ that both enantiomers of enniatins B and C exert, in fact, the same biological activity.

2.2.1.3 Sodium binding studies for cyclohexapeptoids 47-52

The structural comparison between **49a** rigid structure and beauvericin (**40**) (Figure 2.22, a) and c)), inferred from theoretical studies, evidenced deep morphological differences. However, it is known that the overall architecture of a cyclic peptoid changes dramatically when complexed with metal cations (*cf.* Paragraph 1.4).⁶⁹ The minimum energy structure of [**49a**·Na]⁺ (Figure 2.22, b)) showed a similar side-chain orientation and backbone morphology to beauvericin.

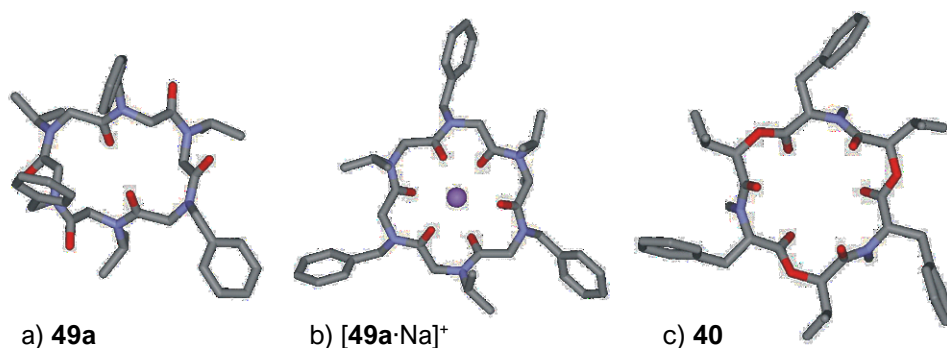


Figure 2.22. Minimum energy structures for a) **49a**; b) [**49a**·Na]⁺; c) beauvericin (**40**). C, silver; N, blue; O, red.

We started the investigation of the sodium complexing ability of our molecules using sodium tetrakis[3,5-bis(trifluoromethyl)phenyl]borate (NaTFPB)⁷⁰ by ¹H-NMR in CDCl₃. We chose the sodium cation considering both its high affinity towards cyclohexapeptoids and its relevance in biological systems.

The main advantage of using such guest relies on the fact that TFPB⁻ forms a loose ion pairing with Na⁺, promoting the complexation by the macrocyclic host.

⁶⁸ a) Shemyakin M. M., Yu Ovchinnikov A., Ivanov V. T., Estratov A. V., *Nature* **1967**, *213*, 412-413; b) Shemyakin M. M., Yu Ovchinnikov A., Ivanov V. T., *Angew. Chem. Int. Ed. Engl.* **1969**, *8*, 492-499.

⁶⁹ a) Baskin M., Panz L., Maayan G., *Chem. Commun.* **2016**, *52*, 10350-10353; b) Baskin M., Maayan G., *Chem. Sci.* **2016**, *7*, 2809-2820; c) Knight A. S., Zhou E. Y., Francis M. B., *Chem. Sci.* **2015**, *6*, 4042-4048; d) Baskin M., Maayan G., *Biopolymers* **2015**, *104*, 577-584; e) *Metallofoldamers. Supramolecular Architectures from Helicates to biomimetics*, ed. Maayan G., Albrecht M., John Wiley & Sons, **2013**; f) Knight A. S., Zhou E. Y., Pelton J. G., Francis M. B., *J. Am. Chem. Soc.* **2013**, *135*, 17488-17493; g) Maayan G., Ward M. D., Kirshenbaum K., *Chem. Commun.* **2009**, 56-58; h) Maayan G., *Eur. J. Org. Chem.* **2009**, 5699-5710; i) Lee B. C., Chu T. K., Dill K. A., Zuckermann R. N., *J. Am. Chem. Soc.* **2008**, *130*, 8847-8855.

⁷⁰ Nishida H., Takada N., Yoshimura M., Sonoda T., Kobayashi H., *Bull. Chem. Soc. Jpn.* **1984**, *57*, 2600-2604.

Moreover, the formation of highly symmetric complexed species and the relative insolubility of NaTFPB in the nonpolar organic solvent gives precious information about the stoichiometry of the complex, and the possibility to perform a titration to obtain the apparent association constant (K_a).

The step-wise addition of the metal salt to chloroform solution of the cyclic peptoids induced the stiffening of the macrocyclic scaffolds into a single, all-*trans* species, as evidenced by the NMR spectra.

The low chemical shift values observed for the *N*Val *Ca*H residues (4.06 ppm in [47·Na]⁺, 3.98 ppm in [48·Na]⁺, 3.89 ppm in [49·Na]⁺), the relatively small $\Delta\delta$ evidenced for the diastereotopic *N*-CH₂-Ph protons (0.49 ppm in [49·Na]⁺, 0.41 in [51·Na]⁺, 0.30 in [52·Na]⁺) attested, for all the complexes, all-*trans* amide bonds geometries. The strong electrostatic forces between the sodium ion and the carbonyl dipoles stabilized the metalated conformers hampering the ring inversion (with no sign of diastereotopic protons' signals coalescence up to 393 K) for the six [47-52·Na]⁺ complexes (¹H-NMR variable temperature experiments: 1.0 mM solutions in C₂D₂Cl₄, 600 MHz).⁶¹

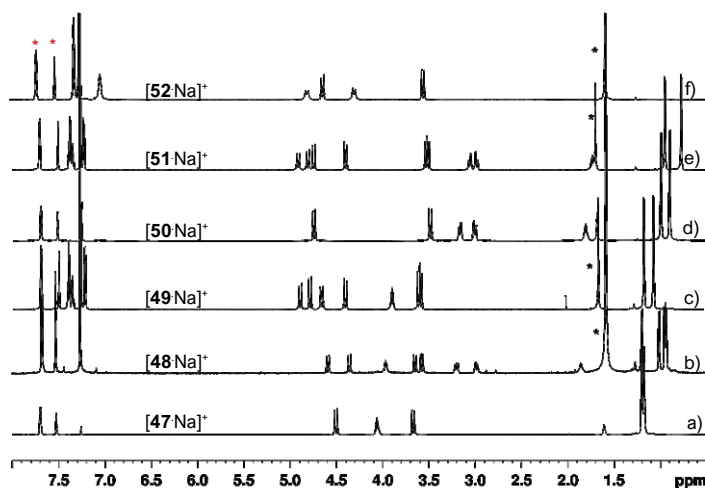


Figure 2.23. ¹H-NMR spectra of complexes [47-52·Na]⁺ (600 MHz, CDCl₃, 5.0 mM). Water or solvent impurities are labelled with a black asterisk. TFPB⁻ signals are labelled with a red asterisk.

The integration values *ratio* between the symmetric host/guest complexes and the TFPB⁻ aromatic resonances were constant during the titrations and documented a fixed 1:1 macrocycle/Na⁺ *ratio* for all the complexes. Further proof of the 1:1 host/guest stoichiometry was deduced by the plots reporting the declining percentage of the free

hosts (calculated on the basis of the 2.5-6.0 ppm range integration) *versus* the molar Na^+ /cyclopeptoid *ratio*. Figure 2.24 b) reports the molar ratio of **51** (with *i*Bu/Bn side-chains, the most soluble host in CDCl_3)/ Na^+ vs. the percentage of the free host. Further addition of NaTFPB induced variation of the chemical shift values, indicating the possible formation of a metalated species with different stoichiometry.

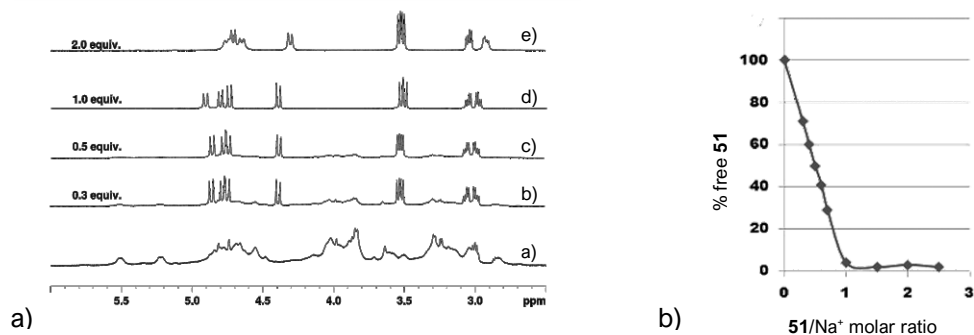


Figure 2.24. a) ^1H -NMR quantitative titration of **51** with NaTFPB at the molar ratio indicated (spectra a-e, 600 MHz, CDCl_3 , 5.0 mM, 6.0-2.5 expansion), and b) plot reporting the percentage of **51** as free host *versus* the molar ratio $\text{Na}^+/\mathbf{51}$.

The relative free host-complexed host integral ratio allowed the evaluation of the apparent association constant K_{a1} (for calculation details, see experimental section, *cfr.* Paragraph 2.2.3.4).⁷¹ The lowest association constant values were recorded for **47** and **49**, bearing isopropyl side-chains; this suggests that, contrary to the natural counterparts, for cyclic peptoids the preorganization of the macrocyclic host hampers the efficient alkali metal capture. In Table 2.2 are reported the $\log K_{a1}$ and the relative Gibbs free energy for the $[\mathbf{47-52}\cdot\text{Na}]^+$ metal complexes.

It is noteworthy that the rigid hexameric metal complexes, with alternating side-chains (**48**, **49**, **51**) are also conformationally chiral, like the free host **49a**.

	47	48	49	50	51	52
$\log K_{a1}^{a,b}$	3.2	4.2	4.0	4.9	4.8	4.9
$-\Delta G^0$	4.4	5.8	5.5	6.6	6.5	6.6

^a From ^1H -NMR experiments, 1.0 mM host/guest in CDCl_3 solutions.

^b Figures within $\pm 10\%$ throughout multiple experiments.

Table 2.2. Log of calculated apparent K_{a1} (M^{-1}) values and $-\Delta G^0$ (kcal/mol) for the $[\mathbf{47-52}\cdot\text{Na}]^+$ complexes.

⁷¹ a) Fielding L., *Tetrahedron* **2000**, *56*, 6151-6170; the term “apparent” is due to the low solubility of the guest in CDCl_3 . See: b) Bright A. A. S., Chudek J. A., Foster R., J. C. S. *Perkin II*, **1975**, *109*, 1256-1259; c) Talotta C., Gaeta C., Neri P., *J. Org. Chem.* **2014**, *79*, 9842-9846.

As for enniatins and beauvericin were also observed 1:2 and 1:3 host/guest stoichiometries, depending on the solvent dielectric constant and cation's radii,⁴² we proceeded the titration studies with further equivalents of NaTFPB, observing the formation of novel species with different host/guest molar ratios. Addition of further equivalents of NaTFPB to $[47\text{-}52\text{Na}]^+$ caused the formation of "inverse sandwich" complexes, characterized by a rare O-bound 1:2 macrocycle/cation for $[48\text{-}52\text{2Na}]^{2+}$ complexes (no variations were recorded in the case of $[47\text{Na}]^+$). The shift of the $^1\text{H-NMR}$ signals, with respect to the monometallic complex spectrum, testified for the formation of novel species, in fast exchange on the NMR time scale. This assumption was corroborated by ESI-MS spectra, and the dissolution of the second equivalent of sodium salt, otherwise insoluble in the nonpolar CDCl_3 .

The bimetallic complexes showed reduced solubility in the chloroform solution, causing the partial precipitation of the adducts for $[48\text{-}50,52\text{2Na}]^{2+}$, which hampered the evaluation of the apparent K_{a2} . Despite our efforts to increase the complexes' solubility, the use of the more polar/coordinating CD_3CN disrupted the bimetal hosts/guest adducts (for the exalted coordination abilities of donor atoms) and re-established the monometallic ones.

Only for the CDCl_3 totally soluble complex $[51\text{2Na}]^{2+}$ we were able to deduce the apparent K_{a2} value ($^1\text{H-NMR}$, 1.0 mM solution, using the program WinEQNMR⁷²) by titration of the monometallic adduct with further NaTFPB. The calculated apparent K_{a2} value was 52 M^{-1} ($\pm 10\%$).

Theoretical calculation disclosed the architecture of the bimetallic adduct $[51\text{2Na}]^{2+}$. In the case of the "inverse sandwich" complex, the two Na^+ ions share half of the amide carbonyl coordination sphere, while in the case of the monometallic adduct the cation is enclosed inside the macrocyclic cavity.

For comparison, in Figure 2.25 are reported the $[51\text{Na}]^+$ and $[51\text{2Na}]^{2+}$ minimum energy structures.

⁷² Hynes M. J., *J. Chem. Soc., Dalton Trans.* **1993**, 311-312.

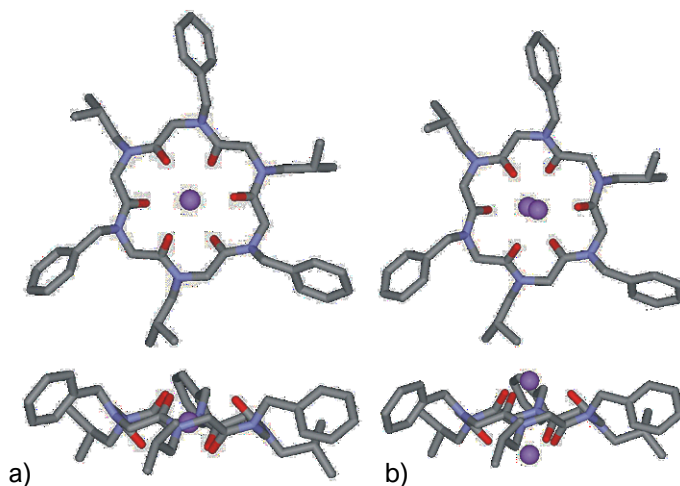


Figure 2.25. Minimum energy structures for a) $[51\cdot\text{Na}]^+$; b) $[51\cdot 2\text{Na}]^{2+}$, top and side view. C, silver; N, blue; O, red; Na^+ , magenta.

Density functional theory studies proved the preferential formation of the disodium complex, rather the monosodium one, as the relative computed energies (ΔG) for the formation of $[51\cdot\text{Na}]^+$ and $[51\cdot 2\text{Na}]^{2+}$, in CHCl_3 , starting from **51** and free Na^+ in solution were calculated as -17.8 and -19.7 kcal/mol, respectively. The ΔG for the formation of $[51\cdot\text{Na}]^+$ and $[51\cdot 2\text{Na}]^{2+}$, in CHCl_3 , starting from **51** and NaTFPB , were calculated to be -32.9 and -49.8 kcal/mol. We concluded that the formation of $[51\cdot 2\text{Na}]^{2+}$ would be favoured either assuming the presence of free Na^+ in solution or considering the undissociated ionic couple.

In order to further validate the computed structures, we tried to crystallize both the monometallic and the bimetallic TFPB adducts, from various solvents (chloroform, toluene and acetonitrile), however obtaining no single crystals suitable for the diffraction measurements. We then chose to prepare the disodium complex using the picrate sodium salt, adding two equivalents to a 2:1 chloroform/toluene solution of **51**. In this way, by slow evaporation, we obtained a yellow crystalline solid, suitable for the X-ray analysis.

The X-ray analysis showed the crystal belonging to an atypical cubic system ($a = 27.36 \text{ \AA}$). The molecular complex is formed in the solid-state by six sodium cations, six picrate anions, three cyclopeptoid molecules, and six water molecules. They are aligned along the crystallographic three-fold rotoinversion axis (determining the positional disorder of benzyl and isobutyl moieties in the central cyclopeptoid molecule).

The central cyclopeptoid molecule binds two sodium ions. Each of them is connected by six bridging water molecules, to two sodium ions, which bind two

cyclopeptoid molecules. Those cyclopeptoid molecules bind two further sodium ions, which complete their coordination sphere by binding three picrate anions each (Figure 2.26). The picrate anions are linked by means of the oxygen atoms of the nitro group, differently from the analogous strontium picrate cyclopeptoid zwitterion complex, where the phenate oxygen atoms were involved.^{30a}

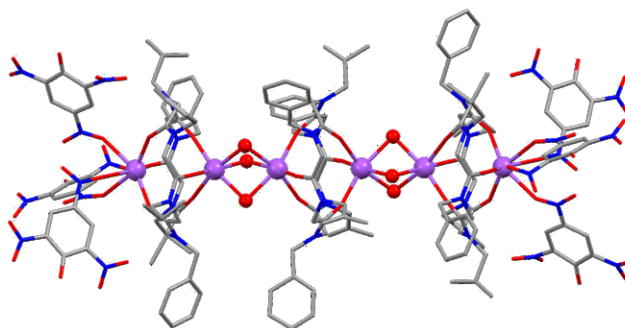


Figure 2.26. X-ray molecular structure of $[51 \cdot 2\text{Na}]^{2+} \cdot 2\text{Pic} \cdot 2\text{H}_2\text{O}$. Hydrogen atoms and disordered sites have been omitted for clarity. Water oxygen atoms and sodium ions are depicted as ball-and-stick. C, silver; N, blue; O, red; Na^+ , magenta.

The solid structure displays an all-*trans* peptoid bond conformation with the carbonyl groups alternately pointing toward the sodium cations and forcing the *N*-linked side-chains to assume an alternate pseudo-equatorial arrangement.

It is possible to compare the **51** complex crystal structure with the beauvericin picrate barium complex. In fact, for the latter, a molecular cation is formed with three picrate anions sandwiched between two barium ions.⁷³

Moreover, also for **51** as sodium complex a solvate form is obtained. The chloroform molecules occupy the void space among the molecular complexes, lying on threefold rotation axis.

2.2.1.4 Ionophoric activity: transmembrane carrier capability of cyclohexapeptoids **47-52**

The encouraging results of the sodium complexation prompted us to test the capability of our macrocycles to transport ions across a phospholipidic membrane, taking advantage of the already mentioned HPTS assay.⁷⁴

⁷³ Braden B., Hamilton J. A., Sabesan M. N., Steinrauf L. K., *J. Am. Chem. Soc.* **1980**, *102*, 2704-2709.

⁷⁴ Sakai N., Matile S., *J. Phys. Org. Chem.* **2006**, *19*, 452-460.

In this test, the pH-sensitive fluorescent dye HPTS (8-hydroxypyrene-1,3,6-trisulfonic acid) is trapped in the internal water pool of liposomes (95:5 phosphatidylcholine (PC) and phosphatidylglycerol (PG) lipid composition) and a pH gradient is established across the membrane by external addition of NaOH. The collapse of the transmembrane pH-gradient, as a consequence of OH⁻ influx or H⁺ efflux, implies basification of the liposome inner water pool which is signalled by an increase of the HPTS fluorescence emission. To maintain trans-membrane electroneutrality this H⁺/OH⁻ movement must be balanced by a flux of counterions which may occur with four possible transport mechanisms: H⁺/M⁺ or OH⁻/X⁻ antiport and H⁺/X⁻ or OH⁻/Na⁺ symport. Therefore, the rate of the pH gradient collapse gives direct information on the transportation of H⁺/OH⁻ and indirect information on the correlated symport/antiport of counterions as well as gives information on the efficiency of the ionophore to promote one of the possible transport mechanisms.

The first part of the study involved the investigation of the cations selectivity, which were added to the system as MCl salt. All alkali metals were evaluated, obtaining, as expected, a selectivity towards Na⁺, the best fitting cation for the hexameric cavity. In Figure 2.27 a) are reported the kinetic profiles for the sodium cation (the profiles for the other metals are not shown). Compound **51** showed the highest activity, while the other cyclopeptoids proved to be almost inactive; for **51** an anion selectivity test was then performed, adding the NaX salt (X= Cl⁻, Br⁻, I⁻) or CaCl₂ to the system.

The overall selectivity, for cations and anions, was obtained comparing the normalized fluorescence intensity measured after 300 s of kinetic in the presence of peptoid **51** corrected for the normalized fluorescence intensity measured in the absence of the peptoid (control trace).

As expected, the anions did not exert a significative effect on the fluorescence emission.

On the contrary, cations displayed a strong selectivity towards Li⁺ and Na⁺, best fitting the macrocycle's cavity, while for the other cations values of fluorescence emission close to zero or negative were observed, suggesting that these ones were not transported.

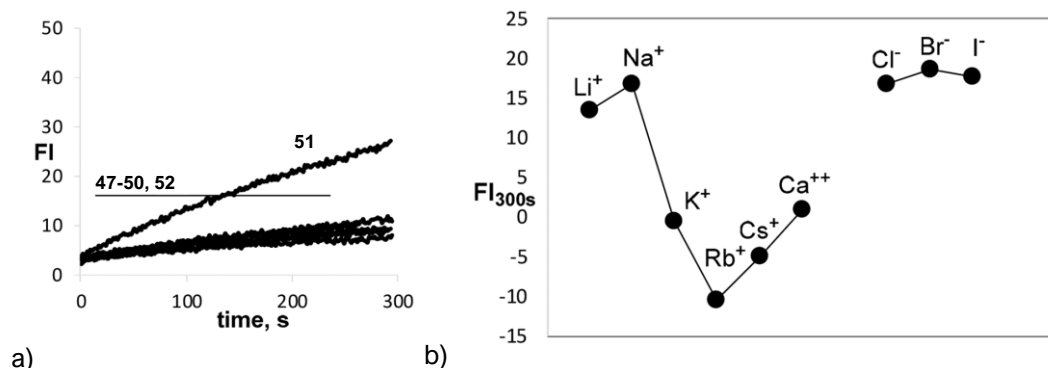
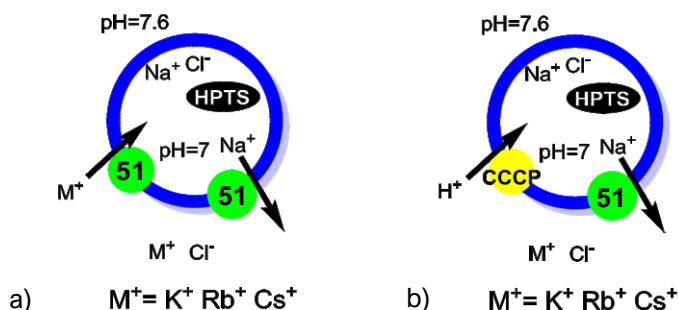


Figure 2.27. a) Normalized fluorescence change in HPTS emission (FI) as a function of time after addition of the base (50 μL of 0.5 M NaOH) to 95:5 EYPC/EYPG LUVs (100 nm diameter) loaded with HPTS (0.1 mM HPTS, 0.17 mM total lipid concentration, 25 mM HEPES, 100 mM NaCl, pH 7.0, total volume 3 mL), in the presence of cyclic peptoids **47-52**. The concentration of the ionophore is 3 mol % with respect to the total concentration of lipids. b) Cations and anions selectivity determined for the cyclic peptoid **51** at 5 mol %, using the HPTS assay (100 mM MCl or NaX, pH 7.0, base pulse by addition of 50 μL of 0.5 M MOH). The figure reports the FI measured at 300 s corrected for the FI measured in the absence of the peptoid.

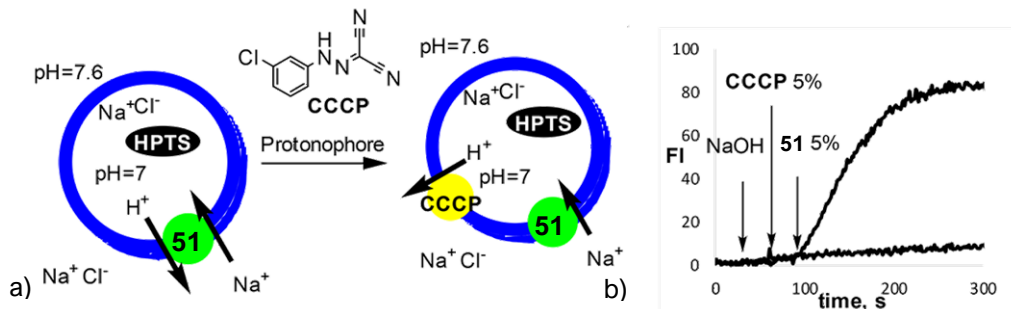
The high selectivity towards Na^+ was further validated by the slight negative emission in fluorescence in the presence of Rb^+ or Cs^+ . The decrease in fluorescence emission implies acidification of the inner water pool of the liposomes which is due to a high Na^+/M^+ selectivity in the transport. In this experiment, the liposomes are prepared in a buffer containing NaCl 100 mM and then diluted in the buffer containing 100 mM MCl. At the beginning of the experiment, when the base pulse is applied, the liposomes contain in the inner water pool Na^+ while outside the concentration of Na^+ is much lower and the concentration of MCl is high. If the ionophore is able to transport both cations this chemical gradient is easily removed by an antiport of the two cations (Scheme 2.4, a)). This process does not affect the pH of the inner water pool of the liposomes and, therefore, it is not signalled by the HPTS. However, if the ionophore is able to transport only Na^+ (high Na^+/M^+ selectivity) the chemical gradient starts a transport of Na^+ from inside to outside counterbalanced by an antiport of H^+ (facilitated by the protonophore CCCP, carbonyl cyanide 3-chlorophenylhydrazone) which results in the acidification of the inner water pool and a lower emission intensity of HPTS (Scheme 2.4, b)).



Scheme 2.4. a) The ionophore is able to transport both cations (low Na^+/M^+ selectivity); the internal pH and the fluorescence emission of HPTS are not affected. b) The ionophore is able to transport only Na^+ (high Na^+/M^+ selectivity) and the gradient is removed by an efflux of Na^+ promoted by **51** counterbalanced by an inverse H^+ flux facilitated by CCCP.

The second part of the study involved the determination of the transport mechanism; in fact, the inner vesicular pH change signalled by HPTS is both consistent with cation transport through an H^+/M^+ antiport or the kinetically equivalent M^+/OH^- symport.

In this case, the experiment was conducted in the presence of the protonophore as well. CCCP can transport H^+ in an electrogenic transport process in which $CCCPH^+$ crosses the membrane and, after delivering the proton, returns back as neutral compounds thus establishing a unidirectional charge flux. The kinetic profiles indicated a strong acceleration of the transport process induced by the protonophore. This proved an H^+/Na^+ antiport mechanism in which the slow step is the antiport of the proton by the ionophore due to high Na^+/H^+ selectivity. The addition of the protonophore decoupled the two processes thus allowing to fully estimate the efficiency of the cyclopeptoid in the Na^+ transport.



Scheme 2.5. a) Schematic representation of the HPTS assay in the presence of the CCCP protonophore. b) Normalized fluorescence change in HPTS emission as a function of time after addition of the base at 25s (50 μL of 0.5 M NaOH), the CCCP protonophore at 50s (5 μL 5.2 mM in DMSO) and the cyclic peptoid **51** at 90s to 95:5 EYPC/EYPG LUVs (100 nm diameter) loaded with

HPTS (0.1 mM HPTS, 0.17 mM total lipid concentration, 25 mM HEPES, 100 mM NaCl, pH 7.0, total volume 3 mL). The concentration of the ionophore is 5 mol % with respect to the total concentration of lipids.

Similar behaviour was observed for Li^+ , the other cation efficiently transported by **51**, without affecting the overall cation selectivity.

The addition of the protonophore did not exert any effect on the other compounds' activities, except for **52** (with all *N*-benzyl side-chains), although with lower efficiency. Similarly, the addition of CCCP increased the fluorescence emission while retaining the cation selectivity order.

Compound **50-52** showed very similar $\log K_{a1}$ values (Table 2.2) but only cyclohexapeptoid **51** exerted significant ionophoric activity; thus, the affinity for Na^+ is not determining the ion transport.

The evaluation of the logP (partition coefficient octanol/water) is reported in Table 2.3.

Compound	47	48	49	50	51	52
logP	2.06	2.64	3.49	2.91	4.02	4.87

Table 2.3. Octanol/water partition coefficients for compounds **47-52**.

There is a strict correlation between the ion affinity and the lipophilicity of the carrier, which is optimal for compound **51**. Carrier type ion transporters often exhibit a specific balance between the need to form a lipophilic complex able to cross the membrane and the need for the ionophore to approach the membrane/water interphase where the ion exchange process takes place.⁷⁵

Finally, to further validate the ion transport mechanism, a series of kinetic experiments at different concentrations of **51**, with or without the protonophore, were performed. Fitting the kinetic profiles, the first-order rate constants (k_i , s^{-1}) for the transport process, were plotted against the concentration of ionophore. In both cases, a linear dependence was observed and this suggested that the transport active species was monomeric (a 1:1 [**51**· Na]⁺ complex was formed). Hill analysis of the kinetic profiles was performed to obtain the EC_{50} ("effective" peptoid concentration needed to reach 50%

⁷⁵ Knight N. J., Hernando E., Haynes C. J. E., Busschaert N., Clarke H. J., Takimoto K., García-Valverde M., Frey J. G., Quesada R., Gale P. A., *Chem. Sci.* **2016**, *7*, 1600-1608.

activity).⁷⁶ EC₅₀ values for compounds **51** of 3.91% ± 0.26 and 1.69% ± 0.08 were obtained in the absence and presence of CCCP, respectively. These values correspond to a 6.65 μM and 2.88 μM ionophore concentrations. Interestingly, the Hill coefficient (n) increased from 1.04 ± 0.15 to 1.65 ± 0.12 on addition of CCCP confirming that **51** alone acts as a monomeric species, but suggesting some participation of complexes with a 2:1 ligand/metal ion stoichiometry to the transport process in the presence of the protonophore (Figure 2.28, a)).

Lastly, the same experiment adding cholesterol to the liposomes composition, ratio 66.5:3.5:30 PC/PG/cholesterol was performed. Cholesterol is known to rigidify the phospholipidic membrane and it is used to discriminate transport mechanisms; in a more rigid membrane environment, the activity of a mobile carrier should decrease while that of a channel system, which is incorporated in the membrane, should be unaffected.⁷⁷

Plotting again the first-order rate constants (k_t , s⁻¹) for the transport process, with or without cholesterol, against **51** mol% (Figure 2.28, b)), a significant decrease of activity associated with the presence of cholesterol was observed. Thus cyclopeptoid **51** transports Na⁺ with a mobile carrier mechanism which is further reinforced by the observation that the active species is essentially monomeric and by the dependence of the transport activity from the lipophilicity of the carrier.

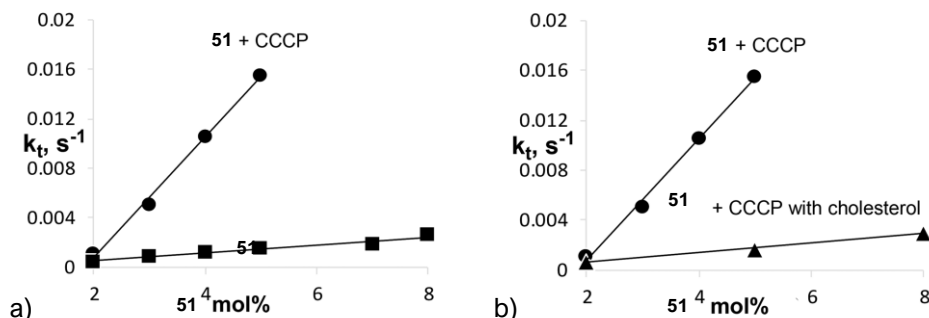


Figure 2.28. a) Dependence of k_t on the concentration of cyclopeptoid **51** in the absence (■) and in the presence of the CCCP protonophore (5%, ●) and b) dependence of k_t on the concentration of cyclopeptoid **51** in the presence of 5 mol % of CCCP with cholesterol (EYPC:PG:CHOL 66.5:3.5:30, ▲) and without cholesterol (PC:PG 95:5, ●).

⁷⁶ Adriaenssens L., Estarellas C., Jentzsch A. V., Belmonte M. M., Matile S., Ballester P., *J. Am. Chem. Soc.* **2013**, *135*, 8324-8330.

⁷⁷ a) Moore S. J., Haynes C. J. E., Gonzalez J., Sutton J. L., Brooks S. J., Light M. E., Herniman J., Langley G. J., Soto-Cerrato V., Pérez-Tomás R., Marques I., Costa P. J., Félix V., Gale P. A., *Chem. Sci.* **2013**, *4*, 103-117; b) Busschaert N., Karagiannidis L. E., Wenzel M., Haynes C. J. E., Wells N. J., Young P. G., Makuc D., Plavec J., Jolliffe K. A., Gale P. A., *Chem. Sci.* **2014**, *5*, 1118-1127.

As discussed before, enniatins cytotoxicity is mainly related to the perturbation of the cation gradient across the inner mitochondrial membrane.^{43a,c} Cyclopeptoid's ion transport mechanism suggested the evaluation of our molecules' cytotoxicity against cancer cells.

2.2.1.5 Cytotoxicity of cyclopeptoids **47-52** against human cancer cell lines

The anti-proliferative capability of our compounds was tested on two human cancer cell lines, PC-3, human metastatic prostate cancer, and A375, human melanoma. To validate the importance of the cyclization for the biological activity also the linear counterparts **58-62** and the known **64** (H-[NPhe]₆-OH) were assayed.

The cell lines were incubated for 72 h with increasing concentration of the compounds (2 μ M - 50 μ M) and cell viability was determined by MTT proliferation assay.⁷⁸ In the MTT assay, the 3-(4,5-dimethyl-2-thiazolyl)-2,5-diphenyl-2H-tetrazolium bromide is reduced by cell dehydrogenases and reducing agents, turning in the violet-blue formazan product (absorbance 562 nm with shoulders at 512 and 587 nm). After the cell incubation with the potential cytostatic/cytotoxic agent, the culture medium is removed, and the formazan deposit recovered and colorimetrically assessed.

No linear peptoid inhibited the cell viability, while four cyclic congeners (**49-52**) exerted a cytostatic effect with IC₅₀ in the μ M range with potencies 5 to 19 lower than the natural beauvericin, used as control in both cancer cell lines (Table 2.4).

Cyclopeptoid	PC-3 Prostate cell line (μ M)	A375 Melanoma cell line (μ M)
47	N. A. ^a	N. A.
48	N. A.	N. A.
49	25.4 \pm 1.5	22.7 \pm 1.2
50	28.4 \pm 2.1	30.1 \pm 2.3
51	9.5 \pm 0.8	8.3 \pm 1.1
52	21.0 \pm 1.2	19.1 \pm 1.6
Beauvericin (40)	1.5 \pm 0.2	1.6 \pm 0.1

^a N.A. not active

Table 2.4. IC₅₀ values of cyclic peptoids **47-52** and beauvericin (**40**) in human cancer cell lines after 72 h treatment.

⁷⁸ Stockert J. C., Horobin R. W., Colombo L. L., Blázquez-Castro A., *Acta Histochem.* **2018**, *120*, 159-167.

The strongest ionophore, **51**, proved to be also the strongest cytotoxic agent, with IC₅₀ values of 8.3 ± 1.1 and 9.5 ± 0.8 µM, respectively. We selected it to further investigate the inhibition mechanism, exploiting flow cytometry.

A375 and PC-3 cells were incubated for 72 h with compound **51** used at a concentration close to its IC₅₀ value and at higher doses (5, 10 and 20 µM) and analysed by flow cytometry. Beauvericin (**40**) was used in the same conditions with a concentration close to its IC₅₀ value as a reference. For cyclic peptoid **51**, in both cancer cell lines, we observed that the phase S significantly increased (between 7-18% in a dose-dependent manner), while the G₀/G₁ phase decreased, without any significant increase of hypodiploid SubG₁ cells, compared to the control cells (Figure 2.29). Beauvericin (**40**), tested in the same conditions, showed similar behaviour, as we detected a substantial increase of the S and G₂/M phase cell fraction, with a reduction of cells in G₀/G₁ phase respect to the control, in accordance with the data reported for the same compound on other cancer cell lines. Moreover, as reported in the literature, the treatment with beauvericin caused an increase of SubG₁ population indicative of apoptotic/necrotic cell death.⁷⁹

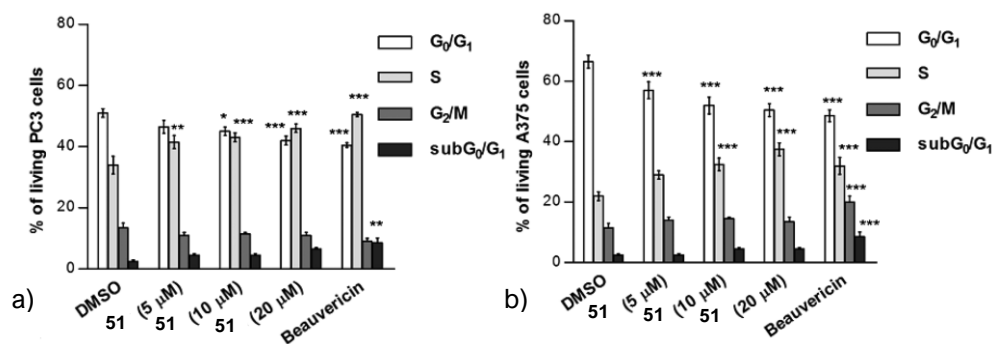


Figure 2.29. Effects of compound **51** and beauvericin (**40**) on cell cycle progression. Cell distribution in the different phases of the cell cycle was analysed by flow cytometry (a) PC-3 cells; b) A375 cells). PI stained viable PC-3 or A375 cells treated with DMSO; compound **51** (5, 10, 20 µM) or beauvericin (**40**) (2 µM) for 72 hours. Results are expressed as means ± SD of three experiments performed in triplicate (***P < 0.001, **P < 0.005, *P < 0.05).

2.2.2 Conclusions

In this study, we evaluated the capability of six cyclohexapeptoids (**47-52**) to act as enniatins and beauvericin analogues, mimicking their ability to transport alkali cations across lipid membrane, and exerting cytotoxic activity against human cancer cell lines.

⁷⁹ a) Prosperini A., Juan-García A., Font G., Ruiz M. J., *Toxicol. Lett.* **2013**, 222, 36-44; b) Lu C. L., Lin H. I., Chen B. F., Jow G. M., *J. Toxicol. Sci.* **2016**, 41, 429-437.

All compounds displayed good affinity for Na⁺ (log K_{a1} 3-5); among these, cyclopeptoid **51**, devoid of a natural direct counterpart, decorated with alternating *N*-isobutyl/*N*-benzyl moieties, exerted the strongest ionophoric activity, thanks to its optimal lipophilicity (logP 4.02), and strong cytotoxic activity, the highest reported for a cyclic peptoid so far in the literature (IC₅₀ in the μM range). Investigation of the mechanism revealed a clear correlation between sodium transport ability and cytotoxic activities on human cancer cell lines. The indication of a carrier H⁺/Na⁺ antiport mechanism suggested the mitochondrial metabolism as possible target (as demonstrated in the case of enniatins).

2.2.3 Experimental section

2.2.3.1 General methods

Starting materials and reagents purchased from commercial suppliers were generally used without purification unless otherwise mentioned. HPLC analyses were performed on a JASCO LC-NET II/ADC equipped with a JASCO Model PU-2089 Plus Pump and a JASCO MD-2010 Plus UV-Vis multiple wavelength detector set at 220 nm. The column used was a C₁₈ reversed-phase analytical column (Waters, Bondapak, 10 μm, 125 Å, 3.9 mm × 300 mm) run with linear gradients of ACN (0.1% TFA) into H₂O (0.1% TFA) over 30 min, at a flow rate of 1.0 mL/min for the analytical runs. ESI-MS analysis in positive ion mode was performed using a Finnigan LCQ Deca ion trap mass spectrometer (ThermoFinnigan, San José, CA, USA) and the mass spectra were acquired and processed using the Xcalibur software provided by Thermo Finnigan. Samples were dissolved in 1:1 CH₃OH/H₂O, 0.1 % formic acid, and infused in the ESI source by using a syringe pump; the flow rate was 5 μL/min. The capillary voltage was set at 4.0 V, the spray voltage at 5 kV, and the tube lens offset at -40 V. The capillary temperature was 220 °C. Data were acquired in MS1 and MS_n scanning modes. Zoom scan was used in these experiments. High-resolution mass spectra (HRMS) were recorded on a Bruker Solarix XR Fourier transform ion cyclotron resonance mass spectrometer (FTICR-MS) equipped with a 7T magnet, using electrospray ionization (ESI) or matrix assisted laser desorption ionization (MALDI). Yields refer to chromatographically and spectroscopically (¹H- and ¹³C-NMR) pure materials. NMR spectra were recorded on a Bruker DRX 600 (¹H at 600.13 MHz, ¹³C at 150.90 MHz), Bruker DRX 400 (¹H at 400.13 MHz, ¹³C at 100.03 MHz), Bruker DRX 300 (¹H at 300.13

MHz, ^{13}C at 75.03 MHz). Chemical shifts (δ) are reported in ppm relative to the residual solvent peak (CHCl_3 , $\delta = 7.26$; $^{13}\text{CDCl}_3$, $\delta = 77.00$; $\text{C}_2\text{D}_2\text{HCl}_4$, TCDE, $\delta = 5.80$, CDH_2CN , $\delta = 1.94$; $^{13}\text{CD}_3\text{CN}$ $\delta = 1.39$) and the multiplicity of each signal is designated by the following abbreviations: s, singlet; d, doublet; dd, double doublet; t, triplet; sept, septet; m, multiplet; br, broad. 2D NMR experiments such as COSY, ROESY, HSQC and HMBC were performed for the full assignment of each signal. Coupling constants (J) are quoted in Hertz.

DFT calculations were performed by prof. C. Costabile, Dpt. of Chemistry and Biology "A. Zambelli", Univ. of Salerno.

X-ray analyses were performed by PhD student G. Pierrri and prof. C. Tedesco, Dpt. of Chemistry and Biology "A. Zambelli", Univ. of Salerno.

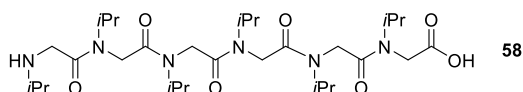
Ionophoric assays were performed by prof. P. Tecilla research group, Dpt. of Chemical and Pharmaceutical Sciences, Univ. of Trieste.

Cytotoxicity assays were performed by prof. I. Bruno research group, Dpt. of Pharmaceutical Sciences, Univ. of Salerno.

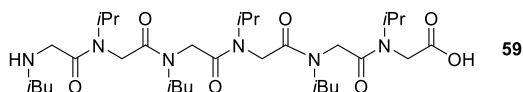
2.2.3.2 General methods for the sub-monomeric solid-phase oligomerization. Synthesis of the linear peptoids 58-62

The 2-chlorotriyl chloride resin (α -dichlorobenzhydryl-polystyrene cross-linked with 1% DVB; 100-200 mesh; 1.63 mmol g^{-1} , 0.400 g, 0.652 mmol) was swelled in dry CH_2Cl_2 (4 mL) for 45 min and washed twice with dry CH_2Cl_2 (4 mL). The first sub-monomer was attached onto the resin by adding bromoacetic acid (0.136 g, 0.978 mmol) in dry CH_2Cl_2 (4 mL) and DIPEA (567 μL , 3.26 mmol) on a shaker platform for 60 min at room temperature, followed by washing with CH_2Cl_2 (3×1 min) and then again with DMF (3×1 min). A solution of the chosen amine (1.6 M in dry DMF, 4 mL) was added to the bromoacetylated resin. The mixture was left on a shaker platform for 40 min at room temperature, then the resin was washed with DMF (3×1 min), DCM (3×1 min) and then again with DMF (3×1 min). Subsequent bromoacetylation reactions were accomplished by reacting the aminated oligomer with a solution of bromoacetic acid (0.910 g, 6.52 mmol) and DIC (1.11 mL, 7.17 mmol) in dry DMF (4 mL) for 60 min at room temperature. The filtrated resin was washed with DMF (4×1 min), DCM (4×1 min), DMF (4×1 min) and treated again with the proper amine under the same conditions reported above. The completion of the acylation reactions was verified by means of the chloranil test. This cycle

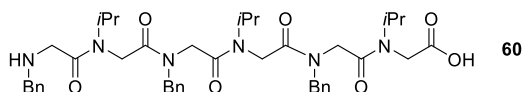
of reactions was iterated until the target linear oligomer was obtained. The cleavage was performed treating the resin, previously washed with DCM (6×1 min), three times with a solution of HFIP in dry CH_2Cl_2 (20% v/v, 4.0 mL each time) on a shaker platform at room temperature for 30 min each time. The resin was then filtered away and the combined filtrates were concentrated *in vacuo*. 1 mg of the final products were dissolved in 60 μL of acetonitrile (0.1% TFA) and 60 μL of HPLC grade water (0.1% TFA) and analysed by RP-HPLC, evaluating their purity; conditions: 5 \rightarrow 100% A in 30 min for the all oligomers (A, 0.1% TFA in acetonitrile, B, 0.1% TFA in water); flow: 1.0 mL min^{-1} , 220 nm; purity >95%. The linear oligomers (isolated as amorphous solids) were subjected to ES-MS or HRMS mass spectrometry and, subsequently, to the cyclization reactions without further purification.



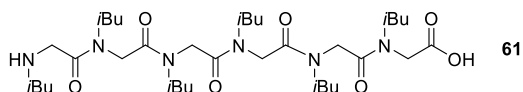
H-[NVal]₆-OH (**58**): white amorphous solid, 0.495 g, 100%; t_R : 9.6 min. ES-MS m/z ; 613.0 [M + H]⁺. HRMS (ESI/FTICR) m/z ; [M + H]⁺ Calcd for $\text{C}_{30}\text{H}_{57}\text{N}_6\text{O}_7^+$ 613.4283; Found 613.4289.



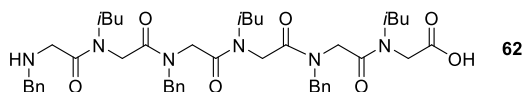
H-[NLeu-NVal]₃-OH (**59**): white amorphous solid, 0.392 g, 92%; t_R : 9.9 min. ES-MS m/z ; 655.1 [M + H]⁺. HRMS (ESI/FTICR) m/z ; [M + H]⁺ Calcd for $\text{C}_{33}\text{H}_{63}\text{N}_6\text{O}_7^+$ 655.4753; Found 655.4741.



H-[NPhe-NVal]₃-OH (**60**): white amorphous solid, 0.430 g, 87%; t_R : 10.0 min. ES-MS m/z ; 757.2 [M + H]⁺. HRMS (ESI/FTICR) m/z ; [M + H]⁺ Calcd for $\text{C}_{42}\text{H}_{57}\text{N}_6\text{O}_7^+$ 757.4283; Found 757.4278.



H-[NLeu]₆-OH (**61**): white amorphous solid, 0.343 g, 76%; t_R : 10.1 min. ES-MS m/z ; 697.0 [M + H]⁺. HRMS (ESI/FTICR) m/z ; [M + H]⁺ Calcd for $\text{C}_{36}\text{H}_{69}\text{N}_6\text{O}_7^+$ 697.5222; Found 697.5211.



H-[N(Phe-NLeu)₃]-OH (**62**): white amorphous solid, 0.406 g, 78%; t_R : 10.8 min. ES-MS m/z ; 799.0 [M + H]⁺. HRMS (ESI/FTICR) m/z ; [M + H]⁺ Calcd for C₄₅H₆₃N₆O₇⁺ 799.4753; Found 799.4749.

2.2.3.3 General methods for the head-to-tail cyclization reaction. Synthesis of the cyclic peptoids **47-51**

The solutions of the linear peptoids (0.150 mmol), previously co-evaporated three times with toluene, were prepared under nitrogen in dry CH₂Cl₂ (5.00 mL). The mixture was added dropwise to a stirred solution of HATU (0.171 g, 0.450 mmol) and DIPEA (105 μL, 0.600 mmol) in dry DMF (45.0 mL) by a syringe pump in 6 h, at room temperature in anhydrous atmosphere. After 12 h the resulting mixture was concentrated *in vacuo*, diluted with CH₂Cl₂ (30.0 mL), washed twice with a solution of HCl (1.0 M, 15.0 mL). The organic phase was washed with water (30.0 mL), dried over anhydrous MgSO₄, filtered and concentrated *in vacuo*. The crude cyclic peptoids were dissolved in 50% acetonitrile in HPLC grade water and analysed by RP-HPLC evaluating their purity; conditions: 5% – 100% A in 30 min (A, 0.1% TFA in acetonitrile, B, 0.1% TFA in water); flow: 1 mL min⁻¹, 220 nm; purity >95%.

The crude cyclic peptoids **47**, **49-51** were dissolved in hot acetonitrile and precipitated by slowly cooling the acetonitrile solutions. The crude **48** was purified on reverse silica gel (C₁₈); conditions: 10% – 100% A (A: acetonitrile; B: water).

cyclo-[NVal]₆ (**47**): white amorphous solid, 0.0320 g, 36%; t_R : 10.7 min. ¹H-NMR: (600 MHz, CDCl₃, mixture of rotamers) δ: 4.91-3.18 (18H, overlapping, O=C-CH₂-N, -CH(CH₃)₂), 1.47-0.93 (36H, overlapping, -CH(CH₃)₂). ¹³C-NMR: (150 MHz, CDCl₃, mixture of rotamers) δ: 171.0, 170.6, 170.1, 169.4, 169.0, 168.3, 167.4, 167.3, 48.5, 48.0, 47.8, 46.1, 45.9, 45.5, 45.4, 44.8, 44.0, 43.5, 43.4, 43.3, 43.2, 43.1, 42.5, 21.8, 21.6, 21.5, 21.2, 20.9, 20.6, 20.4, 20.3, 19.9, 19.5, 19.4, 19.1. ES-MS m/z : 595.1 (100, [M + H]⁺); 617.2 (95, [M + Na]⁺). HRMS (ESI/FTICR) m/z ; [M + H]⁺ Calcd for C₃₀H₅₅N₆O₆⁺ 595.4178; Found 595.4178.

cyclo-[NVal-NLeu]₃ (**48**): white amorphous solid, 0.0620 g, 65%; t_R : 11.4 min. ¹H-NMR: (600 MHz, CDCl₃, mixture of rotamers) δ: 4.81-2.85 (21H, overlapping, br signals, O=C-CH₂-N, N-CH(CH₃)₂, -CH₂-CH(CH₃)₂), 2.12-1.82 (3H, overlapping, br signals, -CH₂-CH(CH₃)₂), 1.43-0.97 (36H, overlapping, br signals, -CH(CH₃)₂), -CH₂-CH(CH₃)₂. ¹³C-NMR: (150 MHz,

CDCl₃, mixture of rotamers) δ : 171.8, 171.5, 171.0, 170.2, 169.7, 169.4, 169.0, 168.6, 168.0, 167.6, 167.3, 166.9, 57.2, 57.0, 56.8, 56.4, 56.1, 55.8, 52.1, 49.8, 49.5, 49.3, 48.5, 48.2, 48.0, 47.8, 47.6, 45.9, 45.7, 45.1, 44.4, 43.1, 42.8, 28.0, 27.3, 27.1, 21.2, 20.1, 19.5, 19.3. ES-MS m/z ; 637.4 (45 [M + H]⁺); 659.3 (100 [M + Na]⁺). HRMS (ESI/FTICR) m/z ; [M + H]⁺ Calcd for C₃₃H₆₁N₆O₆⁺ 637.4647; Found 637.4661.

cyclo-[*cis*-NVal¹-*cis*-NPhe¹-*trans*-NVal²-*cis*-NPhe²-*cis*-NVal³-*trans*-NPhe³] (**49a**): white amorphous solid, 0.0500 g, 45%; t_R : 11.5 min. NMR data are reported in Table 2.1. ES-MS m/z ; 761.4 (100 [M + H + Na]⁺); 739.2 (10 [M + H]⁺). HRMS (ESI/FTICR) m/z ; [M + H]⁺ Calcd for C₄₂H₅₅N₆O₆⁺ 739.4178; Found 739.4178.

cyclo-[NLeu]₆ (**50**): white amorphous solid, 0.0610 g, 60%; t_R : 10.9 min. ¹H-NMR: (600 MHz, CDCl₃, mixture of rotamers) δ : 4.68-3.08 (24H, overlapping, br signals, O=C-CH₂-N, -CH₂-CH(CH₃)₂), 2.15-1.79 (6H, overlapping, br signals, -CH₂-CH(CH₃)₂), 0.99-0.86 (36H, overlapping, br signals, -CH(CH₃)₂). ¹³C-NMR: (150 MHz, CDCl₃, mixture of rotamers) δ : 171.4, 170.9, 170.5, 169.9, 169.7, 169.5, 168.9, 168.8, 168.6, 168.5, 168.0, 167.5, 57.1, 57.0, 56.7, 56.6, 56.3, 56.0, 55.9, 55.5, 55.2, 53.5, 51.7, 49.9, 49.6, 49.5, 49.2, 49.1, 49.0, 48.6, 48.1, 46.4, 28.2, 28.1, 28.0, 27.7, 27.5, 27.3, 27.2, 27.1, 27.0, 26.5, 20.2, 20.0. ES-MS m/z ; 679.3 (90 [M + H]⁺); 701.2 (100 [M + Na]⁺). HRMS (ESI/FTICR) m/z ; [M + H]⁺ Calcd for C₃₆H₆₇N₆O₆⁺ 679.5117; Found 679.5102.

cyclo-[NPhe-NLeu]₃ (**51**): white amorphous solid, 0.0560 g, 48%; t_R : 12.8 min. ¹H-NMR: (600 MHz, CDCl₃, mixture of rotamers) δ : 7.57-7.03 (15H, overlapping, br signals, Ar-H), 5.51-2.84 (24H, overlapping, br signals, O=C-CH₂-N, CH₂-Ph, -CH₂-CH(CH₃)₂), 2.16-1.71 (3H, overlapping, br signals, -CH₂-CH(CH₃)₂), 0.95-0.92 (18H, overlapping, br signals, -CH(CH₃)₂). ¹³C-NMR: (150 MHz, CDCl₃, mixture of rotamers) δ : 171.8, 171.5, 170.3, 169.6, 169.5, 168.5, 167.5, 137.0, 136.6, 135.3, 129.1, 128.8, 128.7, 128.4, 128.0, 127.8, 127.7, 127.4, 127.2, 126.9, 125.5, 56.7, 56.5, 56.1, 52.8, 51.7, 51.6, 51.5, 50.8, 50.3, 49.8, 49.5, 49.2, 48.7, 47.6, 27.6, 27.3, 20.1, 20.0. ES-MS m/z ; 781.1 (10 [M + H]⁺); 803.1 (100 [M + Na]⁺). HRMS (ESI/FTICR) m/z ; [M + H]⁺ Calcd for C₄₅H₆₁N₆O₆⁺ 781.4647; Found 781.4653.

2.2.3.4 General procedure for the monometallic complexes formation and evaluation of the apparent K_{a1} . Preparation of the complexes [47-52·Na]⁺TFPB⁻

Titration. To 1.0-10.0 mM (depending on the solubility) solutions of cyclic peptoids in CDCl₃ (0.5 mL), were added increasing amounts of sodium tetrakis[3,5-bis(trifluoromethyl)phenyl]borate (NaTFPB) till 1.0 equivalent. After any addition, the

mixtures were sonicated for 5 minutes and the NMR spectra were recorded.

K_{a1} evaluation. To a solution of cyclic peptoids CDCl₃ (0.50 mL, 3.0 mM) 1.0 equivalent of NaTFPB was added. After the addition, the mixture was sonicated for 5 minutes (25 °C). The H·G complex concentration, at the equilibrium – [H·G]_{eq} – was evaluated by integration of the ¹H-NMR complex signals (2.5-6.5 range) versus the total integration of the free host plus complexed molecules at 298 K. With the addition of 1 equivalent of guest, the equilibrium (2.1) is established:



Equation (2.2) was used to obtain the concentration of the [H·G]_{eq} species.

$$[H \cdot G]_{eq} = \frac{F_a}{F_b} \times [C]_i \quad (2.2)$$

Where F_a and F_b are the areas of the signals of the host/guest adduct and host plus host/guest adduct, respectively (recorded in the 2.5-6.5 range); [C]_i is the host initial concentration (3.0 mM).

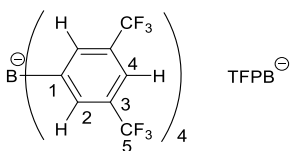
In the case of the formation of a monosodium complex, the evaluation of the concentration of the species, at the equilibrium, follows the relation (2.3):

$$[H]_{eq} = [G]_{eq} = [H]_i - [H \cdot G]_{eq} \quad (2.3)$$

The apparent K_{a1}, was calculated following (2.4):

$$K_{a1} = \frac{[H \cdot G]_{eq}}{[H]_{eq} \times [G]_{eq}} \quad (2.4)$$

In order to have reliable integration values, the delay times (D1) among successive scans, in the ¹H-NMR, were set at 5 seconds.



[⁴⁷Na]⁺TFPB[−]: white amorphous solid. ¹H-NMR (600 MHz, CDCl₃) δ: 7.70 (8H, s, TFPB-*o*-H), 7.53 (4H, s, TFPB-*p*-H), 4.51 (6H, d, *J* 17.2 Hz, O=C-CHH-N), 4.06 (6H, ept, *J* 6.4 Hz, -CH(CH₃)₂), 3.66 (6H, d, *J* 17.2 Hz, O=C-CHH-N), 1.20 (18 H, d, *J* 6.4 Hz, -CH(CH₃)(CH₃)), 1.18 (18 H, d, *J* 6.4 Hz, -CH(CH₃)(CH₃)). ¹³C-NMR: (150 MHz, CDCl₃:CD₃CN 4:1, the CD₃CN was added to avoid precipitation of the salt) δ: 169.1 (C=O), 161.6 (q, *J* 50 Hz, C-1), 134.8 (C-2), 128.8 (q, *J* 30 Hz C-3), 124.6 (q, *J* 270 Hz, C-5), 117.4 (C-4), 48.0 (O=C-CH₂-N), 42.9 (-CH(CH₃)₂), 21.6 (-CH₃), 20.0 (-CH₃). ES-MS *m/z*; 617.3 [M + Na]⁺.

[48Na]⁺TFPB: white amorphous solid. ¹H-NMR (600 MHz, CDCl₃) δ: 7.70 (8H, s, TFPB-*o*-H), 7.52 (4H, s, TFPB-*p*-H), 4.74 (3H, d, *J* 16.2 Hz, O=C-CHH-N-*i*Bu), 4.51 (3H, d, *J* 16.1 Hz, O=C-CHH-N-*i*Pr), 3.98 (3H, ept, *J* 6.3 Hz, -CH(CH₃)₂), 3.61 (3H, d, *J* 16.1 Hz, O=C-CHH-N-*i*Pr), 3.54 (3H, d, *J* 16.2 Hz, O=C-CHH-N-*i*Bu), 3.26 (3H, dd, *J* 14.0 and 7.0 Hz, -CHH-CH(CH₃)₂), 3.01 (3H, dd, *J* 14.0 and 7.0 Hz, -CHH-CH(CH₃)₂), 1.84 (3H, m, -CH₂-CH(CH₃)₂), 1.19 (9H, d, *J* 6.3 Hz, -CH(CH₃)(CH₃)), 1.16 (9H, d, *J* 6.3 Hz, -CH(CH₃)(CH₃)), 1.01 (9H, d, *J* 6.7 Hz, -CH₂-CH(CH₃)(CH₃)), 0.90 (9H, d, *J* 6.7 Hz, -CH₂-CH(CH₃)(CH₃)). ¹³C-NMR: (150 MHz, CDCl₃) δ: 168.9 (C=O), 167.0 (C=O), 161.1 (q, *J* 50 Hz, C-1), 134.2 (C-2), 128.3 (q, *J* 30 Hz C-3), 124.0 (q, *J* 270 Hz, C-5), 117.0 (C-4), 56.2 (-CH₂-CH(CH₃)₂), 48.9 (O=C-CH₂-N), 47.6 (O=C-CH₂-N), 42.1 (N-CH(CH₃)₂), 27.2 (-CH₂-CH(CH₃)₂), 20.6 (-CH₃), 19.4 (-CH₃), 19.3 (-CH₃), 19.2 (-CH₃). ES-MS *m/z*; 659.4 [M + Na]⁺.

[49Na]⁺TFPB: white amorphous solid. ¹H-NMR (600 MHz, CDCl₃) δ: 7.70 (8H, s, TFPB-*o*-H), 7.50 (4H, s, TFPB-*p*-H), 7.40 (6H, t, *J* 7.0 Hz, Ar-*m*-H), 7.36 (3H, t, *J* 7.0 Hz, Ar-*p*-H), 7.22 (6H, d, *J* 7.0 Hz, Ar-*o*-H), 4.88 (3H, d, *J* 16.0 Hz, N-CHH-Ph), 4.77 (3H, d, *J* 17.0 Hz, O=C-CHH-N-Bn), 4.65 (3H, d, *J* 17.0 Hz, O=C-CHH-N-*i*Pr), 4.39 (3H, d, *J* 16.0 Hz, N-CHH-Ph), 3.89 (3H, ept, *J* 6.3 Hz, -CH(CH₃)₂), 3.60 (3H, d, *J* 17.0 Hz, O=C-CHH-N-*i*Pr), 3.57 (3H, d, *J* 17.0 Hz, O=C-CHH-N-Bn), 1.15 (9H, d, *J* 6.3 Hz, -CH(CH₃)(CH₃)), 1.05 (9H, d, *J* 6.3 Hz, -CH(CH₃)(CH₃)). ¹³C-NMR: (150 MHz, CDCl₃) δ: 171.5 (C=O), 168.4 (C=O), 161.7 (q, *J* 50 Hz, C-1), 134.8 (CH-Ph), 134.6 (C-2), 129.4 (CH-Ph), 128.9 (q, *J* 30 Hz C-3), 128.7 (CH-Ph), 126.9 (CH-Ph), 124.6 (q, *J* 270 Hz, C-5), 117.4 (C-4), 53.1 (CH₂- Benzyl), 48.9 (O=C-CH₂-N), 48.1 (O=C-CH₂-N), 43.1 (-CH(CH₃)₂), 21.3 (-CH₃), 20.0 (-CH₃). ES-MS *m/z*; 761.3 [M + Na]⁺.

[50Na]⁺TFPB: white amorphous solid. ¹H-NMR (600 MHz, CDCl₃) δ: 7.70 (8H, s, TFPB-*o*-H), 7.52 (4H, s, TFPB-*p*-H), 4.75 (6H, d, *J* 17.2 Hz, O=C-CHH-N-*i*Bu), 3.50 (6H, d, *J* 17.2 Hz, O=C-CHH-N-*i*Bu), 3.18 (6H, dd, *J* 14.0 and 6.0 Hz, -CHH-CH(CH₃)₂), 3.02 (6H, dd, *J* 14.0 and 6.0 Hz, -CHH-CH(CH₃)₂), 1.83 (6H, m, -CH₂-CH(CH₃)₂), 1.00 (18H, d, *J* 6.4 Hz, -CH₂-CH(CH₃)(CH₃)), 0.92 (18H, d, *J* 6.4 Hz, -CH₂-CH(CH₃)(CH₃)). ¹³C-NMR: (150 MHz, CDCl₃) δ: 170.2 (C=O), 161.7 (q, *J* 50 Hz, C-1), 134.8 (C-2), 128.8 (q, *J* 30 Hz C-3), 124.6 (q, *J* 270 Hz, C-5), 117.4 (C-4), 57.0 (-CH₂-CH(CH₃)₂), 49.9 (O=C-CH₂-N), 27.9 (-CH₂-CH(CH₃)₂), 20.2 (-CH₃), 20.0 (-CH₃). ES-MS *m/z*; 701.2 [M + Na]⁺.

[51Na]⁺TFPB: white amorphous solid. ¹H-NMR (600 MHz, CDCl₃) δ: 7.71 (8H, s, TFPB-*o*-H), 7.51 (4H, s, TFPB-*p*-H), 7.38 (6H, t, *J* 7.0 Hz, Ar-*m*-H), 7.34 (3H, t, *J* 7.0 Hz, Ar-*p*-H), 7.22 (6H, d, *J* 7.0 Hz, Ar-*o*-H), 4.91 (3H, d, *J* 17.0 Hz, N-CHH-Ph), 4.80 (3H, d, *J* 17.4 Hz,

O=C-CHH-N-Bn), 4.74 (3H, d, J 17.4 Hz, O=C-CHH-N-*i*Bu), 4.39 (3H, d, J 17.0 Hz, N-CHH-Ph), 3.53 (3H, d, J 17.4 Hz, O=C-CHH-N-*i*Bu), 3.50 (3H, d, J 17.4 Hz, O=C-N-CHH-N-Bn), 3.05 (3H, dd, J 14.0 and 6.0 Hz, -CHH-CH(CH₃)₂), 2.98 (3H, dd, J 14.0 and 6.0 Hz, -CHH-CH(CH₃)₂), 1.72 (3H, m, -CH₂-CH(CH₃)₂), 0.95 (9H, d, J 6.0 Hz, -CH₂-CH(CH₃)(CH₃)), 0.77 (9H, d, J 6.0 Hz, -CH₂-CH(CH₃)(CH₃)). ¹³C-NMR: (150 MHz, CDCl₃) δ: 171.1 (C=O), 169.9 (C=O), 161.7 (q, J 50 Hz, C-1), 134.8 (C-2), 134.1 (C-Ph), 129.4 (CH-Ph), 128.9 (q, J 30 Hz C-3), 128.8 (CH-Ph), 127.4 (CH-Ph), 124.6 (q, J 270 Hz, C-5), 117.4 (C-4), 56.7 (-CH₂-CH(CH₃)₂), 52.9 (CH₂- Benzyl), 49.9 (O=C-CH₂-N), 49.2 (O=C-CH₂-N), 27.8 (-CH₂-CH(CH₃)₂), 20.0 (-CH₃), 19.8 (-CH₃). ES-MS m/z ; 803.1 [M + Na]⁺.

[52Na]⁺TFPB⁻: white amorphous solid. ¹H-NMR (600 MHz, CDCl₃) δ: 7.71 (8H, s, TFPB-*o*-H), 7.50 (4H, s, TFPB-*p*-H), 7.40 (18H, m, Ar-*m*-H and Ar-*p*-H), 7.09 (12H, d, J 7.0 Hz, Ar-*o*-H), 4.86 (6H, d, J 17.3 Hz, O=C-CHH-), 4.65 (6H, d, J 16.2 Hz, N-CHH-Ph), 4.35 (6H, d, J 16.2 Hz, N-CHH-Ph), 3.53 (6H, d, J 17.3 Hz, O=C-CHH-). ¹³C-NMR: (150 MHz, CDCl₃) δ: 169.4 (C=O), 161.7 (q, J 50 Hz, C-1), 134.8 (C-2), 132.9 (C-Ph), 129.6 (CH-Ph), 128.9 (q, J 30 Hz C-3), 128.8 (CH-Ph), 128.3 (q, J 270 Hz, C-5), 125.4 (CH-Ph), 117.6 (C-4), 53.0 (CH₂- Benzyl), 49.0 (O=C-CH₂-N). ES-MS m/z ; 906.3 [M + Na]⁺.

2.2.3.5 General procedure for the bimetallic complexes formation. Preparation of the complexes [48-52·2Na]²⁺2TFPB⁻

Titration. To 1.0 mM solutions of cyclic peptoids in CDCl₃ (0.50 mL), were added increasing amounts of sodium tetrakis[3,5-bis(trifluoromethyl)phenyl]borate (NaTFPB) till 2.0 equivalents. After any addition, the mixtures were sonicated for 5 minutes and the NMR spectra were recorded.

Only in the case of the cyclic peptoid **47** we obtained the same spectrum reported for [47Na]⁺TFPB⁻ (there was no appreciable formation of the bimetallic complex). The low solubility of [48-50, 52·2Na]²⁺2TFPB⁻ hampered the acquisition of their ¹³C-NMR spectra.

[48·2Na]²⁺2TFPB⁻: white amorphous solid. ¹H-NMR (600 MHz, CDCl₃) δ: 7.55 (16H, s, TFPB-*o*-H), 7.43 (8H, s, TFPB-*p*-H), 4.49 (3H, d, J 16.7 Hz, O=C-CHH-N-*i*Bu), 4.28 (3H, d, J 16.6 Hz, O=C-CHH-N-*i*Pr), 3.93 (3H, ept, J 6.3 Hz, -CH(CH₃)₂), 3.54 (3H, d, J 16.6 Hz, O=C-CHH-N-*i*Pr), 3.53 (3H, d, J 16.7 Hz, O=C-CHH-N-*i*Bu), 3.14 (3H, dd, J 14.3 and 6.2 Hz, -CHH-CH(CH₃)₂), 2.93 (3H, dd, J 14.3 and 6.0 Hz, -CHH-CH(CH₃)₂), 1.78 (3H, m, -CH₂-CH(CH₃)₂), 1.08 (9H, d, J 6.3 Hz, -CH(CH₃)(CH₃)), 1.02 (9H, d, J 6.3 Hz, -CH(CH₃)(CH₃)),

0.88 (9H, d, J 6.2 Hz, $-\text{CH}_2\text{-CH}(\text{CH}_3)(\text{CH}_3)$), 0.82 (9H, d, J 6.2 Hz, $-\text{CH}_2\text{-CH}(\text{CH}_3)(\text{CH}_3)$). ES-MS m/z ; 341.1 (100 $[\text{M} + 2\text{Na}]^{2+}$); 658.9 (70 $[\text{M} + \text{Na}]^+$).

[49 $2\text{Na}]^{2+}2\text{TFPB}$: white amorphous solid. $^1\text{H-NMR}$ (600 MHz, CDCl_3) δ : 7.69 (16H, s, TFPB-*o-H*), 7.52 (8H, s, TFPB-*p-H*), 7.40 (9H, m, Ar-*m-H* and Ar-*p-H*), 7.10 (6H, d, J 7.1 Hz, Ar-*o-H*), 4.79 (3H, d, J 16.4 Hz, N-*CHH-Ph*), 4.65 (3H, d, J 17.2 Hz, O=C-*CHH-N-Bn*), 4.45 (3H, d, J 17.4 Hz, O=C-*CHH-N-iPr*), 4.28 (3H, d, J 16.4 Hz, N-*CHH-Ph*), 3.87 (3H, ept, J 6.1 Hz, $-\text{CH}(\text{CH}_3)_2$), 3.61 (3H, d, J 17.4 Hz, O=C-*CHH-N-iPr*), 3.59 (3H, d, J 17.2 Hz, O=C-*CHH-N-Bn*), 1.06 (9H, d, J 6.1 Hz, $-\text{CH}(\text{CH}_3)(\text{CH}_3)$), 0.97 (9H, d, J 6.1 Hz, $-\text{CH}(\text{CH}_3)(\text{CH}_3)$). ES-MS m/z ; 392.1 (100 $[\text{M} + 2\text{Na}]^{2+}$); 761.1 (20 $[\text{M} + \text{Na}]^+$).

[50 $2\text{Na}]^{2+}2\text{TFPB}$: white amorphous solid. $^1\text{H-NMR}$ (600 MHz, CDCl_3) δ : 7.68 (16H, s, TFPB-*o-H*), 7.53 (8H, s, TFPB-*p-H*), 4.58 (6H, d, J 16.7 Hz, O=C-*CHH-N-iBu*), 3.50 (6H, d, J 16.7 Hz, O=C-*CHH-N-iBu*), 3.14 (6H, dd, J 14.7 and 6.2 Hz, $-\text{CHH-CH}(\text{CH}_3)_2$), 2.94 (6H, dd, J 14.7 and 6.5 Hz, $-\text{CHH-CH}(\text{CH}_3)_2$), 1.76 (6H, m, $-\text{CH}_2\text{-CH}(\text{CH}_3)_2$), 0.92 (18H, d, J 6.0 Hz, $-\text{CH}_2\text{-CH}(\text{CH}_3)(\text{CH}_3)$), 0.89 (18H, d, J 6.0 Hz, $-\text{CH}_2\text{-CH}(\text{CH}_3)(\text{CH}_3)$). ES-MS m/z ; 362.2 (100 $[\text{M} + 2\text{Na}]^{2+}$); 701.6 (10 $[\text{M} + \text{Na}]^+$).

[51 $2\text{Na}]^{2+}2\text{TFPB}$: white amorphous solid. $^1\text{H-NMR}$ (600 MHz, CDCl_3) δ : 7.69 (16H, s, TFPB-*o-H*), 7.51 (8H, s, TFPB-*p-H*), 7.35 (9H, bs, Ar-*m-H* and Ar-*p-H*), 7.10 (6H, bs, Ar-*o-H*), 4.73 (3H, overlapping, br signals, N-*CHH-Ph*), 4.72 (3H, overlapping, br signals, O=C-*CHH-N-Bn*), 4.61 (3H, d, J 17.3 Hz, O=C-*CHH-N-iBu*), 4.28 (3H, d, J 17.0 Hz, N-*CHH-Ph*), 3.54 (3H, d, J 17.3 Hz, O=C-*CHH-N-iBu*), 3.51 (3H, d, J 17.0 Hz, N-*CHH-N-Bn*), 3.04 (3H, dd, J 14.1 and 6.1 Hz, $-\text{CHH-CH}(\text{CH}_3)_2$), 2.91 (3H, dd, J 14.1 and 6.3 Hz, $-\text{CHH-CH}(\text{CH}_3)_2$), 1.69 (3H, m, $-\text{CH}_2\text{-CH}(\text{CH}_3)_2$), 0.84 (9H, bs, $-\text{CH}_2\text{-CH}(\text{CH}_3)(\text{CH}_3)$), 0.73 (9H, d, J 6.1 Hz, $-\text{CH}_2\text{-CH}(\text{CH}_3)(\text{CH}_3)$). $^{13}\text{C-NMR}$: (150 MHz, CDCl_3) δ : 169.4 (C=O), 168.9 (C=O), 161.7 (q, J 50 Hz, C-1), 134.8 (C-2), 133.5 (C-Ph), 129.6 (CH-Ph), 128.7 (q, J 30 Hz C-3), 128.5 (CH-Ph), 127.3 (CH-Ph), 124.6 (q, J 270 Hz, C-5), 117.5 (C-4), 56.8 ($-\text{CH}_2\text{-CH}(\text{CH}_3)_2$), 53.1 (CH₂- Benzyl), 49.3 (O=C-CH₂-N), 48.9 (O=C-CH₂-N), 27.7 ($-\text{CH}_2\text{-CH}(\text{CH}_3)_2$), 19.7 ($-\text{CH}_3$), 19.4 ($-\text{CH}_3$). ES-MS m/z ; 413.5 (100 $[\text{M} + 2\text{Na}]^{2+}$); 803.0 (20 $[\text{M} + \text{Na}]^+$).

[52 $2\text{Na}]^{2+}2\text{TFPB}$: white amorphous solid. $^1\text{H-NMR}$ (600 MHz, CDCl_3) δ : 7.72 (16H, s, TFPB-*o-H*), 7.52 (8H, s, TFPB-*p-H*), 7.30 (18H, m, Ar-*m-H* and Ar-*p-H*), 6.96 (12H, d, J 7.3 Hz, Ar-*o-H*), 4.72 (6H, d, J 17.2 Hz, O=C-*CHH-*), 4.61 (6H, d, J 16.4 Hz, N-*CHH-Ph*), 4.22 (6H, d, J 16.4 Hz, N-*CHH-Ph*), 3.57 (6H, d, J 17.2 Hz, O=C-*CHH-*). ES-MS m/z : 464.7 (100 $[\text{M} + 2\text{Na}]^{2+}$); 906.1 (10 $[\text{M} + \text{Na}]^+$).

2.2.3.6 Procedure for the evaluation of the apparent K_{a2} in $[51\cdot 2Na]^{2+}2TFPB^-$

The apparent K_{a2} in $[51\cdot 2Na]^{2+}2[TFPB]^-$ was evaluated in the following way: to 1.0 mM solutions of $[51\cdot Na]^+$ in $CDCl_3$ were added proper amounts of NaTFPB (0.2 equivalent at a time till 2.0 equivalents and then 0.5 equivalents till 3.0 equivalents). After every addition, the mixture was sonicated for 5 minutes in a heated bath (35 °C). The 1H -NMR spectra were then acquired at 298 K. The apparent K_{a2} was evaluated observing the variation of the chemical shift of the doublet initially at 4.39 ppm, gradually downshifted due to the formation of the bimetallic complex. The data were analysed by a nonlinear regression analysis using the program WinEQNMR.

2.2.3.7 General procedure for the 1H -NMR VT (variable temperature) experiments and ΔG^\ddagger evaluation

The cyclopeptoids were dissolved in $C_2D_2Cl_4$ (TCDE, 5.0 mM solution), then 1H -NMR spectra were acquired at different temperatures, increasing 10 Kelvin each time. Subsequently, in the cases where the coalescence was reached, the ΔG^\ddagger was evaluated according to following relation:

$$\Delta G_c^\ddagger = aT_c \left[9.972 + \log \left(\frac{T_c}{\sqrt{\Delta\nu^2 + 6J^2}} \right) \right] \quad (2.5)$$

Where T_c is the coalescence temperature, $\Delta\nu$ is the difference in Hertz between the two coupled signals and J is the coupling constant between the two signals.

2.2.3.8 General procedure for the Pirkle's alcohol addition to racemic mixtures of cyclic peptoids

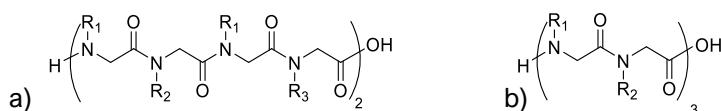
To a $CDCl_3$ (0.50 mL) solution of cyclic peptoids increasing quantities of Pirkle's alcohol ((*R*)-(-)-1-(9-anthryl)-2,2,2-trifluoroethanol) were added, up to 1.0 equivalent. After each addition the mixture was sonicated for 1 minute and the 1H -NMR spectrum was recorded. Further equivalents of Pirkle's alcohol were added in order to increase the protons resonances' splitting (usually up to 3.0 equivalents). NMR spectra were recorded on a Bruker DRX 600 (1H at 600.13 MHz).

2.3 Cyclopeptoids as mimics of bassianolide, verticilide and PF1022s congeners⁸⁰

2.3.1 Results and discussion

2.3.1.1 Synthesis and structural analysis of cyclopeptoids 53-57

The synthesis of the linear oligomers was performed as previously described according the sub-monomeric protocol, using 2-chlorotrityl chloride resin as solid support, bromoacetic acid as acyl synthon, and commercially available primary amines isopropylamine, isobutylamine, benzylamine, methylamine and *n*-amylamine. The detachment from the resin provided the five linear oligomers in acceptable purity ($\geq 71\%$) (Figure 2.30).



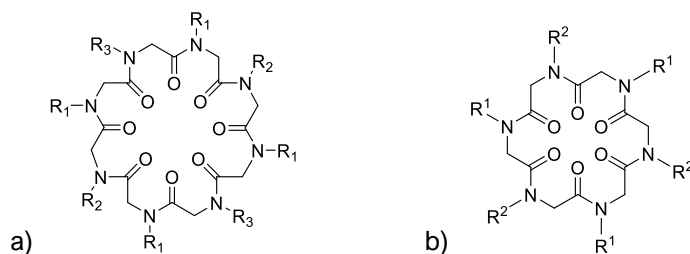
Oligomer	R ₁	R ₂	R ₃	Sequence	Yield
65 ^a	<i>i</i> Bu	<i>i</i> Pr	<i>i</i> Pr	H-[NVal-NLeu] ₄ -OH	100%
66 ^a	Me	<i>n</i> Am	<i>n</i> Am	H-[NAm-NAla] ₄ -OH	54%
67 ^b	Me	<i>n</i> Am	/	H-[NAm-NAla] ₃ -OH	100%
68 ^a	<i>i</i> Bu	Bn	Me	H-[NPhe-NLeu-NAla-NLeu] ₂ -OH	49%
69 ^a	<i>i</i> Bu	Bn	Bn	H-[NPhe-NLeu] ₄ -OH	89%

^a General structure a)

^b General structure b)

Figure 2.30. Linear oligomers **65-69** and their yields.

The head-to-tail cyclization gave the cyclic oligomers **53-57** in high purity (>98%), and acceptable yields (reported in Figure 2.31).



⁸⁰ D'Amato A., Della Sala G., Izzo I., Costabile C., Masuda Y., De Riccardis F., *Cyclic Octamer Peptoids: Simplified Isosters of Bioactive Fungal Cyclodepsipeptides*. *Molecules* **2018**, *23*, 7, 1779-1795.

Cyclic peptoid	R ₁	R ₂	R ₃	Yield
53^a (bs)	<i>i</i> Bu	<i>i</i> Pr	<i>i</i> Pr	21%
54^a (vtA1)	Me	<i>n</i> Am	<i>n</i> Am	34%
55^b (vtB1)	Me	<i>n</i> Am	/	28%
56^a (PF1022A)	<i>i</i> Bu	Bn	Me	31%
57^a (PF1022B)	<i>i</i> Bu	Bn	Bn	29%

^a General structure a)^b General structure b)

Figure 2.31. Cyclopeptoids' structures and their yields. In parentheses are reported the natural congeners. bs = bassianolide; vtA1 = verticillide A1; vtB1 = verticillide B1.

Three out of four 24-membered macrocycles showed good conformational stability, as assessed via ¹H-NMR (CDCl₃, Figure 2.32, a, d, e)), with a single prevalent conformational isomer (>85%). The β-branched isobutyl side-chains seemed to hamper the macrocycles interconversion. On the contrary, the *N*-methyl/*N*-amyl combination caused the presence of multiple conformational isomers, in slow (**54** and **55**) equilibrium on the NMR time scale, for both the octamer and the hexamer (Figure 2.32, b) and c)).

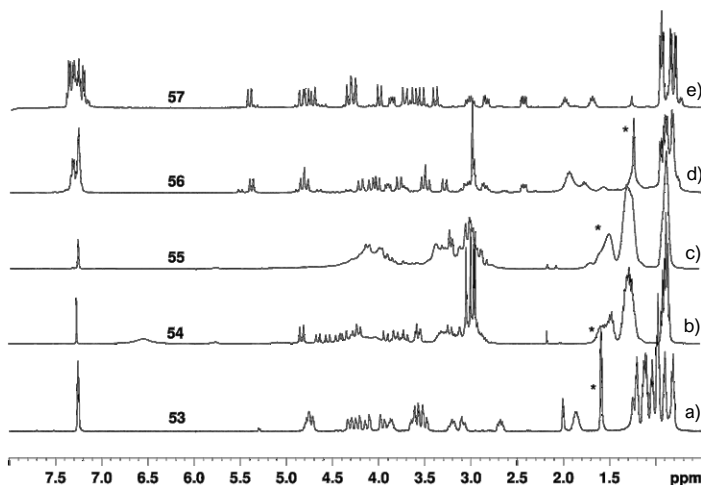


Figure 2.32. ¹H-NMR spectra of cyclic peptoids **53-57** (400 MHz, CDCl₃, 5.0 mM). Water or solvent impurities are labelled with a black asterisk.

The conformational rigidity of **53**, **56** and **57** is particularly interesting, considering that the natural congeners, in solution, are present as mixtures of rotamers.^{53,55b,81}

⁸¹ Scherkenbeck J., Plant A., Harder A., Mencke N., *Tetrahedron* **1995**, *51*, 8459-8470.

Conformational interconversion barriers were quantified by variable-temperature (VT) $^1\text{H-NMR}$ experiments for conformationally homogeneous **53**, **56**, **57**. Coalescence temperatures were experimentally determined to be 110 °C ($\text{C}_2\text{D}_2\text{Cl}_4$, $\Delta G^\ddagger = 17.4 \pm 0.9$ kcal/mol, 300 MHz), 90 °C ($\text{C}_2\text{D}_2\text{Cl}_4$, $\Delta G^\ddagger = 15.9 \pm 0.8$ kcal/mol, 300 MHz) and 90 °C ($\text{C}_2\text{D}_2\text{Cl}_4$, $\Delta G^\ddagger = 16.4 \pm 0.8$ kcal/mol, 300 MHz) for cyclopeptoids **53**, **56** and **57**, respectively.⁶¹

The relative amide bond geometry pattern was assigned through 2D-NMR experiments, homonuclear (COSY) and heteronuclear (HSQC, HMBC) as C_2 -symmetric (**53**, **57**) and C_1 -symmetric (**56**) (*ccttcctt*), as previously reported^{62,37a,82} for cyclic octapeptoids.

The relative amide bond geometry was inferred thanks to the chemical shifts values of the $N\alpha$ -branched isopropyl side-chain (low values testify for a *trans* amide bond, high values for a *cis* amide bond) or the $\Delta\delta$ for diastereotopic $C\alpha\text{-H}_2$ (in the case of the *N*Leu or *N*Phe residues), following the same criteria.

Compound **56** showed an unprecedented case of symmetry breaking in the case of a conformationally stable, symmetrically substituted, cyclic octamer peptoid, evidenced by accurate analysis of the $^1\text{H-NMR}$ spectra.

For cyclic peptoids **53** and **57**, two conformational diastereoisomers were, in principle, possible (**53a/b**, **57a/b**, Figure 2.33).

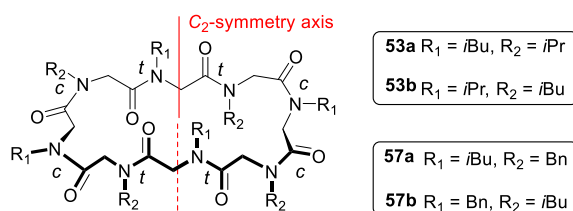


Figure 2.33. Possible conformational diastereoisomers for **53** and **57**.

With the help of DFT calculations, we were able to determine the minimum energy structures in CHCl_3 . Isomers **53a** and **57b** were found to be more stable than the corresponding conformational diastereoisomers **53b** and **57a** of 2.2 and 0.8 kcal/mol, respectively. The energy differences are mainly due to steric interactions among the *N*-

⁸² a) Titlestad K., *Acta Chem. Scand. B* **1975**, 29, 2, 153-167; b) Vollrath S. B. L., Bräse S., Kirshenbaum K., *Chem. Sci.* **2012**, 3, 2726-2731; c) Vollrath S. B. L., Hu C., Bräse S., Kirshenbaum K., *Chem. Commun.* **2013**, 49, 2317-2319; c) Tedesco C., Meli A., Macedi E., Iuliano V., Ricciardulli A. G., De Riccardis F., Vaughan G. B. M., Smith V. J., Barbour L. J., Izzo I., *Cryst. Eng. Comm.* **2016**, 18, 8838-8848.

substituents and the macroring. Specifically, **53b** shows isobutyl-ring distances shorter than **53a**, whereas interactions among the phenyl groups and the ring are responsible for the higher energy of **57a** with respect to **57b** (Figure 2.34). Furthermore, the higher energy difference between **53a** and **53b** (2.2 kcal/mol) is consistent with the NMR spectrum of **53**, which shows only one conformational isomer, whereas the $^1\text{H-NMR}$ spectrum of **57** shows a small amount of the other isomer (Figure 2.32, e)). These data were also coherent with the VT-experiments (the coalescence temperature and therefore the conformational interconversion barrier, resulted higher for cyclopeptoid **53**).

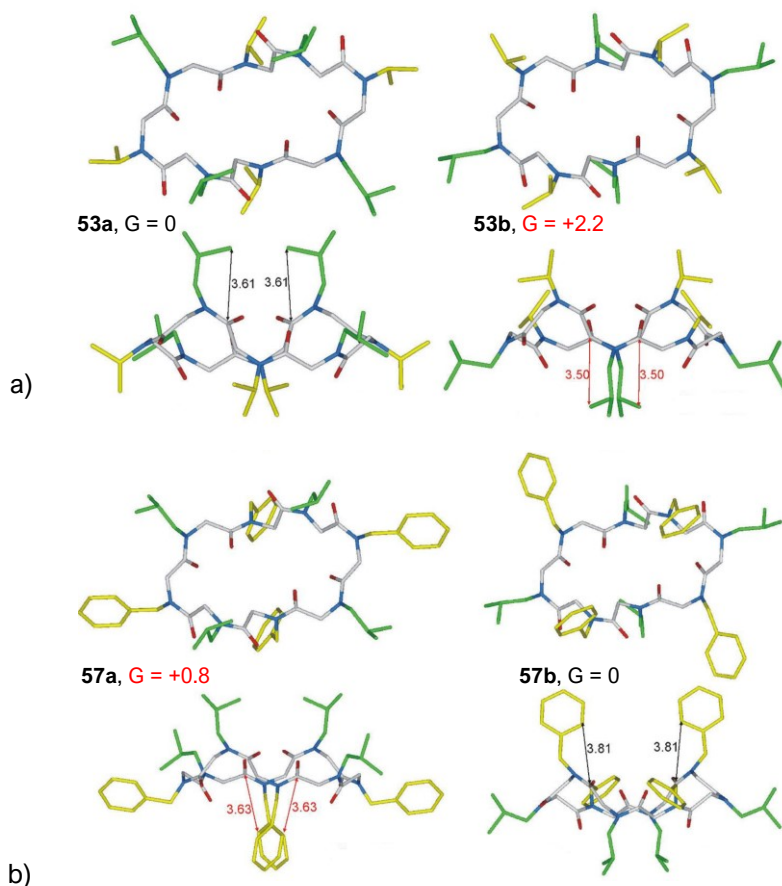


Figure 2.34. Top and side view of minimum energy structures of conformational diastereoisomers a) **53a/b** and b) **57a/b**. Isobutyl groups, green; isopropyl and benzyl groups, yellow; C, silver; N, blue; O, red. Free energies calculated in CHCl_3 and reported in kcal/mol. Distances in Å.

Conformational isomerism in rigid, cyclic octapeptoids is a case of conformational chirality, as in the case of the cyclic hexamer **49**, already described in Paragraph 2.2.1.2. Rigid C_1 - or C_2 -symmetric octamers **53**, **56** and **57**, displaying a

relatively high energy interconversion barrier ($\Delta G^\ddagger \geq 10$ kcal/mol) are chiral and observable as conformational enantiomers in solution by NMR spectroscopy (which, at room temperature, reveals species with lifetimes exceeding 10^{-2} s).

In Figure 2.35 is reported the stepwise addition of the Pirkle's alcohol to a chloroform solution of cyclopeptoid **57**; the splitting of the signals evidenced the two enantiomeric species of the major conformational diastereoisomer, **57b** and *ent*-**57b**.

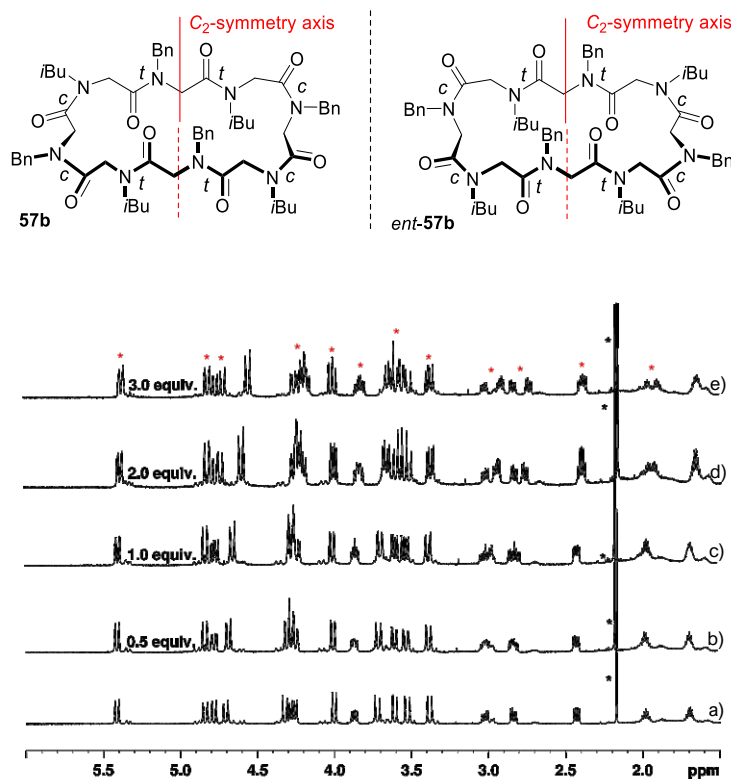


Figure 2.35. Quantitative stepwise addition of Pirkle's alcohol to **57**. $^1\text{H-NMR}$ (600 MHz, CDCl_3 , 298 K, 5.0 mM solution). 6.0-1.5 ppm expansion. Split signals are denoted with a red asterisk, water or solvent impurities are labelled with a black asterisk.

2.3.1.2 Complexation studies for cyclopeptoids **53-57**

Like the enniatins' family, also for cyclooctadepsipeptides the biological activity is related to the ability of the macrocycle to act as ionophore (Paragraph 2.1.3 and references cited therein). Therefore, we tested our compound for alkali metal complexation, starting with sodium. The addition of a single equivalent of NaTFPB showed the formation of a mixture of multiple complexes in slow equilibrium on the NMR time scale for the four octamers **53**, **54**, **56** and **57**; as for hexamer **55**, the monometallic complex

showed an all-*trans* C₃-symmetry, but a low binding constant ($\log K_{a1} = 3.3$, $-\Delta G^0 = 4.4$ kcal/mol), comparable to cyclohexapeptoid **47**, bearing isopropyl side-chains. Further addition of a second equivalent of complexing agent caused no variation in the structure of **55**, while induced the rigidification of the structures into highly symmetric derivatives for the octamers. The all-*trans* geometry of the amide bonds was inferred based on the observation of the chemical shifts (similarly to the hexameric compounds described in Paragraph 2.2.1.3). The relatively low chemical shift values observed for the *N*Ala (2.90 ppm in **[55·Na]**⁺, 2.85 ppm in **[56·2Na]**²⁺; 2.88 ppm in **[54·2Na]**²⁺) and *N*Val (3.96 ppm in **[53·2Na]**²⁺) C α H resonances; the small $\Delta\delta$ evidenced for the diastereotopic -N-CH₂-CH(CH₃)₂ protons of *N*Leu (0.22 in **[53·2Na]**²⁺; 0.30 in **[56·2Na]**²⁺), -N-CH₂-Ph protons of *N*Phe (0.48 in **[56·2Na]**²⁺; 0.51 in **[57·2Na]**²⁺) and -N-CH₂-(CH₂)₃-CH₃ protons of *N*am (0.23 in **[54·2Na]**²⁺) residues, suggested all-*trans* geometry of the amide bonds (similarly to the hexameric compounds described in Paragraph 2.2.1.3).

The host/guest ratio (calculated integrating the signals of the host/guest complex respect to those of dissolved guest, NaTFPB) remained constant during all the titration experiments and documented a 1:2 macrocycle/Na⁺ ratio for all the octameric complexes. VT ¹H-NMR experiments testified the stability of such complexes; no sign of coalescence was observed up to 110 °C (C₂D₂Cl₄, 600 MHz). The efficient ion-dipole interactions between the carbonyl groups and the sodium cation increase the conformational stability of the macrorings.

	53	54	56	57
log K_{aTOT}^{a,b}	7.3	7.1	6.8	6.3
-\Delta G⁰	9.9	9.7	9.4	8.6

^a From ¹H-NMR experiments, 1.0 mM host/guest in CDCl₃ solutions.

^b Figures within $\pm 10\%$ throughout multiple experiments.

Table 2.5. Log of calculated apparent K_{aTOT} (M⁻²) values and $-\Delta G^0$ (kcal/mol) for the **[53-54, 56-57·2Na]**²⁺ complexes.

Figure 2.36 reports the ¹H-NMR spectra of the **53-57** sodium complexes.

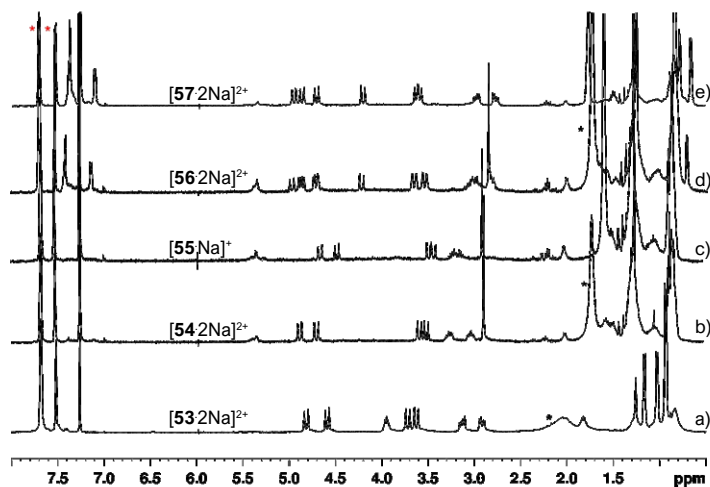


Figure 2.36. $^1\text{H-NMR}$ spectra of complexes $[\mathbf{53-57}\cdot\text{Na}]^+$ (400 MHz, CDCl_3 , 1.0 mM). Water or solvent impurities are labelled with a black asterisk. TFPB $^-$ signals are labelled with a red asterisk.

The rigid architecture of the disodium complexes led to the presence of couples of enantiomorphous cyclooligomers. In particular, cyclic peptoids $[\mathbf{53c}\cdot 2\text{Na}]^{2+}$ and $[\mathbf{53d}\cdot 2\text{Na}]^{2+}$, showing alternating side-chains, are C_4 -symmetric conformational enantiomers, similarly to compounds **54** and **57** (not shown); macrorings $[\mathbf{56a}\cdot 2\text{Na}]^{2+}$ and $[\mathbf{56b}\cdot 2\text{Na}]^{2+}$ are C_2 -symmetric species.

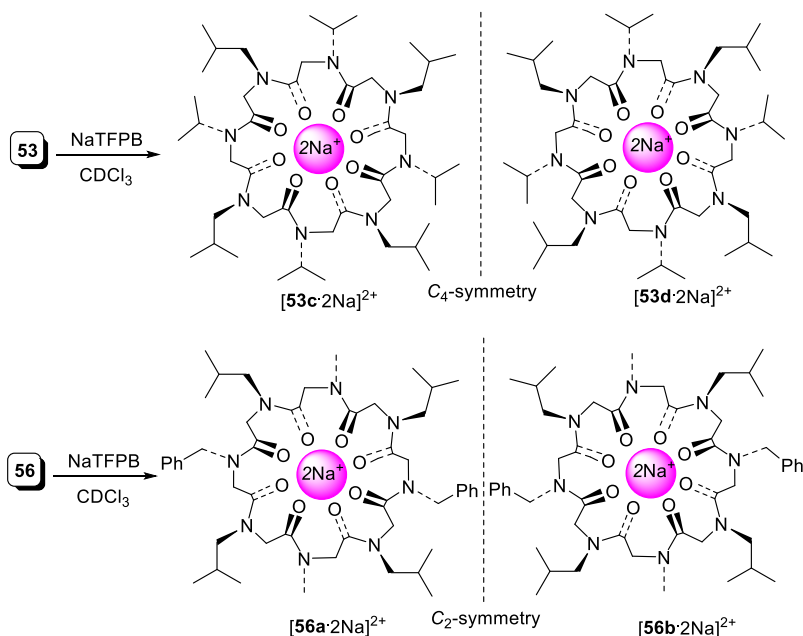


Figure 2.37. Schematic structures of the enantiomeric couples of all-*trans* complexes for $[\mathbf{53}, \mathbf{56}\cdot 2\text{Na}]^{2+} 2\text{TFPB}^-$.

The increased dimension of the macrocyclics' octameric cavities prompted us to attempt complex formation of compounds **53**, **54**, **56** and **57** also with potassium tetrakis[3,5-bis(trifluoromethyl)phenyl]borate (KTFPB). Addition of the potassium salt caused the formation of multiple conformations in slow equilibrium on the NMR time scale with formation of very complex NMR spectra.

2.3.1.3 Biological activity of cyclopeptoids **53-57**

Compounds **53-57** were tested for anti-proliferative action on A375 (human melanoma) cancer cell line, as for the first generation of compounds (Paragraph 2.2.1.5). The cells were incubated for 72 h with increasing concentration of compounds (10-25-50 μM) and cell viability was determined by MTT proliferation assay. The results indicated that the assayed compounds did not affect the cell vitality.

Cyclic octameric depsipeptides exert their cytotoxic activity targeting a specific receptor or molecular target in the cell; thus, we hypothesized that the conformational rigidity of our molecules and complexes could be detrimental to such activity.

Given that all the corresponding natural effectors are potent anthelmintics (Paragraph 2.1.3 and references cited therein), we tested our cyclopeptoids in a toxicity test against silkworm larvae.

Fourth-instar larvae of *Bombyx mori* were subjected to injection of a DMSO solution of suspension of the cyclopeptoid mycotoxin; a total of 10 larvae were tested and the number of dead ones was counted.

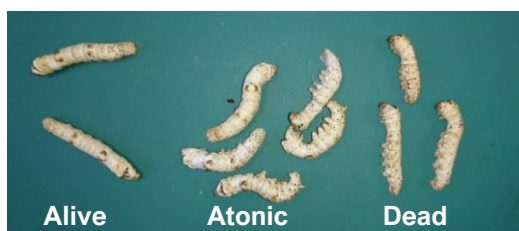


Figure 2.38. Photograph of the tested silkworm larvae after the treatment with the cyclopeptoids.

The administration of the cyclopeptoid compounds caused the death of a few larvae, rather than atony, at a dose of 300 nmol/larva after 72-120 h (Table 2.6). However, the toxicity displayed resulted much lower than the natural reference, bassianolide (**41**), which induces atonic symptoms within 0.5 h and 100% mortality in a week at a dose of 5 μg (= 5.5 nmol)/larva.

Compound	Number of dead larvae ($n = 10$)					
	time after injection (h)					
	1	6	24	72	120	168
vehicle	0	0	0	0	0	0
53	0	0	0	2	2	2
54	0	0	0	1	1	1
55	0	0	0	1	1	1
56	0	0	0	1	2	2
57	0	0	0	2	2	2

Each compound in DMSO was injected into 4th-instar larvae (ca 0.9 g body weight) at a dose of 300 nmol/larva.

Table 2.6. Toxicity of cyclopeptoids **53-57** against silkworms by haemolymph injection.

2.3.2 Conclusions

In this study, we outlined the synthesis and the structural analysis of five cyclopeptoids derivatives, whose design was based on natural cyclodepsipeptides effectors bassianolide, verticilide derivatives and PF1022s congeners. The accurate comprehension of the architecture of the macrocyclic' scaffolds, inferred by NMR and computational analysis, resulted important to better understand the biological activity.

Overall, the intrinsic conformational stability of cyclooctamer peptoids, resulted detrimental to the biological activity, which resulted scarce, compared to the natural counterparts, due to the reduced conformational adaptability of the peptoid effectors.

2.3.3 Experimental section

2.3.3.1 General methods

Refer to Paragraph 2.2.3.1.

For the VT NMR experiments, refer to Paragraph 2.2.3.7; for the Pirkle experiments, refer to Paragraph 2.2.3.8.

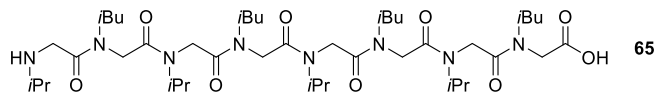
DFT calculations were performed by prof. C. Costabile, Dpt. of Chemistry and Biology "A. Zambelli", Univ. of Salerno.

Cytotoxicity assays were performed by prof. I. Bruno research group, Dpt. of Pharmaceutical Sciences, Univ. of Salerno.

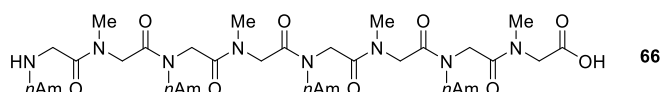
Anthelmintic assays were performed by Dr. Y. Masuda, Graduate School of Bioresources, Univ. Mie, Japan.

2.3.3.2 Synthesis of linear peptoids **65-69**

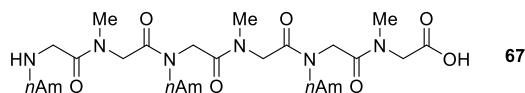
Refer to Paragraph 2.2.3.2. The synthesis was performed using the sub-monomer protocol, on a 0.400 g 2-chlorotrytil chloride resin batch (1.63 mmol g⁻¹); purity of the linear oligomers $\geq 71\%$.



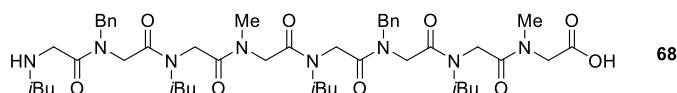
H-[NVal-NLeu]₄-OH (**65**): white amorphous solid, 0.565 g, 100%; *t_R*: 11.2 min. ES-MS *m/z*; 867.5 [M + H]⁺. HRMS (ESI/FTICR) *m/z*; [M + H]⁺ Calcd for C₄₄H₈₃N₈O₉⁺ 867.6278; Found 867.6277.



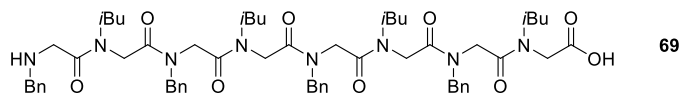
H-[NAm-NAla]₄-OH (**66**): white amorphous solid, 0.285 g, 54%; *t_R*: 11.1 min. ES-MS *m/z*; 811.5 [M + H]⁺. HRMS (ESI/FTICR) *m/z*; [M + H]⁺ Calcd for C₄₀H₇₅N₈O₉⁺ 811.5652; Found 811.5653.



H-[NAm-NAla]₃-OH (**67**): white amorphous solid, 0.399 g, 100%; *t_R*: 9.7 min. ES-MS *m/z*; 613.3 [M + H]⁺. HRMS (ESI/FTICR) *m/z*; [M + H]⁺ Calcd for C₃₀H₅₇N₆O₇⁺ 613.4283; Found 613.4286.



H-[NPhe-NLeu-NAla-NLeu]₂-OH (**68**): white amorphous solid, 0.290 g, 49%; *t_R*: 11.4 min. ES-MS *m/z*; 908.2 [M + H]⁺. HRMS (ESI/FTICR) *m/z*; [M + H]⁺ Calcd for C₄₈H₇₅N₈O₉⁺ 907.5652; Found 907.5650.



H-[NPhe-NLeu]₄-OH (**69**): white amorphous solid, 0.690 g, 89%; *t_R*: 12.3 min. ES-MS *m/z*; 1059.6 [M + H]⁺. HRMS (ESI/FTICR) *m/z*; [M + H]⁺ Calcd for C₆₀H₈₃N₈O₉⁺ 1059.6278; Found 1059.6280.

2.3.3.3 Synthesis of the cyclic peptoids **53-57**

Refer to Paragraph 2.2.3.3.

The cyclization reaction was performed on a 0.150 mmol scale of the linear oligomers, which were dissolved in 5.0 mL of dry DCM and added by a syringe pump in 5 hours to the reaction mixture. The crude cyclic peptoids (purity >90%) **53**, **57** were dissolved in hot acetonitrile and precipitated by slowly cooling the acetonitrile solutions. The crude **54-56** were purified on reverse silica gel (C₁₈); conditions: 10–100% A (A: acetonitrile; B: water).

cyclo-[NVal-NLeu]₄ (**53**): white amorphous solid, 0.0270 g, 21%; *t_R*: 12.1 min. ¹H-NMR (400 MHz, CDCl₃, *c* stands for *cis* amide bond, *t* stands for *trans* amide bond) δ: 4.77 (2H, m, N-CH(CH₃)₂, *c*), 4.74 (2H, d, *J* 16.1 Hz, O=C-CHH-N-*i*Bu, *t*), 4.32 (2H, d, *J* 17.8 Hz, O=C-CHH-N-*i*Bu, *c*), 4.23 (2H, d, *J* 17.7 Hz, O=C-CHH-N-*i*Pr, *t*), 4.13 (2H, d, *J* 17.8 Hz, O=C-CHH-N-*i*Pr, *c*), 3.96 (2H, d, *J* 17.8 Hz, O=C-CHH-N-*i*Pr, *c*), 3.87 (m, 2H, N-CH(CH₃)₂, *t*), 3.64 (2H, dd, *J* 14.1, 7.4 Hz, N-CHH-CH(CH₃)₂, *c*), 3.60 (4H, d, O=C-CHH-N-*i*Bu, *t* and O=C-CHH-N-*i*Bu, *c*, overlapping), 3.51 (2H, d, *J* 17.7 Hz, O=C-CHH-N-*i*Pr, *t*), 3.22 (2H, dd, *J* 13.9, 5.0 Hz, N-CHH-CH(CH₃)₂, *t*), 3.09 (2H, dd, *J* 13.9, 5.0 Hz, N-CHH-CH(CH₃)₂, *t*), 2.68 (2H, dd, *J* 14.1, 7.4 Hz, N-CHH-CH(CH₃)₂, *c*), 1.87 (4H, m, N-CH₂-CH(CH₃)₂, *c* and *t*), 1.21 (6H, d, *J* 6.7 Hz, N-CH(CH₃)₂, *t*), 1.14 (6H, d, *J* 6.7 Hz, N-CH(CH₃)₂, *c*), 1.11 (6H, d, *J* 6.7 Hz, N-CH(CH₃)₂, *t*), 1.05 (6H, d, *J* 6.7 Hz, N-CH(CH₃)₂, *c*), 0.98 (12H, d, *J* 6.5 Hz, N-CH₂-CH(CH₃)₂, *c* and *t*), 0.91 (6H, d, *J* 6.5 Hz, N-CH₂-CH(CH₃)₂, *t*), 0.82 (6H, d, *J* 6.5 Hz, N-CH₂-CH(CH₃)₂, *c*). ¹³C-NMR (100 MHz, CDCl₃) δ: 170.3 (x2), 169.4 (x2), 169.3 (x2), 166.1 (x2), 56.2 (x2), 55.8 (x2), 50.6 (x2), 49.0 (x2), 48.0 (x2), 45.6 (x2), 43.2 (x2), 42.8 (x2), 27.8 (x2), 27.0 (x2), 20.9 (x2), 20.6 (x3), 20.4 (x3), 19.9 (x4), 19.6 (x2), 19.6 (x2). HRMS (ESI/FTICR) *m/z*; [M + H]⁺ Calcd for C₄₄H₈₁N₈O₈⁺ 849.6172; Found 849.6170.

cyclo-[Nam-NAla]₄ (**54**): white amorphous solid, 0.0400 g, 34%; *t_R*: 13.3 min. ¹H-NMR (400 MHz, CDCl₃, mixture of rotamers) δ: 4.84–2.94 (36H, overlapping signals, O=C-CH₂-N-CH₃, O=C-CH₂-N-CH₂CH₂CH₂CH₂CH₃, N-CH₂CH₂CH₂CH₂CH₃, O=C-CH₂-N-CH₃), 1.58–1.44 (8H, br signals, overlapping, N-CH₂CH₂CH₂CH₂CH₃), 1.33–1.22 (16H, overlapping signals, N-CH₂CH₂CH₂CH₂CH₃), 0.92–0.83 (12H, overlapping signals, N-CH₂CH₂CH₂CH₂CH₃). ¹³C-NMR (100 MHz, CDCl₃) δ: 169.9, 169.3, 169.2, 169.0, 168.0, 167.0, 51.6, 50.8, 50.5, 50.3, 49.0, 48.9, 48.6, 48.4, 48.0, 47.7, 36.6, 35.9, 35.5, 29.1, 29.0, 28.9, 28.7, 28.5, 27.5, 27.3, 27.0, 22.4, 22.2, 14.0. HRMS (ESI/FTICR) *m/z*; [M + H]⁺ Calcd for C₄₀H₇₃N₈O₈⁺ 793.5546; Found 793.5540.

cyclo-[Nam-NAla]₃ (**55**): white amorphous solid, 0.0250 g, 28%; *t_R*: 11.4 min. ¹H-NMR (400 MHz, CDCl₃, mixture of rotamers) δ: 4.02–2.86 (27H, overlapping signals, O=C-CH₂-N-CH₃,

$\text{O}=\text{C}-\text{CH}_2-\text{N}-\text{CH}_2\text{CH}_2\text{CH}_2\text{CH}_2\text{CH}_3$, $\text{N}-\text{CH}_2\text{CH}_2\text{CH}_2\text{CH}_2\text{CH}_3$, $\text{O}=\text{C}-\text{CH}_2-\text{N}-\text{CH}_3$, 1.48-1.23 (18H, br signals, overlapping, $\text{N}-\text{CH}_2\text{CH}_2\text{CH}_2\text{CH}_2\text{CH}_3$ and $\text{N}-\text{CH}_2\text{CH}_2\text{CH}_2\text{CH}_2\text{CH}_3$), 0.86 (9H, br s, $\text{N}-\text{CH}_2\text{CH}_2\text{CH}_2\text{CH}_2\text{CH}_3$). ^{13}C -NMR (100 MHz, CDCl_3) δ : 171.9, 170.2, 169.7, 169.3, 169.2, 168.9, 168.3, 168.0, 167.5, 160.2, 159.8, 159.4, 159.1, 52.1, 51.8, 50.9, 50.3, 49.7, 49.5, 48.9, 48.5, 48.1, 47.4, 37.6, 36.9, 36.5, 36.0, 35.7, 35.4, 34.8, 28.9, 28.5, 28.1, 27.6, 27.3, 27.2, 26.9, 26.6, 26.3, 22.3, 13.9. HRMS (ESI/FTICR) m/z ; $[\text{M} + \text{H}]^+$ Calcd for $\text{C}_{30}\text{H}_{55}\text{N}_6\text{O}_6^+$ 595.4178; Found 595.4175.

cyclo-[*N*Phe-*N*Leu-*N*Ala-*N*Leu]₂ (**56**): white amorphous solid, 0.0410 g, 31%; t_R : 12.6 min. ^1H -NMR (400 MHz, CDCl_3 , *c* stands for *cis* amide bond, *t* stands for *trans* amide bond) δ : 7.36-7.34-7.23 (10H, overlapping, *Ar-H*), 5.52 (1H, d, J 15.6 Hz, $\text{N}-\text{CHH}-\text{Ph}$, *c*), 5.39 (1H, d, J 14.5 Hz, $\text{N}-\text{CHH}-\text{Ph}$, *c*), 4.91 (1H, d, J 16.8 Hz, $\text{O}=\text{C}-\text{CHH}-\text{N}-\text{CH}_3$, *t*), 4.84 (1H, d, J 17.0 Hz, $\text{O}=\text{C}-\text{CHH}-\text{N}-\text{CH}_3$, *t*), 4.71 (1H, d, J 17.8 Hz, $\text{O}=\text{C}-\text{CHH}-\text{N}-i\text{Bu}$, *t*), 4.67 (1H, d, J 16.0 Hz, $\text{O}=\text{C}-\text{CHH}-\text{N}-i\text{Bu}$, *t*), 4.37 (1H, d, J 16.8 Hz, $\text{O}=\text{C}-\text{CHH}-\text{N}-i\text{Bu}$, *c*), 4.22 (1H, d, J 17.9 Hz, $\text{O}=\text{C}-\text{CHH}-\text{N}-\text{Bn}$, *c*), 4.14 (1H, d, J 15.6 Hz, $\text{O}=\text{C}-\text{CHH}-\text{N}-\text{Bn}$, *c*), 4.09 (1H, d, J 18.3 Hz, $\text{O}=\text{C}-\text{CHH}-\text{N}-i\text{Bu}$, *c*), 4.03 (1H, d, J 14.5 Hz, $\text{N}-\text{CHH}-\text{Ph}$, *c*), 3.92 (1H, dd, J 13.5, 7.2 Hz, $\text{N}-\text{CHH}-\text{CH}(\text{CH}_3)_2$, *c*), 3.79 (1H, d, J 18.5 Hz, $\text{O}=\text{C}-\text{CHH}-\text{N}-i\text{Bu}$, *c*), 3.77 (2H, d, J 15.6 Hz, $\text{N}-\text{CHH}-\text{Ph}$, *c* and $\text{O}=\text{C}-\text{CHH}-\text{N}-\text{Bn}$, *c*, overlapping), 3.75 (1H, m, overlapping signals, $\text{N}-\text{CHH}-\text{CH}(\text{CH}_3)_2$, *c*), 3.71 (1H, d, J 16.8 Hz, $\text{O}=\text{C}-\text{CHH}-\text{N}-i\text{Bu}$, *c*), 3.52 (1H, d, J 16.0 Hz, $\text{O}=\text{C}-\text{CHH}-\text{N}-i\text{Bu}$, *t*), 3.51 (1H, d, J 17.0 Hz, $\text{O}=\text{C}-\text{CHH}-\text{N}-\text{CH}_3$, *t*), 3.48 (1H, d, J 17.9 Hz, $\text{O}=\text{C}-\text{CHH}-\text{N}-\text{Bn}$, *c*), 3.30 (1H, d, J 17.8 Hz, $\text{O}=\text{C}-\text{CHH}-\text{N}-i\text{Bu}$, *t*), 3.10 (1H, d, J 16.8 Hz, $\text{O}=\text{C}-\text{CHH}-\text{N}-\text{CH}_3$, *t*), 3.05 (1H, dd, J 13.2, 6.5 Hz, $\text{N}-\text{CHH}-\text{CH}(\text{CH}_3)_2$, *t*), 3.00 (3H, s, $\text{N}-\text{CH}_3$, *t*), 2.99 (2H, m, overlapping signals, $\text{N}-\text{CH}_2-\text{CH}(\text{CH}_3)_2$, *t*), 2.97 (3H, s, $\text{N}-\text{CH}_3$, *t*), 2.96 (1H, dd, J 13.2, 6.5 Hz, $\text{N}-\text{CHH}-\text{CH}(\text{CH}_3)_2$, *t*), 2.87 (1H, dd, J 14.0, 7.6 Hz, $\text{N}-\text{CHH}-\text{CH}(\text{CH}_3)_2$, *c*), 2.44 (1H, dd, J 13.5, 7.2 Hz, $\text{N}-\text{CHH}-\text{CH}(\text{CH}_3)_2$, *c*), 1.97-1.72 (4H, m, overlapping signals, $\text{N}-\text{CH}_2-\text{CH}(\text{CH}_3)_2$, *c* and *t*), 0.97-0.77 (24H, overlapping signals, $\text{N}-\text{CH}_2-\text{CH}(\text{CH}_3)_2$, *c* and *t*). ^{13}C -NMR (150 MHz, CDCl_3) δ : 170.2, 169.8, 169.6, 169.3 (x2), 168.5, 167.2, 166.7, 136.6 (x2), 129.2, 129.0 (x3), 128.8 (x2), 128.6, 127.8, 127.4, 127.0, 56.1 (x2), 55.8, 55.1, 52.0, 50.9, 50.8, 50.4, 50.1, 49.8, 49.5, 49.2, 48.0, 46.9, 36.8, 35.4, 29.7, 27.8, 27.2 (x2), 20.6 (x2), 20.5, 20.3 (x2), 20.0, 19.9, 19.7. HRMS (ESI/FTICR) m/z ; $[\text{M} + \text{H}]^+$ Calcd for $\text{C}_{48}\text{H}_{73}\text{N}_8\text{O}_8^+$ 889.5546; Found 889.5543.

cyclo-[*N*Phe-*N*Leu]₄ (**57**): white amorphous solid, 0.0450 g, 29%; t_R : 14.6 min. ^1H -NMR (400 MHz, CDCl_3 , *c* stands for *cis* amide bond, *t* stands for *trans* amide bond) δ : 7.36-7.18 (20H, overlapping, *Ar-H*), 5.40 (2H, d, J 15.0 Hz, $\text{N}-\text{CHH}-\text{Ph}$, *c*), 4.83 (2H, d, J 17.3 Hz, $\text{O}=\text{C}-$

CHH-N-iBu, *t*), 4.77 (2H, d, *J* 16.1 Hz, O=C-*CHH-N-Bn*, *t*), 4.71 (2H, d, *J* 16.6 Hz, N-*CHH-Ph*, *t*), 4.32 (2H, d, *J* 17.8 Hz, N-*CHH-Ph*, *t*), 4.27 (4H, d, *J* 19.0 Hz, O=C-*CHH-N-Bn*, *c* and O=C-*CHH-N-iBu*, *c*, overlapping), 3.98 (2H, d, *J* 15.0 Hz, N-*CHH-Ph*, *c*), 3.85 (2H, dd, *J* 13.6, 7.2 Hz, N-*CHH-CH(CH₃)₂*, *c*), 3.71 (2H, d, *J* 19.0 Hz, O=C-*CHH-N-iBu*, *c*), 3.61 (2H, d, *J* 16.1 Hz, O=C-*CHH-N-Bn*, *t*), 3.53 (2H, d, *J* 19.0 Hz, O=C-*CHH-N-Bn*, *c*), 3.38 (2H, d, *J* 17.3 Hz, O=C-*CHH-N-iBu*, *t*), 3.03 (2H, dd, *J* 14.9, 7.6 Hz, N-*CHH-CH(CH₃)₂*, *t*), 2.83 (2H, dd, *J* 14.9, 7.6 Hz, N-*CHH-CH(CH₃)₂*, *t*), 2.42 (2H, dd, *J* 13.6, 7.2 Hz, N-*CHH-CH(CH₃)₂*, *c*), 1.97 (2H, m, N-*CH₂-CH(CH₃)₂*, *t*), 1.68 (2H, m, N-*CH₂-CH(CH₃)₂*, *c*), 0.92 (12H, t, *J* 7.3 Hz, N-*CH₂-CH(CH₃)₂*, *t*, overlapping signals), 0.82 (6H, d, *J* 6.5 Hz, N-*CH₂-CH(CH₃)₂*, *c*), 0.77 (6H, d, *J* 6.5 Hz, N-*CH₂-CH(CH₃)₂*, *c*). ¹³C-NMR (100 MHz, CDCl₃) δ: 169.8 (x2), 169.7 (x2), 169.3 (x2), 167.4 (x2), 136.6 (x2), 135.9 (x2), 129.1 (x4), 128.8 (x4), 128.6 (x4), 128.0 (x2), 127.3 (x2), 126.7 (x4), 55.8 (x2), 55.1 (x2), 52.3 (x2), 50.1 (x2), 49.7 (x2), 49.4 (x2), 48.0 (x2), 47.1 (x2), 27.2 (x2), 20.4 (x2), 20.3 (x2), 20.2 (x2), 19.9 (x4). HRMS (ESI/FTICR) *m/z*; [M + H]⁺ Calcd for C₆₀H₈₁N₈O₈⁺ 1041.6172; Found 1041.6171.

2.3.3.4 Preparation of the monometallic complex [55·Na]⁺TFPB⁻

Refer to Paragraph 2.2.3.4.

Titration. To 2.0 mM solution of cyclic peptoid **55** in CDCl₃ (0.50 mL), were added increasing amounts of sodium tetrakis[3,5-bis(trifluoromethyl)phenyl]borate (NaTFPB) till 1.0 equivalent. After any addition the mixtures were sonicated for 5 minutes and the NMR spectra were recorded.

Note: for cyclic octamers **53**, **54**, **56**, **57** the NMR characterization was performed on the bimetallic adduct.

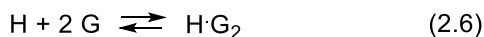
[55·Na]⁺TFPB⁻: white amorphous solid. ¹H-NMR (600 MHz, CDCl₃) δ: 7.68 (8H, s, TFPB-*o-H*), 7.53 (4H, s, TFPB-*p-H*), 4.79 (2H, d, *J* 16.2 Hz, O=C-*CHH-N-CH₃*), 4.67 (2H, d, *J* 16.1 Hz, O=C-*CHH-N-CH₂CH₂CH₂CH₂CH₃*), 3.51 (2H, d, *J* 16.1 Hz, O=C-*CHH-N-CH₂CH₂CH₂CH₂CH₃*), 3.46 (2H, d, *J* 16.2 Hz, O=C-*CHH-N-CH₃*), 3.23 (3H, m, O=C-*CH₂-N-CHHCH₂CH₂CH₂CH₃*), 2.98 (9H, s, O=C-*CH₂-N-CH₃*), 1.55 (3H, m, O=C-*CH₂-N-CHHCH₂CH₂CH₂CH₃*), 1.30-1.26 (18H, overlapping signals, O=C-*CH₂-N-CH₂CH₂CH₂CH₂CH₃*), 0.87 (9H, m, O=C-*CH₂-N-CH₂CH₂CH₂CH₂CH₃*). ¹³C-NMR (100 MHz, CDCl₃, for the TFPB numbering refer to Paragraph 2.2.3.4) δ: 170.8 (x3), 168.7 (x3), 160.1 (q, *J* 50 Hz, C-1), 134.8 (C-2), 129.0 (q, *J* 30 Hz, C-3), 124.6 (q, *J* 270 Hz, C-5), 117.6 (C-4), 51.7 (x3), 49.6 (x6), 36.8 (x3), 28.8 (x3), 28.0 (x3), 22.3 (x3), 13.8

(x3).

2.3.3.5 General procedure for the bimetallic complexes formation and evaluation of the apparent association constant K_{aTOT} . Preparation of the disodium complexes [53-54, 56-57·2Na]²⁺·2TFPB⁻

Titration. To 2.0 mM solution of cyclic octameric peptoids **53**, **54**, **56**, **57** in CDCl₃ (0.50 mL), were added increasing amounts of sodium tetrakis[3,5-bis(trifluoromethyl)phenyl]borate (NaTFPB) or potassium tetrakis[3,5-bis(trifluoromethyl)phenyl]borate (KTFPB) till 2.0 equivalents. After any addition the mixtures were sonicated for 5 minutes and the NMR spectra were recorded.

K_{aTOT} evaluation. To a solution of cyclic peptoids in CDCl₃ (0.50 mL) 2.0 equivalents of NaTFPB were added. After the addition, the mixtures were sonicated for 5 minutes in a rt bath (25 °C). The H·G₂ complex concentration, at the equilibrium – [H·G₂]_{eq} – was evaluated by integration of the ¹H-NMR complex signals (2.5-6.0 range) versus the total integration of the free host plus complexed molecules at 298 K (Relation 2.2). With the addition of 2 equivalents of guest, the equilibrium (2.6) is established:



$$[H]_{eq} = [H]_i - [H \cdot G_2]_{eq} \quad (2.7)$$

$$[G]_{eq} = [G]_i - 2[H \cdot G_2]_{eq} \quad (2.8)$$

(where $[G]_i = 2[H]_i$).

The K_{aTOT} ($= K_{a1} \cdot K_{a2}$, where K_{a1} is the equilibrium constant associated with the formation of the monometallic complex, K_{a2} is the equilibrium constant associated with the formation of the bimetallic complex, starting from the monometallic one), was calculated as follows:

$$K_{aTOT} = \frac{[H \cdot G]_{eq}}{[H]_{eq} \times [G]_{eq}^2} \quad (2.9)$$

for the equilibrium (2.6).

In order to have the reliable integration values, the delay times (D1) among successive scans, in the ¹H-NMR, were set at 5 seconds. For the TFPB numbering refer to Paragraph 2.2.3.4.

[53·2Na]²⁺·2TFPB⁻: white amorphous solid. ¹H-NMR (400 MHz, CDCl₃) δ: 7.68 (16H, s,

TFPB-*o*-H), 7.52 (8H, s, TFPB-*p*-H), 4.82 (4H, d, J 16.5 Hz, O=C-CHH-N-*i*Bu), 4.59 (4H, d, J 16.6 Hz, O=C-CHH-N-*i*Pr), 3.96 (4H, ept, J 6.8 Hz, -CH(CH₃)₂), 3.72 (4H, d, J 16.6 Hz, O=C-CHH-N-*i*Pr), 3.63 (4H, d, J 16.5 Hz, O=C-CHH-N-*i*Bu), 3.14 (4H, dd, J 14.7, 7.2 Hz, N-CHH-CH(CH₃)₂), 2.92 (4H, dd, J 14.7, 7.2 Hz, N-CHH-CH(CH₃)₂), 1.83 (4H, m, N-CH₂-CH(CH₃)₂), 1.18 (12H, d, J 5.6 Hz, N-CH(CH₃)(CH₃)), 1.03 (12H, d, J 5.6 Hz, N-CH(CH₃)(CH₃)), 0.95 (24H, d, J 5.3 Hz, N-CH₂-CH(CH₃)₂). ¹³C-NMR (100 MHz, CDCl₃) δ: 170.0 (x4), 168.1 (x4), 161.7 (q, J 50 Hz, C-1), 136.2, 134.8, (C-2), 128.8 (q, J 30 Hz, C-3), 124.6 (q, J 270 Hz, C-5), 117.4 (C-4), 56.1 (x6), 48.4 (x2), 48.1 (x4), 42.2 (x4), 27.3 (x4), 20.9 (x4), 19.9 (x12).

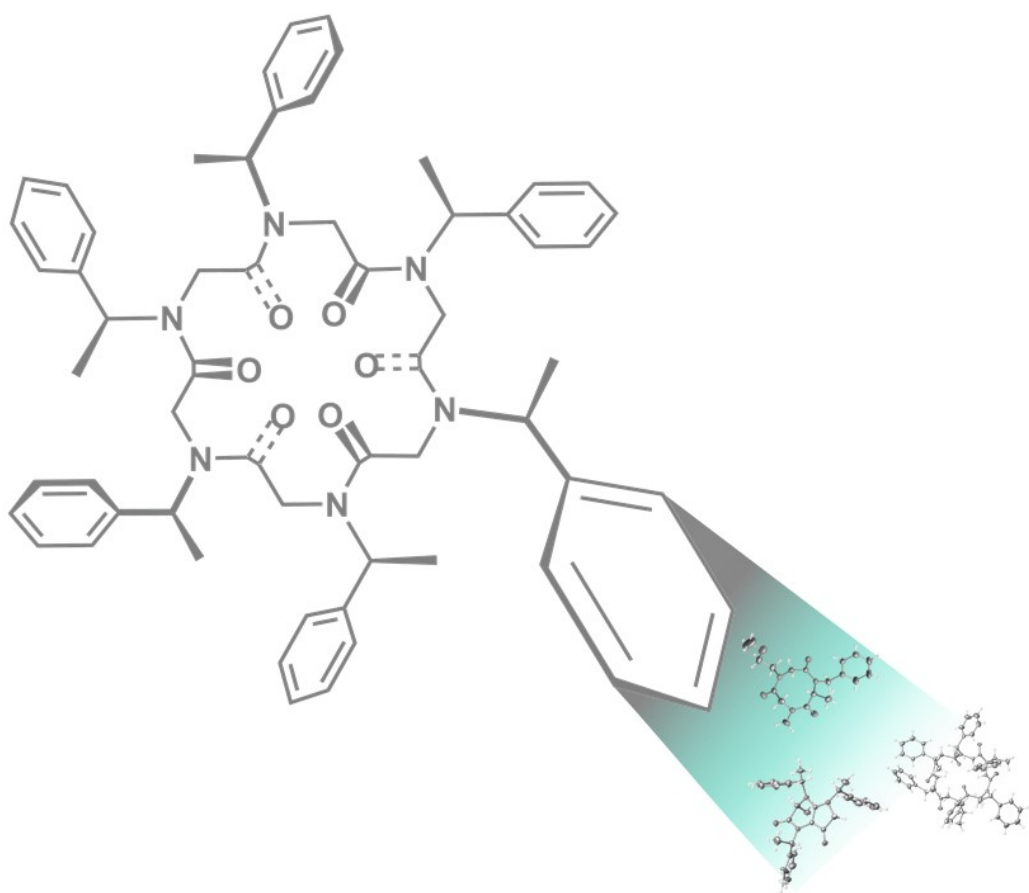
[54·2Na]²⁺·2TFPB⁻: white amorphous solid. ¹H-NMR (400 MHz, CDCl₃) δ: 7.68 (16H, s, TFPB-*o*-H), 7.53 (8H, s, TFPB-*p*-H), 4.88 (4H, d, J 16.8 Hz, O=C-CHH-N-CH₃), 4.70 (4H, d, J 17.0 Hz, O=C-CHH-N-CH₂CH₂CH₂CH₂CH₃), 3.58 (4H, d, J 17.0 Hz, O=C-CHH-N-CH₂CH₂CH₂CH₂CH₃), 3.51 (4H, d, J 16.8 Hz, O=C-CHH-N-CH₃), 3.26 (4H, m, O=C-CH₂-N-CHHCH₂CH₂CH₂CH₃), 3.03 (4H, m, O=C-CH₂-N-CHHCH₂CH₂CH₂CH₃), 2.88 (12H, s, O=C-CH₂-N-CH₃), 1.59-1.48 (8H, m, overlapping signals, O=C-CH₂-N-CH₂CH₂CH₂CH₂CH₃), 1.26 (16H, m, O=C-CH₂-N-CH₂CH₂CH₂CH₂CH₃), 0.87 (12H, m, O=C-CH₂-N-CH₂CH₂CH₂CH₂CH₃). ¹³C-NMR (100 MHz, CDCl₃) δ: 170.3 (x4), 168.8 (x4), 160.1 (q, J 50 Hz, C-1), 134.8 (C-2), 129.0 (q, J 30 Hz, C-3), 124.6 (q, J 270 Hz, C-5), 117.6 (C-4), 50.2 (x4), 48.8 (x4), 45.5 (x4), 35.8 (x4), 29.7 (x4), 22.2 (x8), 13.6 (x4).

[56·2Na]²⁺·2TFPB⁻: white amorphous solid. ¹H-NMR (400 MHz, CDCl₃) δ: 7.69 (16H, s, TFPB-*o*-H), 7.52 (8H, s, TFPB-*p*-H), 7.43-7.41 (6H, overlapping, Ar-H), 7.13 (4H, d, J 6.9 Hz, Ar-H), 4.97 (2H, d, J 17.0 Hz, O=C-CHH-N), 4.88 (2H, d, J 16.8 Hz, O=C-CHH-N-CH₃), 4.86 (2H, d, J 16.7 Hz, O=C-CHH-N), 4.72 (2H, d, J 16.7 Hz, O=C-CHH-N), 4.70 (2H, d, J 16.7 Hz, O=C-CH₂-N-CHH-Ph), 4.22 (2H, d, J 16.7 Hz, O=C-CH₂-N-CHH-Ph), 3.66 (2H, d, J 17.0 Hz, O=C-CHH-N), 3.65 (2H, d, J 16.7 Hz, O=C-CHH-N), 3.54 (2H, d, J 16.8 Hz, O=C-CHH-N-CH₃), 3.53 (2H, d, J 16.7 Hz, O=C-CHH-N), 3.10 (6H, overlapping, N-CH₂-CH(CH₃)₂), 2.85 (6H, s, N-CH₃), 2.80 (2H, overlapping, N-CH₂-CH(CH₃)₂), 2.01 (4H, m, N-CH₂-CH(CH₃)₂), 0.85 (24H, d, J 6.3 Hz, N-CH₂-CH(CH₃)₂). ¹³C-NMR (150 MHz, CDCl₃) δ: 169.2 (x4), 161.7 (q, J 50 Hz, C-1), 161.5 (x4), 136.2, 134.8, C-2), 129.7 (x2), 129.0 (x2), 128.8 (x4), 128.8 (q, J 30 Hz, C-3), 126.5 (x4), 124.6 (q, J 270 Hz, C-5), 117.4 (C-4), 34.1 (x4), 30.1 (x4), 29.7 (x4), 27.3 (x3), 22.6 (x3), 22.3 (x2), 19.7 (x4), 14.0 (x4).

[57·2Na]²⁺·2TFPB⁻: white amorphous solid. ¹H-NMR (400 MHz, CDCl₃) δ: 7.71 (16H, s,

TFPB-*o*-H), 7.53 (8H, s, TFPB-*p*-H), 7.38 (12H, bs, Ar-*m*-H and Ar-*p*-H), 7.11 (8H, d, *J* 6.8 Hz, Ar-*o*-H), 4.95 (4H, d, *J* 16.7 Hz, O=C-CHH-N-*i*Bu), 4.86 (4H, d, *J* 16.5 Hz, O=C-CHH-N-Bn), 4.71 (4H, d, *J* 16.6 Hz, N-CHH-Ph), 4.20 (4H, d, *J* 16.6 Hz, N-CHH-Ph), 3.62 (4H, d, *J* 16.5 Hz, O=C-CHH-N-Bn), 3.60 (4H, d, *J* 16.7 Hz, O=C-N-CHH-N-*i*Bu), 2.97 (4H, dd, *J* 15.2 and 7.7 Hz, N-CHH-CH(CH₃)₂), 2.77 (4H, dd, *J* 15.2 and 7.7 Hz, -CHH-CH(CH₃)₂), 1.50 (4H, m, N-CH₂-CH(CH₃)₂), 0.77 (12H, d, *J* 6.6 Hz, N-CH₂-CH(CH₃)(CH₃)), 0.65 (12H, d, *J* 6.6 Hz, -CH₂-CH(CH₃)(CH₃)). ¹³C-NMR: (100 MHz, CDCl₃) δ: 169.9 (x4), 169.3 (x4), 161.7 (q, *J* 50 Hz, C-1), 134.8 (C-2), 133.2 (x6), 129.6 (x6), 128.9 (q, *J* 30 Hz C-3), 126.5 (x6), 127.3 (x6), 124.7 (q, *J* 270 Hz, C-5), 117.5 (C-4), 55.9 (x4), 52.0 (x4), 48.1 (x8), 27.2 (x4), 19.7 (x4), 19.4 (x4).

Chapter 3



3 Conformational chirality in cyclic peptoids and its control

3.1 Introduction

3.1.1 Foldamers: a synthetic approach

The tri-dimensional arrangement of a biological effector is crucial for its efficiency, meaning both its activity and selectivity towards the molecular target. Nature relies onto two main classes of macromolecules, proteins and RNA, to accomplish several sophisticated tasks, such as catalysis, information, signal transduction and so on.

The macromolecules compact conformation generates active sites, arranging the functional groups in a precise architecture.

The artificial reproduction of the motifs adopted by such biofoldamers has been a hot topic since the early years of the new millennium.⁸³ The design of a synthetic foldamer involves, first of all, the accurate prediction of all the non-covalent interactions that will guide the oligomer folding (*i.e.* the preferred, stable, solution secondary structure).

For example, in proteins this secondary structure is dictated by H-bonding between sites embedded in the polymeric backbone. The main goal in envisioning a synthetic foldamer is, undoubtedly, the need to simplify the biopolymer, while retaining the biological functions.

Small, oligomeric chains should participate in short-range intrachain interactions, able to induce the proper folded state. Moreover, the primary sequence of the oligomer should be simple and allow the *ab initio* determination of the folded state, dependent by the sequence composition. Finally, the foldamer should have high designability, meaning the same secondary structure should be formed by many different, highly foldable, primary structures.⁸⁴

In particular, the development of a peptide-like foldamer involves the reproduction of peptides' secondary structures, such as α -helix, β -sheet and γ -turns. To accomplish such task, the monomers can be developed using β -, γ -, or δ -amino acids, α - or β -peptoids, units containing cycloalkane rings, meant to rigidify the overall structure, or isosteres of γ -amino acids, such as oligoureas and carbamates.

⁸³ Gellmann S. H., *Acc. Chem. Res.* **1998**, *31*, 173-180.

⁸⁴ Hill D. J., Mio M. J., Prince R. B., Hughes T. S., Moore J. S., *Chem. Rev.* **2001**, *101*, 3893-4011.

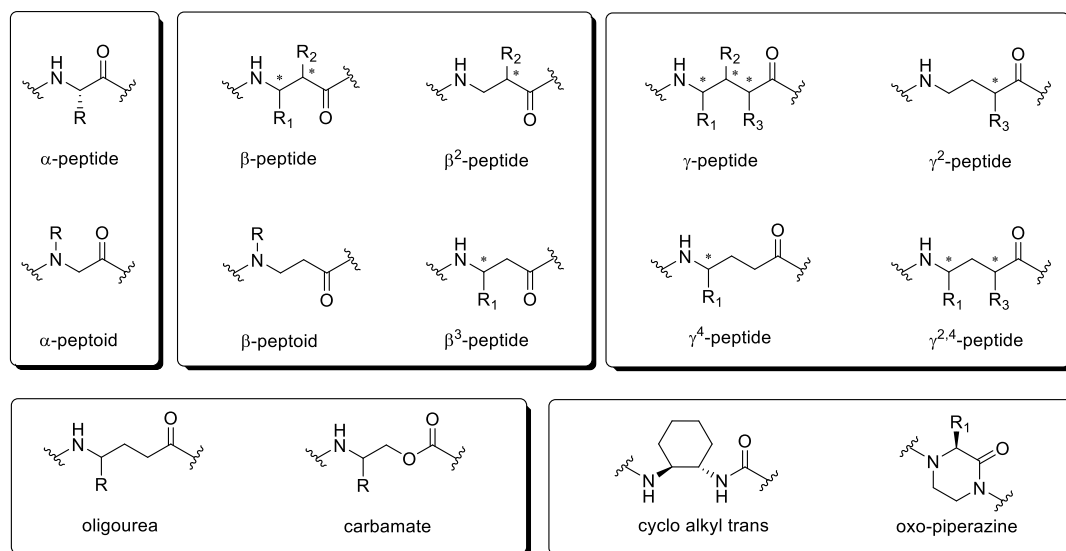


Figure 3.1. Selected structures of peptide foldamers backbone.

Peptide-like foldamers have already been used for biomedical applications.²⁴ The main task was the protein-protein interactions mimicry (*i.e.*: virus entry sequences, in order to block the infection or hormones modelling), and the preparation of systems able to act as vessels for small molecules.

The final goal will be the preparation of the so-called “miniproteins”, small, oligomeric systems able to reproduce not only the 3D-assembly of the parent protein, but also its functions, morphologies, molecular packing and overall physico-chemical properties.⁸⁵

3.1.2 Definition conformational chirality and its application to macrocyclic systems

Stereochemistry is a crucial feature of biomacromolecules, in particular proteins. The specific primary sequence, constituted, of course, by enantiopure amino acids, generates the unique secondary structure.

The tri-dimensional disposition of a chiral oligomer generates a chiral structure, which has, in principle, two enantiomeric conformations. For example, peptides' α-helix is

⁸⁵ a) Yoo S. H., Lee H.-S., *Acc. Chem. Res.* **2017**, *50*, 832-841; b) Baker E. G., Bartlett G. J., Porter Goff K. L., Woolfson D. N., *Acc. Chem. Res.* **2017**, *50*, 2085-2092.

right-handed, whereas a synthetic helix, generated by a polymer constituted by achiral monomers, can adopt both the two enantiomeric (*M* and *P*) screw senses (Figure 3.2).⁸⁶

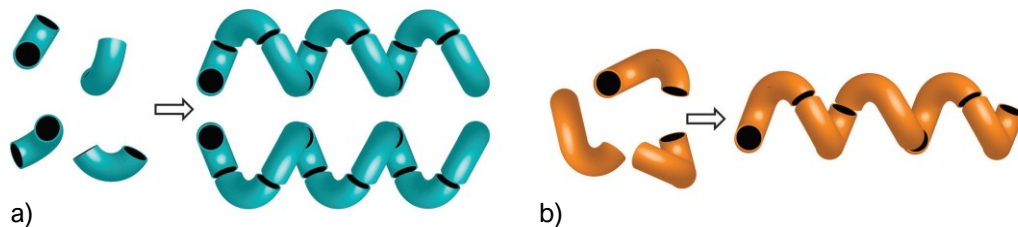


Figure 3.2. An a) achiral monomer can generate both screw senses; a b) chiral monomer generates a single screw sense.

Importantly, though, the biological efficiency is strictly related also to the conformational chirality proper of the secondary structure; it is therefore evident the need to determine and predict this kind of chirality.

A precise definition of conformational chirality was given in the early 90s, by Dodziuk,^{87,66a} who pointed out the incomplete definition in the CIP (Cahn, Ingold, Prelog) classification. The only necessary and sufficient condition for a molecule to be chiral is that it not be superimposable with its mirror image; so a molecule can be chiral but devoid of chiral centres. Indeed, chirality is associated with the presence of stereogenic centres, axes of chirality, double bonds, but it can arise also from the tri-dimensional disposition of compounds whose sp^3 - sp^3 bond rotation is energetically restricted.^{66d}

The energy barriers that separates conformational isomers, usually, is of the order of 5-20 kcal/mol, which corresponds to an extremely rapid interconversion, with rate constants ranging from 10^9 to 10^2 s⁻¹. In this case, the species cannot be separated and, at a given temperature, are referred to as *rotational isomers*, whose ratio composition is determined by the energy difference.⁸⁸

The *plane of chirality* is a further stereogenic element related to this concept. In the presence of four coplanar atoms, if the rotation about the single bonds is somewhat restricted, the system can generate two enantiomeric forms (or diastereomeric in the presence of further chirality elements). To distinguish the isomers, a *sequence-rule-preferred-path* should be established. For example, in Figure 3.3 the sequence is Y-X-A

⁸⁶ Le Bailly B. A. F., Clayden J., *Chem. Commun.* **2016**, 52, 4852-4863.

⁸⁷ Dodziuk H., *Tetrahedron: Asymmetry* **1990**, 1, 3, 171-186.

⁸⁸ Testa B., *Helv. Chim. Acta* **2013**, 96, 564-623.

(plus B, coplanar atom). Another atom, Z, is defined as *pilot atom*, and is the *point of view* from where the sequence is observed.

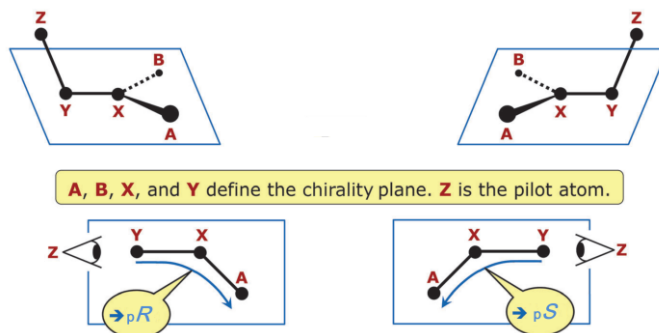


Figure 3.3. Pictorial definition of planar chirality.

Watching from the *pilot atom*, if the *sequence-preferred-path* Y-X-A traces a clockwise rotation, the configuration is denoted ${}_pR$; *vice versa*, ${}_pS$.

Planar chirality can be included, together with axial chirality, in a form of helicity, according to Prelog and Helmchen.^{66f} In this way, the forms of chirality are reduced to two macroclasses, each one defined by four internal, atomic, coordinates: the stereogenic centre and the helix (Figure 3.4).

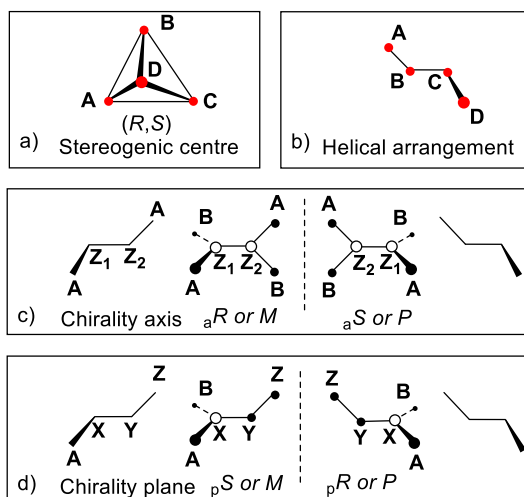


Figure 3.4. Four points three-dimensional chiral nonplanar arrangements and their configurational descriptors. a) Asymmetric tetrahedron (stereogenic centre ($A \neq B \neq C \neq D$)), b) helix, which is present in: c) the axis ($A \neq B$), and d) the plane of chirality ($A \neq B$).

Examples of molecules bearing planar chirality are cyclophanes, annulenes, *trans*-cycloalkenes, aryl metal complexes, quinol polymethylene ethers and so on. Figure 3.5 reports a few cases with the relative configuration assignment.

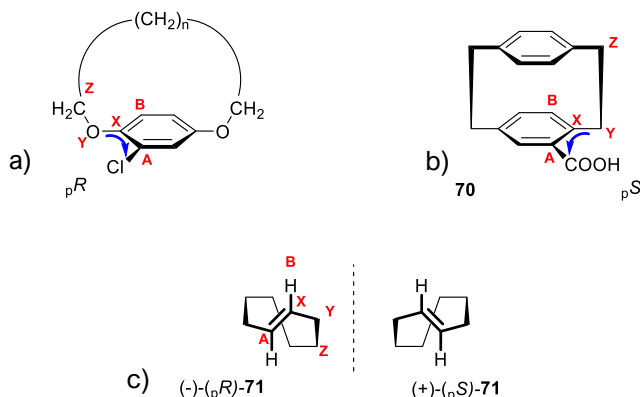


Figure 3.5. Chemical structure and planar chirality assignment in a) generic quinol polymethylene ether; b) [2.2]paracyclophanecarboxylic acid (**70**) and c) *trans*-Cyclooctene (**71**).

Planar chirality often arises in cyclic structures. Szumna indicated the lower energetical limit for the inversion barrier as $\Delta G \geq 10$ kcal/mol, as the critical parameter used to define such chirality; this corresponds to molecules that can only be detected *via* NMR (which reveals species with lifetimes exceeding 10^{-2} s).⁸⁹

Cyclochirality was first coined to describe cyclopeptides in 1974; it is referred to a number of chiral building blocks (usually α -amino acids) which are disposed in a clockwise or a counter-clockwise array, defining a directionality in the ring. The main peculiarity regards the presence of chiral units; for this reason, the inversion of the curvature does not cause racemization.^{66d}

The directionality of the amide bond adds another element of chirality, and the reversal of the peptide structure generates an isomer which is not topochemically related to its parent analogue. A cycloenantiomer is defined as an isomer derived by the reflection in a plane which results in the same distribution of the chiral centres, but reversed peptide bonds (Figure 3.6).⁹⁰

⁸⁹ Szumna A., *Chem. Soc. Rev.* **2010**, 39, 4274-4285.

⁹⁰ Goodman M., Chorev M., *Acc. Chem. Res.* **1979**, 12, 1, 1-7.

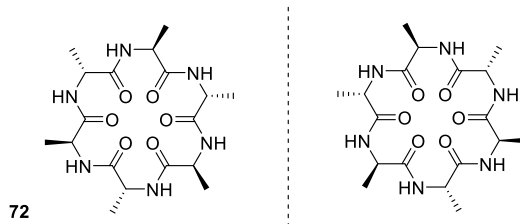


Figure 3.6. Cycloenantiomers of cyclohexaalanyl (**72**).

Similarly, a cyclodiastereoisomer is an isomer with the same distribution of chiral centres and opposite ring directionality, but not a mirror image of the parent cyclopeptide; lastly, a cycloretro-enantiomer is a cycloisomer with reversed sequence and each residue with opposite absolute configuration.

A cyclic amide, devoid of stereogenic centres, is conformationally chiral because of the directionality of the macroring; cyclic amides (with sufficiently high rotational barriers) exist in enantiomeric conformations.

For example, calix[3]amides have been reported, whose crystal structures showing a dimeric, self-complementary bowl-shaped structure, constituted by the two conformational enantiomers, which can also be referred to as inherently chiral.⁹¹

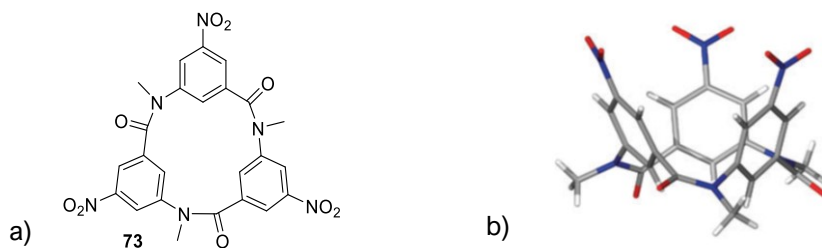


Figure 3.7. Inherently chiral a) *p*-nitrocalix[3]amide (**73**) and b) its X-ray structure. C, silver; N, blue; O, red; H, white.

It is noteworthy that, up to date, there is no systematic nomenclature reported in the literature for cyclic, tertiary amides, or its planar unit in linear oligoamides. In some cases, like the ones mentioned above (compound **73**), the system is assimilated to an inherently chiral one, but this definition is not omnicomprehensive.

⁹¹ Imabeppu F., Katagiri K., Masu H., Kato T., Tominaga M., Therrien B., Takayanagi H., Kaji E., Yamaguchi K., Kagechika H., Azumaya I., *Tetrahedron Lett.* **2006**, *47*, 413-416.

3.1.3 Conformational control and secondary assembly in linear peptoids

In this Paragraph, the conformational characteristics of the peptoid bond, as well as the structural assembly of linear oligopeptoids and the ways to control it, will be discussed in depth, as anticipated in Paragraph 1.3.

First of all, it should be noted that, to address the conformational issue, a few parameters must be considered. The molecular conformation is dictated by bond length, bond angle, and internal rotation angle. In a peptide, the *trans* conformation of the amide bond is preferred; in this structure, for convention, the angles defined by the C α are labelled ϕ for the N-C α bond, and ψ for the C α -C bond; ω defines the O-C-N angle (Figure 3.8 a)). In principle, ϕ and ψ could assume all the values between -180° and $+180^\circ$, but steric hindrance prohibits many values.⁹²

In a peptoid, the dihedral angles are defined in the same manner, plus the introduction of χ , defined as the C α -N-R angle (Figure 3.8 b)).

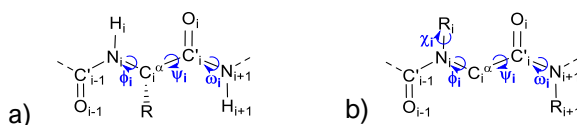


Figure 3.8. Internal rotation angles in a) peptide and b) peptoid.

Besides the mentioned structures of *Nspe*₈ and *Nspe*₉,²⁵⁻²⁷ efforts have been made to understand the dynamics of the folding of an oligopeptoid into a PPI-type structure. At first, it was hypothesized that such structure could be obtained only using α -branched side-chains, due to a pure steric factor.

Although monomers of *Nspe* and *Nrpe* are, by far, the most studied, oligomers up to dodecamers with various α -chiral branched side-chains have been synthesized. Circular dichroism was (and still is) the most useful tool to investigate chiral secondary structures of oligopeptoids. Generally, the spectra show a double minimum around 200 and 220 nm, plus a maximum at 190 nm, reminiscent of peptides' α -helix.

In *Nspe*₈,^{25c} the conformational maps showed that the minimum energy conformation was stabilized by the lack of detrimental steric interactions between the two N-C β carbons of the (*S*)-1-(phenylethyl) moiety, and the carbonyl oxygen of the residue

⁹² Ramachandran G. N., Ramakrishnan C., Sasisekharan V., *J. Mol. Biol.* **1963**, 7, 95-99.

i-1. This constraint forced the angles to $\omega \sim 0^\circ$, $\phi \sim -75^\circ$, $\psi \sim 170^\circ$, values compatible with a polyproline helix of type I; the peculiarity of this structure is the presence of *cis* amide bonds, favoured in peptoid oligomers, a right-handed twist, and a periodicity of three residues per turn.

Soon the main advantages of the peptoid helices emerged; first of all, the stability of the structure in pH ranges from 3 to 7, plus a thermal stability up to 65 degrees for a nonamer with alternating *Nspe/Nsce* (*N*-(*S*)-(1-carboxyethyl)glycine) residues (**74**) (pH 7).^{25a} Moreover, (*NsceNsceNspe*)₁₂ (**75**) resulted stable in aqueous media even in the presence of 8 M urea (a known chaotrope; urea disrupts the water's solvophobic force that causes folding).⁹³

What's interesting is that peptoid helices show properties similar to the peptide ones, like unfolding at extreme pH or temperature, but lack of the stabilization forces typical of the polypeptides, mainly H-bonding.

Further studies evidenced how the presence of an aromatic side-chain is not necessary to obtain the helix folding; in fact, oligomers constituted by α -chiral aliphatic side-chains, such as *Nsch* (*N*-(*S*)-(1-cyclohexylethyl)glycine) or *Nssb* (*N*-(*S*)-(2-butyl)glycine) showed CD spectra of increasing intensity according to the main chain length, like the aromatic counterparts. In this case as well, the headedness of the helix was predictable on the bases of the absolute configuration of the stereogenic centre (*R* gives a left-handed helix and *vice versa*). The structures were further elucidated thanks to 2D-NMR and X-ray.⁹⁴

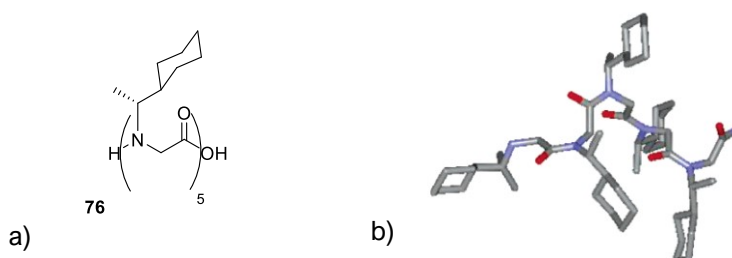


Figure 3.9. a) *Nrch*₅ (**76**) and b) its X-ray structure (perpendicular to the long axis of the helix). C, silver; N, blue; O, red.

⁹³ Sanborn T. J., Wu C. W., Zuckermann R. N., Barron A. E., *Biopolymers* **2002**, *63*, 12-20.

⁹⁴ Wu C. W., Kirshenbaum K., Sanborn T. J., Patch J. A., Huang K., Dill K. A., Zuckermann R. N., Barron A. E., *J. Am. Chem. Soc.* **2003**, *125*, 13525-13530.

According to a systematic study performed by Barron and co-workers,^{25b} to obtain a stable helix structure in a short peptoid oligomer, is sufficient to have either of the following conditions:

- 50% of α -chiral, or α -chiral aromatic side-chains;
- an α -chiral aromatic unit placed at the carboxy terminus;
- design of sequences with recurrent residues.

The steric hindrance, however, is not the only determining factor; carbonyl-carbonyl and carbonyl-aromatic $n \rightarrow \pi^*$ interactions play a key role in the *cis/trans* amide bond equilibrium. This interaction can manifest itself in two forms; $n \rightarrow \pi^*_{Am}$ (Am stands for amide) interaction, characterized by donation of electron density from a carbonyl oxygen lone pair into the π^* orbital of an adjacent amide carbonyl. In a peptoid, this can happen only in the case of a *trans* amide bond, because the geometrical constraints ($O_{i-1} \cdots C_i=O_i$ distance $\leq 3.2 \text{ \AA}$, angle = $109 \pm 10^\circ$) are satisfied. Secondly, the presence of an α -aromatic side-chain, $n \rightarrow \pi^*_{Ar}$ (Ar stands for aromatic) can stabilize *cis* amide bonds, *via* interaction between a backbone carbonyl and proximal side-chain aromatic group (geometrical constraints are carbonyl oxygen to ring centroid distance 2.8-3.8 \AA , dihedral angle between aryl and carbonyl planes $\leq 90^\circ$).⁹⁵

These interactions can be exploited to tune the *cis/trans* amide bond geometry equilibrium to generate folded structures. As demonstrated shortly after,²³ the ratio between the conformational isomers can be evaluated, as well as the rate of exchange, exploiting NMR techniques.

The exchange mechanism involves the shift of a lone pair if the nitrogen atom from a p_z orbital to a sp^3 orbital, followed by a rotation around the C-N bond. It was also observed that, for peptoid oligomers with more than two residues, like the Ac-*N*(butyl)-*N*(methyl)-*N*(benzyl)-NH₂ (**77**) analysed, the isomerization is strictly dependent on the conformation of the other amide bonds present in the molecule; the rate constants displayed a variation of a factor up to three, depending on the conformations of the links between the *N*-acetyl and the *N*-butyl and the *N*-butyl and the *N*-methyl residues. It should be noted that the *cis* average population in linear peptoids is estimated around 35%, while for proline amide bonds in acyclic peptides is less than 10%, meaning that for oligopeptoids all the isomers could be relatively high populated.

⁹⁵ Gorske B. C., Bastian B. L., Geske G. D., Blackwell H. E., *J. Am. Chem. Soc.* **2007**, *129*, 8928-8929.

This strategy, however, was immediately recognized to be not sufficient to induce proper folding in longer oligomers; in fact, the *cis/trans* free energy differences usually do not exceed 1 kcal/mol. Kirshenbaum and co-workers were then prompted to ideate a second, complementary strategy, that would intertwine with the idea of inducing stable, non-covalent interactions. The introduction of an *N*-aryl side-chain was firstly proposed in 2008.⁹⁶

The authors analysed computationally a set of *N*-methylacetanilides, varying the substitution at the phenyl moiety; the *cis/trans* free energy differences were evaluated, and found ranging from 1.05 to 3.55 kcal/mol, with a *trans* amide bond preference. Electron-withdrawing groups tended to decrease (and electron-donating groups increase) this preference.

The conformational analysis of *N*(phenyl)glycine hexamer **78** (Figure 3.10 a)) revealed that, for this oligomer, many isomers were not favoured due to steric clashes. Moreover, a helical secondary structure was observed (Figure 3.10 b)), displaying *trans* amide bonds, similarly to polyproline helix of type II (PPII). The modelled helix showed 3.1 residues *per* turn and a helical pitch of approximately 9 Å *per* turn. The spacing between repeating aromatic side-chains was demonstrated to be sufficiently large to preclude significant aromatic/aromatic interactions. This computed structure, observable in two enantiomeric forms, *i.e.* the right- and the left-handed helices, displayed an additional stabilization energy of about 2 kcal/mol, compared to all the other possible conformational isomers.

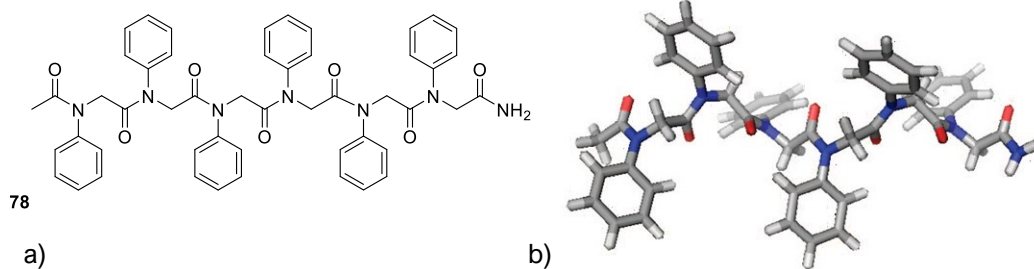


Figure 3.10. a) *N*(phenyl)glycine hexamer **78** and b) its lowest energy conformation (PPII type helix). C, silver; N, blue; O, red.

⁹⁶ Shah N. H., Butterfoss G. L., Nguyen K., Yoo B., Bonneau R., Rabenstein D. L., Kirshenbaum K., *J. Am. Chem. Soc.* **2008**, *130*, 16622-16632.

Further investigations by the Blackwell group⁹⁷ pointed out the strict interplay between $n \rightarrow \pi^*$ interactions, hydrogen bonding and steric interactions. Particularly, properly functionalized $N\alpha$ -chiral side-chains or the N -1-naphtylethyl side-chain can favour *cis* amide bonds, thanks to $n \rightarrow \pi^*_{C=O}$ /hydrogen bonding interactions and $n \rightarrow \pi^*_{Ar}$ /steric interactions, respectively.

The overall control of the amide bond isomerization and, consequently, the folding of the oligopeptoid can be accomplished only with an accurate consideration of all these intertwining factors.

3.1.4 Early studies on cyclic peptoids' conformational control

Despite the formal invention of cyclic peptoids only in the early 00s, as already mentioned, early studies about the synthesis and the conformational properties of cyclic oligomers of sarcosine (*i.e.* N -(methyl)glycine) were already known in the mid-70s.^{98,62,82a}

In particular, cyclic oligomers ranging from dimers to octamers were synthesized and analysed *via* NMR. The intrinsic rigidity of smaller macrocycles, such as the cyclotrimers and cyclotetramers, allowed the determination of the relative amide bond geometry; for example, cyclotrisarcosyl showed an all-*cis* conformation, assigned observing a C_3 -symmetry, with a single couple of doublets relative to the methylene protons, coalescing at 135 °C (corresponding to a barrier for the ring inversion of 20.1 kcal/mol). Cyclic trimers can only form if the three amides are in a *cis* geometry, and the ring shows a preference for a “crown” conformation, which implies that the three $C\alpha$ atoms are on one side of the plane defined by the N atoms (**79a**, Figure 3.11 a)). The alternative is the “boat” conformation, characterized by one $C\alpha$ atom lying on the opposite side of the two others relative to the plane of the N atoms (**79b**, Figure 3.11 b)).

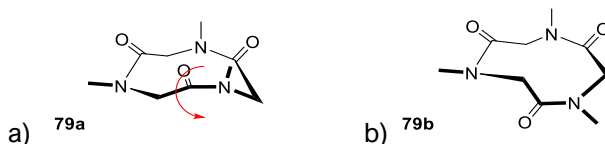


Figure 3.11. Cyclotrisarcosyl in a) crown conformation and b) boat conformation.

The assigned structure for the crown conformer was further validated by X-ray analysis.⁹⁹ The same architecture was later observed in cyclic trimers variously

⁹⁷ Gorske B. C., Stringer J. R., Bastian B. L., Fowler S. A., Blackwell H. E., *J. Am. Chem. Soc.* **2009**, *131*, 16555-16567.

⁹⁸ Sugihara T., Imanishi Y., Higashimura T., *Biopolymers* **1975**, *14*, 723-731.

decorated.¹⁰⁰ Particularly, as denoted also in prolinated compounds,¹⁰¹ the proportion of the crown conformer increases with the polarity of the solvent (acetone, acetonitrile, dimethylsulfoxide, water).

Cyclic tetramers usually display alternated *cis* and *trans* amide bonds, which results in a centrosymmetric structure, as foreseen *via* NMR and X-ray in cyclotetrasarcosyl,^{82a} and later on observed in *cyclo*-[Nbe]₄ (**8**) crystal structure,^{30a} and in *cyclo*-[Npm]₄ (**80**) (Figure 3.12).^{100b}

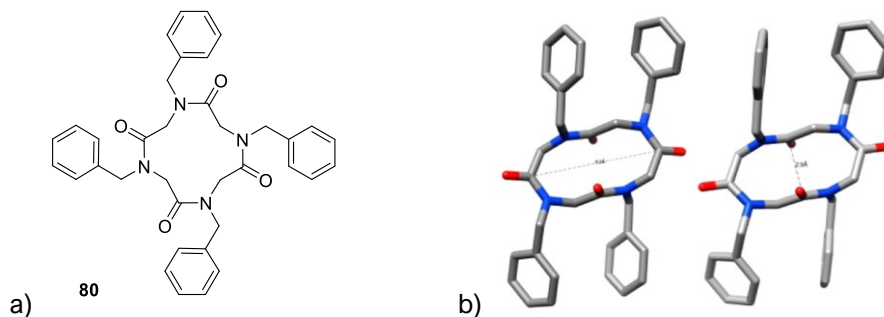


Figure 3.12. *cyclo*-[Npm]₄ (**80**) a) structure and b) X-ray in two projections. C, silver; N, blue; O, red.

Cyclic pentamers display rigid structures in the solution state, with *ttccc* amide geometry,^{62,82a,100b} and also cyclic hexamers⁵⁸ and octamers^{62,82a} can, depending on the type and arrangement of the side-chains, show a single or a prevalent conformational isomer in the solution state.

3.1.5 Purpose of the research

The literature regarding the conformational control in linear peptoids is quite vast, and it was shown that it is possible to obtain stable secondary structures in the solution state, tuning the conformation exploiting side-chains functionalities. In the case of cyclic oligomers this field is rather unexplored.

First of all, we clarified the stereochemical definitions for the peptoids' conformations, filling a gap in the existing literature. A planar chirality descriptor will be described, with a rigorous definition regarding peptoid monomers (Paragraph 3.2).

⁹⁹ Groth P., *Acta Chem. Scand. A* **1976**, *30*, 10, 838-840.

¹⁰⁰ a) Hioki H., Kinami H., Yoshida A., Kojima A., Kodama M., Takaoka S., Ueda K., Katsu T., *Tetrahedron Lett.* **2004**, *45*, 1091-1094; b) Culf A. S., Čuperlović-Culf M., Léger D. A., Decken A., *Org. Lett.* **2014**, *16*, 2780-2783.

¹⁰¹ a) Bats J. W., Fuess H., *J. Am. Chem. Soc.* **1980**, *102*, 6, 2065-2070; b) de Leeuw F. A. M., Altona C., Kessler H., Bermel W., Friedrich A., Krack G., Hull W. E., *J. Am. Chem. Soc.* **1983**, *105*, 8, 2237-2246.

Secondly, we tackled the conformational control in cyclic peptoids; of course, the added strain given from the macrocyclization gives rise to a preferred alternation of amide bond geometries, as stated above.

However, our aim was to induce the stereoselective synthesis of a single conformational isomer. This task was performed exploiting a central-to-conformational chirality induction on macrocycles ranging from tri- to octamers; firstly, adding a single enantiopure stereocenter on the backbone of the macrocycle (Paragraph 3.3), then on the side-chain(s) of the cyclic scaffold (Paragraph 3.4). I will describe both the syntheses and the conformational properties of such compounds.

The structures will be fully appreciated and extensively characterized *via* NMR, DFT computation, X-ray, UV-Vis and CD spectroscopy, when accessible.

3.2 Conformational chirality in cyclic peptoids and its specification¹⁰²

3.2.1 Results and discussion

The presence of a directionality imposed by the amide bond confers to cyclic peptoids, with a restrained rotational barrier for the macrocyclic inversion, the property of conformational chirality. However, as anticipated before (Paragraph 3.1.2), up to date the literature lacks systematic chirality descriptors for cyclic, conformationally stable, oligoamides. In Figure 3.13 is reported the general case of a cyclic peptoid; **A** and **B** are defined as conformational enantiomers, as they are the mirror image of each other, and can be interconverted through a complete inversion of all the amide bond planes (**C**), plus a 180° degree out-of-plane rotation. For comparison, **D** is included; in this molecule, only one amide bond plane is inverted, generating a conformational diastereoisomer.

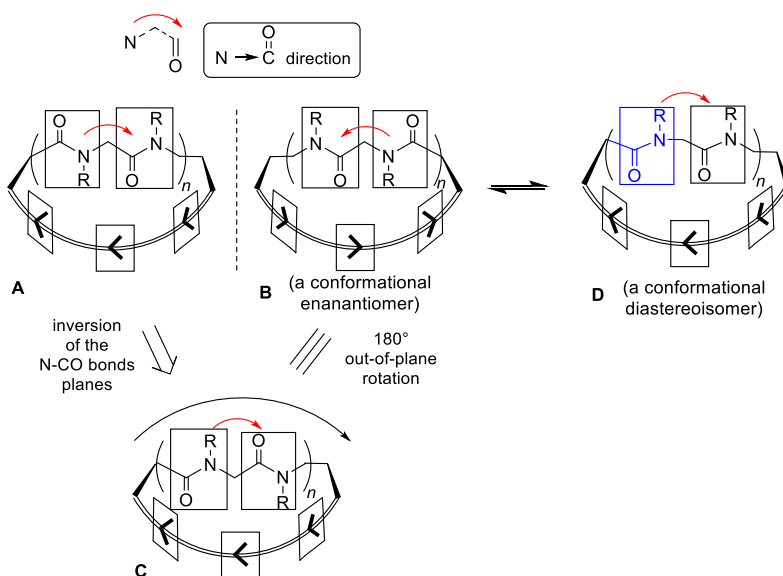


Figure 3.13. Conformational isomerism in a generic cyclic peptoid. **A** and **B**, conformational enantiomers. **D**, conformational diastereoisomers.

We proposed a nomenclature system based on the CIP rules, assuming the single amide bonds present in the macrocyclic scaffold as single planar units. A cyclic peptoid will then be viewed as constituted by several planar units, corresponding to the

¹⁰² D'Amato A., Schettini R., Della Sala G., Costabile C., Tedesco C., Izzo I., De Riccardis F., *Conformational Isomerism in Cyclic Peptoids and its Specification*. *Org. Biomol. Chem.* **2017**, *15*, 9932-9942.

number of monomers of the macroring. The complete description of the nomenclature will then include the assignment of the conformational chirality descriptor for all the amide units of the compound.

Starting with a tri-dimensional view of the peptoid unit (using the wedged bonds), “a preferred side of the plane [...] from which observation of the model is made in applying the Chirality Rule. [...] The most preferred atom of the set directly bound to plane, the leading atom or ‘pilot’ atom, [...] marks the preferred side of the plane” (as stated by Cahn, Ingold and Prelog).^{66e}

In Figure 3.14 is reported a generic assignment of the conformational chirality descriptor, using as model monomer a Npm unit.

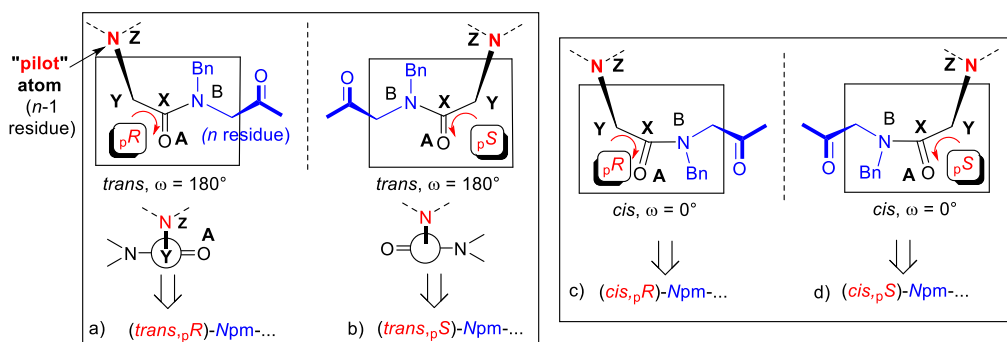


Figure 3.14. Assignment of the conformational chirality descriptor in a peptoid monomer.

The ‘pilot’ atom (*i.e.*: the highest priority atom outside the amide bond plane) is the nitrogen atom of the preceding ($n-1$) residue (marked as Z, in red; in case the nitrogen is in the same plane of the amide bond, the pilot atom is the carbonyl carbon linked to it). Then: “the sequence starts with the in-plane atom directly bound to the pilot atom, and continues, to and through other atoms, by way of succession of bonds along that in-plane path, which at each branch leads to the atom more preferred by the Standard Sub-rules”.^{66e}

The *sequence-rule-preferred* path Y-X-A defines the configuration (clockwise rotation: pR configuration; counter-clockwise rotation: pS configuration) of the amino acid n residue. The four *cis/trans*, pR/pS possible permutations of a hypothetical amide group are illustrated in Figure 3.14 a)-d). The only difference with the classic peptides conformational designation is the addition of the chirality plane descriptor.

In a cyclic system, the definition of the chirality descriptors continues following the usual N→C direction; the complete nomenclature of the molecule will then comprise

the *cis/trans*, ${}_pR/{}_pS$ stereochemical notation preceding the three letter code of the single residue; equal residues will be differentiated by increasing superscript numbers.

It is worth remembering that peptoid sequences are not palindromic, so it was necessary to define priority rules in the nomenclature. In the case of hetero-oligomeric chains, the sequence will start with the highest priority *N*-side-chain (according to the CIP priority rules). In the case of identical residues (cyclic homo-oligomers), the priority will be given to (*cis*, ${}_pR$) residues over the (*cis*, ${}_pS$), (*trans*, ${}_pR$), and (*trans*, ${}_pS$), in this order.

As examples, the full nomenclature assignment of *cyclo*-[Npm]₃ (**81**), *cyclo*-[Npm]₄ (**80**) and *cyclo*-[*cis*-NVal¹-*cis*-NPhe¹-*trans*-NVal²-*cis*-NPhe²-*cis*-NVal³-*trans*-NPhe³] (**49a**) follow.

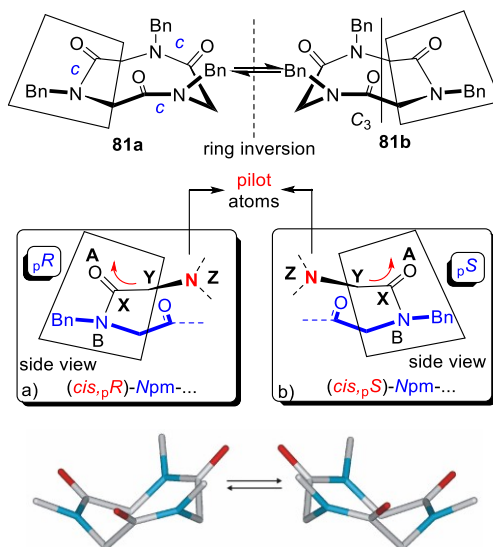


Figure 3.15. Configurational assignment in terms of planar chirality descriptors for *cyclo*-[Npm]₃ (**81**), plus minimum energy structures. In the enantiomeric models, hydrogen atoms and side-chains have been omitted for clarity. C, silver; N, blue; O, red.

The C_3 -symmetric cyclotribenzyl **81**^{100b} (already reported in the literature and synthesized by us to perform conformational stability experiments) is constituted by the two conformational enantiomers **81a** and **81b**, whose nomenclature will be *cyclo*-{[(*cis*, ${}_pR$)Npm]₃} and *cyclo*-{[(*cis*, ${}_pS$)Npm]₃}, respectively. The two can be interconverted by simultaneous inversion of the three amide bonds, which means that **81a** and **81b** are, at the same time, enantiomers and conformational isomers.

As already mentioned before, energy barriers are crucial to observe conformational chirality in the solution state; it should be also pointed out that the rotamers can be physically separated if their half-life τ is at least 1000 sec (16.7 min),^{103,86} which corresponds to a free energy barrier (ΔG^\ddagger) between the conformational isomers higher than 20 kcal/mol.¹⁰⁴

Moreover, conformational enantiomers can be detected using HPLC with chiral stationary phase. In this case, the separation is possible if two conditions are met; first, the analyte enantiomers form transient diastereomeric adsorbates with free energy differences of, at least, 0.025 kcal mol⁻¹;¹⁰⁵ secondly, the energetic barriers separating the two species is high enough ($\Delta G^\ddagger \geq 20$ kcal mol⁻¹) to avoid fast racemization^{86,103,104} in the eluent.

For compound **81**, we found no evidence of coalescence up to 120 °C,⁶¹ but we were not able to separate the racemic mixture of conformational enantiomers with chiral stationary phases (CHIRALPAK® AD, CHIRALPAK® AS-H, CHIRALPAK® AD-H, CHIRALCEL® OD-H).¹⁰⁶

Another method to evidence the presence of racemic mixture is adding a chiral solvating agent, causing the formation of two diastereomeric adducts, as already mentioned in Paragraph 2.2.1.2. As expected, the addition of the Pirkle's alcohol to a chloroform solution of **81** caused the splitting of the ¹H-NMR signals, attesting the presence of two enantiomers.

¹⁰³ a) Oki K., *Top. Stereochem.* **1983**, *14*, 1-81; b) Clayden J., Moran W. J., Edwards P. J., LaPlante S. R., *Angew. Chem. Int. Ed.* **2009**, *48*, 35, 6398-6401.

¹⁰⁴ Bringmann G., Mortimer A. J. P., Keller P., Gresser M. J., Garner J., Breuning M., *Angew. Chem. Int. Ed.* **2005**, *44*, 34, 5384-5427.

¹⁰⁵ Welch C. J., *ACS Cent. Sci.* **2017**, *3*, 8, 823-829.

¹⁰⁶ Elution conditions: 85:15 hexane:isopropanol; 1.0 mg/mL; flow: 1.0 mL min⁻¹, 220 nm. CHIRALPAK® AD chromatographic column (0.46 x 25 cm). The conditions of enantioseparation were varied increasing or decreasing the percentage of isopropanol $\pm 5\%$, varying the flux to 0.5 mL/min and changing the chromatographic column (CHIRALPAK® AS-H (0.46 x 25 cm), CHIRALPAK® AD-H (0.46 x 25 cm), CHIRALCEL® OD-H (0.46 x 25 cm)).

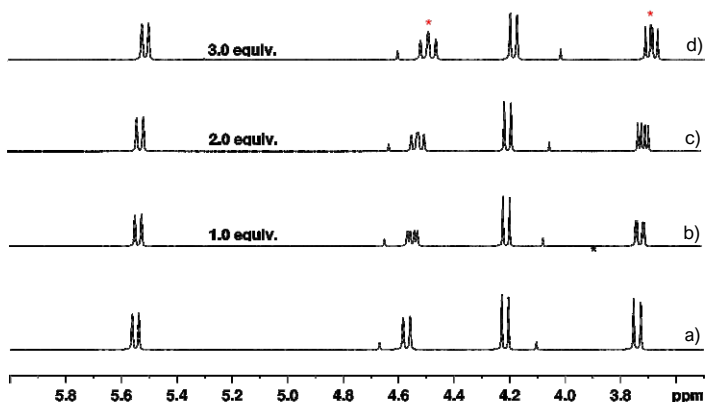


Figure 3.16. Quantitative step-wise addition of Pirkle's alcohol to **81**. $^1\text{H-NMR}$ (600 MHz, CDCl_3 , 298 K, 9.0 mM solution). 6.0-2.5 ppm expansion. Split signals are denoted with a red asterisk.

Cyclic tetramer **80**^{100b} is a conformationally *meso* compound, constituted by two topologically nonequivalent halves; the assigned nomenclature is *cyclo*-[(*cis*,*pR*)*Npm*¹-(*trans*,*pR*)*Npm*²-(*cis*,*pS*)*Npm*³-(*trans*,*pS*)*Npm*⁴].

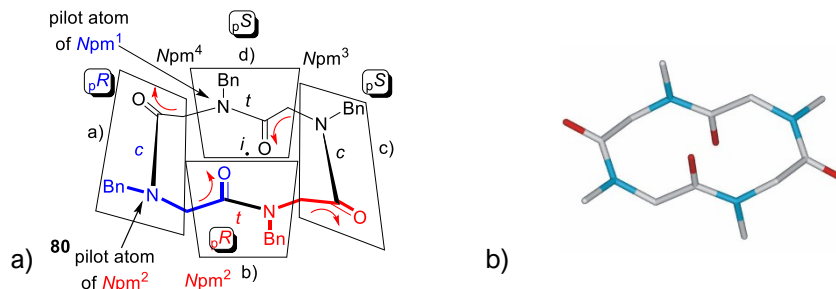


Figure 3.17. Configurational assignment in terms of planar chirality descriptors for *cyclo*-[*Npm*]₄ (**80**), plus minimum energy structure. In the reported model, hydrogen atoms and side-chains have been omitted for clarity. C, silver; N, blue; O, red.

In this case as well, no coalescence was observed up to 120 °C.

The addition of the Pirkle's alcohol clarified the nonequivalence of the two halves in the *S*₂-symmetric *cyclo*-[*Npm*]₄ **80**, using as chiral solvating agent.

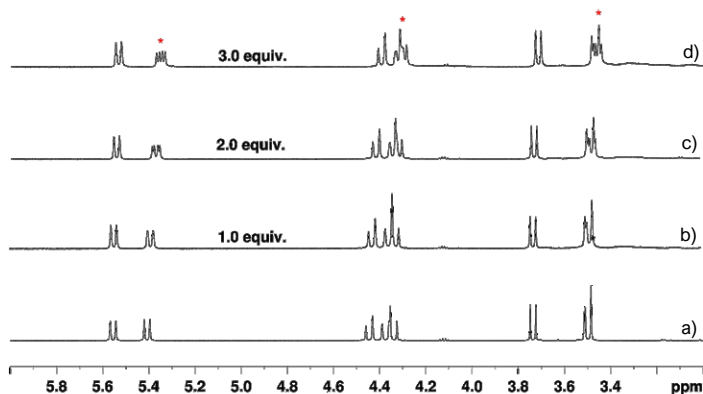


Figure 3.18. Quantitative step-wise addition of Pirkle's alcohol to **80**. $^1\text{H-NMR}$ (600 MHz, CDCl_3 , 298 K, 4.0 mM solution). 6.0-3.0 ppm expansion. Split signals are denoted with a red asterisk.

Regarding the hexamers, I already showed the splitting of the $^1\text{H-NMR}$ signals of **49a**, caused by the stepwise addition of the Pirkle's alcohol, in Paragraph 2.2.1.2 (Figure 2.21). Accordingly, the two forms are named: *cyclo*-[(*cis*,*pR*)NPh 1 -(*cis*,*pR*)NVal 1 -(*trans*,*pR*)NPh 2 -(*cis*,*pR*)NVal 2 -(*cis*,*pS*)NPh 3 -(*trans*,*pS*)NVal 3], **49a**, and its enantiomer (*ent*-**49a**) (~85%). The residual 15% was constituted by a mixture of conformational diastereoisomers, like **49c** *cyclo*-[(*cis*,*pS*)NPh 1 -(*cis*,*pR*)NVal 1 -(*trans*,*pS*)NPh 2 -(*cis*,*pR*)NVal 2 -(*cis*,*pS*)NPh 3 -(*trans*,*pS*)NVal 3] (and relative enantiomer), generated by the overturn of one or more amide bonds inversion.

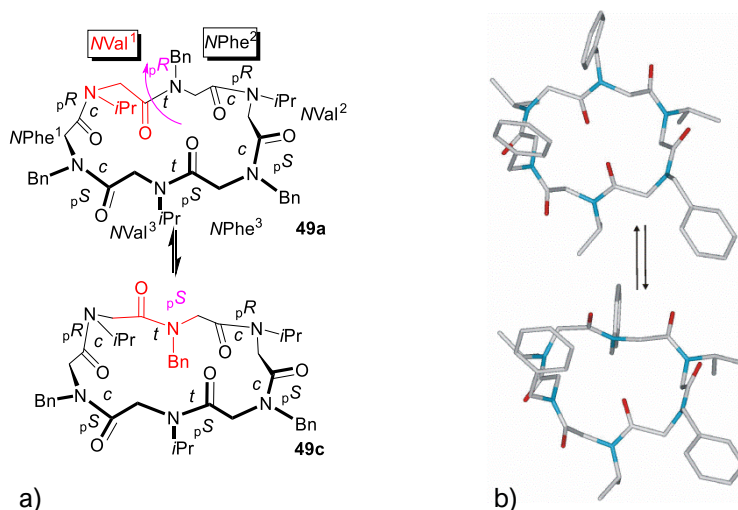


Figure 3.19. a) Assignment of the conformational chirality nomenclature of **49a** and its conformational diastereoisomer **49c** (the respective enantiomers are not shown), plus b) their relative minimum energy structures. C, silver; N, blue; O, red.

Although, also in this case, it was not possible to separate the enantiomers, we were able to detect both **49a** and *ent*-**49a** in the unit cell of the crystal packing. I already showed **49a** solid state arrangement in Figure 2.18; in Figure 3.20 is reported the whole crystallographic cell, displaying both the enantiomers, linked in pairs through an intermolecular inversion centre.

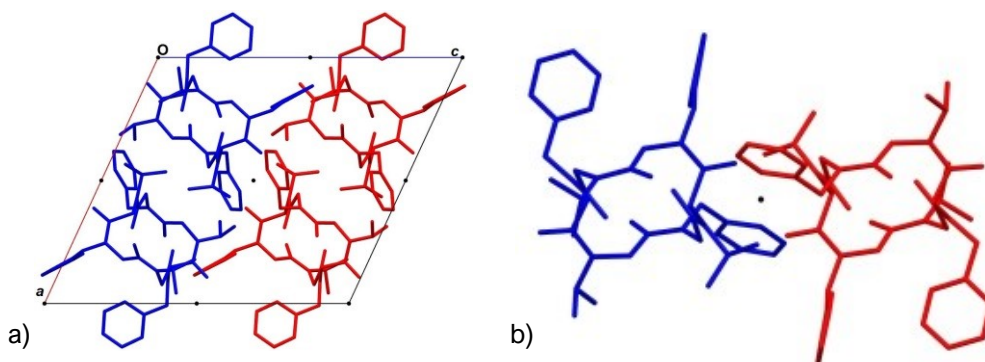


Figure 3.20. a) Crystal packing of **49a** as viewed along the *b* axis. Red and blue molecules represent enantiomeric pairs; crystallographic inversion centers are indicated by black dots. Chloroform molecules and hydrogen atoms have been omitted for clarity. b) View of a single pair of enantiomers as related by the inversion center. C, silver; N, blue; O, red.

The formation of rigid metal complexes, for example for cyclic hexamers, can generate mixtures of conformational stereoisomers. Ion-dipole electrostatic forces can stiffen the structure of the macrocycle, resulting in a raise of the coalescence temperature up to 150 °C.^{30a} The all-*trans* complex [**49a**·Na]⁺, already mentioned in Chapter 2, is chiral, and the two conformational enantiomers can be interconverted *via* ring inversion (Figure 3.21).

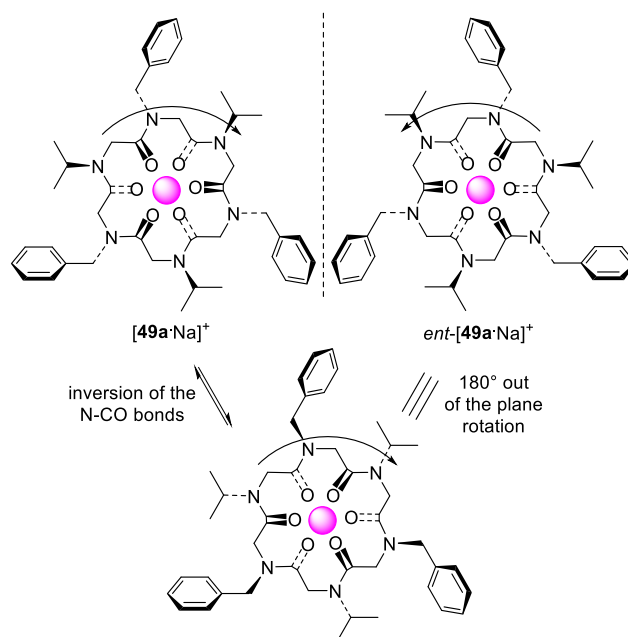


Figure 3.21. The metalation of a cyclic peptoid generates a mixture of conformational enantiomers. $[49a\cdot Na]^+$ and its enantiomer are related by inversion of the amide bonds present in the macrocyclic ring plus 180° out-of-the-plane rotation.

The fact that we were not able to physically separate any of the racemic mixture, and the seek for an enantioselective process towards a single conformational stereoisomer, prompted us to conceive a selective synthesis to obtain macrocycles with a ring inversion barrier higher than 22 kcal/mol.

In Paragraph 3.3 and 3.4 two central-to-conformational chirality transfer approaches that allowed us to perform this task will be presented.

3.2.2 Experimental section

3.2.2.1 General methods

Refer to Paragraph 2.2.3.1.

Chiral HPLC analyses were performed using JASCO LC-NET II/ADC model with a JASCO PU-4180 Plus Pump and a Photo Diode Array UV detector JASCO MD-4015, set at 220 nm or 254 nm.

For the VT NMR experiments, refer to Paragraph 2.2.3.7; for the Pirkle experiments, refer to Paragraph 2.2.3.8.

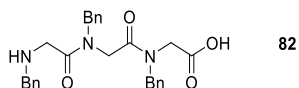
X-ray analyses were performed by prof. C. Tedesco, Dpt. of Chemistry and

Biology “A. Zambelli”, Univ. of Salerno.

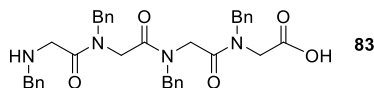
DFT calculations were performed by prof. C. Costabile, Dpt. of Chemistry and Biology “A. Zambelli”, Univ. of Salerno.

3.2.2.2 Synthesis of linear peptoids **82-83**

Refer to Paragraph 2.2.3.2. The synthesis was performed using the sub-monomer protocol, on a 0.400 g 2-chlorotrytil chloride resin batch (1.63 mmol g⁻¹), using commercially available benzylamine; purity of the linear oligomers ≥ 95%.



H-[Npm]₃-OH (**82**): white amorphous solid, 0.180 g, 100%; *t_R*: 6.6 min. ES-MS *m/z*; 460.2 [M + H]⁺.



H-[Npm]₄-OH (**83**): white amorphous solid, 0.250 g, 100%; *t_R*: 8.2 min. ES-MS *m/z*; 607.3 [M + H]⁺.

3.2.2.3 Synthesis of cyclic peptoids **80-81**

Refer to Paragraph 2.2.3.3.

The cyclization reaction was performed on a 0.150 mmol scale of the linear oligomers, which were dissolved in 5.0 mL of dry DMF and added by a syringe pump in 6 hours to the reaction mixture. The crude **81** was purified on flash silica gel; conditions: 80% – 50% A (A: petroleum ether; B: ethyl acetate). The crude cyclic peptoid **80** was dissolved in hot acetonitrile and precipitated by slowly cooling the acetonitrile solution.

cyclo-[Npm]₃ (**81**): white amorphous solid, 0.0340 g, 35%; *t_R*: 9.0 min. ¹H-NMR (400 MHz, CDCl₃) δ: 7.40-7.30 (15H, m), 5.54 (3H, d, *J* 14.4 Hz), 4.58 (3H, d, *J* 15.5 Hz), 4.21 (3H, d, *J* 14.4 Hz), 3.73 (3H, d, *J* 15.5 Hz). ES-MS *m/z*; 442.2 [M + H]⁺.

cyclo-[Npm]₄ (**80**): white amorphous solid, 0.115 g, 95%; *t_R*: 11.6 min. ¹H-NMR (600 MHz, CDCl₃) δ: 7.32-7.08 (20H, m), 5.56 (2H, d, *J* 14.4 Hz), 5.41 (2H, d, *J* 14.9 Hz), 4.45 (2H, d, *J* 17.2 Hz), 4.38 (2H, d, *J* 17.2 Hz), 4.34 (2H, d, *J* 17.2 Hz), 3.74 (2H, d, *J* 14.4 Hz), 3.50 (2H, d, *J* 14.9 Hz), 3.49 (2H, d, *J* 17.2 Hz). ES-MS *m/z*; 589.3 [M + H]⁺.

3.3 Central-to-conformational chirality transfer. Stereogenic centre present in the backbone¹⁰⁷

In this Paragraph, I will describe the syntheses and the conformational properties of several cyclopeptoids, including a residue of *N*(Bn)Ala. We hypothesized that the introduction of a single stereocenter on the backbone of the macrocycle could raise the energy for the macroring's inversion, thanks to the added steric hindrance.

Moreover, for each compound, we prepared an analogue bearing a unit of *N*pm (*N*-(phenylmethyl)glycine) (instead of *N*(Bn)Ala) in the corresponding position, to understand the effect of the methyl unit on the conformational order. Each molecule was thoroughly characterized via NMR, DFT calculations, UV-Vis, CD, and, when possible, X-ray diffraction analysis.

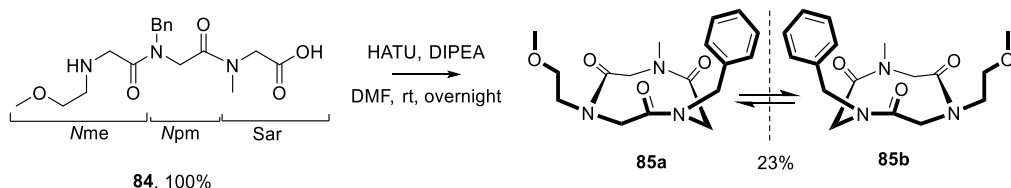
Note: diastereoisomers are indicated with progressive numbering, while conformational isomers are indicated with progressive lettering.

Chiral *N*(Bn)Ala residue is indicated in red.

3.3.1 Results and discussion

3.3.1.1 Cyclic trimers

We started our investigation with the smallest set of macrocycles; in particular, we chose the linear oligomer H-[*N*mme-*N*pm-Sar]-OH (**84**) as a starting point. The presence of different side-chains eased the ¹H-NMR assignment. As expected, the cyclization gave a racemic mixture of the two crown conformational enantiomers *cyclo*-[(*cis*,*pR*)*N*mme-(*cis*,*pR*)*N*pm-(*cis*,*pR*)Sar] (**85a**) and *cyclo*-[(*cis*,*pS*)*N*mme-(*cis*,*pS*)*N*pm-(*cis*,*pS*)Sar] (**85b**).



Scheme 3.1. Cyclization of H-[*N*mme-*N*pm-Sar]-OH (**84**) gives the racemic mixture **85a/b**.

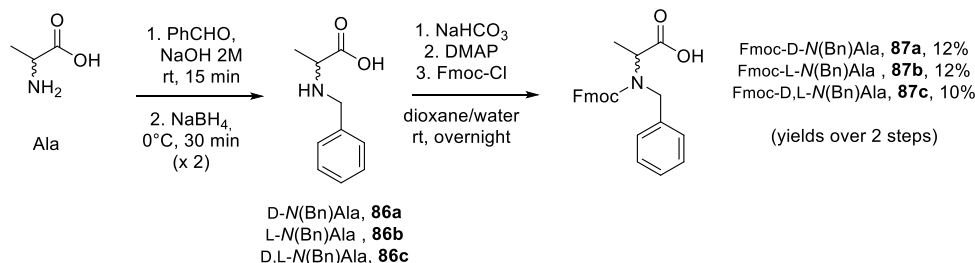
The energy barrier for the ring inversion, calculated *via* VT NMR,⁶¹ was $\Delta G^\ddagger = 17.9$ kcal/mol ($T_c = 383$ K); this relatively low value hampered the separation *via* chiral

¹⁰⁷ D'Amato A., Pierrri G., Costabile C., Della Sala G., Tedesco C., Izzo I., De Riccardis F., *Cyclic Peptoids as Topological Templates: Synthesis via Central to Conformational Chirality Induction*. *Org. Lett.* **2018**, *20*, 640-643.

HPLC. The presence of a racemic mixture, similarly to the examples shown in Paragraph 3.2.1, was spectroscopically confirmed with the addition of a chiral solvating agent to a chloroform solution of **85a/b** (spectra not shown).

The substitution of the *N*-(phenylmethyl)glycine residue with an *N*-benzyl alanine unit affected dramatically the conformational stability of the trimeric scaffold.

First, we prepared the necessary monomer, according to literature procedures,¹⁰⁸ starting from alanine.



Scheme 3.2. Synthesis of the Fmoc-*N*(Bn)Ala monomer (**87a-c**).

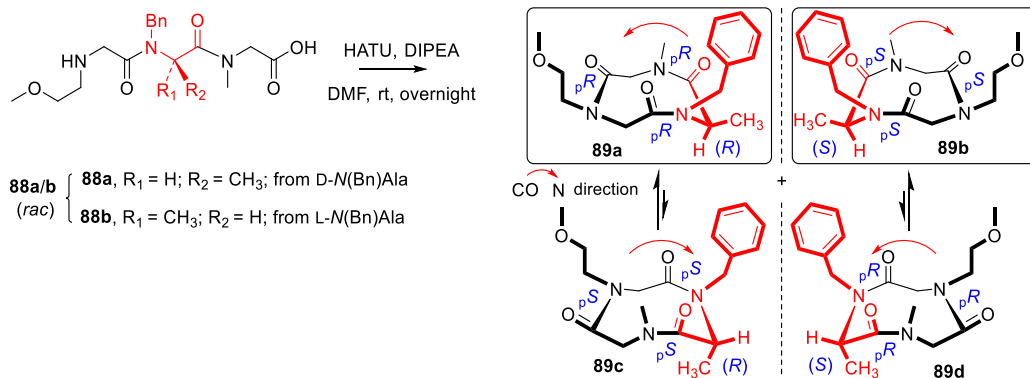
The incorporation of D-*N*(Bn)Ala in the linear oligomer, exploiting a mixed sub-monomeric/monomeric synthesis approach, directed the cyclization of the linear oligomer **88a** towards the preferential formation of *cyclo*-[(*cis*,*pR*)*N*me-(*cis*,*pR*)D(Bn)Ala-(*cis*,*pR*)Sar] (**89a**) with the alanine methyl group in the pseudo-equatorial position.¹⁰⁹

Correspondingly, the incorporation of the L-amino acid derivative led to the mirror image cyclic product, and, lastly, the use of the racemic monomer **87c** caused the formation of both the conformational stereoisomers in equal ratio (Scheme 3.3).

Theoretically, the conformational diastereoisomers **89c/d**, with the methyl group in pseudo-axial position could have been obtained, but no trace of these derivatives was detected *via* NMR; the accurate determination of the structure was inferred thanks to two-dimensional analyses.

¹⁰⁸ a) Huy P. H., Koskinen A. M. P., *Org. Lett.* **2013**, *15*, 20, 5178-5181; b) Meli A., Gambaro S., Costabile C., Talotta C., Della Sala G., Tecilla P., Milano D., Tosolini M., Izzo I., De Riccardis F., *Org. Biomol. Chem.* **2016**, *14*, 38, 9055-9062.

¹⁰⁹ The stability of this product was also assessed *via* VT NMR experiments; no coalescence was observed up to 120 °C (300 MHz, C₂D₂Cl₄, 5.0 mM solution).



Scheme 3.3. Enantioselective synthesis of the cyclotrimeric derivatives **89a/b**. Yields: **88a**, 92%; **88b**, 73%; **88a/b**, 97%; **89a**, 65%; **89b**, 69%; **89a/b**, 56%.

The key ROE cross-correlation among the three intra-annular protons allowed us to confirm the formation of only **89a/b**; this result was later corroborated by DFT calculations. Enantiomers **89a/89b** ($E = 0$ kcal/mol in DMSO) showed much higher stability than their conformational diastereoisomers **89c/89d** ($\Delta E = 6.9$ kcal/mol in DMSO).

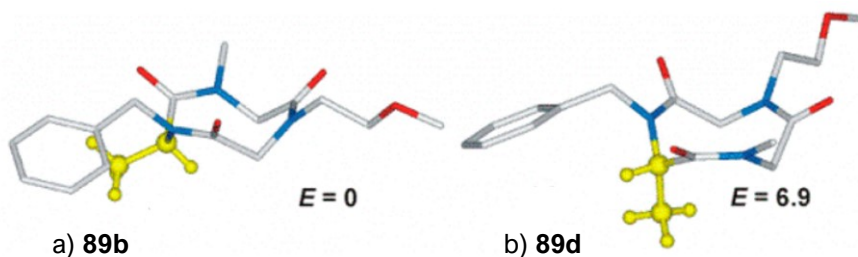


Figure 3.22. Minimum energy structures and relative internal energies (kcal/mol) of conformational diastereoisomers **89b/d**. C, silver; N, blue; O, red; CH₃, yellow.

The chiral HPLC analysis, as expected, gave a perfectly superimposable elution profile of the racemic mixture with the enantiopure compounds (Figure 3.23 a)); moreover, conformational enantiomers **89a** and **89b** showed opposite CD spectra (Figure 3.23 b)).

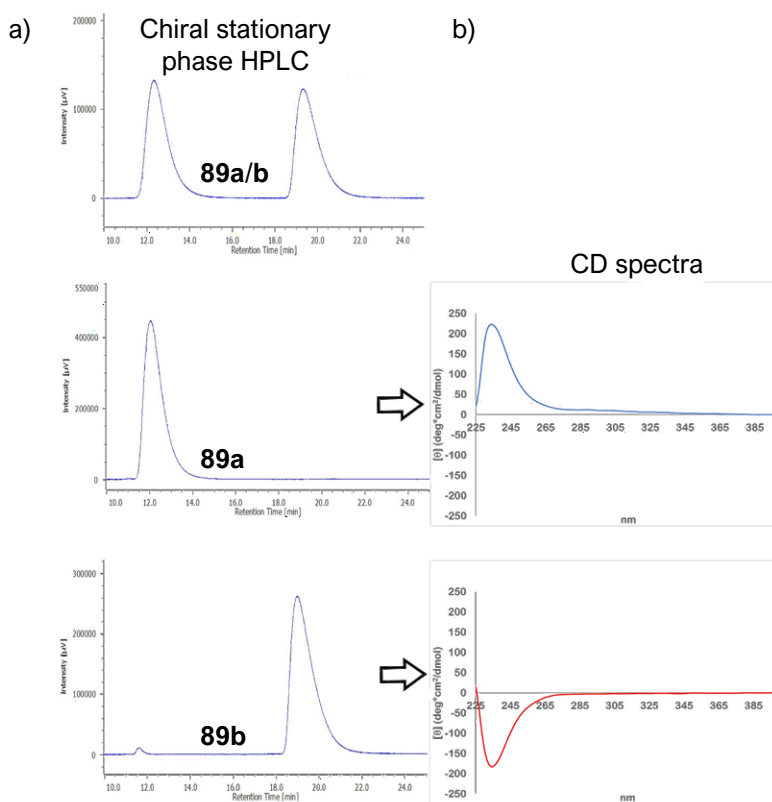


Figure 3.23. a) Resolution of the racemic mixture **89a/b**, in comparison with chiral non-racemic **89a** and **89b**. CHIRALPAK AD-H, 85:15 hexane:isopropanol, 1 mL min⁻¹, 220 nm. b) Respective CD spectra (CHCl₃).

We were also able to obtain single crystals suitable for X-ray diffraction analysis from both the single enantiomers, and their racemic mixture (from slow evaporation of a 1:1 hexane:ethyl acetate solution, or slow diffusion of hexane vapors into an ethyl acetate solution of the peptoids). The enantiopure compounds crystallized as enantiomorph crystals in the space group $P2_12_12_1$ and from the special arrangement was possible to confirm both the absolute stereochemistry and the conformational chirality assignment. On the other hand, the racemic mixture provided crystals in space group $P-1$ with two crystallographically independent molecules in the asymmetric unit. The CH₂⋯OC hydrogen bonding caused, in all three cases, the assembling in a *T*-shape arrangement.

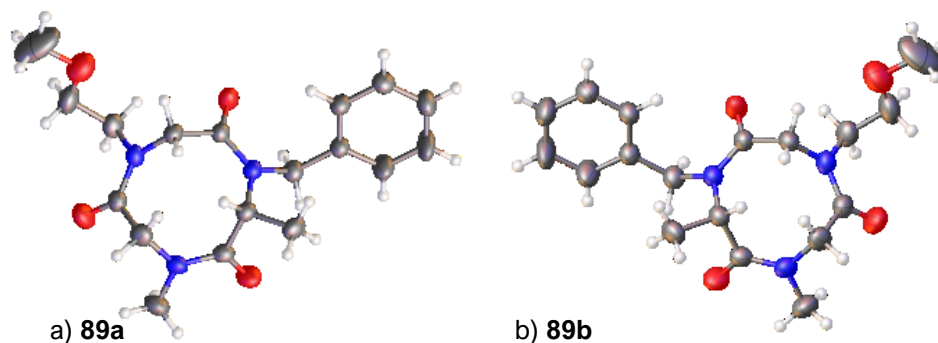
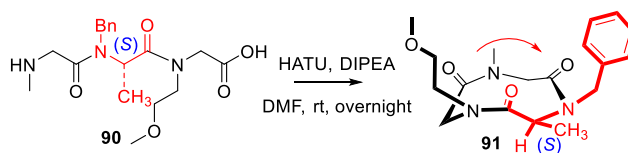


Figure 3.24. X-ray molecular structures of the enantiomorph cyclic peptoids a) **89a** and b) **89b**. Thermal ellipsoids are drawn at 30% probability level. C, silver; N, blue; O, red.

Peptoid sequences, similarly to peptide ones, are not palindromic; cyclization of linear reverse sequences leads to constitutional cycloisomers. We prepared H-[Sar-L(Bn)Ala-Nme]-OH (**90**), a retro-inverso isomer of **88a**; its cyclization gave the cyclotripeptoid **91**, *cyclo*-[(*cis,pR*)Sar-(*cis,pR*)L(Bn)Ala-(*cis,pR*)Nme], (Scheme 3.4), which is defined as the *cycloretro-enantiomer* of **89a**.⁹⁰ Compound **91** is topologically equivalent to **89a**, even though they show a stereocenter with opposite absolute configuration. In conformationally stable peptoid scaffolds the backbone stereogenic center or their primary sequences are powerful tools meant to control the absolute three-dimensional orientation of the side-chains.



Scheme 3.4. Synthesis of **91** (cycloretro-enantiomer of **89a**).

Conformationally stable cyclic peptoids constitute a promising platform for molecular recognition. We tested **89b** capability to complex benzylammonium tetrakis[3,5-bis(trifluoromethyl)phenyl]borate (**92**) in a ¹H-NMR experiment. The crown conformation of our effector oriented the three carbonyls in a cone shape that allowed the formation of a complex in fast equilibrium with the free host on the NMR time scale.

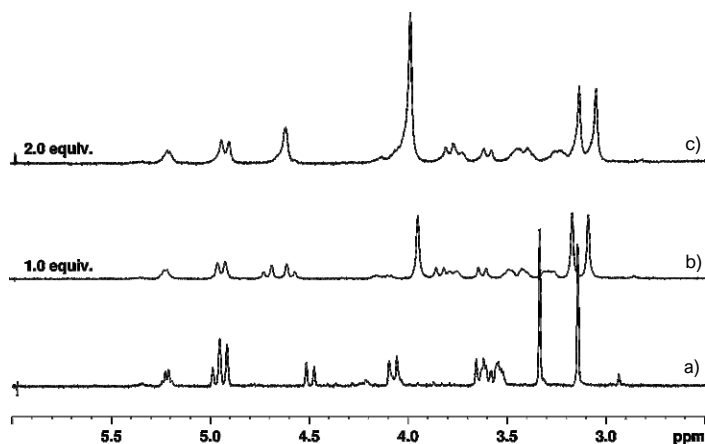
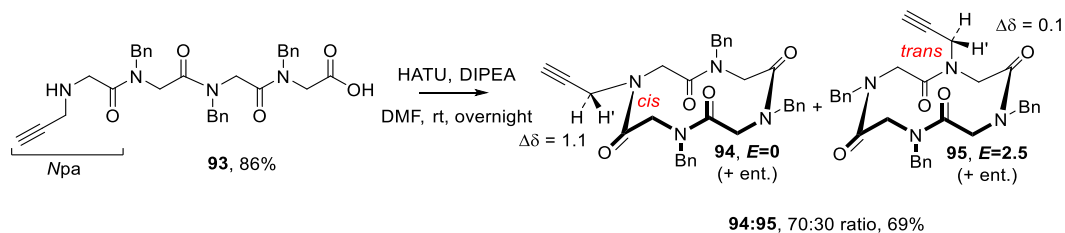


Figure 3.25. Stepwise addition of $\text{BnNH}_4^+\text{TFPB}^-$ to **89b**. $^1\text{H-NMR}$ (400 MHz, CDCl_3 , 298 K). 6.0-2.5 ppm expansion.

3.3.1.2 Cyclic tetramers

We chose as model tetrameric compound *cyclo*-[Npa-Npm₃] (Npa = *N*-(propargyl)glycine). The cyclization of the linear oligomer H-[Npa-Npm₃]-OH **93** afforded an inseparable mixture of conformational *ctct* diastereoisomers **94/95** (plus the respective enantiomers). The spectroscopic analyses provided full assignment of the structures, with 70% of preference for the diastereoisomer with the propargyl moiety on the *cis* amide bond (already reported in the literature).¹¹⁰ As reported in Chapter 2, the relative amide bond geometry of the four residues was inferred thanks to the diastereotopic CH_2 $\Delta\delta$ of the side-chains, and then corroborated by comparison of calculated internal energies (**94**, $E = 0$ kcal/mol; **95**, $\Delta E = 2.5$ kcal/mol; CHCl_3).

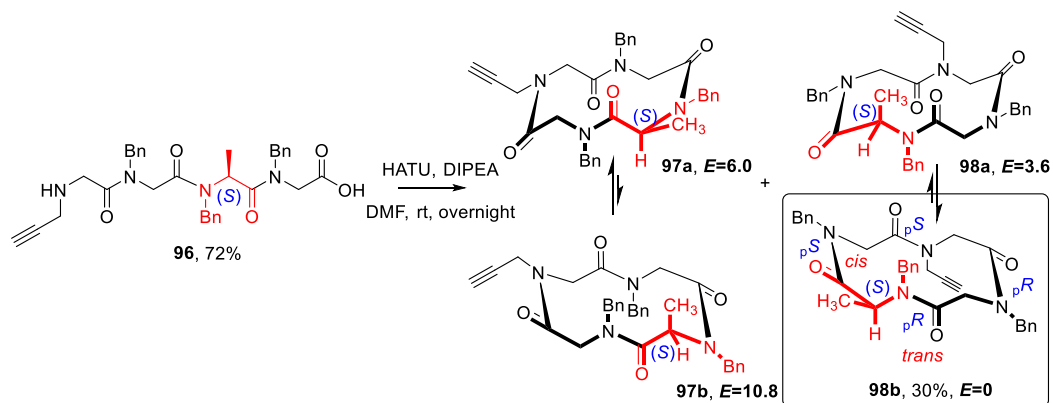


Scheme 3.5. Synthesis of cyclic tetramers **94/95**. $\Delta\delta$ of the propargyl side-chain reported in ppm. Internal energies reported in kcal/mol (CHCl_3).

¹¹⁰ Tedesco C., Macedi E., Meli A., Pierri G., Della Sala G., Drathen C., Fitch A. N., Vaughan G. B. M., Izzo I., De Riccardis F., *Acta Cryst. B* **2017**, 73, 399-412.

The introduction of the L(Bn)Ala unit in H-[Npa-Npm-L(Bn)Ala-Npm]-OH (**96**) switched completely the diastereoselection towards the product with the propargyl residue on the *trans* amide bond.

Of the four possible isomers, only *cyclo*-[(*trans*,*pR*)L(Bn)Ala-(*cis*,*pS*)Npm-(*trans*,*pS*)Npa-(*cis*,*pR*)Npm] **98b** was, in fact, detected (¹H-NMR analysis), with the bulky methyl group in the pseudo-equatorial position, indicating the remarkable stereodirecting effect of the alanine unit. Assignment of the possible diastereoisomers with *trans*-propargyl group (**98a/b**) was accomplished *via* DFT.



Scheme 3.6. Enantioselective synthesis of cyclotetramer **98b**. The four possible stereoisomers are depicted, with the relative computed internal energies (kcal/mol, CHCl₃).

Cyclic tetramer **98b** was able to complex BnNH₄⁺TFPB⁻ as well (spectra not shown). This result was remarkable, as the only other case of cyclic tetramers molecular recognition is related to benzene.¹¹¹

Moreover, both the free cyclic tetramers showed no sign of coalescence up to 120 °C (300 MHz, C₂D₂Cl₄, 5.0 mM solution), corroborating the exceptional stability of the tetrameric scaffolds.

3.3.1.3 Cyclic hexamers

The enlargement of the macrocyclic cavity had an overall detrimental effect on the conformational control. In order to appreciate the effect of the *N*(Bn)Ala residue in the presence of different side-chains, we synthesized two oligomeric cyclic derivatives. One including one chiral and five *Npm* residue (*cyclo*-[Npm₄-L(Bn)Ala-Npm] (**100**), from linear

¹¹¹ Sugihara T., Imanishi Y., Higashimura T., *Biopolymers* **1975**, *14*, 733-747.

H-[Npm₄-L(Bn)Ala-Npm]-OH (**99**), and one bearing alternated isopropyl and benzyl *N*-side-chains, including a *N*(Bn)-Ala residue (*cyclo*-[Npm-NVal-L(Bn)Ala-NVal-Npm-NVal] (**102**) from linear H-[Npm-NVal-L(Bn)Ala-NVal-Npm-NVal]-OH (**101**). The corresponding cyclic hexamers, devoid of the *N*(Bn)Ala residue were available in our laboratory and have been described in Chapter 2 (compounds **52** and **49**, respectively).

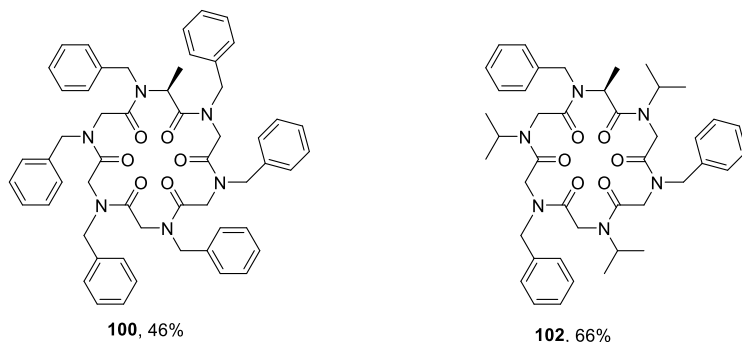


Figure 3.26. Structures of cyclohexamers **100** and **102**.

In both the cases we observed multiple conformations in slow equilibrium on the NMR time scale; however, addition of one equivalent of NaTFPB induced the formation of 1:1 complexes with Na⁺ (Figure 3.27, b) and d)). As previously reported,^{58,30a} the cyclic peptoids complexes [100·Na]⁺ and [102·Na]⁺ displayed an all-*trans* amide bond conformation, with relatively high apparent association constants (log *K_a* = 4.7, -Δ*G*⁰ = 6.4 kcal/mol, and log *K_a* = 4.4, -Δ*G*⁰ = 6.0 kcal/mol, respectively), and extended chirality (evidenced by CD spectra, not shown).

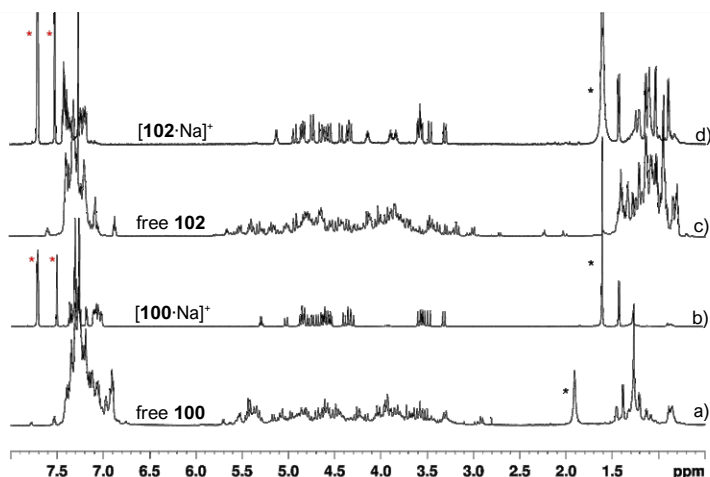


Figure 3.27. ¹H-NMR spectra of cyclic hexamers **100** and **102** (a, c) and their relative complexes [100, 102·Na]⁺ (b, d) (600 MHz, CDCl₃, 5.0 mM). Water or solvent impurities are labelled with a black asterisk. TFPB⁻ signals are labelled with a red asterisk.

DFT calculations disclosed the conformational chirality assignment of the two complexes; as easily appreciated, the complexes with the methyl group in pseudo-axial position were unfavoured ($\Delta E = + 2.4$ kcal/mol and $+ 2.1$ kcal/mol for $[\mathbf{100a}\cdot\text{Na}]^+$ and $[\mathbf{102a}\cdot\text{Na}]^+$, respectively, Figure 3.28). The planar amide configurations of the chiral complexes $[\mathbf{100}\cdot\text{Na}]^+$ and $[\mathbf{102}\cdot\text{Na}]^+$ were consequently assigned as: *cyclo*- $[(trans,{}_pR)L(\text{Bn})\text{Ala}-(trans,{}_pS)\text{Npm}-(trans,{}_pR)\text{Npm}-(trans,{}_pS)\text{Npm}-(trans,{}_pR)\text{Npm}-(trans,{}_pS)\text{Npm}]$ and *cyclo*- $[(trans,{}_pR)L(\text{Bn})\text{Ala}-(trans,{}_pS)\text{NVal}-(trans,{}_pR)\text{Npm}-(trans,{}_pS)\text{NVal}-(trans,{}_pR)\text{Npm}-(trans,{}_pS)\text{NVal}]$, respectively.

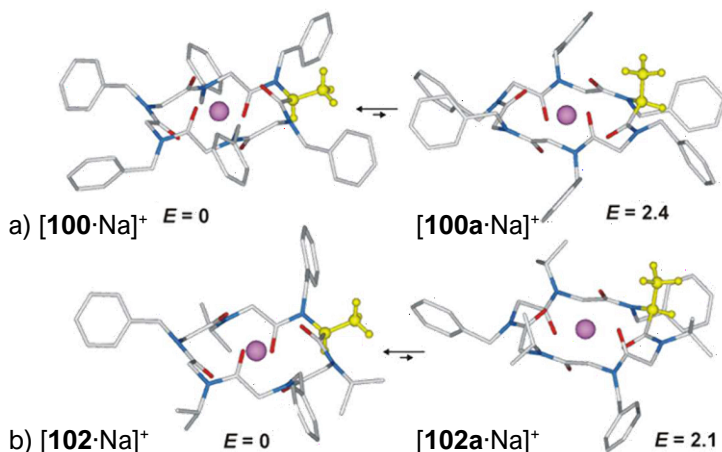


Figure 3.28. Minimum energy structures of chiral metal complexes a) $[\mathbf{100}\cdot\text{Na}]^+ / [\mathbf{100a}\cdot\text{Na}]^+$ and b) $[\mathbf{102}\cdot\text{Na}]^+ / [\mathbf{102a}\cdot\text{Na}]^+$ and their respective internal energies (kcal/mol). C, silver; N, blue; O, red; CH₃, yellow; Na, magenta.

Finally, we tested the molecular recognition capability of cyclic hexamer **100**. The macrocycle complexed efficiently $\text{BnNH}_4^+\text{TFPB}^-$, forming a 1:2 host:guest stoichiometry complex (in slow equilibrium with the free host on the NMR time scale), whose association constant was assessed as $\log K_a = 6.8 \text{ M}^{-2}$ ($-\Delta G^0 = 9.3$ kcal/mol).

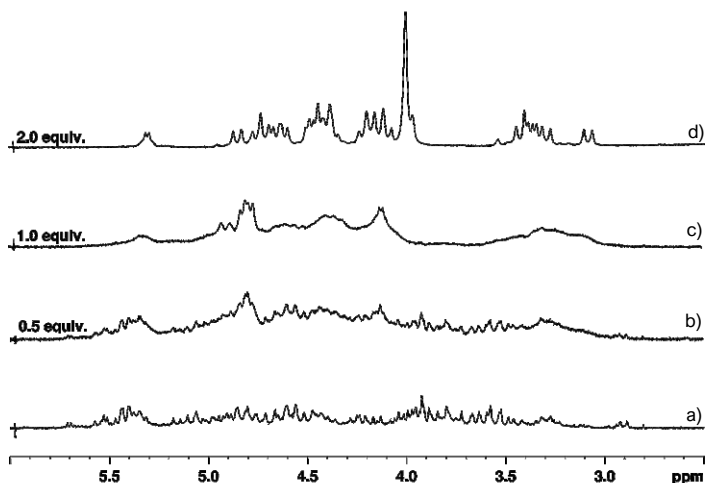


Figure 3.29. Stepwise addition of $\text{BnNH}_4^+\text{TFPB}^-$ to **100**. $^1\text{H-NMR}$ (400 MHz, CDCl_3 , 298 K). 6.0-2.5 ppm expansion.

3.3.2 Conclusions

In this study we presented an effective approach for the synthesis of conformationally chiral cyclopeptoids, stable in the solution state. We prepared a variety of compounds, with increasing macrocycle's cavity, and investigated the central-to-conformational chirality transfer from a single, enantiopure, stereogenic centre, in the form of a L-N(Bn)Ala residue, on the overall conformation of the macroring, comparing the results with the corresponding glycinate molecules. This strategy resulted efficient for cyclic trimers and tetramers; as for the conformationally unstable hexamers, metal complexation was necessary to provide rigidity of chiral scaffolds.

3.3.3 Experimental section

3.3.3.1 General methods

Refer to Paragraph 2.2.3.1.

Chiral HPLC analyses were performed using JASCO LC-NET II/ADC model with a JASCO PU-4180 Plus Pump and a Photo Diode Array UV detector JASCO MD-4015, set at 220 nm or 254 nm.

UV-Vis spectra were recorded on a Varian® Cary 1E UV-Vis Spectrophotometer; the samples were dissolved in acetonitrile and the measurement were performed between 400 and 220 nm.

CD spectra were acquired using a JASCO rapid scanning monochromator. Spectra were collected at 25 °C from 200 to 400 nm in 0.5 nm or 1 nm increments in a circular quartz cell with 1 mm path length. Data were averaged for 5 s at each wavelength.

Additional NMR solvents used in this work: (CH₃)₂SO, DMSO, δ = 2.50; (¹³CH₃)₂SO, DMSO, δ = 39.51, CO(CH₃)₂, δ = 2.05 ppm.

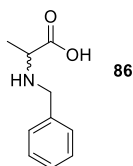
For the VT NMR experiments, refer to Paragraph 2.2.3.7; for the Pirkle experiments, refer to Paragraph 2.2.3.8.

DFT calculations were performed by prof. C. Costabile, Dpt. of Chemistry and Biology "A. Zambelli", Univ. of Salerno.

X-ray analyses were performed by PhD student G. Pierri and prof. C. Tedesco, Dpt. of Chemistry and Biology "A. Zambelli", Univ. of Salerno.

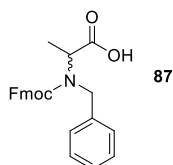
3.3.3.2 Synthesis of *N*-Fmoc-*N*-benzyl-alanine (**87**)

Alanine (2.00 g, 10.4 mmol) was dissolved in 2 M NaOH (11.2 mL, 22.4 mmol) under stirring. Benzaldehyde (2.28 mL, 22.4 mmol) was added dropwise and the mixture was stirred for 15 minutes, then brought to 0 °C; NaBH₄ (0.3 eq., 0.249 g, 6.73 mmol) was added. The mixture was brought to room temperature and stirred for an additional 30 minutes. This procedure was repeated by twice. The reaction mixture was then diluted with H₂O (4.00 mL) and the aqueous phase was extracted with MTBE (3 times x 6.00 mL), then cooled to 0 °C and HCl 3 M (2.80 mL) was added dropwise to start the precipitation, followed by HCl 1 M (17.2 mL). The resulting precipitate was filtered away and the water phase was cooled again to 0 °C and further acidified with HCl 1 M (17.2 mL) to induce further precipitation. The combined resulting precipitates were washed with cold acetone:H₂O 2:1 (12.0 mL) and then with cold acetone. Once dry, the *N*-benzyl alanine was derivatized without further purification.



N-benzyl alanine (**86**): white amorphous solid, 2.47 g, average yield (D, L and D,L), 61%. ¹H-NMR (400 MHz, D₂O) δ : 7.44 (5H, s, Ar-*H*), 4.15 (1H, d, *J* 12.7 Hz, N-*CHH*-Ph), 4.08 (1H, d, *J* 12.7 Hz, N-*CHH*-Ph), 3.59 (1H, q, *J* 7.3 Hz, C=O-*CHCH*₃), 1.43 (3H, d, *J* 7.2 Hz, C=O-*CHCH*₃). ES-MS: 179.1 *m/z* [M+H⁺].

N-benzyl alanine (2.47 g, 13.8 mmol) was dispersed in dioxane:H₂O 1:1 (81.0 mL) under stirring; NaHCO₃ (2.4 eq., 2.78 g, 33.0 mmol), DMAP (0.05 eq., 0.841 g, 0.690 mmol) and Fmoc-Cl (1.3 eq., 4.63 g, 17.9 mmol) were subsequently added, one portion at a time. The reaction mixture was left under agitation at room temperature for 20 hours, after which KHSO₄ 1 M (23 mL) was added to pH 3, then the dioxane was evaporated and the pH was adjusted. The water phase was extracted with AcOEt (3 times), anhydriified with MgSO₄ and dried under *vacuum*. The crude product was purified on flash silica gel, 90:10 (1% AcOH) to 70:30 (1% AcOH) petroleum ether (EP):AcOEt.

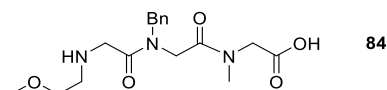


N-Fmoc-*N*-benzyl alanine (**87**): white amorphous solid, 0.945 g, average yield (D, L and D,L), 51%. ¹H-NMR (300 MHz, CDCl₃, mixture of rotamers) δ : 7.73-7.19 (13H, br signals, overlapping, Ar-*H*), 4.65-4.35 (4H, br signals, overlapping, N-CH₂-Ph, C=O-O-CH₂), 4.22-4.12 (1H, br signals, overlapping, CHCH₃), 1.40 (3H, d, *J* 7.1 Hz, CHCH₃). ES-MS: 401.2 *m/z* [M+H⁺].

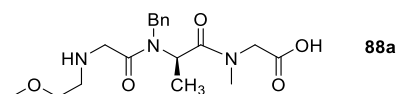
3.3.3.3 General methods for the sub-monomeric/monomeric solid-phase oligomerization. Synthesis of the linear peptoids **84**, **88**, **90**, **93**, **96**, **99**, **101**

The 2-chlorotrityl chloride resin (α -dichlorobenzhydryl-polystyrene cross-linked with 1% DVB; 100-200 mesh; 1.63 mmol g⁻¹, 0.400 g, 0.652 mmol) was swelled in dry CH₂Cl₂ (4 mL) for 45 min and washed twice with dry CH₂Cl₂ (4 mL). The first sub-monomer was attached onto the resin by adding bromoacetic acid (0.136 g, 0.978 mmol) in dry CH₂Cl₂ (4 mL) and DIPEA (567 μ L, 3.26 mmol) on a shaker platform for 60 min at room temperature, followed by washing with DCM (3 \times 1 min) and then again with DMF (3 \times 1 min). A solution of the chosen amine (1.6 M in dry DMF, 4 mL) was added to the bromoacetylated resin. The mixture was left on a shaker platform for 40 min at room temperature, then the resin was washed with DMF (3 \times 1 min), DCM (3 \times 1 min) and then again with DMF (3 \times 1 min). Subsequent bromoacetylation reactions were accomplished by reacting the aminated oligomer with a solution of bromoacetic acid (0.910 g, 6.52 mmol) and DIC (1.11 mL, 7.17 mmol) in dry DMF (4 mL) for 60 min at room temperature. The filtrated resin was washed with DMF (4 \times 1 min), DCM (4 \times 1

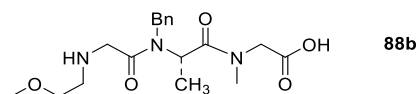
min), DMF (4 × 1 min) and treated again with the proper amine under the same conditions reported above. Alternatively, according to the monomeric protocol, a solution of the proper monomer (L, D or D,L *N*-Fmoc-*N*-benzyl alanine, 0.785, 1.96 mmol), HATU (0.719 g, 1.89 mmol), DIPEA (0.400 mL, 2.61 mmol) in dry DMF (4 mL) was added, and left to shake for 60 min. The completion of the acylation reactions was verified by means of the chloranil test. The monomer was subsequently deprotected using a 20% solution of piperidine in dry DMF (two treatments, 3 minutes and 7 minutes, respectively, 4 mL each time) and then washed in the usual manner. This cycle of reactions was iterated until the target linear oligomer was obtained. The cleavage was performed treating the resin, previously washed with DCM (3 × 1 min), three times with a solution of HFIP in dry CH₂Cl₂ (20% v/v, 4.00 mL each time) on a shaker platform at room temperature for 30 min each time. The resin was then filtered away and the combined filtrates were concentrated *in vacuo*. 1 mg of the final products were dissolved in 60 μL of acetonitrile (0.1% TFA) and 60 μL of HPLC grade water (0.1% TFA) and analysed by RP-HPLC; purity >85% (except for **96**, purity ~73%); conditions: 5 → 100% A in 30 min for the all oligomers (A, 0.1% TFA in acetonitrile, B, 0.1% TFA in water); flow: 1.0 mL min⁻¹, 220 nm]. The linear oligomers (isolated as amorphous solids) were subjected to ESI mass spectrometry and, subsequently, to the cyclization reactions without further purification.



H-[*N*me-*N*pm-Sar]-OH (**84**): white amorphous solid, 0.229 g, 100%; t_R : 5.1 min. ES-MS m/z ; 352.8 [M + H]⁺. HRMS (ESI/FTICR) m/z ; [M + H]⁺ Calcd for C₁₇H₂₆N₃O₅⁺ 352.1867; Found 352.1872.

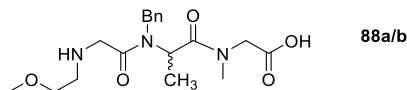


H-[*N*me-D(Bn)Ala-Sar]-OH (**88a**): white amorphous solid, 0.219 g, 92%; t_R : 5.0 min. ES-MS m/z ; 366.0 [M + H]⁺. HRMS (ESI/FTICR) m/z ; [M + H]⁺ Calcd for C₁₈H₂₈N₃O₅⁺ 366.2023; Found 366.2022.

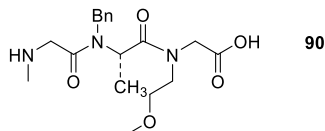


H-[*N*me-L(Bn)Ala-Sar]-OH (**88b**): white amorphous solid, 0.174 g, 73%; t_R : 5.1 min. ES-

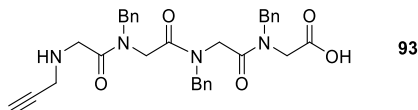
MS m/z ; 366.2 $[M + H]^+$. HRMS (ESI/FTICR) m/z ; $[M + H]^+$ Calcd for $C_{18}H_{28}N_3O_5^+$ 366.2023; Found 366.2019.



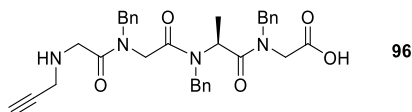
H-[Nme-D,L(Bn)Ala-Sar]-OH (**88a/b**): white amorphous solid, 0.231 g, 97%; t_R : 4.8 min. ES-MS m/z ; 366.0 $[M + H]^+$. HRMS (ESI/FTICR) m/z ; $[M + H]^+$ Calcd for $C_{18}H_{28}N_3O_5^+$ 366.2023; Found 366.2024.



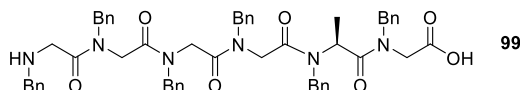
H-[Sar-L(Bn)Ala-Nme]-OH (**90**): white amorphous solid, 0.238 g, 100%; t_R : 4.6 min. ES-MS m/z ; 365.7 $[M + H]^+$. HRMS (ESI/FTICR) m/z ; $[M + H]^+$ Calcd for $C_{18}H_{28}N_3O_5^+$ 366.2023; Found 366.2023.



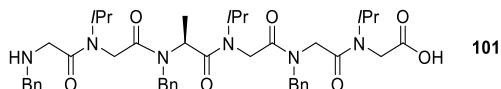
H-[Npa-Npm₃]-OH (**93**): white amorphous solid, 0.311 g, 86%; t_R : 8.0 min. ES-MS m/z ; 555.1 $[M + H]^+$. HRMS (ESI/FTICR) m/z ; $[M + H]^+$ Calcd for $C_{32}H_{35}N_4O_5^+$ 555.2602; Found 555.2599.



H-[Npa-Npm-L(Bn)Ala-Npm]-OH (**96**): white amorphous solid, 0.267 g, 72%; t_R : 8.2 min. ES-MS m/z ; 569.2 $[M + H]^+$. HRMS (ESI/FTICR) m/z ; $[M + H]^+$ Calcd for $C_{33}H_{37}N_4O_5^+$ 569.2758; Found 569.2757.



H-[Npm₄-L(Bn)Ala-Npm]-OH (**99**): white amorphous solid, 0.525 g, 88%; t_R : 10.8 min. ES-MS m/z ; 915.4 $[M + H]^+$. HRMS (ESI/FTICR) m/z ; $[M + H]^+$ Calcd for $C_{55}H_{59}N_6O_7^+$ 915.4440; Found 915.4446.



H-[Npm-NVal-L(Bn)Ala-NVal-Npm-NVal]-OH (**101**): white amorphous solid, 0.377 g, 75%; t_R : 9.4 min. ES-MS m/z ; 771.8 [M + H]⁺, HRMS (ESI/FTICR) m/z ; [M + H]⁺ Calcd for C₄₃H₅₉N₆O₇⁺ 771.4440; Found 771.4447.

3.3.3.4 Synthesis of the cyclic peptoids **85**, **89**, **91**, **94/95**, **98b**, **100**, **102**

Refer to Paragraph 2.2.3.3.

The cyclization reaction was performed on a 0.150 mmol scale of the linear oligomers, which were dissolved in 5.0 mL of dry DMF (5.0 mL of dry DCM for compound **84**) and added by a syringe pump in 6 hours to the reaction mixture. The crude cyclic peptoids **94/95**, **98b**, **100** were dissolved in hot acetonitrile and precipitated by slowly cooling the acetonitrile solutions. The crude **102** was purified on reverse silica gel (C₁₈); conditions: 10% – 100% A (A: acetonitrile; B: water). The crude **85**, **89a**, **89b**, **89a/b**, **91** were purified on flash silica gel; conditions: 10% – 100% A (A: ethyl acetate; B: petroleum ether), then 90:10 ethyl acetate: methanol.

cyclo-[Nme-Npm-Sar] (**85a/b**): white amorphous solid, 0.0110 g, 23%; t_R : 4.6 min. ¹H-NMR (600 MHz, CDCl₃) δ: 7.27-7.19 (5H, br signals, overlapping, Ar-H), 5.38 (1H, d, J 14.4 Hz, N-CHH-Ph), 4.84 (1H, d, J 15.2 Hz, O=C-CHH-N-CH₃), 4.73 (1H, d, J 15.3 Hz, O=C-CHH-N-CH₂CH₂OCH₃), 4.52 (1H, d, J 15.2 Hz, O=C-CHH-N-Bn), 4.08 (1H, d, J 14.4 Hz, N-CHH-Ph), 3.99 (m, 1H, N-CHHCH₂OCH₃), 3.96 (1H, d, J 15.3 Hz, O=C-CHH-N-CH₂CH₂OCH₃), 3.55 (2H, d, J 15.2 Hz, O=C-CHH-N-CH₃ and O=C-CHH-N-Bn, overlapping), 3.52-3.49 (3H, br signals, overlapping, N-CHHCH₂OCH₃), 3.26 (3H, s, N-CH₂CH₂OCH₃), 3.06 (3H, s, N-CH₃). ¹³C-NMR (150 MHz, CDCl₃) δ: 167.1, 166.9, 166.7, 136.1, 129.0 (x2), 128.7 (x2), 127.8, 70.4, 58.7, 51.5, 50.1, 49.0, 47.0, 47.3, 35.5. HRMS (ESI/FTICR) m/z ; [M + H]⁺ Calcd for C₁₇H₂₄N₃O₄⁺ 334.1761; Found 334.1763.

cyclo-[Nme-D(Bn)Ala-Sar] (**89a**): white amorphous solid, 0.0340 g, 65%; t_R : 5.4 min; t_R : 12.0 min (HPLC analysis, with chiral stationary phase). ¹H-NMR (400 MHz, CDCl₃) δ: 7.33-7.16 (5H, br signals, overlapping, Ar-H), 5.22 (1H, q, J 6.5 Hz, O=C-CHCH₃), 4.97 (1H, d, J 12.2 Hz, O=C-CHH-N-CH₃), 4.93 (2H, d, J 15.1 Hz, O=C-CHH-N-CH₂CH₂OCH₃ and N-CHH-Ph, overlapping), 4.50 (1H, d, J 15.1 Hz, N-CHH-Ph), 4.07 (m, 1H, N-CHHCH₂OCH₃), 4.07 (1H, d, J 15.1 Hz, O=C-CHH-N-CH₂CH₂OCH₃), 3.63 (1H, d, J 12.1 Hz, O=C-CHH-N-CH₃), 3.62-3.52 (3H, br signals, overlapping, N-CHHCH₂OCH₃), 3.33 (3H, s, N-CH₂CH₂OCH₃), 3.14 (3H, s, N-CH₃), 1.40 (3H, d, J 6.5 Hz, O=C-CHCH₃).

cyclo-[Nme-L(Bn)Ala-Sar] (**89b**): white amorphous solid, 0.0360 g, 69%; t_R : 5.2 min; t_R :

19.0 min (HPLC analysis, with chiral stationary phase). $^1\text{H-NMR}$ (400 MHz, CDCl_3) δ : 7.33-7.16 (5H, br signals, overlapping, Ar-*H*), 5.22 (1H, q, J 6.5 Hz, O=C-*CHCH*₃, *pseudo-ax*), 4.95 (3H, d, J 15.1 Hz, O=C-*CHH-N-CH*₃, *pseudo-ax*, O=C-*CHH-N-CH*₂CH₂OCH₃, *pseudo-ax*, N-*CHH-Ph*, overlapping), 4.50 (1H, d, J 15.1 Hz, N-*CHH-Ph*), 4.07 (m, 1H, N-*CHHCH*₂OCH₃), 4.07 (1H, d, J 15.1 Hz, O=C-*CHH-N-CH*₂CH₂OCH₃, *pseudo-eq*), 3.64 (1H, d, J 15.1 Hz, O=C-*CHH-N-CH*₃, *pseudo-eq*), 3.63-3.51 (3H, br signals, overlapping, N-*CHHCH*₂OCH₃), 3.34 (3H, s, N-*CH*₂CH₂OCH₃), 3.14 (3H, s, N-*CH*₃), 1.40 (3H, d, J 6.5 Hz, O=C-*CHCH*₃, *pseudo-eq*). $^{13}\text{C-NMR}$ (100 MHz, CDCl_3) δ : 169.3, 168.9, 166.8, 138.5, 128.3 (x2), 126.7 (x3), 70.4, 58.7, 51.2, 50.4, 49.9, 46.7, 45.8, 35.6, 16.7.

$^1\text{H-NMR}$ (600 MHz, DMSO-d_6) δ : 7.25-7.23 (2H, br signals, overlapping, Ar-*H*), 7.18-7.15 (1H, br signals, overlapping, Ar-*H*), 7.07 (2H, d, J 7.6 Hz, Ar-*H*), 5.64 (1H, q, J 6.3 Hz, O=C-*CHCH*₃), 5.36 (2H, d, J 15.5 Hz, O=C-*CHH-N-CH*₃ and O=C-*CHH-N-CH*₂CH₂OCH₃, overlapping), 4.61 (1H, d, J 15.5 Hz, O=C-*CHH-N-CH*₂CH₂OCH₃ and N-*CHH-Ph*, overlapping), 4.50 (1H, d, J 15.5 Hz, N-*CHH-Ph*), 4.38 (1H, d, J 15.5 Hz, O=C-*CHH-N-CH*₂CH₂OCH₃), 3.81 (m, 1H, N-*CHHCH*₂OCH₃), 3.72 (1H, d, J 15.5 Hz, O=C-*CHH-N-CH*₃), 3.30-3.26 (3H, br signals, overlapping, N-*CHHCH*₂OCH₃), 3.33 (3H, s, N-*CH*₂CH₂OCH₃), 2.94 (3H, s, N-*CH*₃), 1.20 (3H, d, J 6.3 Hz, O=C-*CHCH*₃). $^{13}\text{C-NMR}$ (150 MHz, DMSO-d_6) δ : 169.8, 168.6, 167.7, 138.8, 128.0 (x2), 126.3, 126.2 (x2), 69.2, 58.1, 50.4, 49.4, 49.4, 45.8, 44.8, 35.0, 16.3. HRMS (ESI/FTICR) m/z ; $[\text{M} + \text{H}]^+$ Calcd for $\text{C}_{18}\text{H}_{26}\text{N}_3\text{O}_4^+$ 348.1918; Found 348.1921.

cyclo-[Nme-D,L(Bn)Ala-Sar] (**89a/b**): white amorphous solid, 0.0290 g, 56%; t_R : 5.3 min; t_R : 12.3, 19.3 min (HPLC analysis, with chiral stationary phase). $^1\text{H-NMR}$ (400 MHz, CDCl_3) δ : 7.33-7.25 (3H, br signals, overlapping, Ar-*H*), 7.21-7.16 (2H, br signals, overlapping, Ar-*H*), 5.22 (1H, q, J 6.5 Hz, O=C-*CHCH*₃), 4.97 (1H, d, J 12.2 Hz, O=C-*CHH-N-CH*₃), 4.93 (2H, d, J 15.1 Hz, O=C-*CHH-N-CH*₂CH₂OCH₃ and N-*CHH-Ph*, overlapping), 4.50 (1H, d, J 15.1 Hz, N-*CHH-Ph*), 4.07 (m, 1H, N-*CHHCH*₂OCH₃), 4.07 (1H, d, J 15.1 Hz, O=C-*CHH-N-CH*₂CH₂OCH₃), 3.63 (1H, d, J 12.1 Hz, O=C-*CHH-N-CH*₃), 3.62-3.52 (3H, br signals, overlapping, N-*CHHCH*₂OCH₃), 3.33 (3H, s, N-*CH*₂CH₂OCH₃), 3.14 (3H, s, N-*CH*₃), 1.39 (3H, d, J 6.5 Hz, O=C-*CHCH*₃).

cyclo-[Sar-L(Bn)Ala-Nme] (**91**): white amorphous solid, 0.0240 g, 46%; t_R : 5.5 min. $^1\text{H-NMR}$ (600 MHz, CDCl_3) δ : 7.27-7.25 (3H, br signals, overlapping, Ar-*H*), 7.20-7.15 (2H, br signals, overlapping, Ar-*H*), 5.23 (1H, q, J 6.5 Hz, O=C-*CHCH*₃, *pseudo-ax*), 5.05 (1H, d, J

15.2 Hz, O=C-CHH-N-CH₃, *pseudo-ax*), 4.87 (1H, d, *J* 15.7 Hz, N-CHH-Ph), 4.85 (1H, d, *J* 15.5 Hz, O=C-CHH-N-CH₂CH₂OCH₃, *pseudo-ax*), 4.49 (1H, d, *J* 15.7 Hz, N-CHH-Ph), 3.97 (m, 1H, N-CHHCH₂OCH₃), 3.96 (1H, d, *J* 15.5 Hz, O=C-CHH-N-CH₂CH₂OCH₃, *pseudo-eq*), 3.69 (1H, d, *J* 15.2 Hz, O=C-CHH-N-CH₃, *pseudo-eq*), 3.66-3.59 (2H, br signals, overlapping, N-CHHCHHOCH₃), 3.53 (1H, m, N-CH₂CHHOCH₃), 3.33 (3H, s, N-CH₂CH₂OCH₃), 3.11 (3H, s, N-CH₃), 1.40 (3H, d, *J* 6.5 Hz, O=C-CHCH₃, *pseudo-eq*). ¹³C-NMR (150 MHz, CDCl₃) δ: 169.1, 167.3, 167.3, 138.4, 128.3 (x2), 126.8 (x2), 126.8, 70.5, 58.7, 51.4, 50.8, 49.5, 46.7, 45.9, 36.0, 16.9. HRMS (ESI/FTICR) *m/z*; [M + H]⁺ Calcd for C₁₈H₂₆N₃O₄⁺ 348.1918; Found 348.1920.

cyclo-[Npa-Npm₃] (**94/95**): white amorphous solid, 0.0550 g, 69%; *t_R*: 10.1 min. ¹H-NMR (300 MHz, CDCl₃, mixture of conformational isomers): δ: 7.42-7.21 (12H, br signals, Ar-H), 7.05-7.03 (4H, br signals, Ar-H), 5.64 (0.2H, d, *J* 15.0 Hz), 5.56 (0.7H, d, *J* 14.3 Hz), 5.43 (1H, d, *J* 15.8 Hz), 5.37 (1H, d, *J* 15.8 Hz), 4.91 (0.8H, dd, *J* 17.8, 2.3 Hz, NCHHCCH, *major conformer, cis*), 4.63 (0.7H, d, *J* 12.6 Hz), 4.57 (0.7H, d, *J* 13.5 Hz), 4.39 (2H, d, *J* 17.0 Hz, overlapping), 4.32 (0.8H, d, *J* 7.2 Hz), 4.23 (1.2H, br signals), 4.07 (1H, d, *J* 17.9 Hz, NCHHCCH, *minor conformer, trans*), 3.96 (0.6H, d, *J* 17.9 Hz, NCHHCCH, *minor conformer, trans*), 3.83 (1.2H, d, *J* 17.8, 2.4 Hz, overlapping, NCHHCCH, *major conformer, cis*), 3.75 (0.8H, d, *J* 14.3 Hz), 3.63 (0.6H, d, *J* 14.1, 13.5 Hz, overlapping), 3.48 (2.7H, d, *J* 15.2, 14.6 Hz, overlapping), 2.23 (0.3H, t, *J* 2.4 Hz), 2.13 (0.7H, t, *J* 2.3 Hz). ¹³C-NMR (75 MHz, CDCl₃, mixture of conformational isomers) δ: 169.1, 169.0, 168.7, 168.0, 167.9, 167.7, 167.6, 136.2, 135.8, 135.7, 135.2, 129.1, 129.1, 129.0, 128.8, 128.7, 128.7, 128.0, 128.0, 127.9, 127.8, 127.8, 126.9, 126.6, 126.6, 73.9, 73.5, 50.6, 50.4, 50.4, 49.6, 49.3, 48.9, 48.8, 48.7, 48.7, 47.5, 47.3, 47.2, 47.1, 36.6, 35.8, 31.9, 29.7, 29.3, 22.7, 22.7, 14.1. HRMS (ESI/FTICR) *m/z*; [M + H]⁺ Calcd for C₃₂H₃₃N₄O₄⁺ 537.2496; Found 537.2493.

cyclo-[Npa-Npm-L(Bn)Ala-Npm] (**98b**): white amorphous solid, 0.0250 g, 30%; *t_R*: 10.5 min. ¹H-NMR (600 MHz, CDCl₃): δ: 7.35-7.24 (8H, br signals, overlapping, Ar-H), 7.16-7.09 (3H, br signals, overlapping, Ar-H), 7.06 (2H, br d, *J* 7.3 Hz, Ar-H), 6.92 (2H, br d, *J* 6.9 Hz, Ar-H), 5.68 (1H, d, *J* 18.0 Hz, N-CHH-Ph), 5.67 (1H, q, *J* 6.7 Hz, O=C-CHCH₃), 5.42 (1H, d, *J* 14.3 Hz, N-CHH-Ph), 5.25 (1H, d, *J* 14.7 Hz, O=C-CHH-N-CH₂CCH), 4.40 (1H, d, *J* 18.1 Hz, O=C-CHH-N-CH₂-Ph), 4.38 (1H, d, *J* 18.2 Hz, O=C-CHCH₃-N-CHHPh), 4.33 (1H, d, *J* 18.2 Hz, O=C-CHCH₃-N-CHHPh), 4.12 (1H, dd, *J* 19.0, 2.2 Hz, N-CHH-CCH), 4.02 (1H, dd, *J* 18.3 Hz, O=C-CHH-N-CH₂-Ph), 3.93 (1H, d, *J* 18.1 Hz,

O=C-CHH-N-CH₂-Ph), 3.91 (1H, d, *J* 19.0 Hz, N-CHH-CCH), 3.88 (1H, d, *J* 18.0 Hz, N-CHH-Ph), 3.57 (1H, d, *J* 14.7 Hz, O=C-CHH-N-CH₂CCH), 3.50 (1H, d, *J* 14.3 Hz, N-CHH-Ph), 3.10 (1H, d, *J* 18.3 Hz, O=C-CHH-N-CH₂-Ph), 2.23 (1H, t, *J* 2.2 Hz, N-CH₂CCH), 1.43 (1H, d, *J* 6.7 Hz, O=C-CHCH₃). ¹³C-NMR (150 MHz, CDCl₃) δ: 170.7, 169.2, 168.6, 167.5, 136.9, 136.4, 135.8, 129.0 (x4), 128.8 (x2), 128.8 (x2), 128.5 (x2), 127.9, 127.7, 127.5, 125.7 (x2), 73.9, 51.0, 50.3, 50.0, 48.9, 47.9, 46.5, 46.4, 35.9, 29.7, 15.63. HRMS (ESI/FTICR) *m/z*; [M + H]⁺ Calcd for C₃₃H₃₅N₄O₄⁺ 551.2653; Found 551.2650.

cyclo-[Npm₄-L(Bn)Ala-Npm] (**100**): white amorphous solid, 0.0620 g, 46%; *t_R*: 13.8 min. ¹H-NMR (600 MHz, CDCl₃, mixture of rotamers) δ: 7.29-6.89 (30H, overlapping, Ar-*H*), 5.73-2.90 (23H, overlapping, O=C-CH₂-N, N-CH₂-Ph, O=C-CHCH₃), 1.46-1.20 (3H, overlapping, O=C-CHCH₃). ¹³C-NMR (150 MHz, CDCl₃, mixture of rotamers) δ: 172.4, 171.6, 170.3, 170.0, 169.3, 169.2, 168.8, 168.6, 168.3, 167.8, 166.8, 137.7, 137.0, 136.6, 136.3, 136.2, 135.9, 135.7, 135.6, 135.2, 129.9, 129.4, 129.0, 129.0, 128.8, 128.7, 128.5, 128.3, 128.0, 127.7, 127.5, 127.3, 127.0, 126.8, 126.7, 126.5, 126.1, 125.9, 125.6, 125.4, 125.1, 124.9, 54.1, 52.7, 51.5, 51.2, 50.8, 50.4, 50.3, 50.0, 49.8, 49.4, 49.3, 49.0, 49.0, 48.6, 48.4, 48.2, 47.8, 47.5, 47.3, 47.0, 46.4, 45.8, 45.1, 44.0, 29.7, 16.5, 15.9, 15.4, 15.1, 14.8, 14.1. HRMS (ESI/FTICR) *m/z*; [M + H]⁺ Calcd for C₅₅H₅₇N₆O₆⁺ 897.4334; Found 897.4338.

cyclo-[Npm-*N*Val-L(Bn)Ala-*N*Val-Npm-*N*Val] (**102**): white amorphous solid, 0.0740 g, 66%; *t_R*: 11.1 min. ¹H-NMR (600 MHz, CDCl₃, mixture of rotamers) δ: 7.39-6.85 (15H, overlapping, Ar-*H*), 5.30-2.70 (20H, overlapping, O=C-CH₂-N, N-CH₂-Ph, N-CH₂-CH(CH₃)₂, O=C-CHCH₃), 1.44-0.79 (21H, overlapping, O=C-CHCH₃, N-CH₂-CH(CH₃)₂). ¹³C-NMR (150 MHz, CDCl₃, mixture of rotamers) δ: 175.8, 172.2, 171.9, 171.5, 171.3, 171.0, 170.0, 169.7, 169.7, 169.2, 169.0, 168.6, 168.4, 167.4, 159.1, 158.8, 137.9, 137.7, 137.3, 136.9, 136.8, 135.9, 129.2, 129.0, 129.0, 128.7, 128.6, 128.4, 128.1, 128.0, 127.9, 127.7, 127.6, 127.3, 126.5, 126.2, 116.1, 114.2, 53.4, 52.5, 52.1, 51.8, 51.6, 51.2, 51.0, 50.5, 49.8, 49.4, 49.1, 48.4, 48.0, 47.8, 47.6, 47.3, 47.0, 46.8, 46.3, 46.2, 46.1, 45.9, 45.7, 45.4, 45.3, 44.7, 44.3, 44.0, 43.8, 43.4, 43.0, 42.8, 21.9, 21.2, 21.0, 20.7, 20.5, 20.3, 20.0, 19.9, 19.8, 19.6, 19.5, 19.3, 19.3, 19.2, 16.8, 15.8, 15.1, 14.9, 14.5. HRMS (ESI/FTICR) *m/z*; [M + H]⁺ Calcd for C₄₃H₅₇N₆O₆⁺ 753.4334; Found 753.4333.

3.3.3.5 Preparation of the monometallic complexes $[100,102\cdot\text{Na}]^+\text{TFPB}^-$ and apparent K_{a1} evaluation

Refer to Paragraph 2.2.3.4.

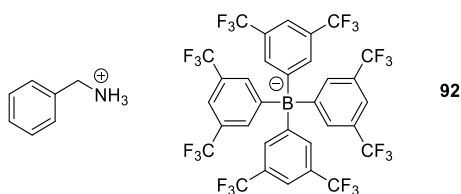
$[100\cdot\text{Na}]^+[\text{TFPB}]^-$: white amorphous solid. $^1\text{H-NMR}$ (600 MHz, CDCl_3) δ : 7.71 (8H, s, TFPB-*o-H*), 7.50 (4H, s, TFPB-*p-H*), 7.38-7.27 (18H, br signals, overlapping, Ar-*H*), 7.18 (2H, br d, J 7.2 Hz, Ar-*H*), 7.11-7.01 (10H, br signals, overlapping, Ar-*H*), 5.29 (1H, q, J 7.7 Hz, O=C-*CHCH*₃), 5.17 (1H, d, J 16.3 Hz, CHCH₃-N-*CHH*-Ph), 4.87 (1H, d, J 16.6 Hz, O=C-*CHH*-N-Bn), 4.84 (1H, d, J 16.7 Hz, O=C-*CHH*-N-Bn), 4.84 (1H, d, J 16.7 Hz, O=C-*CHH*-N-Bn), 4.81 (1H, d, J 16.5 Hz, O=C-*CHH*-N-Bn), 4.76 (1H, d, J 19.0 Hz, O=C-*CHH*-N-Bn), 4.71 (1H, d, J 16.9 Hz, N-*CHH*-Ph), 4.66 (1H, d, J 16.0 Hz, N-*CHH*-Ph), 4.61 (1H, d, J 16.6 Hz, N-*CHH*-Ph), 4.60 (1H, d, J 16.6 Hz, N-*CHH*-Ph), 4.58 (1H, d, J 19.0 Hz, O=C-*CHH*-N-Bn), 4.55 (1H, d, J 16.5 Hz, N-*CHH*-Ph), 4.54 (1H, d, J 16.3 Hz, CHCH₃-N-*CHH*-Ph), 4.39 (1H, d, J 15.8 Hz, N-*CHH*-Ph), 4.34 (2H, d, N-*CHH*-Ph and N-*CHH*-Ph, overlapping), 4.30 (1H, d, J 16.0 Hz, N-*CHH*-Ph), 3.58 (1H, d, J 16.6 Hz, O=C-*CHH*-N-Bn), 3.55 (1H, d, J 16.7 Hz, O=C-*CHH*-N-Bn), 3.52 (1H, d, J 16.7 Hz, O=C-*CHH*-N-Bn), 3.47 (1H, d, J 16.5 Hz, O=C-*CHH*-N-Bn), 3.31 (1H, d, J 16.9 Hz, N-*CHH*-Ph), 1.41 (3H, d, J 7.7 Hz, O=C-*CHCH*₃). $^{13}\text{C-NMR}$ (150 MHz, CDCl_3) δ : 171.8, 170.8 (x4), 170.2, 161.7 (q, J 50 Hz, C-1 of TFPB), 136.2, 134.8 (one resonance belongs to the host plus C-2 resonance of TFPB), 133.7 (x4), 133.5, 129.3 (x6), 129.0 (x4), 128.9 (q, J 30 Hz, C-3 of TFPB), 128.8, 128.0, 127.3 (x5), 127.1 (x4), 126.9 (x4), 125.1 (x4), 124.6 (q, J 270 Hz, C-5 of TFPB), 117.4 (C-4 of TFPB), 54.2, 52.9 (x2), 52.8 (x2), 49.8, 49.4 (x2), 49.2, 48.2, 47.9, 14.4 (x2); ESI-MS m/z 919.4 $[\text{M} + \text{Na}]^+$. HRMS (ESI/FTICR) m/z ; $[\text{M} + \text{Na}]^+$ Calcd for $\text{C}_{55}\text{H}_{56}\text{N}_6\text{NaO}_6^+$ 919.4154; Found 919.4153.

$[102\cdot\text{Na}]^+[\text{TFPB}]^-$: white amorphous solid. $^1\text{H-NMR}$ (600 MHz, CDCl_3) δ : 7.70 (8H, s, TFPB-*o-H*), 7.51 (4H, s, TFPB-*p-H*), 7.43-7.32 (9H, br signals, overlapping, Ar-*H*), 7.24-7.17 (6H, br signals, overlapping, Ar-*H*), 5.13 (1H, q, J 7.4 Hz, O=C-*CHCH*₃), 4.93 (1H, d, J 18.9 Hz, CHCH₃-N-*CHH*-Ph), 4.85 (1H, d, J 16.4 Hz, N-*CHH*-Ph), 4.84 (1H, d, J 16.5 Hz, N-*CHH*-Ph), 4.74 (2H, d, O=C-*CHH*-N-Bn and O=C-*CHH*-N-Bn, overlapping), 4.65 (1H, d, J 19.9 Hz, CHCH₃-N-*CHH*-Ph), 4.60 (1H, d, J 16.7 Hz, O=C-*CHH*-N-*iPr*), 4.55 (1H, d, J 16.5 Hz, O=C-*CHH*-N-*iPr*), 4.43 (1H, d, J 16.4 Hz, N-*CHH*-Ph), 4.36 (1H, d, J 16.8 Hz, O=C-*CHH*-N-*iPr*), 4.33 (1H, d, J 16.5 Hz, N-*CHH*-Ph), 4.14 (1H, m, N-*CH*(CH₃)₂), 3.90 (1H, m, N-*CH*(CH₃)₂), 3.84 (1H, m, N-*CH*(CH₃)₂), 3.59 (1H, d, J 16.7 Hz, O=C-*CHH*-N-*iPr*), 3.58 (1H, d, J 16.7 Hz, O=C-*CHH*-N-Bn), 3.57 (1H, d, J 16.5 Hz,

O=C-CHH-N-*i*Pr), 3.47 (1H, d, *J* 16.7 Hz, O=C-CHH-N-Bn), 3.31 (1H, d, *J* 16.8 Hz, O=C-CHH-N-*i*Pr), 1.44 (3H, d, *J* 7.4 Hz, O=C-CHCH₃), 1.15 (3H, d, *J* 6.5 Hz, N-CH(CH₃)₂), 1.04 (3H, d, *J* 6.5 Hz, N-CH(CH₃)₂), 0.90 (3H, d, *J* 7.3 Hz, N-CH(CH₃)₂). ¹³C-NMR (150 MHz, CDCl₃) δ: 173.2, 172.3, 170.7 (x2), 167.8 (x2), 161.6 (q, *J* 50 Hz, C-1 of TFPB), 134.8 (x4 host, plus C-2 resonances of TFPB), 129.5 (x3), 129.2, 129.0 (x2), 128.9 (q, *J* 30 Hz, C-3 of TFPB), 128.8 (x2), 128.5, 128.2, 126.6 (x2), 124.9, 124.6 (q, *J* 270 Hz, C-5 of TFPB), 117.5 (x3 host, plus C-5 of TFPB), 54.0, 53.4, 53.1, 50.1, 49.5, 49.0, 48.3 (x2), 43.5, 42.8, 42.5, 21.1, 21.0 (x2), 20.6, 19.9, 19.7, 14.3 (x2); ESI-MS *m/z* 775.4 [M + Na]⁺. HRMS (ESI/FTICR) *m/z*; [M + Na]⁺ Calcd for C₄₃H₅₆N₆NaO₆⁺ 775.4154; Found 775.4149.

3.3.3.6 Synthesis of benzylammonium tetrakis(3,5-bis(trifluoromethyl)phenyl)borate [BnNH₃]⁺[TFPB]⁻¹¹²

To a solution of benzyl amine hydrochloride salt (0.020 g, 0.140 mmol) in dry methanol (0.8 mL) was added a solution of sodium tetrakis(3,5-bis(trifluoromethyl)phenyl)borate (NaTFPB) (0.160 g, 0.181 mmol) in dry methanol (0.5 mL). The reaction was stirred overnight, then the methanol was evaporated. The resulting yellow oil was sonicated with deionized water for 1 hour, then the water was removed and the resulting solid was kept at high *vacuum* overnight.



[BnNH₃]⁺[TFPB]⁻ (**92**): yellow amorphous solid, 0.0850 g, 63%. ¹H-NMR (400 MHz, CO(CD₃)₂): δ: 7.80 (8H, s, TFPB-*o*-H), 7.68 (4H, s, TFPB-*p*-H), 7.51-7.46 (5H, br signals, overlapping, Ar-*H*), 5.19 (2H, s, N-CH₂-Ph).

3.3.3.7 General procedure for the evaluation of the apparent *K*_{ATOT} in [100·(BnNH₃)₂]²⁺2[TFPB]⁻

For the BnNH₃TFPB complex, to a 3.0 mM solution of **100** in CDCl₃ were added 2.0 equivalents of the guest salt; after the addition the mixture was sonicated for 5 minutes

¹¹² Gaeta C., Troisi F., Neri P., *Org. Lett.* **2010**, *12*, 9, 2092-2095.

in a rt bath (25 °C), then the $^1\text{H-NMR}$ spectra were acquired. The H-G complex concentration, at the equilibrium – $[\text{H-G}]_{\text{eq}}$ – was evaluated by integration of the $^1\text{H-NMR}$ complex signals (2.5-6.0 range) *versus* the total integration of the free host plus complexed molecules at 298 K.

In the case of a complex with two benzyl ammonium ions, the evaluation of the species at the equilibrium follows the relations already indicated in Paragraph 2.3.3.5 for the disodium complexes.

Note: for the benzyl ammonium complex, to F_a were added 4 protons to consider the integration of the guest.

3.3.3.8 UV-Vis spectroscopy

The following transitions were observed: compounds **100**, **102** and $[\mathbf{100}\cdot\text{Na}]^+$ λ_{max} 258 nm ($\pi \rightarrow \pi^*$); compound $[\mathbf{102}\cdot\text{Na}]^+$ λ_{max} 269 nm (side band 281 nm).

Concentration of the samples: **89a**, 0.3 mg mL⁻¹; **89b**, 0.3 mg mL⁻¹; **100**, 0.03 mg mL⁻¹; $[\mathbf{100}\cdot\text{Na}]^+$, 0.03 mg mL⁻¹; **102**, 0.3 mg mL⁻¹; $[\mathbf{102}\cdot\text{Na}]^+$, 0.3 mg mL⁻¹. All samples were prepared in UV-Vis grade acetonitrile.

3.3.3.9 Circular dichroism (CD) spectroscopy

Data were originally collected in millidegrees and then converted to per-residue molar ellipticity (deg·cm²/dmol). A spectrum of the solvent (chloroform or acetonitrile) was subtracted from peptoid solution spectra, recorded using a 500 μM solution of the sample in either chloroform or acetonitrile.

3.4 Central-to-conformational chirality transfer. Stereogenic centre(s) present in the side-chain(s)¹¹³

In this Paragraph, I will describe the syntheses and conformational properties of a family of cyclic peptoids, whose scaffold was decorated with a single, or multiple stereocenters, on the α position of the amine side-chain(s).

The sub-monomer (S)-(-)-1-phenylethylamine was chosen as the chiral inducer for two main reasons. First, this unit is known to induce stable secondary structures in linear peptoids (Paragraph 3.1.3 and references cited therein). Second, to assess the relevance of the methyl substitution on the side-chain(s) rather than the backbone (Paragraph 3.3).

For each macrocyclic scaffold, we varied the number and the position of the chiral side-chain(s) and combined them with *Npm* as achiral monomer. Our investigation was extended to cyclic octamers.

Each molecule was thoroughly characterized *via* NMR, DFT calculations and, when possible, X-ray diffraction analyses.

Note: diastereoisomers of the same molecular formula are indicated with progressive numbering, while conformational isomers are indicated with progressive lettering.

Chiral *Nspe* residue is indicated in red.

3.4.1 Results and discussion

3.4.1.1 Cyclic trimers

We started with the introduction of a single *Nspe* unit in the linear oligomer H-[*Npm-Nspe-Npm*]-OH (**103**), whose cyclization afforded two crown conformational isomers in 70:30 ratio (in slow equilibrium on the NMR time scale, ¹H-NMR analysis, DMSO-*d*₆), *cyclo*-[(*cis*,*pS*)*Nspe*-(*cis*,*pS*)*Npm*-(*cis*,*pS*)*Npm*] (**104a**), and *cyclo*-[(*cis*,*pR*)*Nspe*-(*cis*,*pR*)*Npm*-(*cis*,*pR*)*Npm*] (**104b**). The structure of the major conformational isomer **104a** was inferred *via* NMR observing the downfield shift of the side-chain methine proton chemical shift (δ 5.47 ppm), which testified for a shorter hydrogen bond in **104a** (compared to δ 5.10 ppm recorded for the same proton in minor atropisomer **104b**).

¹¹³ D'Amato A., Pierri G., Tedesco C., Della Sala G., Izzo I., Costabile C., De Riccardis F., *Reverse Turn and Loop Secondary Structures in Stereodefined Cyclic Peptoid Scaffolds*. *J. Org. Chem.* **2019**, *84*, 10911-10928.

This assignment was further corroborated by DFT calculations; higher internal energy of conformational isomer **104b** ($\Delta E = + 1.3$ kcal/mol, DMSO) was caused by steric clash between methyl group and carbonyl residue (3.03 Å) and the weaker hydrogen bond between the C α -H group of the *N*-(*S*)-(1-phenylethyl) side-chain and the carbonyl residue¹¹⁴ (2.39 Å). On the contrary, model **104a** was stabilized by the sterically inter-residue beneficial Ph(Me)NC-H/C=O eclipsing, relieving the 1,3-allylic strain.¹¹⁵

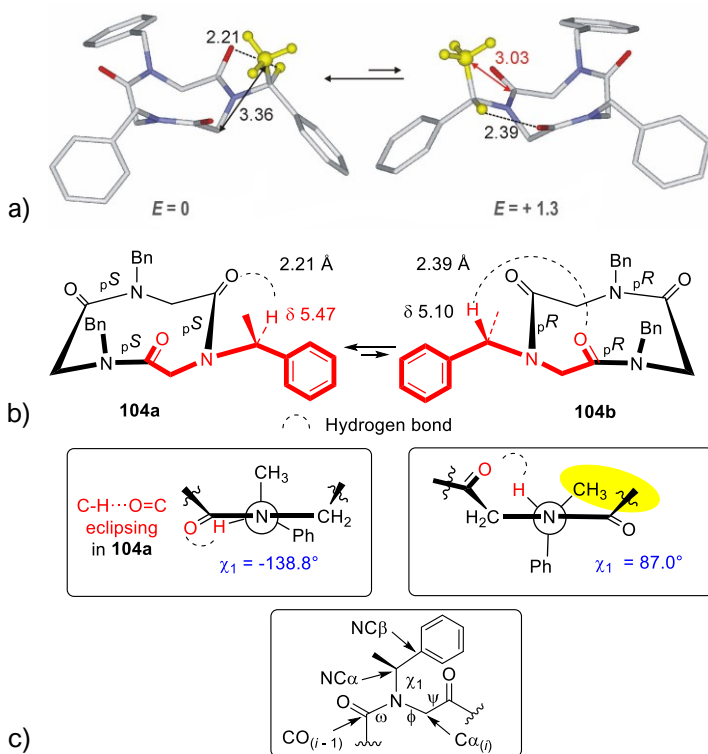


Figure 3.30. a) Minimum energy structures (kcal/mol, DMSO; distances in Å; distances in black, favorable hydrogen bonds; red, unfavorable C-C distance) of conformational diastereoisomers **104a** and **104b** (yield 19%) with their b) schematic structures. C, silver; N, blue; O, red; CH₃, yellow. c) Newman projections indicating angle χ_1 in both conformational isomers. In yellow is the steric clash between methyl and carbonyl group, plus dihedral angles definition for general residue i : ω [$\text{C}\alpha_{(i-1)}$; $\text{CO}_{(i-1)}$; $\text{N}_{(i)}$; $\text{C}\alpha_{(i)}$], ϕ [$\text{CO}_{(i-1)}$; $\text{N}_{(i)}$; $\text{C}\alpha_{(i)}$; $\text{CO}_{(i)}$], ψ [$\text{N}_{(i)}$; $\text{C}\alpha_{(i)}$; $\text{CO}_{(i)}$; $\text{N}_{(i+1)}$], χ_1 [$\text{CO}_{(i-1)}$; $\text{N}_{(i)}$; $\text{NC}\alpha$; $\text{NC}\beta$] (exemplified also in Paragraph 3.1.3).

The favourable pairing between *S* stereogenic centre and pS planar chirality is due to a $\chi_1 \approx -130^\circ$ torsion angle, generated by inter-residue Ph(Me)NC-H/C=O eclipsing. This arrangement, with similar χ_1 values, had already been observed in linear peptoids

¹¹⁴ Already observed in linear peptoid helices. Stringer J. R., Crapster J. A., Guzei I. A., Blackwell H. E., *J. Am. Chem. Soc.* **2011**, *133*, 15559-15567.

¹¹⁵ Hoffmann R. W., *Chem. Rev.* **1989**, *89*, 1841-1860.

already mentioned, such as $Nspe_8$ ($\chi_1 \approx -120^\circ$),^{25c} $Nrch_5$ ⁹⁴ (enantiomorphous R/pR configurational pairing) and $cyclo-[Nspe]_9$ (**105**)²⁷ ($\chi_1 \approx -130^\circ$). The mismatch S/pR caused a $\chi_1 \approx 90^\circ$ and a higher energy.

The third most common secondary structure in peptides, after α -helices and β -strands, are γ -turns.¹¹⁶ Based on the values of the torsion angles, we were able to classify the turn present in **104b** as a “classic” γ -turn (φ from 70 to 95° ; ψ from -75 to -45°),^{16b} while **104a** values fell within the definition of an “inverse” γ -turn ($\varphi = -79 \pm 40^\circ$; $\psi = 69 \pm 40^\circ$) (the most common one).¹¹⁷

However, the presence of *cis* amide bonds in cyclic trimeric peptoids required a different classification. We, therefore, introduced the acronym “CP” (from “Cyclic Peptoid”) to identify these turns, a subscript number to identify the type and, as in the classic notation, a prime symbol for motifs with opposite torsion angles (“inverse” turns). According to this notation, cyclic peptoids **104a** and **104b** showed CP'_1 and CP_1 type γ -turns, respectively (Figure 3.31), with $Ca_{(i)}-Ca_{(i+2)}$ distances shorter than 5.5 \AA .¹¹⁸

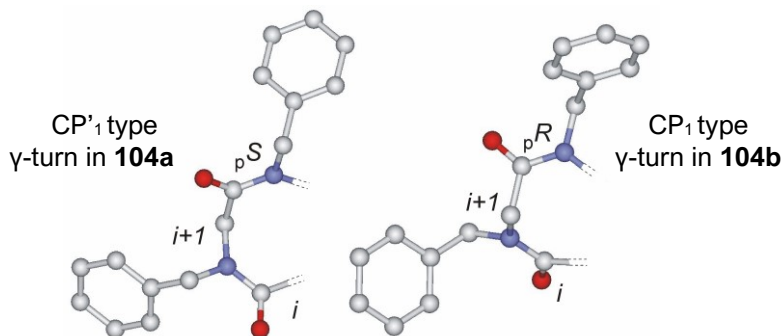


Figure 3.31. Folding of cyclic peptoids **104a** and **104b** in CP'_1 and CP_1 type γ -turns, respectively. C, silver; N, blue; O, red.

Table 3.1 reports a comparison among φ , ψ and ω torsion angles values in γ -turns and compounds **104a/104b**.

Compound	Turn type	ω_{i+1} (planar chirality)	φ_{i+1}	ψ_{i+1}	Distance $Ca_{(i)}-Ca_{(i+2)}$ (\AA)
104a	CP'_1	2.0 (pS)	-99.3	94.2	2.97
-	CP'_1 ^a	0 (pS)	-95	95	≤ 5.5
-	Inverse γ ¹¹⁶	180	-79	69	≤ 5.5 ¹¹⁸

¹¹⁶ a) Guruprasad K., Rajkumar S., *J. Biosci.* **2000**, *25*, 143-156; b) Kahn M., Eguchi M., in *Synthesis of Peptides and Peptidomimetics*, Thieme, Stuttgart, **2004**, Vol. E22c, Chapter 12.2, pp. 741-758.

¹¹⁷ Nemethy G., Printz M. P., *Macromolecules* **1972**, *5*, 755-758.

¹¹⁸ Kaewpet M., Odell B., King M. A., Banerji B., Schofield C. J., Claridge T. D. W., *Org. Biomol. Chem.* **2008**, *6*, 3476-3485.

104b	CP ₁	-1.8 (<i>pR</i>)	95.9	-98.3	2.96
-	CP ₁ ^a	0 (<i>pR</i>)	95	-95	≤5.5
-	Classic γ ¹¹⁶	180	75	-64	≤5.5 ¹¹⁸

^a Idealized torsion angles values.

Table 3.1. Central residue dihedral angle values, amide bonds planar chirality and C $\alpha_{(i)}$ -C $\alpha_{(i+2)}$ distances for CP₁- and CP₁-type γ -turns in **104a** and **104b**.

With the aim to induce formation of a prevailing conformational isomer, we designed other two compounds, bearing two and three *Nspe* units, respectively. To our surprise, the cyclization reaction of the linear counterparts led to rearrangement products. *Cyclo*-[*Nspe*₂-*Npm*], **106**, and *cyclo*-[*Nspe*]₃, **107**, were not obtained; instead, the usual cyclization protocol gave bicyclic dehydrated congeners **108** and **109**, in 25 and 26% yield, respectively.

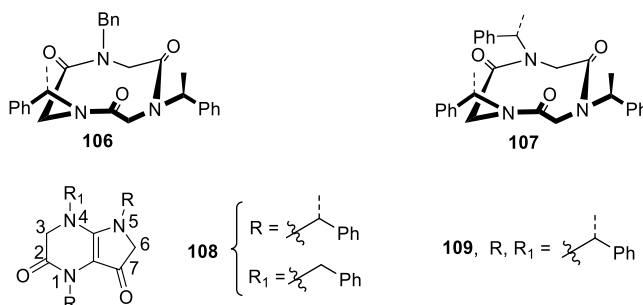
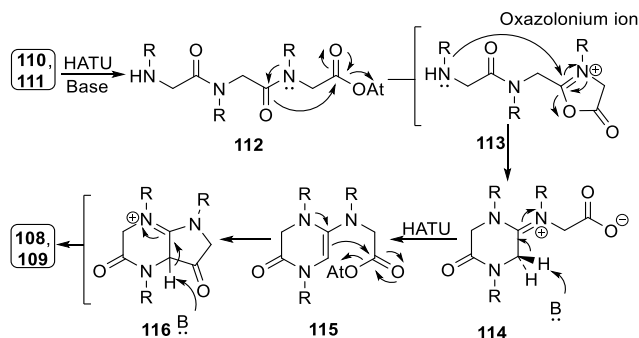


Figure 3.32. Expected cyclic tripeptoids **106** and **107**, and respective rearranged products **108** and **109**, deriving from the cyclization of H-[*Npm*-*Nspe*]₂-OH (**110**), and H-[*Nspe*]₃-OH (**111**), respectively.

The structure of 3,4,5,6-tetrahydro-1H-pyrrolo[2,3-b]pyrazine-2,7-dione heterocyclic nucleus has never been reported before in the literature, and inferred by one- and two-dimensional NMR techniques. Changing the cyclization conditions (PyBOP/DIPEA^{30b} or EDC/HOBt/TEA^{100b}) led to rearrangement products.

We postulated the rearrangement mechanism as depending on the formation of an oxazolonium ion intermediate¹¹⁹ (**113**), *N*-terminal aminolysis (from **114** to **115**) and pyrrole ring closure (to form hypothetical immonium **116**), leading to a double intramolecular segment coupling linking the oligomers termini to the central amide junction (Scheme 3.7).

¹¹⁹ a) Oxazolonium ions are reported as unwanted reactive species during the carbodiimide-mediated amide condensations (their intrinsic ability to enolize induces epimerization of stereogenic centres of chiral amino acid residues); b) Kates S. A., Albericio F. (Eds.), in *Solid Phase Synthesis: A Practical Guide*, Marcel Dekker, Inc., New York, 2000.



Scheme 3.7. Postulated mechanism for the formation of pyrrolopyrazines **108** and **109**. At = 7-azabenzotriazole; R = benzyl or *N*-(*S*)-(1-phenylethyl) side-chain.

Similar rearrangement products were observed in the cyclization reaction of (H-[Nr1npe]₃-OH, **117**) with the bulkier (*R*)-(+)-1-(1-naphthyl)ethylamine (to give bicyclic **118**). Cyclization of H-[Npm-Nr1npe-Npm]-OH (**119**) gave a complex mixture of products. Cyclization of linear oligomer H-[Nnpm-Nr1npe-Nnpm]-OH (**120**), comprising two 1-naphthylmethylamine moieties, gave a complex mixture of products, too.

We investigated *via* DFT calculations the formation of bicyclic **109** over cyclic peptoid **107**, and found a conspicuous energy difference (-15.1 kcal/mol vs. -7.5 kcal/mol, DMF), justified by the entropically favorable development of two water molecules for the formation of pyrrolopyrazine **109** (instead of one, as in **107**).

To further validate our assigned structure, we tried and crystallize compound **109**, obtaining single crystals suitable for X-ray diffraction; X-ray analysis confirmed the formation of a pyrrolopyrazine nucleus but revealed the presence of a hydroxyl group on C-3, due to an autoxidation process.¹²⁰

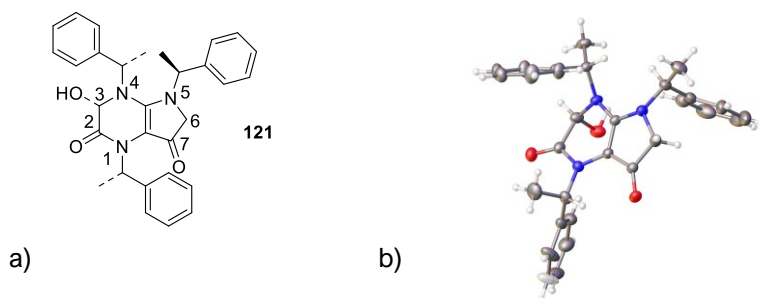


Figure 3.33. a) Oxidized product **121** and its b) ORTEP drawing. Ellipsoids are drawn at 20% probability level. C, silver; N, blue; O, red; H, white.

¹²⁰ Formation of (*S*)-3,4,5,6-tetrahydro-3-hydroxy-1,4,5-tris((*S*)-1-phenylethyl)-1H-pyrrolo[2,3-*b*]pyrazine-2,7-dione (**121**) was reasonably due to autoxidation processes. Its structure was confirmed by spectroscopic and spectrometric analyses of the crystalline sample. Crystals obtained by slow evaporation of an ethyl acetate solution of **109**.

The crystallization of **121** was facilitated by an intermolecular hydrogen bonding between C-7 carbonyl oxygen and hydroxyl group (OH \cdots O 2.677 Å, O-H \cdots O 169.3°), giving rise to a left-handed helix through the crystallographic 2_1 screw axis parallel to the shortest cell axis (*i.e.* *a* axis).

3.4.1.2 Cyclic tetramers

We then moved our attention to cyclic tetramers; also in this case, we designed two scaffolds, the first one bearing a single *Nspe* unit, *cyclo*-[*Npm*₂-*Nspe*-*Npm*] (**122**), the second, *cyclo*-[*Npm*-*Nspe*]₂ (**123**), comprising alternated chiral and achiral side-chains. The accurate NMR analyses allowed the full assignment of the two *ctct* structures, in the first case displaying a major conformational diastereomer (~85%, **122a**, plus a minor one, ~15%, **122b**), in the second case a single compound.

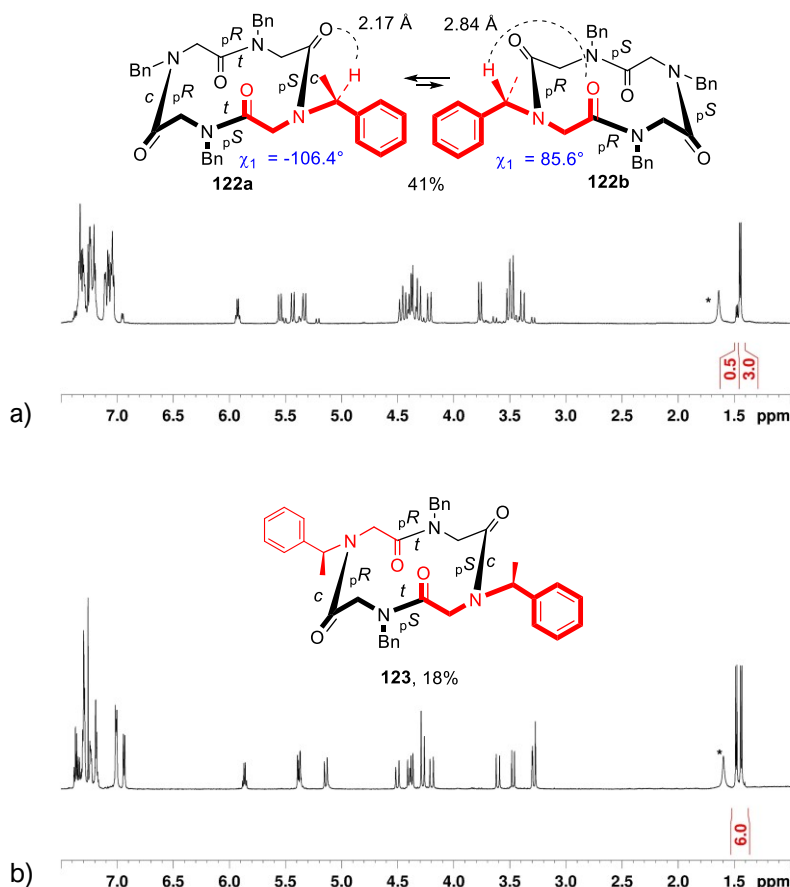


Figure 3.34. Schematic structure and relative $^1\text{H-NMR}$ spectrum (600 MHz, CDCl_3 , 298 K, 7.5-1.0 ppm expansion) of a) **122a/122b** and b) **123**. In red are reported the resonances relative to the side-chain methyl group(s). Water impurities are labelled with a black asterisk.

DFT calculations testified for the preferred formation of *cyclo*-[(*cis*,*pR*)Npm-(*trans*,*pR*)Npm-(*cis*,*pS*)Nspe-(*trans*,*pS*)Npm] **122a**, showing a favorable *S*_{*p*}*S* configurational pairing due to a reduced allylic strain ($\chi_1 = -106.4^\circ$), over *cyclo*-[(*cis*,*pS*)Npm-(*trans*,*pS*)Npm-(*cis*,*pR*)Nspe-(*trans*,*pR*)Npm] **122b**, displaying a *S*_{*p*}*R* configurational mismatch originated by the unfavorable ($\chi_1 = 85.6^\circ$), ($\Delta E = + 1.3$ kcal/mol, CHCl₃).

In both of the conformational diastereoisomers the bulky *N* α -chiral side-chain is located on a *cis* amide bond, however the *S*_{*p*}*S* match in **122a** allows a shorter C-H \cdots O=C hydrogen bonding (also testified by the higher methine resonance, δ 5.92 ppm), like in the case of trimer **104a**.

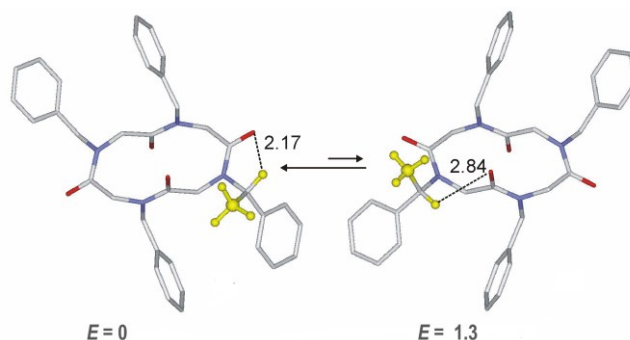


Figure 3.35. Minimum energy structures of conformational diastereoisomers **122a/122b** plus respective internal energies (kcal/mol, CHCl₃). Distances in Å; distances in black, favorable hydrogen bonds. C, silver; N, blue; O, red; CH₃, yellow.

We were able to obtain single crystals of **122a/122b**¹²¹ suitable for X-ray diffraction analysis, which showed the selective crystallization of major conformational isomer **122a** (Figure 3.36).

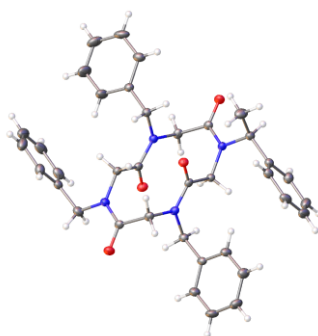


Figure 3.36. ORTEP drawing of compound **122a**. Ellipsoids are drawn at 20% probability level. C, silver; N, blue; O, red; H, white.

¹²¹ Needle-like crystals obtained by slow cooling of a hot dichloromethane solution of **122a/b**.

As for compound **123** (>98%, $^1\text{H-NMR}$), theoretical studies showed a marked preference for *cyclo*-[(*cis*,*pR*)*Nspe*-(*trans*,*pR*)*Npm*-(*cis*,*pS*)*Nspe*-(*trans*,*pS*)*Npm*], with both the *Nspe* residues on *cis* amide bonds (also testified by the high resonances of the methine protons (5.86 and 5.38 ppm and the small $\Delta\delta$ values detected for the diastereotopic methylene protons, 0.22 and 0.10 ppm, attesting *trans* *Npm* junctions). The higher energy of the hypothetical isomer **124** ($\Delta E = + 3.9$ kcal/mol) was caused by steric strain between the methine of the side-chains on *trans* amide bonds and the intra-annular CH_2 (Figure 3.37 b)).

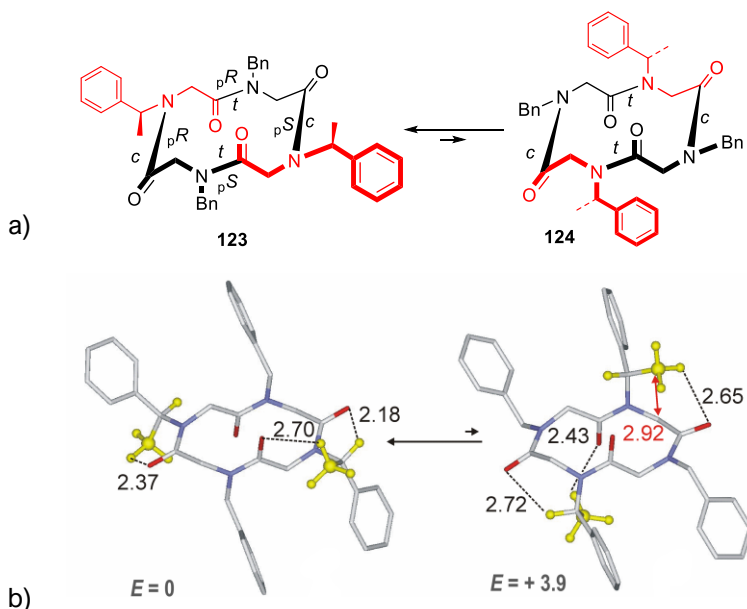


Figure 3.37. a) Schematic and b) minimum energy structures of cyclic tetramers **123** and **124** (kcal/mol, CHCl_3). Distances in Å; distances in black, favorable hydrogen bonds; red, unfavorable C-C distance. C, silver; N, blue; O, red; CH_3 , yellow.

Again, the structural assignment was confirmed by X-ray, as compound **123** crystallized from a solution of chloroform/toluene (2:1) as single crystals suitable for the measurements. Figure 3.40 reports the ORTEP drawing. In agreement with the other studies, **123** crystallized in space group $P2_1$ with a *ctct* tetralactam core geometry and overall rectangular shape of the peptoid backbone.

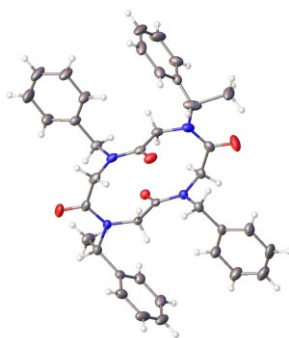


Figure 3.38. ORTEP drawing of compound **123**. Ellipsoids are drawn at 20% probability level. C, silver; N, blue; O, red; H, white.

The close evaluation of ω , ϕ and ψ torsion angles allowed the association of cyclic tetramers structures with type VI β -turns. These foldings are characterized by the presence of a *cis* proline at the $i+2$ residue;^{117,118,122} in our case, the large deviations from the canonical angle values suggested a better classification as non-classified type IV β -turns. Turn motifs in **122a** and **122b** were therefore defined as type CP₂ and CP'₂ β -turns; the same accounts for the two halves of compound **123**. The following Table 3.2 reports the dihedral angle values of compounds **122-123**, compared with type VIb β -turn, which is the closest to the CP'₂ turn.

Cpd	β -turn type	ω_{i+1} (planar chirality)	ϕ_{i+1}	ψ_{i+1}	ω_{i+2} (planar chirality)	ϕ_{i+2}	ψ_{i+2}	Distance $C\alpha_{(i)}-C\alpha_{(i+3)}$ (Å)
122a	CP ₂	-170.7 (<i>pS</i>) (-169.5)	118.8 (118.9)	-65.8 (-69.4)	-6.6 (<i>pR</i>) (0.8)	93.8 (91.6)	-169.9 (-172.4)	2.93 (2.89)
122b	CP ₂	-170.4 (<i>pS</i>)	119.6	-59.2	-13.8 (<i>pR</i>)	100.3	-171.7	2.91
123	CP ₂	-170.4 (<i>pS</i>) (-171.1)	121.3 (118.4)	-67.4 (-60.0)	-2.7 (<i>pR</i>) (-13.4)	93.0 (99.6)	-173.0 (-170.8)	2.93 (2.87)
-	CP ₂ ^b	180 (<i>pS</i>)	120	-65	0 (<i>pR</i>)	95	-170	≤ 7
122a	CP' ₂	170.0 (<i>pR</i>) (170.4)	-119.6 (-121.5)	65.3 (63.4)	5.4 (<i>pS</i>) (7.2)	-91.0 (-95.1)	171.8 (171.2)	2.93 (2.86)
122b	CP' ₂	169.0 (<i>pR</i>)	-119.1	64.2	7.4 (<i>pS</i>)	-95.1	170.0	2.94
123	CP' ₂	169.4 (<i>pR</i>) (171.8)	-119.0 (-120.9)	64.3 (63.4)	5.5 (<i>pS</i>) (6.5)	-91.7 (-93.8)	171.5 (170.4)	2.91 (2.83)
-	CP' ₂ ^b	180 (<i>pR</i>)	-120	65	0 (<i>pS</i>)	-95	170	≤ 7

¹²² a) de Brevern A. G., *Sci. Rep.* **2016**, 6, 33191; b) Pelay-Gimeno M., Glas A., Koch O., Grossmann T. N., *Angew. Chem. Int. Ed.* **2015**, 54, 8896-8927.

-	Vib ¹¹⁶	180	-135	135	0	-75	160	≤ 7 ^{122a}
---	--------------------	-----	------	-----	---	-----	-----	---------------------

^a In parenthesis data from the X-ray crystal structures.

^b Idealized torsion angles values.

Table 3.2. Central residues dihedral angle values, amide bonds planar chirality and $\text{Ca}_{(i)}\text{-Ca}_{(i+3)}$ distances for CP_2 and CP'_2 *tct* β -turns in **122a**, **122b**, and **123**.

Interestingly, in the case of diastereomeric **122a/122b**, for the peculiar symmetry properties of the *ctct* oligoamide scaffold (which, in the absence of a chiral side-chain, would show an inversion centre),¹²³ both CP_2 and CP'_2 turns are present in each half of the same molecule (indicated in blue and black, Figure 3.39).

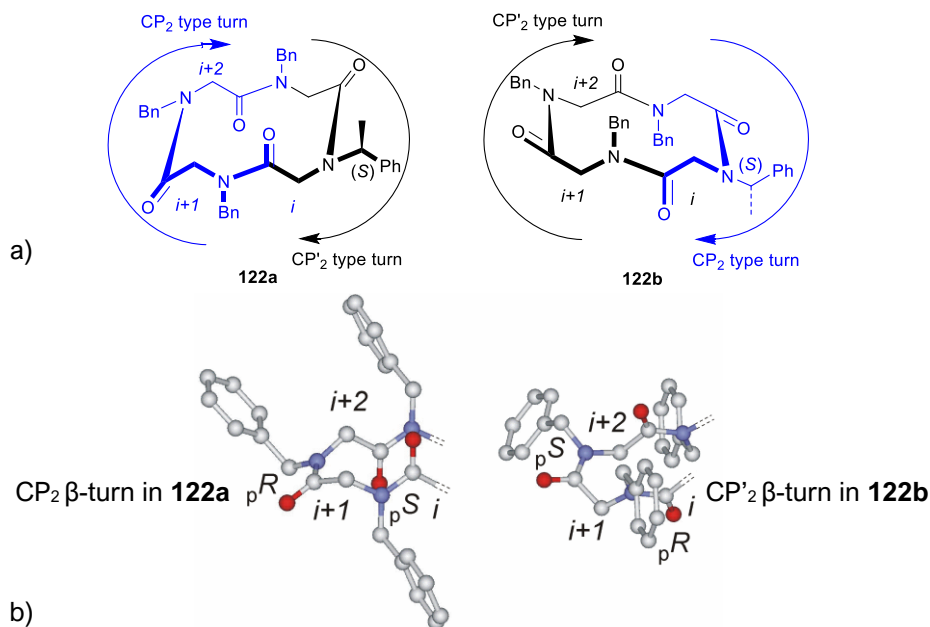


Figure 3.39. a) Schematic structures of conformational diastereoisomers depicting type CP_2 and CP'_2 β -turns present in **122a** and **122b**. The arrows point toward the $\text{CO}\rightarrow\text{N}$ direction. b) Portion of models of CP_2 and CP'_2 β -turns extracted from the minimum energy structures of **122a** and **122b**, respectively. C, silver; N, blue; O, red.

As for asymmetric **123**, the two halves of the molecule show opposite orientation of the same turn as well (structures not shown).

Lastly, seeking additional stability, we attempted the cyclization of $\text{H-[Nspe]}_4\text{-OH}$, **125**, and $\text{H-[Npm}_2\text{-Nr1npe-Npm]-OH}$, **126**. The ¹H-NMR analysis of the crude products revealed, in the first case, no cyclization product (probably due to the proximity of two

¹²³ Schettini R., Costabile C., Della Sala G., Iuliano V., Tedesco C., Izzo I., De Riccardis F., *J. Org. Chem.* **2018**, *83*, 12648-12663.

*N*spe bulky residues); in the second case, a complex mixture of conformational isomers in slow equilibrium on the NMR time scale.

3.4.1.3 Cyclic hexamers

While the transannular strain has a beneficial effect in stabilizing the macrocycle conformation in trimers and tetramers, resulting in a ΔG^\ddagger for the ring inversion > 20 kcal/mol,^{102,124} the stabilization of the eighteen-membered cyclic hexamers is more challenging, as the barrier for the ring inversion is lower ($\Delta G^\ddagger \sim 14$ -16 kcal/mol).^{102,21b,58,28,82a}

The introduction of a single stereocenter on the backbone of the macroring, in **100** and **102**, resulted in the presence of multiple conformational isomers in slow equilibrium on the NMR time scale (Paragraph 3.3.1.3).

We, therefore, decided to proceed with the preparation of three model compounds, showing respectively one, three and six *N*spe residues, shown in Figure 3.40.

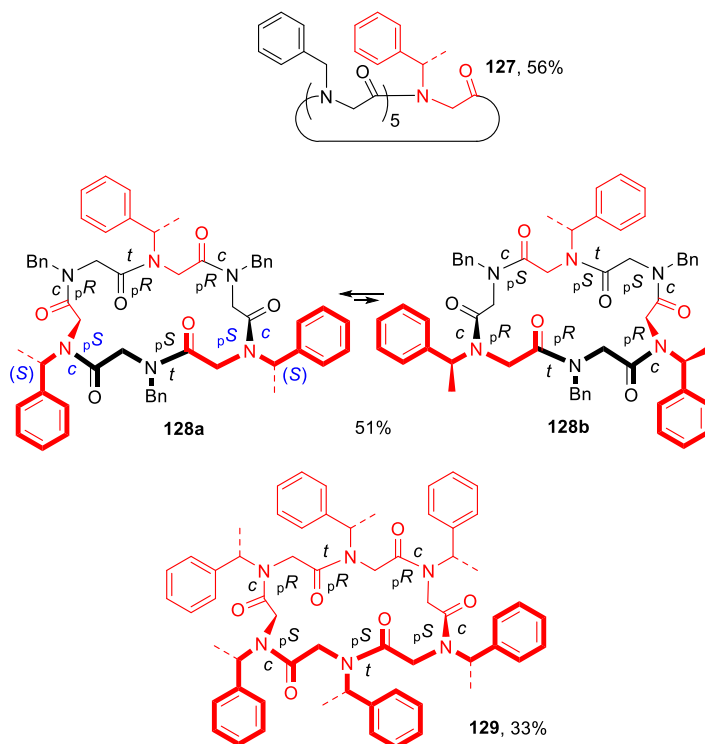


Figure 3.40. Model cyclic hexamers *cyclo*-[*Npm*₄-*Nspe*-*Npm*] (**127**), *cyclo*-[*Nspe*-*Npm*]₃ (**128a/128b**), *cyclo*-[*Nspe*]₆ (**129**).

¹²⁴ Shaug J., *Acta Chem. Scand.* **1971**, 25, 2771-2772.

While the cyclization of (H-[Npm₄-Nspe-Npm]-OH, **130**) led to the formation a complex mixture of multiple species in slow equilibrium on the NMR time scale, the introduction of three and six *N*α-chiral side-chains (H-[Nspe-Npm]₃-OH, **131** and H-[Nspe]₆-OH, **132**) yielded *cctcct*-**128a** (or *cctcct*-**128b**, as a possible alternative conformational isomer) and *cctcct*-**129** as a major conformationally homogeneous species. The accurate observation of the chemical shifts of the (*S*)-(1-phenylethyl) Cα-H groups and the Δδ of the CH₂ benzyl side-chains (Figure 3.41), together with the NMR two-dimensional analyses, allowed the full assignment for **128a/128b** and **129**. It is noteworthy that these two compounds, together with *cyclo*-[N*Phe*-N*Val*]₃ (**49a**) constitute the only examples present in the literature of conformationally stable cyclohexapeptoids (non-complexed or non-arylated).

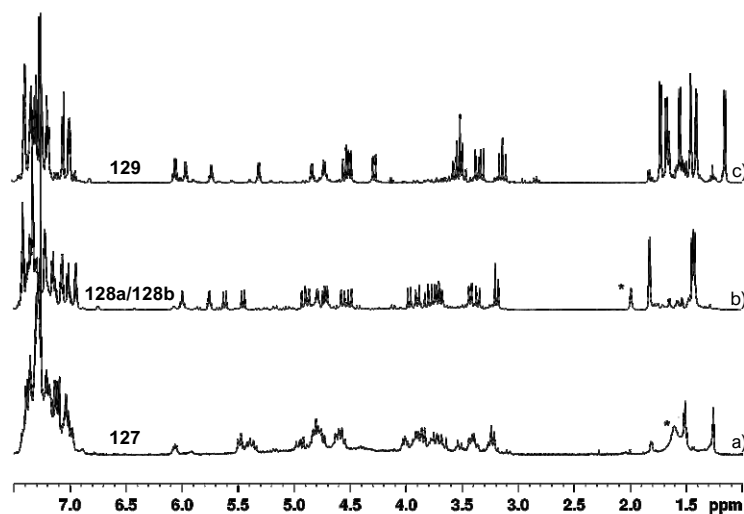


Figure 3.41. ¹H-NMR spectra of a) *cyclo*-[Npm₄-Nspe-Npm] (**127**), b) *cyclo*-[Nspe-Npm]₃ (**128a/128b**), c) *cyclo*-[Nspe]₆ (**129**). 600 MHz, CDCl₃, 7.5-1.0 ppm.

The preferential formation of *cyclo*-[(*cis*,_p*R*)Npm-(*trans*,_p*R*)Nspe-(*cis*,_p*R*)Npm-(*cis*,_p*S*)Nspe-(*trans*,_p*S*)Npm-(*cis*,_p*S*)Nspe] **128a** (70%, ¹H-NMR analysis) was confirmed by DFT calculations. The matching *cis*-(_p*S,S*) configurations (blue in the schematic structure of Figure 3.40) allowed the formation of key hydrogen bonds between side-chains methine groups on *cis* amide bonds and adjacent carbonyl groups (C-H⋯O=C distance: 2.19 and 2.33 Å, respectively). The _p*R/S* mismatch in **128b** induced a higher internal energy (Δ*E* = + 3.5 kcal/mol, Figure 3.42).

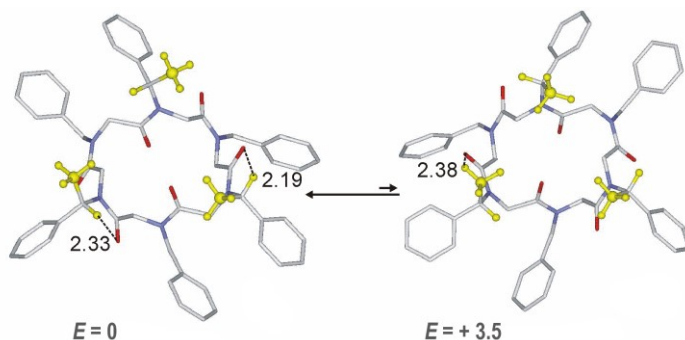


Figure 3.42. Minimum energy structures of conformational diastereoisomers **128a** and **128b** (kcal/mol, CHCl_3). Distances in Å; distances in black, favorable hydrogen bonds. C, silver; N, blue; O, red; CH_3 , yellow.

Interestingly, in the case of *cyclo*-[Nspe]₆ (**129**), the configurational inversion of all the amide bonds gives back the same structure, *cyclo*-[(*cis*,*pR*)Nspe-(*trans*,*pR*)Nspe-(*cis*,*pR*)Nspe-(*cis*,*pS*)Nspe-(*trans*,*pS*)Nspe-(*cis*,*pS*)Nspe] (shown in Figure 3.40) and therefore just one *cctcct*-conformational isomer was possible for this macrocyclic species.

The structural hypothesis on **129** was confirmed by X-ray studies.¹²⁵ We obtained single crystals suitable for the measurements by slow evaporation from a 2:1 ethyl acetate:diethyl ether solution of **129**.

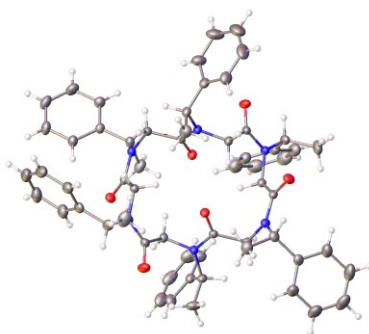


Figure 3.43. ORTEP drawing of conformational isomer **129**. Ellipsoids are drawn at 20% probability level. C, silver; N, blue; O, red; H, white.

Kirshenbaum and co-workers had already classified the turn observed in cyclohexamer *cyclo*-[Nme-Npm]₃ (**133**) as morphologically similar to type I (and III) β -turns.²⁸

¹²⁵ Butterfoss G. L., Renfrew P. D., Kuhlman B., Kirshenbaum K., Bonneau R., *J. Am. Chem. Soc.* **2009**, *131*, 16798-16807. In this paper the structure of **129** is mentioned, but no NMR or X-ray diffraction data are provided.

However, the large deviations observed for the torsion angles, together with the presence of two *cis* amide bonds, suggested a better fitting with a type I polyproline helix (PPI). According to our definition, we introduced CP₃ and CP'₃ turn motifs, which are, respectively, similar to the right-handed polyproline I (PPI) helix ($\varphi = -75^\circ$; $\psi = 160^\circ$) and the left-handed PPI helix ($\varphi = 75^\circ$; $\psi = -160^\circ$).

Figure 3.44 reports the turn motifs in compound **128a**. Similarly to the case of cyclic tetramers **122-123**, both the classic turn and its inverse are present in the two halves of the same molecule.

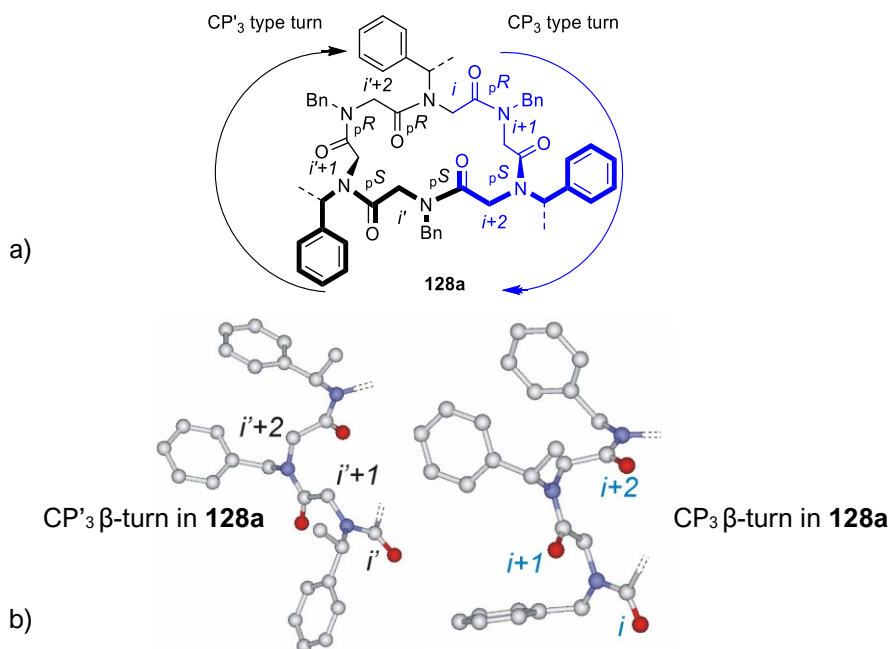


Figure 3.44. a) Schematic structures of conformational diastereoisomers depicting type CP'₃ and CP₃ β -turns present in **128a**. The arrows point toward the CO \rightarrow N direction. b) Portion of models of CP'₃ and CP₃ β -turns extracted from the minimum energy structures of **128a**. C, silver; N, blue; O, red.

Table 3.3 reports the dihedral angle values and distances relative to hexamers **128a** and **129**, compared with the classic PPI peptide helix. It is interesting to note that in terms of torsion angles, CP₃ is assimilable to right-handed polyproline I (PPI) helix ($\varphi = -75^\circ$; $\psi = 160^\circ$), while CP'₃ is more similar to the left handed PPI helix ($\varphi = 75^\circ$; $\psi = -160^\circ$). The main difference between CP₃ and CP'₃ and PPI models is the planar chirality of the amide bond (which is opposite in the peptoid and peptide models). In larger cyclic peptoids (with six or more residues), where the ring strain is lower, the φ and ψ torsion

angles ($\varphi \approx 70^\circ$ and -70° and $\psi \approx 180^\circ$ and -180°) are similar to those reported for the majority of published peptoid structures.¹²⁶

Cpd	β -turn type	ω_{i+1} (planar chirality)	φ_{i+1}	ψ_{i+1}	ω_{i+2} (planar chirality)	φ_{i+2}	ψ_{i+2}	Distance $C\alpha_{(i)}-C\alpha_{(i+3)}$ (Å)
128a	CP ₃	12.4 (pR)	-74.0	176.7	-7.6 (pS)	-69.4	168.6	5.35
129^a	CP ₃	18.4 (pR)	-75.8	167.6	-0.2 (pS)	-79.1	-179.2	5.41
-	CP ₃ ^b	0 (pR)	-75	175	0 (pS)	-75	175	≤ 7
-	Right-handed PPI helix	0 (pS)	-75	160	-	-	-	-
128a	CP' ₃	-16.1 (pS)	77.9	-176.4	5.7 (pR)	74.6	-170.4	5.35
129^a	CP' ₃	-19.9 (pS)	75.7	-174.7	-2.0 (pR)	78.6	-159.9	5.41
-	CP' ₃ ^b	0 (pS)	75	-175	0 (pR)	75	-175	≤ 7
-	Left-handed PPI helix	0 (pR)	75	-160	-	-	-	-

^a In parenthesis data from the X-ray crystal structures.

^b Idealized torsion angles values.

Table 3.3. Central residues dihedral angle values, amide bonds planar chirality and $C\alpha_{(i)}-C\alpha_{(i+3)}$ distances for type CP₃ and CP'₃ β -turns in **128a** and **129**, plus typical PPI values.

3.4.1.4 Cyclic octamers

Cyclooctapeptoids often show multiple conformations in the solution state.^{80,102,123,82a} For this class of macrocycles, we designed three compounds, again with increasing number of *N*-(S)-(1-phenylethyl) side-chains. The cyclization of H-[Npm₆-Nspe-Npm]-OH (**134**), containing a single *Nspe* monomer, led to a mixture of conformational isomers. Likewise, H-[Npm-*Nspe*₂-Npm₂-*Nspe*₂-Npm]-OH (**135**), designed to match the *ccttcctt* amide bond geometry pattern often shown by rigid cyclic octamers (*Nspe* residue favors *cis* amide bonds),^{95,102} produced a conformational heterogeneous macrocycle. Only the cyclization of homooligomer H-[*Nspe*]₈-OH (**136**) showed the presence of a single, prevalent, C₂-symmetric species (~62%, ¹H-NMR analysis, C₆D₅CD₃), with four side-chains located on *cisoid* bonds (δ 6.14/5.47 for the C α -H groups) and four positioned on *transoid* junctions (δ 4.40/4.22). It should be noted that, for the symmetry properties of *ccttcctt*-

¹²⁶ Spencer R. K., Butterfoss G. L., Edison J. R., Eastwood J. R., Whitlam S., Kirshenbaum K., Zuckermann R. N., *Biopolymers* **2019**, *110*, e23266.

cyclic octamers, two possible inequivalent C_2 -symmetric¹²³ conformational diastereoisomers are possible (shown in Figure 3.45).

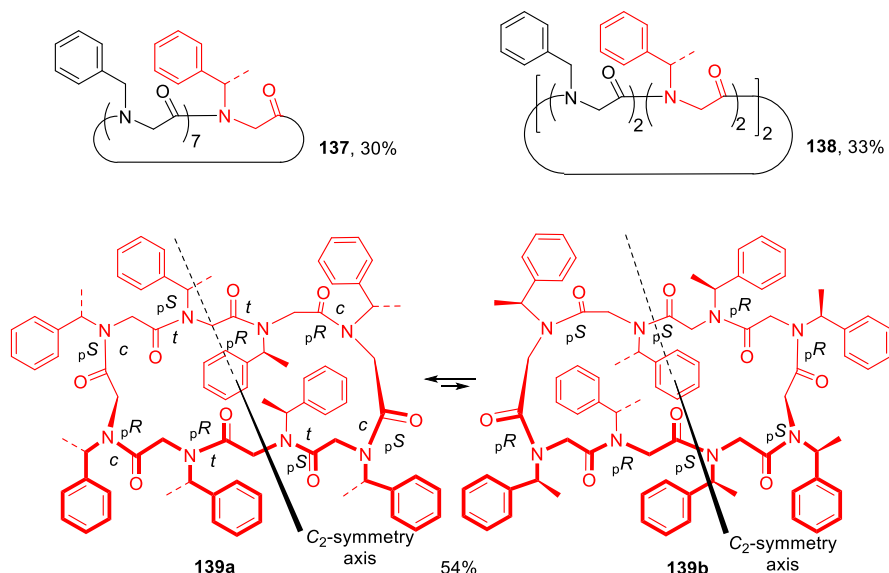


Figure 3.45. Schematic structures of cyclic octamers **137**, **138** and conformationally non-equivalent **139a/b**.

Thanks to DFT calculations we were able to assign the framework of the major conformational isomer to *cyclo-[[$(cis,{}_pR)$ Nspe- $(cis,{}_pS)$ Nspe- $(trans,{}_pS)$ Nspe- $(trans,{}_pR)$ Nspe] $_2$]*, **139a**. The isomer *cyclo-[[$(cis,{}_pS)$ Nspe- $(cis,{}_pR)$ Nspe- $(trans,{}_pR)$ Nspe- $(trans,{}_pS)$ Nspe] $_2$]*, **139b**, was unfavored due to the presence of multiple steric clashes between methyl and carbonyl groups ($\Delta E = +2.6$ kcal/mol).

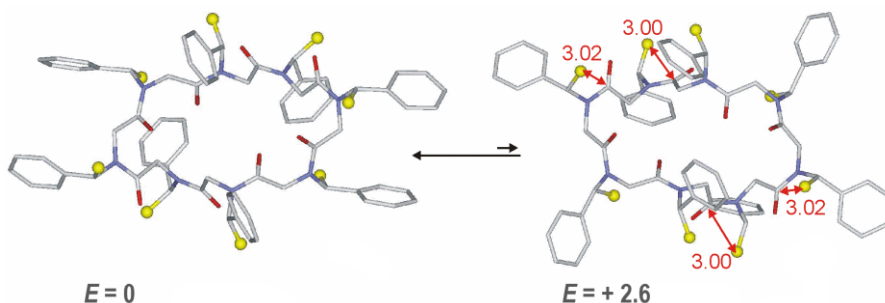


Figure 3.46. Minimum energy structures of cyclic octamers **139a** and **139b** (kcal/mol, $CHCl_3$). Distances in Å; distances in red, unfavorable C-C distance. C, silver; N, blue; O, red; CH_3 , yellow.

The turn motif shown in **139a** was compatible with CP_3 β -turn (dihedral angle values in Table 3.4, the canonical values were already reported in Table 3.3).

Hypothetically, the inverse turn (CP'_3) could be observed in cyclooctamer with *N*-(*R*)-(1-phenylethyl) side-chains (*i.e.*: *ent*-**139a**).

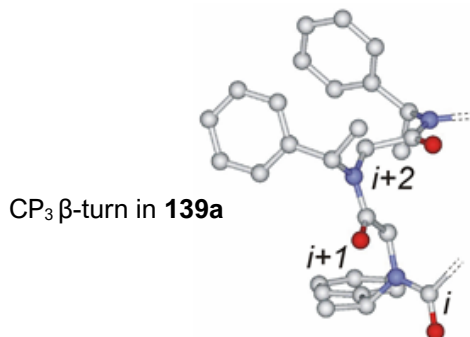


Figure 3.47. Portion of model of CP_3 β -turns extracted from the minimum energy structure of **139a**. C, silver; N, blue; O, red.

Cpd	β -turn type	ω_{i+1} (planar chirality)	ϕ_{i+1}	ψ_{i+1}	ω_{i+2} (planar chirality)	ϕ_{i+2}	ψ_{i+2}	Distance $Ca_{(i)}-Ca_{(i+3)}$ (Å)
139a	CP_3	-4.8 (<i>pR</i>)	-78.8	-173.7	-9.1 (<i>pS</i>)	-69.2	164.2	5.28

Table 3.4. Central residues dihedral angles values, amide bonds planar chirality and $Ca_{(i)}-Ca_{(i+3)}$ distances for type CP_3 *cct* turn in **139a**.

3.4.1.5 Metal complexes

The addition of one equivalent of NaTFPB to hexameric compounds **127**, **128**, **129** caused the formation of 1:1 cycloheptoid:Na⁺ all-*trans* complexes, as previously reported.^{58,107}

Particularly, the complexation of **127** led to two non-equivalent species (78:12 ratio) whose signals overlapping hampered the assignment of the structures.

On the other hand, metalation of **128** caused the formation of a single three-fold, all-*trans* species, in slow equilibrium with the free host; we were able to quantify the association constant ($\log K_a = 4.4$, $-\Delta G^0 = 6.0$ kcal/mol) and to fully assign the structure. The same accounts for cyclic hexamer **129**, as testified by the methine upfield shift (δ 4.91 ppm, CDCl₃) ($\log K_a = 4.3$, $-\Delta G^0 = 5.9$ kcal/mol).

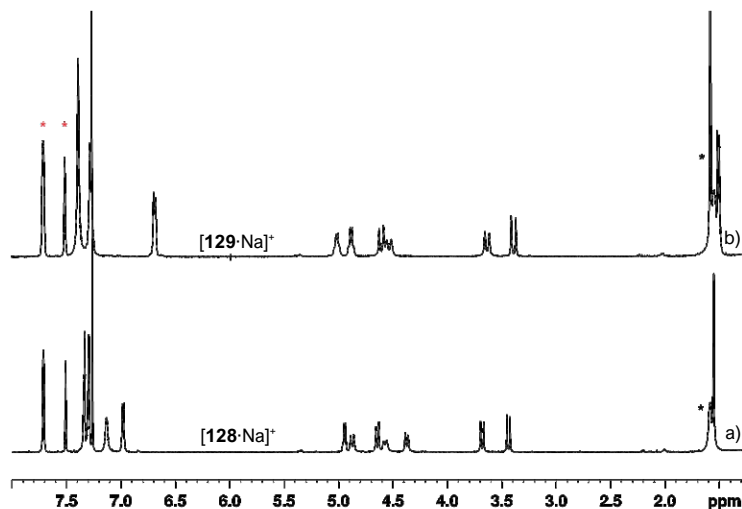
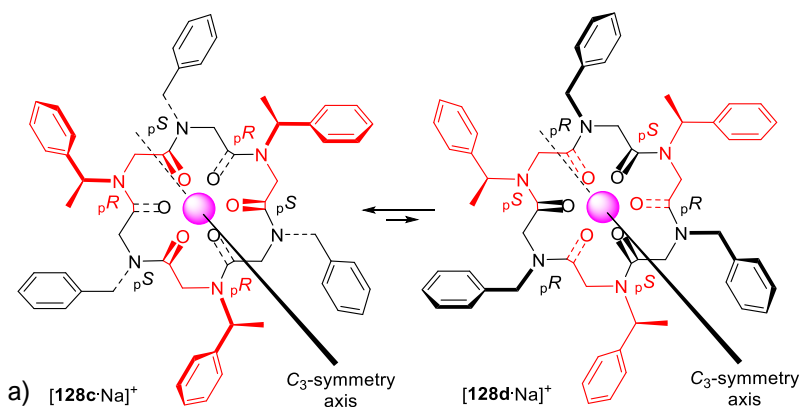


Figure 3.48. $^1\text{H-NMR}$ spectra of monosodium complexes a) $[\mathbf{128}\cdot\text{Na}]^+$ and b) $[\mathbf{129}\cdot\text{Na}]^+$ (600 MHz and 400 MHz, respectively, 3.0 mM solution, CDCl_3). Water or solvent impurities are labelled with a black asterisk. TFPB $^-$ signals are labelled with a red asterisk.

Metalation of **128** could have given two conformational diastereoisomers, both all-*trans* C_3 -symmetric, $[\text{cyclo}-[(\text{trans},pR)\text{Nspe}-(\text{trans},pS)\text{Npm}]_3\text{Na}]^+$ $[\mathbf{128c}\cdot\text{Na}]^+$ and $[\text{cyclo}-[(\text{trans},pS)\text{Nspe}-(\text{trans},pR)\text{Npm}]_3\text{Na}]^+$ $[\mathbf{128d}\cdot\text{Na}]^+$. DFT studies clarified the preferential formation of $[\mathbf{128c}\cdot\text{Na}]^+$; higher energy of $[\mathbf{128d}\cdot\text{Na}]^+$ ($\Delta E = + 14.1$ kcal/mol) was due to repulsive steric interactions between the methyl side-chains and intra-annular methylene groups. Contrarily to free hosts, where the pS/S pairing (for *cis* peptoid junctions) is stabilizing, in metalated compounds, presenting *trans* amide junctions, pR planar chirality is stabilized by *S* stereogenic center.



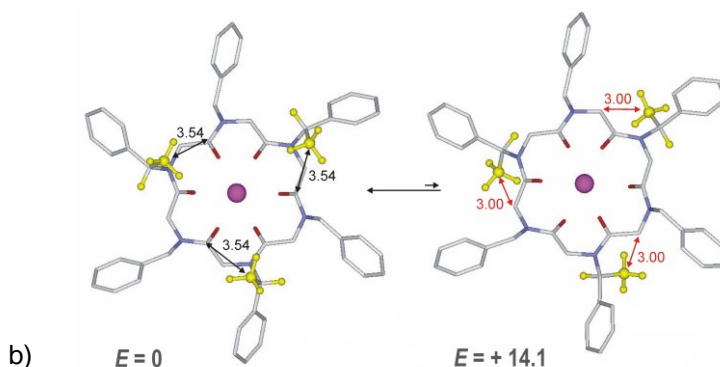


Figure 3.49. a) Schematic structures of all-*trans* conformational diastereoisomers [128c-Na]⁺/[128d-Na]⁺ and their b) minimum energy structures (internal energies, kcal/mol, CHCl₃). Hydrogen atoms have been omitted for clarity except for selected H residues of *Nspe* (in yellow). Distances in Å; distances in black, favorable hydrogen bonds; distances in red, unfavorable C-C distance. C, silver; N, blue; O, red; CH₃, yellow; Na, magenta.

For symmetry reasons, metalation of cyclohomooligomer **129** formed a unique all-*trans* atropisomer: [cyclo-[(*trans*,*pR*)*Nspe*-(*trans*,*pS*)*Nspe*]₃-Na]⁺ ([129-Na]⁺).

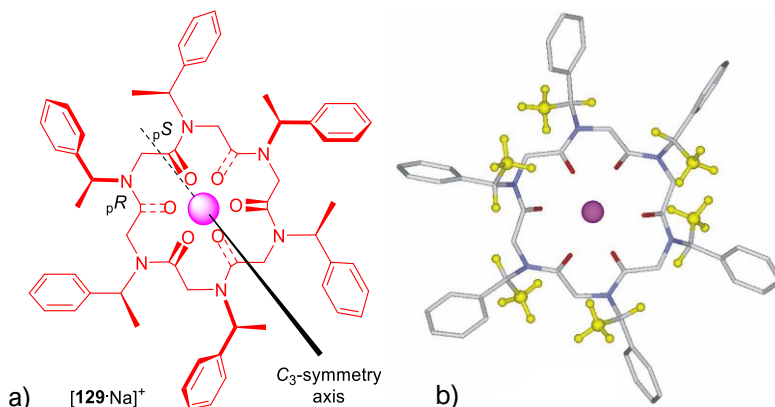


Figure 3.50. a) Schematic structures of all-*trans* [129-Na]⁺ and its b) minimum energy structure. Hydrogen atoms have been omitted for clarity except for selected H residues of *Nspe* (in yellow). C, silver; N, blue; O, red; CH₃, yellow; Na, magenta.

Contrarily to the free hosts, metal complexes show a secondary structure resembling PPII rather than PPI. In fact, the pleated *ttt* arrangement present in both of the metal complexes displayed a loop structure (distance between the Cα_(i) and the Cα_(i+3) is larger than 7.0 Å) similar to left-handed polyproline helix of type II. We indicated this folding as “CPM₁ loop” (M stands for metal).

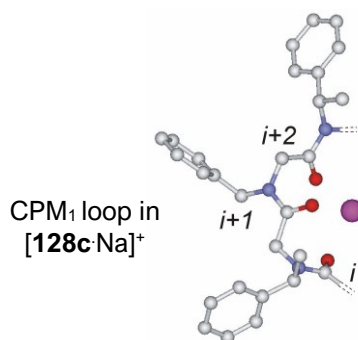


Figure 3.51. CPM₁ loop present in the minimum energy structure of [128c-Na]⁺. C, silver; N, blue; O, red; Na, magenta.

In Table 3.5 the values of ω , ϕ and ψ dihedral angles and the $\text{Ca}_{(i)}-\text{Ca}_{(i+3)}$ distances are reported. The right-handed helix (CPM'₁) could be obtained using *N*-(*R*)-(1-phenylethyl)amine instead of (*S*).

Cpd	Loop type	ω_{i+1} (planar chirality)	ϕ_{i+1}	ψ_{i+1}	ω_{i+2} (planar chirality)	ϕ_{i+2}	ψ_{i+2}	Distance $\text{Ca}_{(i)}-\text{Ca}_{(i+3)}$ (Å)
[128c-Na] ⁺	CPM ₁	174.2 (<i>pR</i>)	-71.5	175.0	-173.5 (<i>pS</i>)	70.5	-174.5	7.59
[129-Na] ⁺	CPM ₁	176.7 (<i>pR</i>)	-73.1	175.4	-179.2 (<i>pS</i>)	75.4	-176.1	7.59
-	CPM ₁ ^a	180 (<i>pR</i>)	-70	175	180 (<i>pS</i>)	70	-175	>7.0
-	Left- handed PPII helix	180 (<i>pS</i>)	-75	150	-	-	-	-
[<i>ent</i> - 128c-Na] ⁺ / [<i>ent</i> -129- Na] ⁺	CPM' ₁ ^a	180 (<i>pS</i>)	70	-175	180 (<i>pR</i>)	-70	175	>7.0

^a Idealized torsion angles values.

Table 3.5. Central residues dihedral angles values, amide bonds planar chirality and $\text{Ca}_{(i)}-\text{Ca}_{(i+3)}$ distances for CPM'₁ type *ttt* turn in hexameric metal complexes.

The addition of two equivalents of sodium to octameric compounds **137**, **138**, **139** caused the formation of 1:2 stoichiometry metal complexes, as stated in previous works.^{80,123,30b}

Similarly to hexameric **127**, the complexation of octameric mono-*N*spe **137** led to multiple conformational isomers in slow equilibrium, whose overlapping signals prevented the assignment of the structures. The NMR analysis evidenced the presence of two C₂-symmetric, almost isoenergetic (58:42 ratio) isomers, [138a₂Na]²⁺ and

[**138b**:2Na]²⁺ ($\log K_a = 4.1$, $-\Delta G^0 = 5.6$ kcal/mol, values referred to the sum of both complexes), and a single C_4 -symmetric species for the homooligomeric [**139**:2Na]²⁺ complex as, for symmetry reasons, simultaneous inversion of all the amide bonds does not change the structure ($\log K_a = 6.3$, $-\Delta G^0 = 8.6$ kcal/mol).

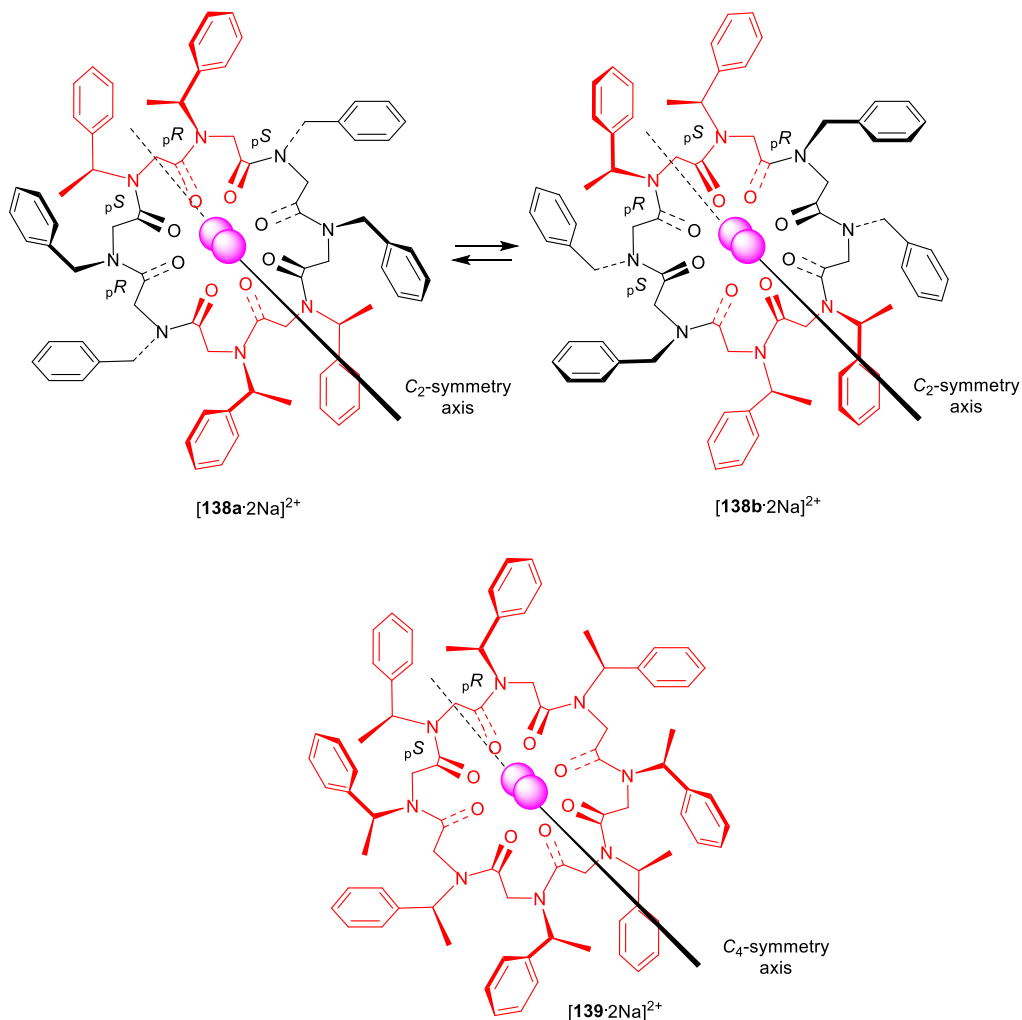


Figure 3.52. Schematic structures of [**138a**:2Na]²⁺, [**138b**:2Na]²⁺ and [**139**:2Na]²⁺.

Octameric cyclopeptoids complexes can be described as a number of multiple fluxional conformations in fast equilibrium on NMR time scale.

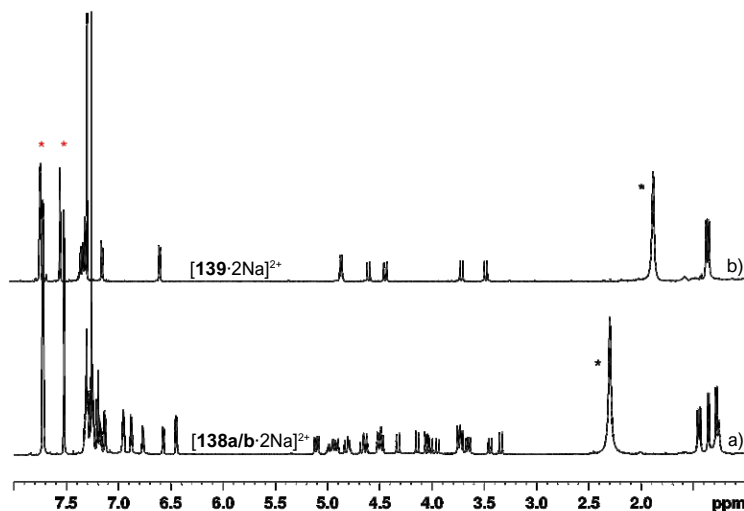


Figure 3.53. ^1H -NMR spectra of disodium complexes a) $[\mathbf{138a/b}\cdot 2\text{Na}]^{2+}$ and b) $[\mathbf{139}\cdot 2\text{Na}]^{2+}$ (600 MHz, 3.0 mM solution, CDCl_3). Water impurities are labelled with a black asterisk. TFPB $^-$ signals are labelled with a red asterisk.

After many crystallization trials of octamer cyclopeptoids in the presence of NaTFPB, we focused our attention on the use PF_6^- as counterion (used in the past to facilitate the crystallization of prolinated compounds).¹²⁷ To our delight, the addition of a *single* equivalent of NaPF_6 to a $\text{CDCl}_3:\text{CD}_3\text{CN}$ (9:1) solution of **139** caused the formation of an unexpected four-fold symmetric species, in slow equilibrium with the free host on the NMR time scale ($\log K_a = 4.5$, $-\Delta G^0 = 6.2$ kcal/mol).

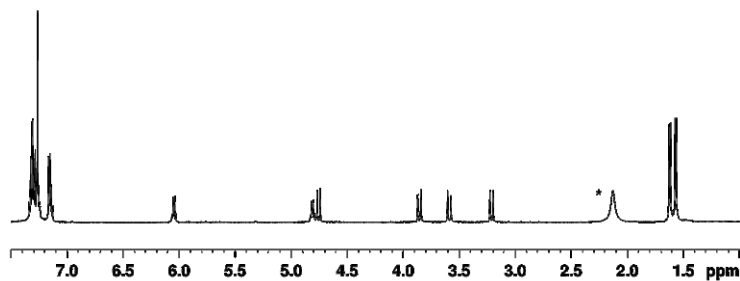


Figure 3.54. ^1H -NMR spectrum showing $[\mathbf{139Na}]^+\text{PF}_6^-$ (600 MHz, $\text{CDCl}_3:\text{CD}_3\text{CN}$ 9:1). Water impurities are labelled with a black asterisk.

¹²⁷ Izzo I., Ianniello G., De Cola C., Nardone B., Erra L., Vaughan G., Tedesco C., De Riccardis F., *Org. Lett.* **2013**, *15*, 598-601.

Interestingly, the addition of further equivalents of NaPF₆ (up to 3.0 equivalents) did not disrupt the 1:1 complex in favor of the 1:2 stoichiometry one but, the addition of increasing quantities of NaTFPB disrupted the monometallic complex in favor of the 1:2 one.

The side-chain methine proton chemical shift values suggested the presence of four *cis* and four *trans* amide bonds (δ 5.94, for the *cis* amide bond, and 4.76, for the *trans* amide bond). According to these data, the only two possible structures were the C₄-symmetric *ctctctct*-[**139c**·Na]⁺PF₆⁻ and *ctctctct*-[**139d**·Na]⁺PF₆⁻ complexes, showing a rare peptoid secondary structures: the “ribbon”,¹²⁸ the “ η -helix”,¹²⁹ or the mixed *cis*-*trans* α,β -oligopeptoids.¹³⁰

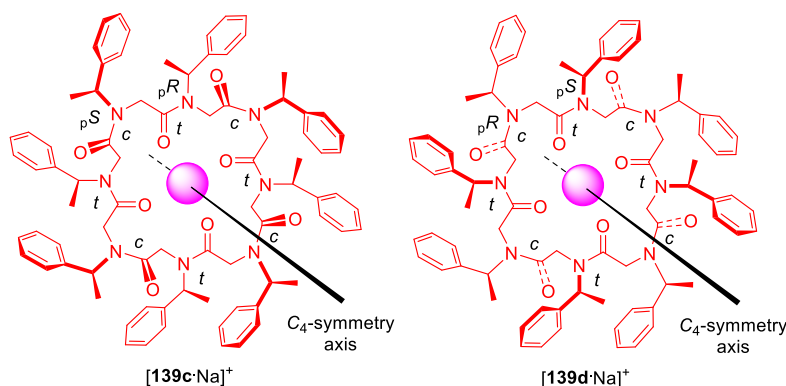


Figure 3.55. Schematic structures of [**139c**·Na]⁺PF₆⁻ and [**139d**·Na]⁺PF₆⁻ conformational isomers.

We were also able to obtain single crystals of [**139**·Na]⁺PF₆⁻, cooling a hot acetonitrile solution of the complex and confirming the NMR assignment. The tetragonal crystalline unit cell contains two symmetry independent [**139c**·Na(H₂O)]⁺PF₆⁻ moieties. Na⁺ ions are located on the crystallographic fourfold rotation axes and are hexacoordinated to four *trans* carbonyl oxygen atoms of the macrocycle, to one water molecule and one PF₆⁻ fluorine atom. The side-chain groups are alternately directed on opposite faces of the macrocycle providing a pocket where PF₆⁻ ion is located. Moreover, [**139c**·Na(H₂O)]⁺PF₆⁻ moieties are aligned along the *c* axis by means of CH \cdots OC hydrogen bonds between *cis* carbonyl groups and aromatic *p*-hydrogen atoms, forming channels parallel to the *c* axis, where acetonitrile molecules are located.

¹²⁸ Crapster J. A., Guzei I. A., Blackwell H. E., *Angew. Chem. Int. Ed.* **2013**, *52*, 5079-5084.

¹²⁹ Gorske B. C., Mumford E. M., Gerrity C. G., Ko I., *J. Am. Chem. Soc.* **2017**, *139*, 8070-8073.

¹³⁰ Dumonteil G., Bhattacharjee N., Angelici G., Roy O., Faure S., Jouffret L., Jolibois F., Perrin L., Taillefumier C., *J. Org. Chem.* **2018**, *83*, 6382-6396.

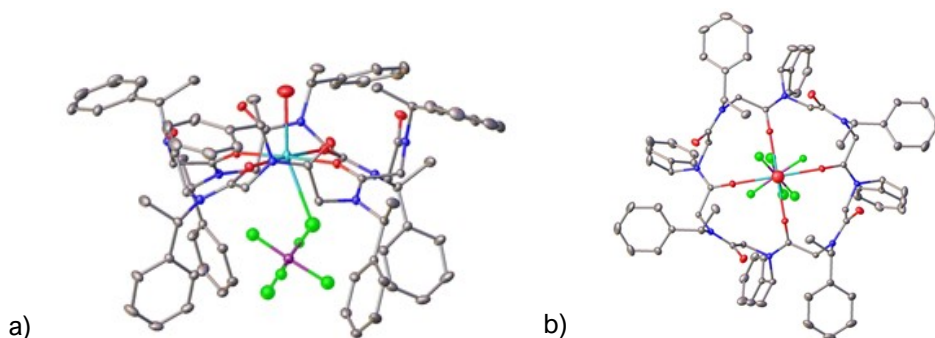


Figure 3.56. ORTEP drawing of $[\mathbf{139c-Na(H_2O)}]^+PF_6^-$: a) side view; b) top view. Ellipsoids are drawn at 10% probability level. For clarity hydrogen atoms have been omitted and only one possible disordered PF_6^- moiety is displayed. C, silver; N, blue; O, red; Na, light blue; P, magenta; F, green.

This novel loop structure was classified as CPM_2 loop (Figure 3.57); similarly to what exemplified for the hexamer complexes, the enantiomorphous CPM'_2 loop could be obtained using *N*-(*R*)-(1-phenylethyl)amine instead of *S*.

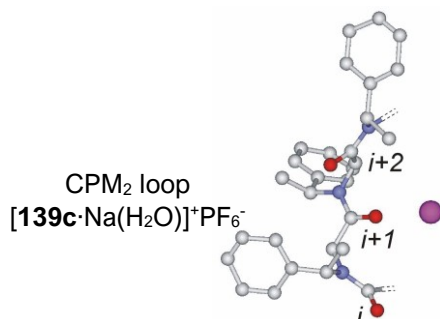


Figure 3.57. Portion of the model of $[\mathbf{139c-Na(H_2O)}]^+PF_6^-$ depicting CPM_2 loop. C, silver; N, blue; O, red; Na, magenta.

Lastly, in Table 3.6 are reported the values of the ω , φ and ψ dihedral angles of the solid state complex $[\mathbf{139c-Na(H_2O)}]^+PF_6^-$, compared with the hypothetical *ent*- $[\mathbf{139c-Na(H_2O)}]^+PF_6^-$.

Cpd	Loop type	ω_{i+1} (planar chirality)	φ_{i+1}	ψ_{i+1}	ω_{i+2} (planar chirality)	φ_{i+2}	ψ_{i+2}	Distance $C\alpha_{(i)}-C\alpha_{(i+3)}$ (Å)
$[\mathbf{139c-Na(H_2O)}]^+$	CPM_2	-4.6 (pS)	-81.5	-164.1	172.5 (pR)	-67.7	170.4	7.94
-	CPM'_2 ^a	0 (pS)	-80	-165	180 (pR)	-70	170	>7.0
<i>ent</i> - $[\mathbf{139c-Na(H_2O)}]^+$	CPM'_2 ^a	0 (pR)	80	165	180 (pS)	70	-170	>7.0

^a Idealized torsion angles values.

Table 3.6. Central residues dihedral angles values, amide bonds planar chirality and $C\alpha_{(i)}-C\alpha_{(i+3)}$ distances for CPM_2 type $[\mathbf{139c-Na(H_2O)}]^+$ metal complex.

3.4.2 Conclusions

In this study, we extended our central-to-conformational chirality approach with a systematic investigation about the side-chains. Particularly, we introduced *N*-(*S*)-(1-phenylethyl)amine as chiral sub-monomer on a single or multiple positions of the cyclic peptoid framework, and analysed the number and type of conformational isomers formed in solution. In some cases, we were able to obtain a single prevalent conformational isomer, even for bigger macrocycles (hexamers and octamers), exploiting the delicate interplay between steric and electronic interactions.

Moreover, for the first time the torsion angle values of the resulting secondary structures were systematically analysed and compared with peptide secondary structures; we introduced a novel nomenclature for cyclic peptoids folding motifs.

We believe that these results, together with the exceptional conformational control found for chiral backbones (Paragraph 3.3), put the bases for an extended use of cyclic peptoids, now envisioned as mimics of natural polypeptides in the forms and, possibly, in the functions.

3.4.3 Experimental section

3.4.3.1 General methods

Refer to Paragraph 2.2.3.1.

For the VT NMR experiments, refer to Paragraph 2.2.3.7.

Additional NMR solvents used in this work: (CH₃)₂SO, DMSO, δ = 2.50; (¹³CH₃)₂SO, DMSO, δ = 39.51; C₆D₅CD₂H, toluene, δ = 2.09; C₆D₅¹³CD₃, toluene, δ = 20.4.

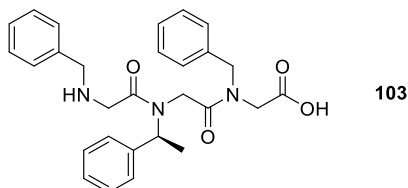
For the VT NMR experiments, refer to Paragraph 2.2.3.7; no sign of coalescence was detected up to 100 °C for compounds **104a/b**, **122a/b**, **123**, **128**, **129**, **139**.

DFT calculations were performed by prof. C. Costabile, Dpt. of Chemistry and Biology “A. Zambelli”, Univ. of Salerno.

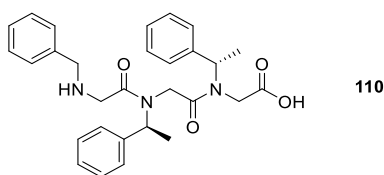
X-ray analyses were performed by PhD student G. Pierri and prof. C. Tedesco, Dpt. of Chemistry and Biology “A. Zambelli”, Univ. of Salerno.

3.4.3.2 Synthesis of linear peptoids **103**, **110**, **111**, **117**, **119**, **120**, **125**, **126**, **130-132**, **134-136**, **140-141**

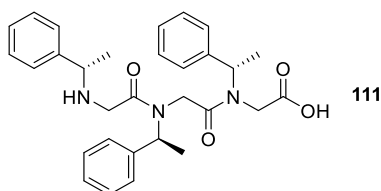
Refer to Paragraph 2.2.3.2. The synthesis was performed exploiting the sub-monomer protocol, on a 0.300 g 2-chlorotrytil chloride resin batch (1.63 mmol g⁻¹), using commercially available benzylamine, (S)-(-)-1-phenylethylamine, (R)-(+)-1-(1-naphthyl)ethylamine, 1-naphthylmethylamine; purity of the linear oligomers >80% (except for **134**, 46%).



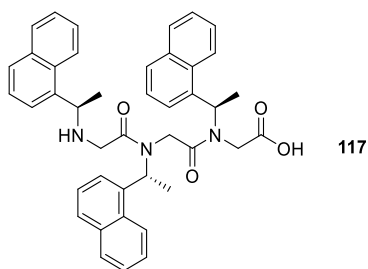
H-[Npm-Nspe-Npm]-OH (**103**): white amorphous solid, 0.231 g, 100%; t_R : 7.1 min. ES-MS m/z ; 474.2 [M + H]⁺, HRMS (ESI/FTICR) m/z ; [M + H]⁺ Calcd for C₂₈H₃₂N₃O₄⁺ 474.2387; Found 474.2375.



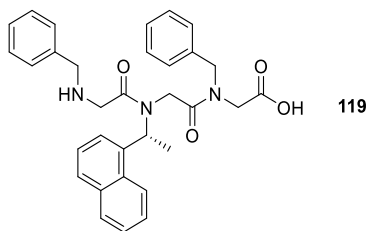
H-[Npm-Nspe₂]-OH (**110**): white amorphous solid, 0.238 g, 100%; t_R : 8.1 min. ES-MS m/z ; 448.2 [M + H]⁺, HRMS (ESI/FTICR) m/z ; [M + H]⁺ Calcd for C₂₉H₃₄N₃O₄⁺ 488.2544; Found 488.2538.



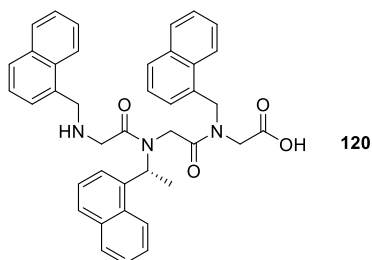
H-[Nspe]₃-OH (**111**): white amorphous solid, 0.245 g, 100%; t_R : 8.0 min. ES-MS m/z ; 502.6 [M + H]⁺, HRMS (ESI/FTICR) m/z ; [M + H]⁺ Calcd for C₃₀H₃₆N₃O₄⁺ 502.2700; Found 502.2709.



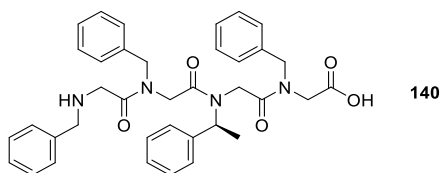
H-[Nr1npe]₃-OH (**117**): white amorphous solid, 0.318 g, 100%; t_R : 11.6 min. ES-MS m/z ; 652.4 [M + H]⁺, HRMS (ESI/FTICR) m/z ; [M + H]⁺ Calcd for C₄₂H₄₂N₃O₄⁺ 652.3170; Found 652.3169.



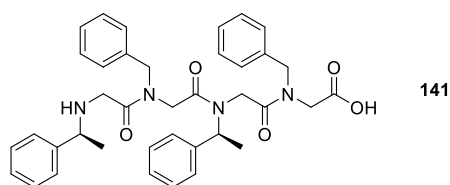
H-[Npm-Nr1npe-Npm]-OH (**119**): white amorphous solid, 0.212 g, 83%; t_R : 9.9 min. ES-MS m/z ; 524.1 [M + H]⁺, HRMS (ESI/FTICR) m/z ; [M + H]⁺ Calcd for C₃₂H₃₄N₃O₄⁺ 524.2544; Found 524.2548.



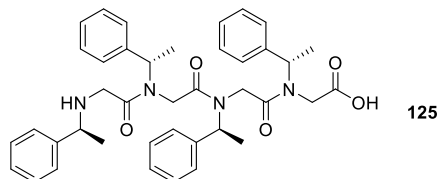
H-[Nnpm-Nr1npe-Nnpm]-OH (**120**): white amorphous solid, 0.0760 g, 25%; t_R : 10.1 min. ES-MS m/z ; 624.4 [M + H]⁺, HRMS (ESI/FTICR) m/z ; [M + H]⁺ Calcd for C₄₀H₃₈N₃O₄⁺ 624.2857; Found 624.2855.



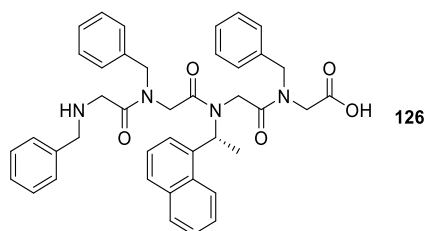
H-[Npm₂-Nspe-Npm]-OH (**140**): white amorphous solid, 0.303 g, 100%; t_R : 8.7 min. ES-MS m/z ; 621.0 [M + H]⁺, HRMS (ESI/FTICR) m/z ; [M + H]⁺ Calcd for C₃₇H₄₁N₄O₅⁺ 621.3071; Found 621.3079.



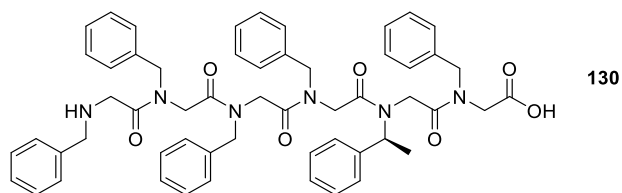
H-[Nspe-Npm-Nspe-Npm]-OH (**141**): white amorphous solid, 0.310 g, 100%; t_R : 8.7 min. ES-MS m/z ; 635.3 [M + H]⁺, HRMS (ESI/FTICR) m/z ; [M + H]⁺ Calcd for C₃₈H₄₃N₄O₅⁺ 635.3228; Found 635.3219.



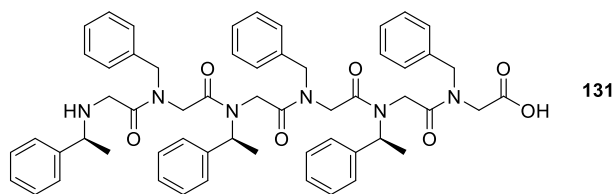
H-[Nspe]₄-OH (**125**): white amorphous solid, 0.324 g, 100%; t_R : 9.4 min. ES-MS m/z ; 662.9 [M + H]⁺, HRMS (ESI/FTICR) m/z ; [M + H]⁺ Calcd for C₄₀H₄₇N₄O₅⁺ 663.3541; Found 663.3553.



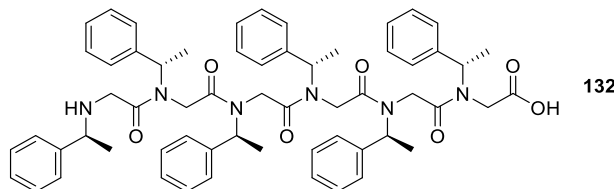
H-[Npm₂-Nr1npe-Npm]-OH (**126**): white amorphous solid, 0.328 g, 100%; t_R : 11.5 min. ES-MS m/z ; 671.5 [M + H]⁺, HRMS (ESI/FTICR) m/z ; [M + H]⁺ Calcd for C₄₁H₄₃N₄O₅⁺ 671.3228; Found 671.3231.



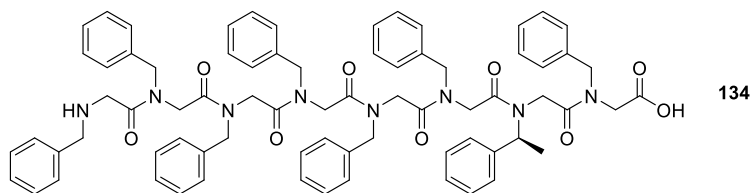
H-[Npm₄-Nspe-Npm]-OH (**130**): white amorphous solid, 0.268 g, 60%; t_R : 11.5 min. ES-MS m/z ; 915.4 [M + H]⁺, HRMS (ESI/FTICR) m/z ; [M + H]⁺ Calcd for C₅₅H₅₉N₆O₇⁺ 915.4440; Found 915.4460.



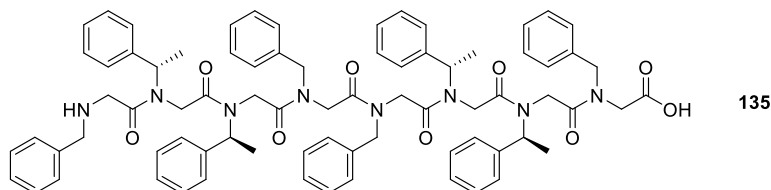
H-[Nspe-Npm]₃-OH (**131**): white amorphous solid, 0.461 g, 100%; t_R : 11.8 min. ES-MS m/z ; 943.5 [M + H]⁺, HRMS (ESI/FTICR) m/z ; [M + H]⁺ Calcd for C₅₇H₆₃N₆O₇⁺ 943.4753; Found 943.4730.



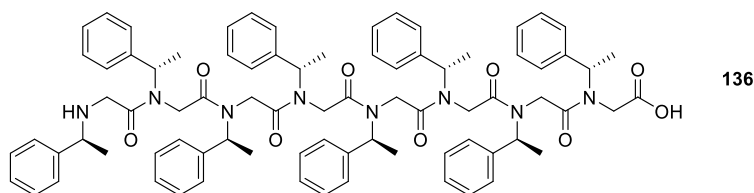
H-[Nspe]₆-OH (**132**): white amorphous solid, 0.481 g, 100%; t_R : 12.8 min. ES-MS m/z ; 985.5 [M + H]⁺, HRMS (ESI/FTICR) m/z ; [M + H]⁺ Calcd for C₆₀H₆₉N₆O₇⁺ 985.5222; Found 985.5201.



H-[Npm₆-Nspe-Npm]-OH (**134**): white amorphous solid, 0.532 g, 90%; t_R : 13.3 min. ES-MS m/z ; 1210.5 [M + H]⁺, HRMS (ESI/FTICR) m/z ; [M + H]⁺ Calcd for C₇₃H₇₇N₈O₉⁺ 1209.5808; Found 1209.5839.



H-[Npm-Nspe₂-Npm₂-Nspe₂-Npm]-OH (**135**): white amorphous solid, 0.483 g, 79%; t_R : 13.1 min. ES-MS m/z ; 1252.7 [M + H]⁺, HRMS (ESI/FTICR) m/z ; [M + H]⁺ Calcd for C₇₆H₈₃N₈O₉⁺ 1251.6278; Found 1251.6299.



H-[Nspe]₈-OH (**136**): white amorphous solid, 0.639 g, 100%; *t_R*: 14.1 min. ES-MS *m/z*; 1307.7 [M + H]⁺, HRMS (ESI/FTICR) *m/z*; [M + H]⁺ Calcd for C₈₀H₉₁N₈O₉⁺ 1307.6904; Found 1307.6943.

3.4.3.3 Synthesis of the cyclic derivatives **104**, **108**, **109**, **118**, **121**, **122a/b**, **123**, **127**, **128a/b**, **129**, **137**, **138**, **139a/b**

Refer to Paragraph 2.2.3.3.

The cyclization reaction was performed on a 0.150 mmol scale of the linear oligomers, which were dissolved in 5.0 mL of dry DMF and added by a syringe pump in 3 hours to the reaction mixture. The crude cyclic peptoids **122a/b**, **123**, **127**, **128a/b**, **129**, **137** were dissolved in hot acetonitrile and precipitated by slowly cooling the acetonitrile solutions. Crude **138**, **139a/b** were purified on reverse silica gel (C₁₈); conditions: 10% – 100% A (A: acetonitrile; B: water). Crude **104**, **108**, **109**, **118** were purified on flash silica gel; conditions: 10% – 50% A (A: ethyl acetate; B: petroleum ether). Cyclic peptoids were dissolved in 50% acetonitrile in HPLC grade water and analysed by RP-HPLC; purity >90%. Conditions: 5% – 100% A in 30 min (A, 0.1% TFA in acetonitrile, B, 0.1% TFA in water); flow: 1 mL min⁻¹, 220 nm.

Note: **122a/b**, **123**, **127**, **128a/b** chromatograms are not reported due to the insolubility of the compounds in the acetonitrile solutions. Their analytical purity was corroborated by the elemental analysis.

*Further cyclization procedures for **110**, **111**, **125**.*^{30b,100b} a) PyBOP/DIPEA. Solutions of linear peptoids (0.150 mmol), previously co-evaporated three times with toluene, were prepared under nitrogen in dry DMF (5.0 mL). The mixture was added dropwise to a stirred solution of PyBOP (0.242 g, 0.465 mmol) and DIPEA (162 μL, 0.930 mmol) in dry DMF (70.0 mL) by a syringe pump in 3 h, at room temperature in anhydrous atmosphere. After 12 h the resulting mixture was concentrated *in vacuo*, diluted with CH₂Cl₂ (30.0 mL), washed twice with a solution of HCl (1.0 M, 15.0 mL). The organic phase was washed with water (30.0 mL), dried over anhydrous MgSO₄, filtered and concentrated *in vacuo*. b) EDC/HOBt/TEA. Solutions of linear peptoids (0.150 mmol), previously co-evaporated three times with toluene, were prepared under nitrogen in dry DMF (5.0 mL). The mixture was added dropwise to a stirred solution of EDC (0.172 g, 0.900 mmol), HOBt (0.122 g, 0.900 mmol) and dry triethylamine (125 μL, 0.900 mmol) in dry DMF (45.0 mL) by a syringe pump in 3 h, at room temperature in anhydrous atmosphere. After 12 h the resulting

mixture was concentrated *in vacuo*, diluted with CH₂Cl₂ (30 mL), washed twice with a solution of HCl (1.0 M, 15.0 mL). The organic phase was washed with water (30.0 mL), dried over anhydrous MgSO₄, filtered and concentrated *in vacuo*.

Note: in the ¹H-NMR assignment, N_c stand for *cis* amide bond, N_t stands for *trans* amide bond.

cyclo-[(*cis*,_p*S*)Nspe-(*cis*,_p*S*)Npm-(*cis*,_p*S*)Npm] (**104a**) and *cyclo*-[(*cis*,_p*R*)Nspe-(*cis*,_p*R*)Npm-(*cis*,_p*R*)Npm] (**104b**): white amorphous solid, 0.0130 g, 19%; *t_R*: 8.9 min. ¹H-NMR (600 MHz, (CD₃)₂SO, as a 70/30 mixture of „crown“ conformational isomers) δ: 7.35-7.22 (15H, br signals, Ar-*H*), 5.47 (0.7H, q, *J* 6.9 Hz, N-CHCH₃-Ph), 5.32 (0.3H, d, *J* 15.9 Hz, N-CH₂-Ph or O=C-CH₂-N), 5.21 (1.3H, overlapping, N-CH₂-Ph and/or O=C-CH₂-N), 5.16 (1.3H, br d, N-CH₂-Ph and/or O=C-CH₂-N), 5.10 (1H, overlapping, N-CH₂-Ph and/or O=C-CH₂-N plus N-CHCH₃-Ph of the minor isomer), 5.03 (1.3H, overlapping, N-CH₂-Ph and/or O=C-CH₂-N), 4.23 (0.7H, d, *J* 14.8 Hz, N-CH₂-Ph and/or O=C-CH₂-N), 4.19 (0.3H, d, *J* 15.0 Hz, N-CH₂-Ph and/or O=C-CH₂-N), 4.14 (0.3H, d, *J* 15.2 Hz, N-CH₂-Ph and/or O=C-CH₂-N), 4.10 (0.7H, d, *J* 14.8 Hz, N-CH₂-Ph and/or O=C-CH₂-N), 3.82 (0.7H, overlapping, N-CH₂-Ph and/or O=C-CH₂-N) 3.46-3.38 (2.4H, overlapping, N-CH₂-Ph and/or O=C-CH₂-N), 1.63 (0.9H, d, *J* 7.1 Hz, N-CHCH₃-Ph), 1.56 (2.1H, d, *J* 7.0 Hz, N-CHCH₃-Ph). ¹³C-NMR (150 MHz, (CD₃)₂SO, as a 70/30 mixture of „crown“ conformational isomers) δ: 169.5, 168.5, 168.2, 140.6, 137.0 (x2), 128.9 (multiple signals), 128.7 (multiple signals), 128.4 (multiple signals), 128.3 (multiple signals), 127.9, 127.7, 126.9, 126.8, 79.6, 58.1, 55.0, 51.4, 50.0, 49.7, 49.5, 49.4, 48.7, 48.4, 48.2, 47.2, 17.6, 16.4. HRMS (ESI/FTICR) *m/z*; [M + H]⁺ Calcd for C₂₈H₃₀N₃O₃⁺ 456.2282; Found 456.2290.

4-Benzyl-3,4,5,6-tetrahydro-1,5-bis((*S*)-1-phenylethyl)-1H-pyrrolo[2,3-*b*]pyrazine-2,7-dione (**108**): white amorphous solid, 0.0170 g, 25%; *t_R*: 11.2 min. ¹H-NMR (600 MHz, CDCl₃) δ: 7.42-7.18 (15H, overlapping, Ar-*H*), 6.24 (1H, q, *J* 7.1 Hz, C=O-N-CHCH₃-Ph), 4.92 (1H, q, *J* 7.1 Hz, C=O-N-CHCH₃-Ph), 4.65 (1H, d, *J* 15.4 Hz, N-CHH-Ph), 4.55 (1H, d, *J* 15.4 Hz, N-CHH-Ph), 3.89 (1H, d, *J* 16.3 Hz, C=O-CHH-N-Bn), 3.76 (1H, d, *J* 16.3 Hz, C=O-CHH-N-Bn), 3.61 (1H, d, *J* 18.1 Hz, C=O-CHH-N-CHCH₃-Ph), 3.46 (1H, d, *J* 18.1 Hz, C=O-CHH-N-CHCH₃-Ph), 1.82 (3H, d, *J* 7.1 Hz, C=O-N-CHCH₃-Ph), 1.55 (3H, d, *J* 7.1 Hz, C=O-N-CHCH₃-Ph). ¹³C-NMR (150 MHz, CDCl₃) δ: 180.6, 165.7, 160.2, 141.7, 139.3, 135.1, 129.7 (x2), 129.3 (x2), 129.0, 128.6, 128.2 (x2), 127.9 (x2), 127.5 (x2), 127.1, 126.9 (x2), 105.7, 56.3 (x2), 54.6, 53.5, 52.4, 17.0 (x2). HRMS (ESI/FTICR) *m/z*; [M + H]⁺ Calcd for C₂₉H₃₀N₃O₂⁺ 452.2333; Found 452.2320.

3,4,5,6-tetrahydro-1,4,5-tris((*S*)-1-phenylethyl)-1H-pyrrolo[3,2-*b*]pyrazine-2,7-dione (**109**): white amorphous solid, 0.0180 g, 26%; t_R : 10.1 min. $^1\text{H-NMR}$ (600 MHz, CDCl_3) δ : 7.43-7.18 (15H, overlapping, Ar-*H*), 6.07 (1H, q, J 7.2 Hz, N-*CHCH*₃-Ph), 5.07 (1H, q, J 7.2 Hz, N-*CHCH*₃-Ph), 4.97 (1H, q, J 7.2 Hz, N-*CHCH*₃-Ph), 3.76 (1H, d, J 16.2 Hz, C-3*HH*), 3.68 (2H, br d, overlapping, C-3*HH* and C-6*HH*), 3.46 (1H, d, J 18.2 Hz, C-6*HH*), 1.69 (3H, d, J 7.2 Hz, C=O-N-*CHCH*₃-Ph), 1.66 (3H, d, J 7.2 Hz, C=O-N-*CHCH*₃-Ph), 1.64 (3H, d, J 7.2 Hz, C=O-N-*CHCH*₃-Ph). $^{13}\text{C-NMR}$ (150 MHz, CDCl_3) δ : 181.5, 166.1, 160.1, 141.1, 139.1, 138.4, 129.1 (x2), 129.0 (x2), 128.5, 128.3, 127.7 (x2), 127.5 (x2), 126.6 (x3), 126.4 (x2), 106.7, 58.8, 56.0, 53.8, 51.7, 48.0, 17.4, 16.8, 16.3. HRMS (ESI/FTICR) m/z ; $[\text{M} + \text{H}]^+$ Calcd for $\text{C}_{30}\text{H}_{32}\text{N}_3\text{O}_2^+$ 466.2489; Found 466.2475.

(*S*)-3,4,5,6-tetrahydro-3-hydroxy-1,4,5-tris((*S*)-1-phenylethyl)-1H-pyrrolo[2,3-*b*]pyrazine-2,7-dione (**121**): white crystalline solid. $^1\text{H-NMR}$ (600 MHz, CDCl_3) δ : 7.39-7.15 (15H, overlapping, Ar-*H*), 6.16 (1H, q, J 7.0 Hz, N-1-*CHCH*₃-Ph), 5.21 (1H, q, J 7.2 Hz, N-4-*CHCH*₃-Ph), 5.09 (1H, s, *CHOH*), 5.03 (1H, q, J 7.2 Hz, N-5-*CHCH*₃-Ph), 3.62 (1H, d, J 18.0 Hz, *CHH*), 3.31 (1H, d, J 18.0 Hz, *CHH*), 1.92 (3H, d, J 7.2 Hz, N-4-*CHCH*₃-Ph), 1.72 (3H, d, J 7.2 Hz, N-5-*CHCH*₃-Ph), 1.68 (3H, d, J 7.0 Hz, N-1-*CHCH*₃-Ph). $^{13}\text{C-NMR}$ (150 MHz, CDCl_3) δ : 181.5, 163.4, 160.0, 140.5, 139.9, 137.6, 129.2 (x3), 128.9 (x3), 127.7 (x3), 127.3 (x2), 127.1 (x2), 126.2 (x2), 104.4, 78.6, 57.8, 56.6, 53.4, 51.4, 17.9, 17.6, 15.9. HRMS (ESI/FTICR) m/z ; $[\text{M} + \text{H}]^+$ Calcd for $\text{C}_{30}\text{H}_{32}\text{N}_3\text{O}_3^+$ 482.2438; Found 482.2429.

1,4,5-tris((*S*)-1-(naphthalen-1-yl)ethyl)-3,4,5,6-tetrahydro-1H-pyrrolo[2,3-*b*]pyrazine-2,7-dione (**118**): white amorphous solid, 0.0280 g, 30%; t_R : 12.6 min. $^1\text{H-NMR}$ (600 MHz, CDCl_3) δ : 7.92-7.36 (21H, overlapping, Ar-*H*), 6.53 (1H, q, J 6.9 Hz, C=O-N-*CHCH*₃-Naph), 5.76 (1H, q, J 6.9 Hz, N-C=O-*CH*₂-N-*CHCH*₃-Naph), 5.73 (1H, q, J 6.9 Hz, N-C-N-*CHCH*₃-Naph), 3.93 (1H, d, J 18.7 Hz, N-C=O-*CHH*-N-*CHCH*₃-Naph), 3.70 (1H, d, J 18.7 Hz, N-C=O-*CHH*-N-*CHCH*₃-Naph), 3.66 (1H, d, J 15.8 Hz, N-C-N-*CHCH*₃-Naph-*CHH*), 3.54 (1H, d, J 15.8 Hz, N-C-N-*CHCH*₃-Naph-*CHH*), 1.88 (3H, d, J 6.9 Hz, C=O-N-*CHCH*₃-Naph), 1.56 (3H, d, J 6.9 Hz, C=O-N-*CHCH*₃-Naph), 1.27 (3H, d, J 6.9 Hz, C=O-N-*CHCH*₃-Naph). $^{13}\text{C-NMR}$ (150 MHz, CDCl_3) δ : 180.8, 166.7, 158.9, 136.2, 136.0, 135.2, 134.3, 134.1, 133.6, 131.6, 130.8, 130.5, 129.3 (x2), 129.2 (x2), 128.6, 127.6, 126.6, 126.5, 126.0 (x3), 125.9, 125.7, 125.2 (x2), 124.8, 124.0, 123.8, 123.3, 122.3 (x2), 55.6, 55.0, 52.9, 49.4, 48.7, 19.1, 18.8, 15.9. HRMS (ESI/FTICR) m/z ; $[\text{M} + \text{H}]^+$ Calcd for $\text{C}_{42}\text{H}_{38}\text{N}_3\text{O}_2^+$ 616.2959; Found 616.2969.

cyclo-[(*cis*,*pR*)*Npm*-(*trans*,*pR*)*Npm*-(*cis*,*pS*)*Nspe*-(*trans*,*pS*)*Npm*] (**122a**) and *cyclo*-

[(*cis*,_p*S*)Npm-(*trans*,_p*S*)Npm-(*cis*,_p*R*)Nspe-(*trans*,_p*R*)Npm] (**122b**): white amorphous solid, 0.0370 g, 41%. ¹H-NMR (600 MHz, CDCl₃, conformational isomers ratio: 85/15; note: the only reported ¹H-NMR signals of the minor conformational isomer are those of the CHCH₃ resonances, the other resonances are hidden under the peaks of the major conformational isomer) δ: 7.34-7.20 (12H, br signals, Ar-*H*), 7.11-7.03 (8H, br signals, Ar-*H*), 5.92 (1H, q, *J* 7.0 Hz, N_c-CHCH₃-Ph), 5.55 (1H, d, *J* 14.5 Hz, N_c-CHH-Ph), 5.43 (1H, d, *J* 14.7 Hz, O=C-CHH-N_t-CH₂-Ph), 5.35 (0.15H, q, *J* 7.0 Hz, N_c-CHCH₃-Ph, minor conformational isomer), 5.33 (1H, d, *J* 14.6 Hz, O=C-CHH-N_t-CH₂-Ph), 4.47 (1H, d, *J* 17.2 Hz, N_t-CHH-Ph), 4.41 (1H, d, *J* 17.8 Hz, O=C-CHH-N_c-CH₂-Ph), 4.39 (2H, br d, overlapping, N_t-CHH-Ph and O=C-CHH-N_t-CH₂-Ph), 4.31 (1H, d, *J* 17.2 Hz, N_t-CHH-Ph), 4.22 (1H, d, *J* 18.4 Hz, O=C-CHH-N_c-CHCH₃-Ph), 3.77 (1H, d, *J* 14.5 Hz, N_c-CHH-Ph), 3.51 (1H, d, *J* 14.7 Hz, O=C-CHH-N_t-CH₂-Ph), 3.49 (2H, overlapping, O=C-CHH-N_c-CH₂-Ph and N_t-CHH-Ph), 3.39 (1H, d, *J* 18.4 Hz, O=C-CHH-N_c-CHCH₃-Ph), 1.47 (0.45H, d, *J* 7.0 Hz, N-CHCH₃-Ph, minor conformational isomer), 1.45 (3H, d, *J* 7.0 Hz, N_c-CHCH₃-Ph). ¹³C-NMR (150 MHz, CDCl₃; note: only the ¹³C-NMR signals of the major conformational isomer are reported) δ: 169.4, 169.2, 168.5, 167.9, 140.0, 136.0, 135.8, 135.3, 129.1 (x2), 129.0 (x4), 128.7 (x2), 128.6 (x2), 128.0, 127.9, 127.8 (x2), 127.5 (x2), 126.8 (x2), 126.4 (x2), 52.6, 50.5, 49.6, 49.5 (x3), 47.2, 45.8, 16.6. Anal. Calcd for C₃₇H₃₈N₄O₄: C, 73.73; H, 6.35; N, 9.30; Found C, 73.98; H, 6.33; N, 9.28. HRMS (ESI/FTICR) *m/z*; [M + H]⁺ Calcd for C₃₇H₃₉N₄O₄⁺ 603.2966; Found 603.2958.

cyclo-[(*cis*,_p*R*)Nspe-(*trans*,_p*R*)Npm-(*cis*,_p*S*)Nspe-(*trans*,_p*S*)Npm] (**123**): white amorphous solid, 0.0170 g, 18%. ¹H-NMR (600 MHz, CDCl₃) δ: 7.35-7.18 (15H, br signals, Ar-*H*), 7.01-7.00 (3H, m, Ar-*H*), 6.94 (2H, d, *J* 7.0 Hz, Ar-*H*), 5.86 (1H, q, *J* 7.0 Hz, N_c-CHCH₃-Ph), 5.38 (1H, d, *J* 14.2 Hz, O=C-CHH-N_t-CH₂-Ph, and 1H, N_c-CHCH₃-Ph, overlapping), 5.14 (1H, d, *J* 14.6 Hz, O=C-CHH-N_t-CH₂-Ph), 4.50 (1H, d, *J* 17.3 Hz, N_t-CHH-Ph), 4.40 (1H, d, *J* 18.1 Hz, O=C-CHH-N_c-CHCH₃-Ph), 4.38 (1H, d, *J* 17.3 Hz, N_t-CHH-Ph), 4.28 (2H, overlapping, d, *J* 17.3 Hz, N_t-CHH-Ph and N_t-CHH-Ph), 4.20 (1H, d, *J* 18.2 Hz, O=C-CHH-N_c-CHCH₃-Ph), 3.61 (1H, d, *J* 18.1 Hz, O=C-CHH-N_c-CHCH₃-Ph), 3.47 (1H, d, *J* 14.2 Hz, O=C-CHH-N_t-CH₂-Ph), 3.28 (2H, overlapping, d, *J* 18.2 Hz, O=C-CHH-N_t-CH₂-Ph and O=C-CHH-N_c-CHCH₃-Ph), 1.48 (3H, d, *J* 7.0 Hz, N_c-CHCH₃-Ph), 1.44 (3H, d, *J* 7.0 Hz, N_c-CHCH₃-Ph). ¹³C-NMR (150 MHz, CDCl₃) δ: 169.4 (x2), 168.5, 167.2, 140.0, 138.8, 135.7, 135.5, 129.0 (x4), 128.6 (x3), 128.1 (x3), 127.9, 127.4 (x3), 126.6 (x3), 126.4 (x3), 56.3, 52.6, 50.5, 49.7 (x2), 49.4, 46.4, 45.8, 17.1,

16.6. Anal. Calcd for $C_{38}H_{40}N_4O_4$: C, 74.00; H, 6.54; N, 9.08; O, 10.38; Found C, 74.11; H, 6.56; N, 9.06; O, 10.40. HRMS (ESI/FTICR) m/z ; $[M + H]^+$ Calcd for $C_{38}H_{41}N_4O_4^+$ 617.3122; Found 617.3134.

cyclo-[Nspe-Npm₅] (**127**): white amorphous solid, 0.0750 g, 56%. 1H -NMR (600 MHz, $CDCl_3$, complex mixture of rotamers) δ : 7.39-7.03 (30H, overlapping, *Ar-H*), 5.47-3.24 (23H, overlapping, br signals, *N-CHCH₃-Ph*, *O=C-CH₂-N-CHCH₃-Ph*, *N-CH₂-Ph*, *O=C-CH₂-N-CH₂-Ph*), 1.82-1.51 (3H, overlapping, br signals, *N-CHCH₃-Ph*). ^{13}C -NMR (150 MHz, $CDCl_3$, complex mixture of rotamers) δ : 171.8, 169.6, 169.5, 169.4, 169.0, 168.9, 168.6, 168.4, 136.8, 136.5, 135.6, 135.4, 135.3, 135.2, 134.9, 129.1, 128.7, 128.4, 127.6, 127.5, 127.3, 125.5, 125.4, 125.2, 53.0, 52.8, 52.7, 51.8, 51.6, 51.4, 51.1, 50.7, 50.4, 50.3, 50.1, 49.7, 49.6, 49.2, 47.7, 46.2, 44.3, 16.3, 15.4. Anal. Calcd for $C_{55}H_{56}N_6O_6$: C, 73.64; H, 6.29; N, 9.37; Found C, 73.47; H, 6.30; N, 9.31. HRMS (ESI/FTICR) m/z ; $[M + H]^+$ Calcd for $C_{55}H_{57}N_6O_6^+$ 897.4334; Found 897.4350.

*cyclo-[(*cis*,*pR*)Npm-(*trans*,*pR*)Nspe-(*cis*,*pR*)Npm-(*cis*,*pS*)Nspe-(*trans*,*pS*)Npm-(*cis*,*pS*)Nspe]* (**128a**): white amorphous solid, 0.0710 g, 51%. 1H -NMR (600 MHz, $CDCl_3$, mixture of conformational isomers with 70% of *cctcct-128a*) δ : 7.42-6.92 (30H, overlapping, *Ar-H*), 5.98 (1H, q, J 7.0 Hz, *N_c-CHCH₃-Ph*), 5.74 (1H, q, J 6.9 Hz, *N_c-CHCH₃-Ph*), 5.61 (1H, d, J 15.0 Hz, *N_c-CHH-Ph*), 5.44 (1H, d, J 15.9 Hz, *N_c-CHH-Ph*), 4.90 (1H, d, J 18.0 Hz, *N_r-CHH-Ph*), 4.87 (1H, d, J 17.8 Hz, *O=C-CHH-N_c-CH₂-Ph*), 4.78 (1H, q, J 7.0 Hz, *N_r-CHCH₃-Ph*), 4.72 (1H, d, J 15.1 Hz, *O=C-CHH-N_r-CH₂-Ph*), 4.70 (1H, d, J 15.0 Hz, *O=C-CHH-N_r-CHCH₃-Ph*), 4.55 (1H, d, J 18.0 Hz, *N_r-CHH-Ph*), 4.49 (1H, d, J 17.9 Hz, *O=C-CHH-N_c-CHCH₃-Ph*), 3.96 (1H, d, J 15.9 Hz, *N_c-CHH-Ph*), 3.88 (1H, d, J 17.8 Hz, *O=C-CHH-N_c-CH₂-Ph*), 3.80 (1H, d, J 17.8 Hz, *O=C-CHH-N_c-CHCH₃-Ph*), 3.74 (1H, d, J 15.0 Hz, *N_c-CHH-Ph*), 3.70 (1H, d, J 17.8 Hz, *O=C-CHH-N_c-CH₂-Ph*), 3.68 (1H, d, J 17.8 Hz, *O=C-CHH-N_c-CHCH₃-Ph*), 3.41 (1H, d, J 15.0 Hz, *O=C-CHH-N_r-CHCH₃-Ph*), 3.34 (1H, d, J 17.8 Hz, *O=C-CHH-N_c-CH₂-Ph*), 3.18 (2H, overlapping, *O=C-CHH-N_r-CH₂-Ph* and *O=C-CHH-N_c-CHCH₃-Ph*), 1.81 (3H, d, J 7.0 Hz, *N_r-CHCH₃-Ph*), 1.43 (3H, d, J 6.9 Hz, *N_c-CHCH₃-Ph*), 1.41 (3H, d, J 7.0 Hz, *N_c-CHCH₃-Ph*). ^{13}C -NMR (150 MHz, $CDCl_3$, mixture of conformational isomers with 70% of *cctcct-128a*) δ : 171.6, 171.5, 170.2, 169.2, 168.2, 168.1, 141.1, 140.8, 138.6, 137.1, 136.8, 135.3, 129.1 (x2), 129.0 (x2), 128.7 (x4), 128.6 (x2), 128.2 (x4), 128.2 (x2), 127.6 (x3), 127.4 (x3), 127.2 (x3), 127.1, 125.4 (x2), 125.0 (x2), 55.4, 54.1, 52.7, 52.0, 51.2 (x2), 50.7, 49.4, 47.8, 45.8, 45.1, 44.8, 20.7, 17.0, 15.8. Anal. Calcd for $C_{57}H_{60}N_6O_6$: C, 74.00; H, 6.54;

N, 9.08; O, 10.38; Found C, 74.19; H, 6.57; N, 9.10; O, 10.40. HRMS (ESI/FTICR) m/z ; $[M + H]^+$ Calcd for $C_{57}H_{61}N_6O_6^+$ 925.4647; Found 925.4670.

cyclo-[(*cis*,*pR*)*Nspe*-(*trans*,*pR*)*Nspe*-(*cis*,*pR*)*Nspe*-(*cis*,*pS*)*Nspe*-(*trans*,*pS*)*Nspe*-(*cis*,*pS*)*Nspe*] (**129**): white amorphous solid, 0.0480 g, 33%; t_R : 15.1 min. 1H -NMR (600 MHz, $CDCl_3$, mixture of conformational isomers with 70% of *cctcct*-**129**) δ : 7.40-7.17 (24H, overlapping, Ar-*H*), 7.05 (2H, d, J 7.2 Hz, Ar-*H*), 7.00-6.98 (4H, overlapping, Ar-*H*), 6.05 (1H, q, J 7.2 Hz, N_c -CHCH₃-Ph), 5.95 (1H, q, J 7.2 Hz, N_c -CHCH₃-Ph), 5.72 (1H, q, J 6.6 Hz, N_c -CHCH₃-Ph), 5.30 (1H, q, J 6.9 Hz, N_c -CHCH₃-Ph), 4.83 (1H, q, J 6.9 Hz, N_t -CHCH₃-Ph), 4.72 (1H, q, J 7.0 Hz, N_t -CHCH₃-Ph), 4.54 (1H, d, J 17.2 Hz, O=C-CHH-N-CHCH₃-Ph), 4.51 (1H, d, J 16.7 Hz, O=C-CHH-N-CHCH₃-Ph), 4.49 (1H, d, J 15.3 Hz, O=C-CHH-N-CHCH₃-Ph), 4.27 (1H, d, J 15.2 Hz, O=C-CHH-N-CHCH₃-Ph), 3.55 (1H, d, J 18.0 Hz, O=C-CHH-N-CHCH₃-Ph), 3.52 (1H, d, J 15.3 Hz, O=C-CHH-N-CHCH₃-Ph), 3.50 (2H, br d, overlapping signals, O=C-CHH-N-CHCH₃-Ph), 3.36 (1H, d, J 18.0 Hz, O=C-CHH-N-CHCH₃-Ph), 3.31 (1H, d, J 15.2 Hz, O=C-CHH-N-CHCH₃-Ph), 3.14 (1H, d, J 16.7 Hz, O=C-CHH-N-CHCH₃-Ph), 3.12 (1H, d, J 17.2 Hz, O=C-CHH-N-CHCH₃-Ph), 1.72 (3H, d, J 7.0 Hz, N_t -CHCH₃-Ph), 1.67 (3H, d, J 6.9 Hz, N_t -CHCH₃-Ph), 1.55 (3H, d, J 6.6 Hz, N_c -CHCH₃-Ph), 1.45 (3H, d, J 7.2 Hz, N_c -CHCH₃-Ph), 1.40 (3H, d, J 7.2 Hz, N_c -CHCH₃-Ph), 1.15 (3H, d, J 6.9 Hz, N_c -CHCH₃-Ph). ^{13}C -NMR (150 MHz, $CDCl_3$, mixture of conformational isomers with 70% of *cctcct*-**129**) δ : 171.5, 171.3, 169.9, 169.0, 168.5, 168.3, 142.0, 141.3, 140.7, 140.5, 139.7, 138.7, 128.9 (x4), 128.7 (x2), 128.5 (x2), 128.1 (x4), 128.0 (x4), 127.6 (x2), 127.4 (x2), 127.2 (x4), 127.1 (x2), 126.6 (x2), 125.4 (x2), 57.9, 55.7, 55.1, 53.8, 51.7, 51.0, 48.9, 47.5, 47.0, 46.8, 46.6, 44.5, 20.4, 20.2, 17.0, 16.6, 16.2, 15.4. HRMS (ESI/FTICR) m/z ; $[M + H]^+$ Calcd for $C_{60}H_{67}N_6O_6^+$ 967.5117; Found 967.5135.

cyclo-[*Nspe*-*Npm*₇] (**137**): white amorphous solid, 0.0540 g, 30%; t_R : 15.9 min. 1H -NMR (400 MHz, $CDCl_3$, complex mixture of rotamers) δ : 7.34-7.22 (32H, overlapping, Ar-*H*), 7.05-7.02 (8H, overlapping, Ar-*H*), 4.63-3.44 (31H, overlapping, N-CHCH₃-Ph, N-CH₂-Ph, O=C-CH₂-N-CH₂-Ph, O=C-CH₂-N-CHCH₃-Ph), 1.63-1.12 (3H, N-CHCH₃-Ph). ^{13}C -NMR (150 MHz, $CDCl_3$, complex mixture of rotamers) δ : 170.4, 169.6, 169.4, 168.8, 168.4, 168.0, 167.6, 167.3, 136.6, 136.4, 136.0, 135.7, 129.0, 128.8, 128.6, 127.9, 127.6, 127.4, 126.8, 126.6, 126.4, 126.3, 55.9, 54.8, 53.0, 52.5, 52.2, 51.6, 51.5, 50.4, 50.2, 49.6, 48.5, 48.4, 47.0, 19.2, 18.1, 15.2; HRMS (ESI/FTICR) m/z ; $[M + H]^+$ Calcd for $C_{73}H_{75}N_8O_8^+$ 1191.5630; Found 1191.5650.

cyclo-[*Nspe*₂-*Npm*₂]₂ (**138**): white amorphous solid, 0.0610 g, 33%; *t*_R: 16.1 min. ¹H-NMR (600 MHz, CDCl₃, complex mixture of rotamers) δ: 7.40-7.03 (40H, overlapping, *Ar-H*), 4.27-3.37 (28H, overlapping, *N-CHCH*₃-Ph, *N-CH*₂-Ph, *O=C-CH*₂-*N-CH*₂-Ph, *O=C-CH*₂-*N-CHCH*₃-Ph), 1.46-0.99 (12H, overlapping, *N-CHCH*₃-Ph). ¹³C-NMR (150 MHz, CDCl₃, complex mixture of rotamers) δ: 170.6, 170.1, 169.8, 169.7, 169.6, 168.7, 168.1, 167.6, 167.5, 167.1, 166.2, 141.2, 141.0, 140.7, 140.6, 140.2, 137.9, 136.8, 136.6, 136.4, 136.1, 135.8, 135.3, 134.9, 129.1, 129.0, 128.9, 128.8, 128.7, 128.5, 128.0, 127.9, 127.8, 127.5, 127.3, 127.1, 126.8, 126.6, 126.5, 126.4, 126.2, 126.1, 126.0, 125.7, 56.2, 54.9, 54.5, 54.1, 53.4, 53.0, 52.6, 52.4, 52.2, 51.9, 51.7, 51.5, 51.1, 50.9, 50.7, 50.3, 50.2, 49.8, 49.6, 49.3, 49.0, 48.5, 48.3, 48.1, 47.9, 47.6, 47.4, 46.6, 46.5, 45.8, 45.3, 44.7, 44.5, 44.3, 44.0, 43.8, 43.2, 19.0, 18.4, 18.2, 17.5, 17.3, 16.8, 16.5, 16.3, 15.7, 15.1, 15.0, 14.6; HRMS (ESI/FTICR) *m/z*; [M + H]⁺ Calcd for C₇₆H₈₁N₈O₈⁺ 1233.6172; Found 1233.6153.

cyclo-{[(*cis*,*pR*)*Nspe*-(*cis*,*pS*)*Nspe*-(*trans*,*pS*)*Nspe*-(*trans*,*pR*)*Nspe*]₂} (**139a**): white amorphous solid, 0.104 g, 54%; *t*_R: 16.6 min. ¹H-NMR (600 MHz, C₆D₅CD₃, mixture of conformational isomers with 62% of *ccttctt*-**139a**) δ: 7.55 (4H, d, *J* 7.7 Hz, *Ar-H*), 7.19-7.03 (32H, overlapping, *Ar-H*), 6.58 (4H, d, *J* 7.4 Hz, *Ar-H*), 6.14 (2H, q, *J* 6.9 Hz, *Nc-CHCH*₃-Ph), 5.47 (2H, q, *J* 7.0 Hz, *Nc-CHCH*₃-Ph), 4.55 (2H, d, *J* 16.9 Hz, *O=C-CHH-Nt-CHCH*₃-Ph), 4.44 (2H, d, *J* 18.0 Hz, *O=C-CHH-Nc-CHCH*₃-Ph), 4.40 (2H, q, *J* 6.8 Hz, *Nt-CHCH*₃-Ph), 4.22 (2H, q, *J* 6.8 Hz, *Nt-CHCH*₃-Ph), 4.09 (2H, d, *J* 16.5 Hz, *O=C-CHH-Nt-CHCH*₃-Ph), 3.65 (4H, br d, overlapping, *O=C-CHH-Nt-CHCH*₃-Ph and *O=C-CHH-Nc-CHCH*₃-Ph), 3.58 (2H, d, *J* 17.7 Hz, *O=C-CHH-Nc-CHCH*₃-Ph), 3.32 (2H, d, *J* 17.7 Hz, *O=C-CHH-Nc-CHCH*₃-Ph), 3.21 (2H, d, *J* 16.5 Hz, *O=C-CHH-Nt-CHCH*₃-Ph), 1.66 (6H, d, *J* 6.9 Hz, *Nc-CHCH*₃-Ph), 1.54 (6H, d, *J* 6.8 Hz, *Nt-CHCH*₃-Ph, *t*), 1.46 (6H, d, *J* 6.8 Hz, *Nt-CHCH*₃-Ph), 1.00 (6H, d, *J* 7.0 Hz, *Nc-CHCH*₃-Ph). ¹³C-NMR (150 MHz, C₆D₅CD₃, mixture of conformational isomers with 62% of *ccttctt*-**139a**; due to the presence of further conformational isomers, the spectrum was assigned also on the basis of the HSQC and HMBC experiments) δ: 170.5 (x2), 168.9 (x2), 167.7 (x2), 167.2 (x2), 141.3 (x2), 140.8 (x2), 139.9 (x2), 139.2 (x2), 129.5-127.4 (x40 C-H signals aromatic overlapping with C₆D₅CD₃ signals), 55.8 (x2), 55.2 (x2), 54.2 (x2), 54.1 (x2), 47.2 (x2), 46.6 (x2), 45.1 (x2), 44.8 (x2), 18.8 (x2), 17.6 (x2), 17.4 (x2), 16.9 (x2). HRMS (ESI/FTICR) *m/z*; [M + H]⁺ Calcd for C₈₀H₈₉N₈O₈⁺ 1289.6798; Found 1289.6817.

3.4.3.4 Preparation of the monometallic complexes [127, 128, 129-Na]⁺TFPB⁻, [139-Na]⁺PF₆⁻ and apparent *K*_{a1} evaluation

Refer to Paragraph 2.2.3.4.

For the [139c-Na]⁺PF₆⁻ complex, increasing quantities of NaPF₆ were added to a CDCl₃:CD₃CN = 9:1 solution of cyclic peptoid **139**, following the usual protocol. The calculations regarding the evaluation of the apparent *K*_{a1} follow the steps reported for TFPB⁻ monometallic complexes.

For the hexameric metal complexes, the complete characterization, including the ¹³C-NMR, was performed on the bimetallic complexes. See following Paragraph.

[128c-Na]⁺[TFPB]⁻: white amorphous solid. ¹H-NMR (600 MHz, CDCl₃) δ: 7.71 (8H, s, TFPB-*o*-H), 7.51 (4H, s, TFPB-*p*-H), 7.34-7.29 (18H, br signals, overlapping, Ar-*H*), 6.99 (6H, m, Ar-*H*), 6.92 (6H, m, Ar-*H*), 4.94 (3H, q, *J* 6.8 Hz, N-CHCH₃-Ph), 4.87 (3H, d, *J* 16.8 Hz, O=C-CHH-N-CH₂-Ph), 4.64 (3H, d, *J* 16.0 Hz, N-CHH-Ph), 4.57 (3H, d, *J* 17.3 Hz, O=C-CHH-N-CHCH₃-Ph), 4.37 (3H, d, *J* 16.0 Hz, N-CHH-Ph), 3.68 (3H, d, *J* 16.8 Hz, O=C-CHH-N-CH₂-Ph), 3.44 (3H, d, *J* 17.3 Hz, O=C-CHH-N-CHCH₃-Ph), 1.56 (9H, br d, N-CHCH₃-Ph). For the ¹³C-NMR see [128c·2Na]²⁺2[TFPB]²⁻. ESI-MS *m/z* 947.8 [M + Na]⁺.

[129-Na]⁺[TFPB]⁻: white amorphous solid. ¹H-NMR (400 MHz, CDCl₃) δ: 7.71 (8H, s, TFPB-*o*-H), 7.50 (4H, s, TFPB-*p*-H), 7.38 (12H, br s, Ar-*H*), 7.28 (6H, br s, Ar-*H*), 6.68 (6H, d, *J* 7.3 Hz, Ar-*H*), 5.00 (3H, q, *J* 6.6 Hz, N-CHCH₃-Ph), 4.87 (3H, q, *J* 6.6 Hz, N-CHCH₃-Ph), 4.60 (3H, d, *J* 16.8 Hz, O=C-CHH-N-CHCH₃-Ph), 4.52 (3H, d, *J* 16.9 Hz, O=C-CHH-N-CHCH₃-Ph), 3.62 (3H, d, *J* 16.8 Hz, O=C-CHH-N-CHCH₃-Ph), 3.38 (3H, d, *J* 16.9 Hz, O=C-CHH-N-CHCH₃-Ph), 1.53 (9H, d, *J* 6.6 Hz, N-CHCH₃-Ph), 1.49 (9H, d, *J* 6.6 Hz, N-CHCH₃-Ph). For the ¹³C-NMR see [129·2Na]²⁺2[TFPB]²⁻. ESI-MS *m/z* 989.7 [M + Na]⁺.

[139c-Na]⁺PF₆⁻: white amorphous solid. ¹H-NMR (600 MHz, CDCl₃:CD₃CN = 9:1) δ: 7.33-7.25 (32H, overlapping, Ar-*H*), 7.16-7.13 (8H, overlapping, Ar-*H*), 6.04 (4H, q, *J* 7.1 Hz, N_c-CHCH₃-Ph), 4.81 (4H, q, *J* 7.0 Hz, N_r-CHCH₃-Ph), 4.75 (4H, d, *J* 16.6 Hz, O=C-CHH-N_r-CHCH₃-Ph), 3.86 (4H, d, *J* 18.0 Hz, O=C-CHH-N_c-CHCH₃-Ph), 3.59 (4H, d, *J* 18.0 Hz, O=C-CHH-N_c-CHCH₃-Ph), 3.21 (4H, d, *J* 16.6 Hz, O=C-CHH-N_c-CHCH₃-Ph), 1.62 (12H, d, *J* 7.0 Hz, N_r-CHCH₃-Ph), 1.57 (12H, d, *J* 7.1 Hz, N_c-CHCH₃-Ph). ¹³C-NMR (150 MHz, CDCl₃:CD₃CN = 9:1) δ: 168.8 (x4), 168.1 (x4), 140.8 (x4), 140.0 (x4), 128.7 (x10), 128.3 (x10), 127.2 (x10), 125.8 (x10), 55.1 (x4), 51.8 (x4), 45.8 (x4), 43.1 (x4), 18.2 (x4), 15.6 (x4). ESI-MS *m/z* 1311.2 [M + Na]⁺.

3.4.3.5 Preparation of the bimetallic complexes [128, 129, 137-139·2Na]²⁺·2TFPB⁻ and apparent K_{aTOT} evaluation for [137-139·2Na]²⁺·2TFPB⁻

Refer to Paragraph 2.3.3.5.

Note: for [138a/b·2Na]²⁺ the K_a is referred to the sum of both the complexes.

[128c·2Na]²⁺·2[TFPB]²⁻: white amorphous solid. ¹H-NMR (600 MHz, CDCl₃) δ: 7.71 (16H, s, TFPB-*o*-H), 7.52 (8H, s, TFPB-*p*-H), 7.33-7.32 (18H, br signals, overlapping, Ar-H), 6.99 (6H, m, Ar-H), 6.92 (6H, m, Ar-H), 4.93 (3H, q, *J* 6.8 Hz, N-CHCH₃-Ph), 4.77 (3H, d, *J* 16.8 Hz, O=C-CHH-N-CH₂-Ph), 4.59 (3H, d, *J* 16.0 Hz, N-CHH-Ph), 4.37 (3H, d, *J* 17.3 Hz, O=C-CHH-N-CHCH₃-Ph), 4.27 (3H, d, *J* 16.0 Hz, N-CHH-Ph), 3.75 (3H, d, *J* 16.8 Hz, O=C-CHH-N-CH₂-Ph), 3.43 (3H, d, *J* 17.3 Hz, O=C-CHH-N-CHCH₃-Ph), 1.40 (9H, d, *J* 6.8 Hz, N-CHCH₃-Ph). ¹³C-NMR (150 MHz, CDCl₃) δ: 169.9 (x3), 168.1 (x3), 161.7 (q, *J* 50 Hz, C-1), 137.1 (x3), 134.8 (C-2), 133.1 (x3), 129.3 (x10), 128.9 (q, *J* 30 Hz, C-3), 126.9 (x10), 126.0 (x10), 124.6 (q, *J* 270 Hz, C-5), 117.6 (C-4), 55.6 (x3), 53.5 (x3), 49.7 (x3), 44.9 (x3), 16.8 (x3). ESI-MS *m/z* 947.7 [M + Na]⁺.

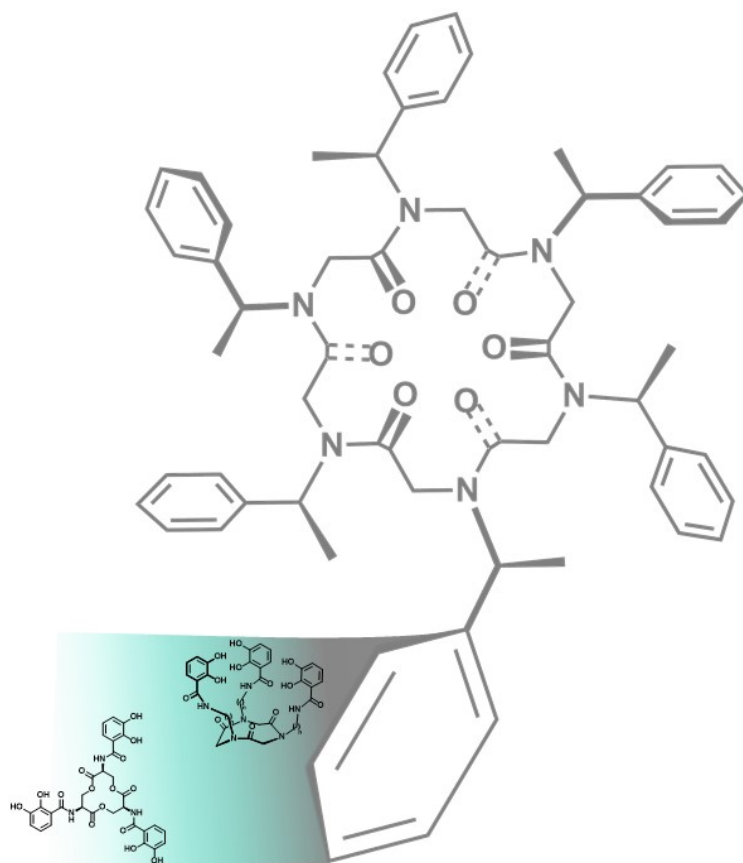
[129·2Na]⁺·2[TFPB]⁻: white amorphous solid. ¹H-NMR (600 MHz, CDCl₃) δ: 7.71 (16H, s, TFPB-*o*-H), 7.51 (8H, s, TFPB-*p*-H), 7.32-7.22 (18H, br signals, overlapping, Ar-H), 7.13 (6H, d, *J* 7.5 Hz, Ar-H), 6.73 (6H, d, *J* 7.5 Hz, Ar-H), 4.91 (6H, q, *J* 6.7 Hz, N-CHCH₃-Ph), 4.51 (3H, d, *J* 16.5 Hz, O=C-CHH-N-CHCH₃-Ph), 4.30 (3H, d, *J* 17.2 Hz, O=C-CHH-N-CHCH₃-Ph), 3.76 (3H, d, *J* 16.5 Hz, O=C-CHH-N-CHCH₃-Ph), 3.34 (3H, d, *J* 17.2 Hz, O=C-CHH-N-CHCH₃-Ph), 1.46 (9H, d, *J* 6.7 Hz, N-CHCH₃-Ph), 1.38 (9H, d, *J* 6.7 Hz, N-CHCH₃-Ph). ¹³C-NMR (150 MHz, CDCl₃) δ: 168.4 (x3), 167.9 (x3), 161.7 (q, *J* 50 Hz, C-1), 137.4 (x3), 136.1 (x3), 134.8 (C-2), 129.5 (x6), 128.8 (q, *J* 30 Hz, C-3), 129.5 (x12), 127.5 (x6), 125.7 (x6), 124.6 (q, *J* 270 Hz, C-5), 117.4 (C-4), 56.2 (x3), 55.1 (x3), 44.2 (x3), 45.0 (x3), 18.2 (x3), 16.5 (x3). ESI-MS *m/z* 989.9 [M + Na]⁺.

[138a·2Na]²⁺·2[TFPB]²⁻/[138b·2Na]²⁺·2[TFPB]²⁻: white amorphous solid. ¹H-NMR (600 MHz, CDCl₃, 50:50 mixture of conformational isomers) δ: 7.72 (16H, s, TFPB-*o*-H), 7.52 (8H, s, TFPB-*p*-H), 7.33-7.12 (28H, br signals, overlapping, Ar-H), 6.97-6.94 (4H, br signals, overlapping, Ar-H), 6.88 (2H, d, *J* 7.1 Hz, Ar-H), 6.77 (2H, d, *J* 7.3 Hz, Ar-H), 6.57 (2H, d, *J* 7.5 Hz, Ar-H), 6.45 (2H, d, *J* 7.7 Hz, Ar-H), 5.12 (1H, d, *J* 7.2 Hz, O=C-CHH-N-CH₂-Ph), 5.09 (1H, d, *J* 7.4 Hz, O=C-CHH-N-CH₂-Ph), 4.99 (1H, q, *J* 6.9 Hz, N-CHCH₃-Ph), 4.95 (1H, q, *J* 7.0 Hz, N-CHCH₃-Ph), 4.93-4.90 (2H, overlapping, N-CHCH₃-Ph and O=C-CHH-N-CH₂-Ph), 4.82 (1H, d, *J* 17.3 Hz, O=C-CHH-N-CHCH₃-Ph), 4.79 (1H, q, *J* 6.8 Hz, N-CHCH₃-Ph), 4.67 (1H, d, *J* 18.2 Hz, O=C-CHH-N-CH₂-Ph), 4.64 (1H, d, *J* 16.6 Hz, O=C-CHH-N-CHCH₃-

Ph), 4.63 (1H, d, J 16.7 Hz, N-*CHH*-Ph), 4.53-4.47 (1H, O=C-*CHH*-N-CHCH₃-Ph and 3H N-*CHH*-Ph, overlapping), 4.33 (1H, d, J 16.8 Hz, O=C-*CHH*-N-CHCH₃-Ph), 4.14 (1H, d, J 16.5 Hz, N-*CHH*-Ph), 4.06 (1H, d, J 16.3 Hz, N-*CHH*-Ph), 4.01 (1H, d, J 16.3 Hz, N-*CHH*-Ph), 3.95 (1H, d, J 16.7 Hz, N-*CHH*-Ph), 3.75-3.71 (4H, overlapping d, O=C-*CHH*-N-CH₂-Ph, O=C-*CHH*-N-CHCH₃-Ph and O=C-*CHH*-N-CHCH₃-Ph), 3.67 (1H, d, J 10.7 Hz, O=C-*CHH*-N-CH₂-Ph), 3.64 (1H, d, J 10.2 Hz, O=C-*CHH*-N-CHCH₃-Ph), 3.45 (1H, d, J 18.2 Hz, O=C-*CHH*-N-CH₂-Ph), 3.34 (1H, d, J 16.8 Hz, O=C-*CHH*-N-CH₂-Ph), 1.46 (3H, d, J 6.9 Hz, N-CHCH₃-Ph), 1.44 (3H, d, J 6.9 Hz, N-CHCH₃-Ph), 1.36 (3H, d, J 7.0 Hz, N-CHCH₃-Ph), 1.28 (3H, d, J 6.8 Hz, N-CHCH₃-Ph). ¹³C-NMR (150 MHz, CDCl₃) δ: 170.2, 170.0, 169.6, 169.1, 169.0, 168.8, 168.2, 167.9, 161.7 (q, J 50 Hz, C-1), 137.7 (x2), 135.4 (x2), 134.8 (C-2), 133.1 (x2), 132.8 (x2), 129.4 (x8), 129.3 (x8), 128.8 (q, J 30 Hz, C-3), 128.0 (x8), 126.7 (x8), 126.5 (x4), 125.6 (x4), 124.6 (q, J 270 Hz, C-5), 117.4 (C-4), 55.7 (x2), 55.5, 55.0, 51.7 (x2), 51.4 (x2), 47.8 (x2), 47.6, 47.3, 46.9, 44.8, 44.3, 44.1, 18.0, 17.7, 17.5 (x2). ESI-MS m/z 1256.0 [M + Na]⁺.

[**139**·2Na]²⁺·2[TFPB]²⁻: white amorphous solid. ¹H-NMR (600 MHz, CDCl₃) δ: 7.71 (16H, s, TFPB-*o*-H), 7.52 (8H, s, TFPB-*p*-H), 7.38-7.27 (24H, br signals, overlapping, Ar-H), 7.12 (8H, d, J 7.5 Hz, Ar-H), 6.57 (8H, d, J 7.5 Hz, Ar-H), 4.84 (8H, q, J 6.9 Hz, N-CHCH₃-Ph), 4.58 (4H, d, J 16.7 Hz, O=C-*CHH*-N-CHCH₃-Ph), 4.42 (4H, d, J 16.8 Hz, O=C-*CHH*-N-CHCH₃-Ph), 3.70 (4H, d, J 16.7 Hz, O=C-*CHH*-N-CHCH₃-Ph), 3.46 (4H, d, J 16.8 Hz, O=C-*CHH*-N-CHCH₃-Ph), 1.36 (12H, d, J 6.9 Hz, N-CHCH₃-Ph), 1.34 (12H, d, J 6.9 Hz, N-CHCH₃-Ph). ¹³C-NMR (150 MHz, CDCl₃) δ: 169.2 (x4), 168.4 (x4), 161.7 (q, J 50 Hz, C-1), 137.9 (x4), 135.5 (x4), 134.8 (C-2), 129.5 (x8), 129.2 (x8), 129.0 (x8), 128.8 (q, J 30 Hz, C-3), 128.2 (x8), 125.5 (x8), 124.6 (q, J 270 Hz, C-5), 117.4 (C-4), 55.6 (x4), 55.0 (x4), 44.5 (x4), 44.2 (x4), 18.0 (x4), 17.4 (x4). ESI-MS m/z 1312.1 [M + Na]⁺.

Chapter 4



4 Cyclic tripeptides as mimics of natural siderophores

4.1 Introduction

4.1.1 Catecholamide-based natural siderophores

Iron is among the most important metals for human health; its correct homeostasis, comprising transport, storage, and utilization, is still a crucial topic in biochemistry.

In humans, iron exists only bound to proteins (hemoprotein), incorporated in heme groups (heme-proteins), or in non-heme compounds (ferritin, transferrin, and so on) at $\sim 10^{-24}$ M concentrations.¹³¹ The quantity of iron adsorbed through the diet is extremely low (ranging from 5 to 35% of the ingested quantity), also due to the absence of an excretion mechanism.¹³²

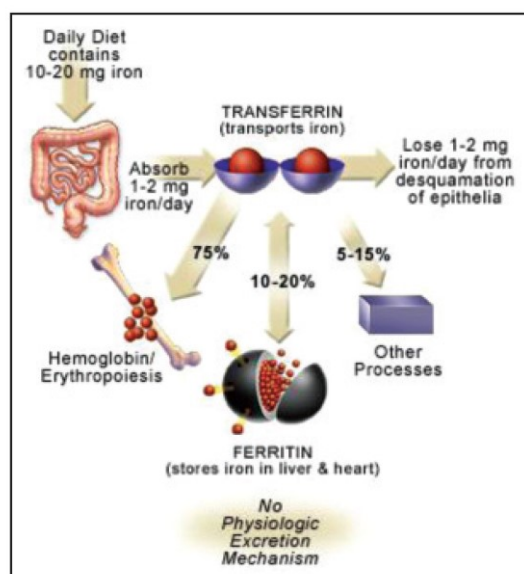


Figure 4.1. Iron metabolism in the human body.¹³²

An excess of iron can lead to a number of pathologies; for example, iron accumulation has been found in brain of patients suffering Alzheimer's disease (AD), particularly in patients showing neuronal death. Similarly, iron excess has been found in

¹³¹ Raymond K. N., Dertz E. A., Kim S. S., *Proc. Natl. Acad. Sci. USA* **2003**, *100*, 7, 3584-3588.

¹³² Abbaspour N., Hurrell R., Kelishadi R., *J. Res. Med. Sci.* **2014**, *19*, 164-174.

patients suffering Parkinson's disease, and in the most advanced stages of the Huntington's disease. In all these cases, iron excess is connected directly to the redox activity in the human brain.¹³³

Iron has a key impact on microbial growth; the optimal $\sim 10^{-6}$ M concentration favours the growth of fungi, microorganisms and bacteria strains. Thus, bacteria have evolved aggressive iron uptake mechanisms. The controlled release of siderophores is a common iron uptake pathway; iron-carriers are secondary metabolites secreted by microorganisms under iron deficiency. These molecules show high affinity for Fe(III), present low molecular weight (usually under 1500 KDa), and are selectively synthesized and secreted under low iron concentrations. Their main task is to increase the low ferric ion solubility, sequestering it from ferric hydroxide polymers.^{131,134}

Among siderophores the most potent, and the first to be isolated was enterobactin (**142**). This compound, isolated from *E. coli* and *Salmonella typhimurium*, is an hexadentate ligand; its scaffold is constituted by a triserine macrolactone, condensed through the side-chain hydroxyl units. Fe(III) complexation occurs through the six oxygens of the catecholate (1,2-dihydroxybenzene) pending moieties.¹³⁵

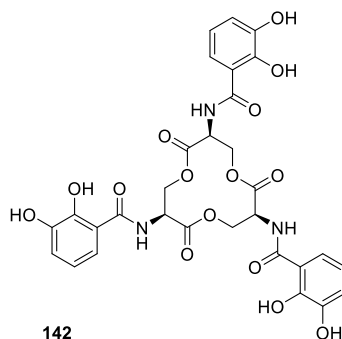


Figure 4.2. Schematic structure of enterobactin (**142**).

The determination of the enterobactin-ferric ion association constant was, at first, challenging, due to the precipitation of an insoluble complex at pH 3.8. Therefore, the association constant was determined through a spectrophotometric competition experiment with the ligand EDTA (ethylenediaminetetraacetic acid) (pH = 5.0), and

¹³³ Barnham K. J., Bush A. I., *Chem. Soc. Rev.* **2014**, 43, 6727-6749.

¹³⁴ a) Hider R. C., Kong X., *Nat. Prod. Rep.* **2010**, 27, 637-657; b) Szebesczyk A., Olshvang E., Shanzer A., Carver P. L., Gumienna-Kontecka E., *Coord. Chem. Rev.* **2016**, 327-328, 84-109.

¹³⁵ a) Knoth W. H., *J. Am. Chem. Soc.* **1979**, 101, 9, 2213-2214; b) Loomis L. D., Raymond K. N., *Inorg. Chem.* **1991**, 30, 906-911.

assessed as 10^{49} M^{-1} . The resulting complex is extremely thermodynamically stable, as EDTA cannot remove substantial amounts of ferric ion at pH 7.0, and the complex itself shows highly negative reduction potential.^{135a}

Another peculiar characteristic of siderophores is their strict selectivity towards Fe(III); in fact, the negatively charged oxygen atoms show a tight interaction with the tripositive cation. Hexadentate ligands are arranged around the metallic center with minimum amount of ligand repulsion, filling the octahedral coordination sphere, forming thermodynamically stable high-spin iron(III) complexes with the two deprotonated ortho-phenolate oxygens of catecholates ($\text{p}K_{\text{a}} = 9.2$ and 13.0).^{134a}

The overall chirality of the complex is crucial as well; in principle, both geometrical and optical isomers could be obtained, meaning Δ -*cis*, Λ -*cis*, Δ -*trans*, Λ -*trans*. Enterobactin, like most of the hexadentate hydroxamates, is restricted to the *cis* form; upon deprotonation, the ortho-oxygen of the catecholate unit changes its conformation, resulting oriented in the same direction of the amide proton. This causes the encapsulation of the ferric ion in a *cis* fashion. Secondly, the overall spatial orientation of the complex results in a Δ (right-handed coordination propeller) chirality.

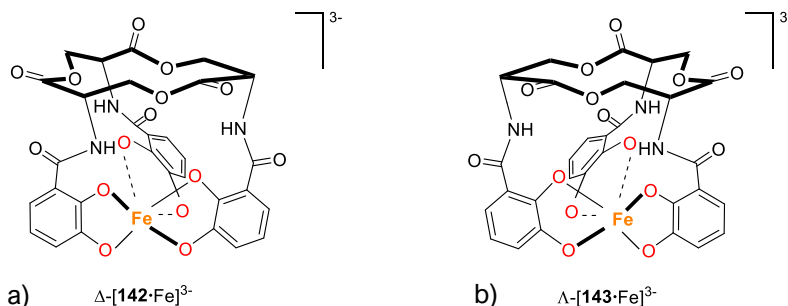


Figure 4.3. Schematic structures of a) Δ -[142·Fe]³⁻ and b) Λ -[143·Fe]³⁻ complexes. The catecholate oxygens participating to iron (orange) bonding are indicated in red.

The overall chirality is crucial for the biological activity; in fact, the Λ -[143·Fe]³⁻ complex, obtained from enantioenterobactin, constituted by D-serine monomers, does not exert the same siderophore activity.¹³⁶ It was proven that the complex chirality drives the biological activity targeting the cytoplasmic esterase (which regulates the iron release), as the substitution of the triserine scaffold with a phenyl unit in the synthetic siderophore H₆-

¹³⁶ Rastetter W. H., Erickson T. J., Venuti M. C., *J. Org. Chem.* **1981**, *46*, 18, 3579-3590.

mecam (**144**) does not affect critically its function, but, on the contrary, Λ -[**143**-Fe]³⁺ is not capable to promote *E. coli* strain growth.¹³⁷

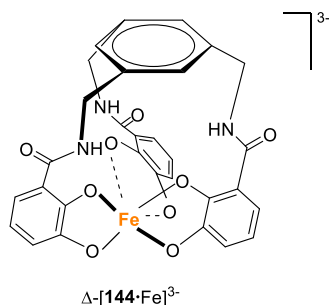


Figure 4.4. Schematic structure of H₆-mecam (**144**) iron(III) complex.

Besides enterobactin, many catechol-based siderophores are known. Corynebactin (**145**), produced by the Gram-positive bacteria *Corynebacterium glutamicum*, possesses a scaffold quite similar to enterobactin (constituted by Thr residues rather than Ser), with the addition of a glycine spacer between the macrolactone ring and the catechol moieties (Figure 4.5).

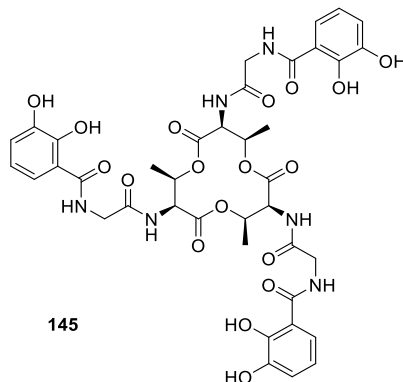


Figure 4.5. Schematic structure of corynebactin (**145**).

The presence of the glycine spacer has a critical impact on the overall chirality of the complex, in fact corynebactin-ferric complex presents a *cis*- Λ chirality.

The stability of the ferric complex is influenced both by the side-chains and by the chirality of the macroring scaffold, resulting, for corynebactin, in a lower energy conformation for the Λ -isomer.¹³¹ The preparation of a serine-corynebactin derivative (**146**), constituted by a triserine macrolactone (typical of enterobactin) plus the

¹³⁷ Cassinelli G., Ruggieri D., Arcamone F., *J. Med. Chem.* **1979**, 22, 2, 123-124.

corynebactin side-chains, evidenced that the latter are determining the chirality of the complex, as the synthetic derivative presented the Λ -isomer as lowest energy as well.¹³⁸

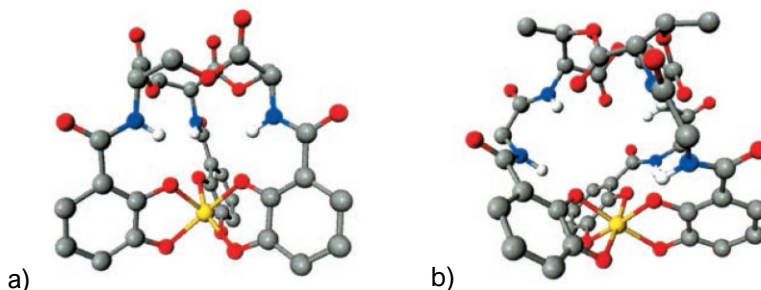


Figure 4.6. Stereoimage of a) enterobactin-ferric complex and b) corynebactin-ferric complex. The two present opposite chirality (Δ and Λ , respectively). C, silver; N, blue; O, red; H, white; Fe, yellow.

Iron overload management is a hot topic in medicinal chemistry, which is why many synthetic siderophores have been prepared.

Iron chelation therapy is based on the administration of a highly selective Fe(III) host, with high binding constant. These compounds are small molecules, linear or cyclic, classified as bi-, tri-, or hexadentate. Often, the main framework resembles the enterobactin one, like the already mentioned H₆-mecam.

The most common iron chelators commercially available are Deferiprone, Deferasirox and Deferoxamine, which are, respectively, bi-, tri- and hexadentate; the scaffolds show *N*-hydroxyl moieties. For example, one of the most common iron chelation therapy (ICT) drugs, Deferoxamine, is constituted by a linear *N*-hydroxy polyamide that binds iron(III) at the myocardial cells level, preventing iron overload in transfusional therapies and thalassemia.

These compounds, however, have dose-related cardiac and neuronal side effects; moreover, nephrotoxicity and dangerous accumulation in the liver have been observed, due to an inefficacious excretion of the drug.¹³⁹

¹³⁸ Bluhm M. E., Kim S. S., Dertz E. A., Raymond K. N., *J. Am. Chem. Soc.* **2002**, *124*, 11, 2436-2437.

¹³⁹ a) Maggio A., *Br. J. Haematol.* **2007**, *138*, 407-421; b) Tyagi P., Kumar Y., Gupta D., Singh H., Kumar A., *Int. J. Pharm. Pharm. Sci.* **2015**, *7*, 35-44; c) Urgesa M. H., Hirpaye B. Y., *J. Chem. Pharm. Res.* **2017**, *9*, 182-187.

4.1.2 Purpose of the research

In this study, we synthesized three cyclotripeptoids, whose scaffold was designed based on natural occurring siderophores. The macroring dimension was chosen on the bases of the natural triserine/trithreonine macrolactone, as well as the catechol side-chains.

The three cyclotripeptoids differ on the basis of the side-chain length linking the macroring core and the chelating units.

UV-Vis titrations were exploited in order to validate the iron(III) binding capability of such compounds, as well as the selectivity compared to transition metal cations commonly occurring in biological systems.

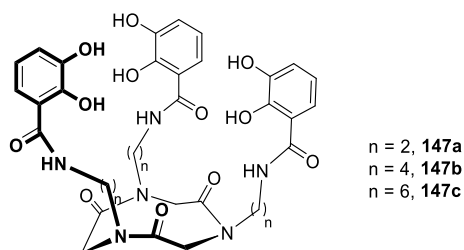


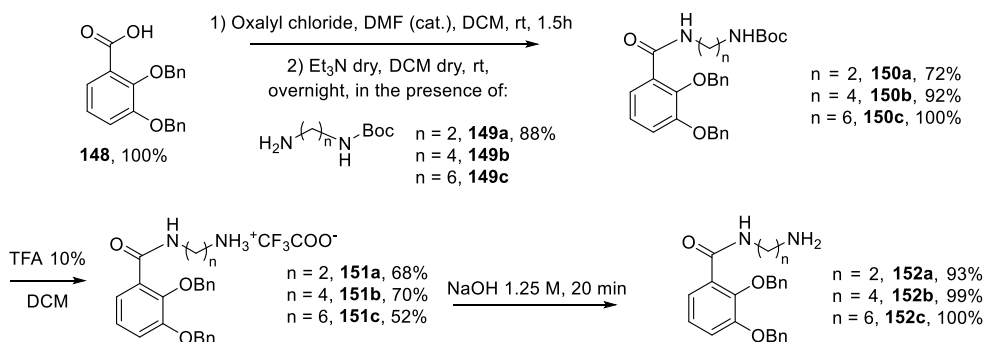
Figure 4.7. Schematic structures of cyclotripeptoid siderophores.

4.2 Catechol-based cyclotripeptoids as transition metal chelators¹⁴⁰

4.2.1 Results and discussion

4.2.1.1 Synthesis and structural analysis of cyclotripeptoids **147a-c**

The synthesis of the three catechol-based derivatives was performed exploiting the sub-monomeric approach. First, the necessary amines were obtained according to reported procedures,¹⁴¹ starting from commercially available 2,3-dihydroxybenzoic acid¹⁴² and 1,2-,¹⁴³ 1,4- and 1,6-alkyldiamines (Scheme 4.1).



Scheme 4.1. Synthesis of *N*-(ω -aminoalkyl)-2,3-bis(benzyloxy)benzamides **152a-c**.

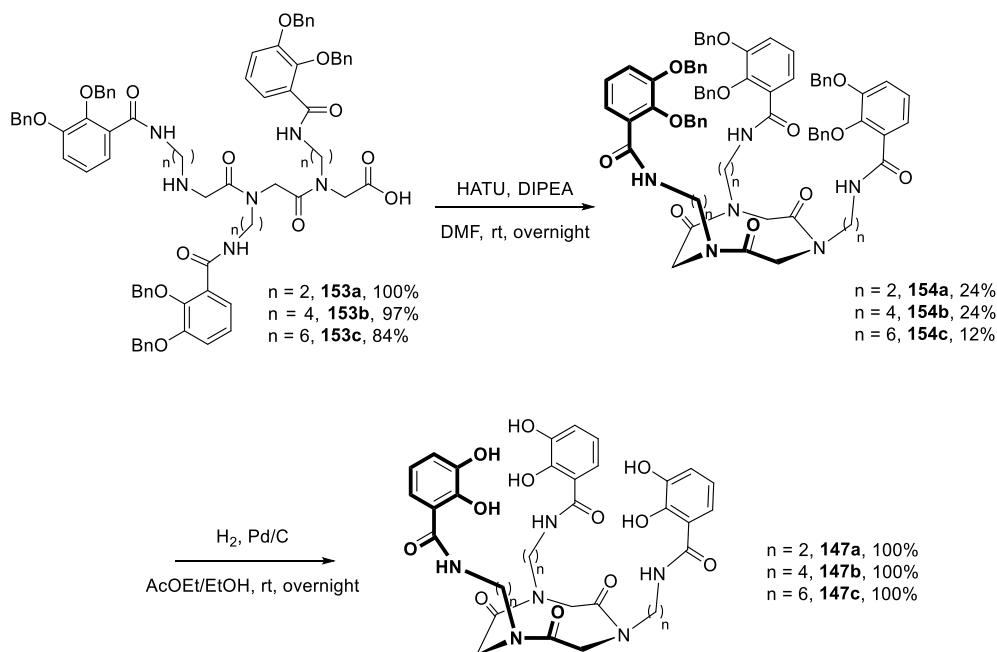
The successful incorporation of amines **152a-c** in the linear oligomers led to the desired compounds, which were subjected to high dilution cyclization to obtain cyclotripeptoids **154a-c**. Finally, such derivatives were deprotected *via* catalytic hydrogenation to obtain the enterobactin mimics **147a-c** in quantitative yields (Scheme 4.2).

¹⁴⁰ D'Amato A., Ghosh P., Della Sala G., Izzo I., Maayan G., De Riccardis F., *Peptoid-based Siderophores with Catecholamide Ligands as Archetype for Ion Complexation*, manuscript in preparation.

¹⁴¹ a) Zhang Q., Jin B., Peng R., Lei S., Chu S., *Polyhedron* **2015**, *34*, 417-423; b) Lei S., Jin B., Zhang Q., Zhang Z., Wang X., Peng R., Chu S., *Polyhedron* **2016**, *35*, 387-395.

¹⁴² 2,3-dihydroxybenzoic acid was benzyl protected according to: Kishimoto S., Nishimura S., Kakeya H., *Chem. Lett.* **2015**, *44*, 1303-1305.

¹⁴³ Ethylenediamine was mono-Boc protected to obtain **149a** according to: Jobin S., Vézina-Dawod S., Herby C., Derson A., Biron E., *Org. Lett.* **2015**, *17*, 5626-5629. **149b** and **149c** were commercially available.



Scheme 4.2. Synthesis of tris-catecholamide cyclotripeptides **147a-c**.

As expected, the cyclization gave C_3 -symmetric, rigid “crown” peptides, with coalescence temperatures above 373 K ($C_2D_2Cl_4$ solution, 600 MHz, $\Delta G^\ddagger > 16.9$ kcal/mol).⁶¹ The same three-fold all-*cis* symmetry was also observed in the deprotected compounds (1H -NMR analysis).

4.2.1.2 Transition metal complexation studies

The complexation capabilities of our compounds were tested with several hexacoordinated transition metal cations, Co^{2+} , Cu^{2+} , Ni^{2+} , Zn^{2+} , Fe^{2+} and Fe^{3+} . The UV-Vis titrations were performed first in methanol, using the respective metal chlorides, in the presence of the cyclic peptides **147a-c**.¹⁴⁴

Figure 4.8 reports the titration curves for **147a**; in all cases, the 319 nm peak typical of the free ligand showed a redshift (to 334 nm for Co^{2+} , Cu^{2+} , Zn^{2+} , 340 nm for Ni^{2+}) and no binding for Fe^{2+} . The most interesting case was Fe^{3+} , with a redshift to 325 nm, plus the appearance of a new peak at 570 nm (Figure 4.8 c)). The ferric complex showed a change of colour to deep blue, testifying the formation of a metal-to-ligand-charge-transfer

¹⁴⁴ Titrations performed at 17 μM concentration of cyclic peptides **147a-c** in methanol, adding increasing quantities of the respective metal chlorides, up to 4 eq.

complex (MLCT). The other two cyclic peptoids displayed similar trends (UV-Vis titration curves not shown).

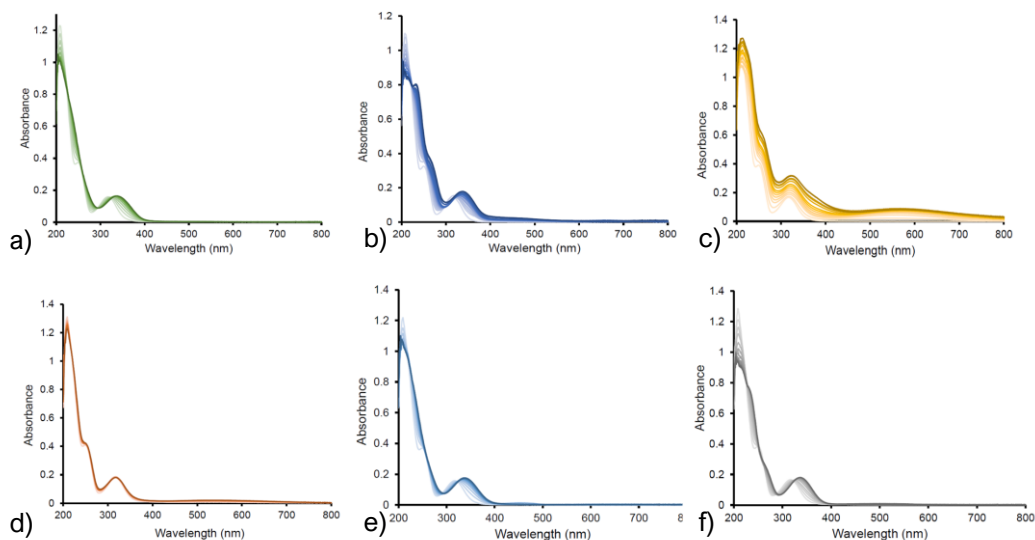


Figure 4.8. UV-Vis titration of **147a** with a) Co^{2+} , b) Cu^{2+} , c) Ni^{2+} , d) Zn^{2+} , e) Fe^{2+} f) Fe^{3+} , concentration: $17\ \mu\text{M}$, solvent: methanol.

Subsequently, the relative stability of our complexes was investigated; the glass vials containing **147a-c** ferric complexes were sealed and the UV-Vis measurement was repeated after four days. Only $[\mathbf{147a}\text{-Fe}]^{3+}$ showed a curve corresponding to the initial one. The stability of the adduct was also testified by the retention of the deep blue colour, faded in the other two cases ($[\mathbf{147b}\text{-Fe}]^{3+}$ and $[\mathbf{147c}\text{-Fe}]^{3+}$).

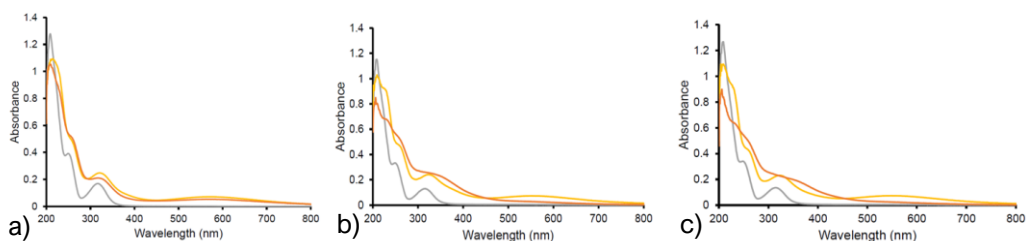


Figure 4.9. UV-Vis ferric ion titration of a) **147a**, b) **147b**, c) **147c**. Grey curve: free ligand; yellow curve: ferric complex; orange curve: ferric complex after four days.

The evaluation of the binding constant, in a competition experiment with known chelator EDTA,¹⁴⁵ corroborated the UV-Vis data; in fact, the highest association constant

¹⁴⁵ Association constants were calculated according to: a) Harvey D., *Modern analytical chemistry*, McGraw-Hill, **1999**; b) Wu S. L., Horrocks W. D. Jr., *Anal. Chem.* **1996**, *68*, 394-401. Measurements performed in MeOH, at different increasing concentrations of the various ligands, cyclopeptoids:EDTA: Fe^{3+} ratio = 1:1:1.

was measured for $[\mathbf{147a}\cdot\text{Fe}]^{3+}$ ($K_a = 3.08 \cdot 10^{20} \text{ M}^{-1}$), while the other two compounds resulted a hundred times less efficient for Fe^{3+} ($[\mathbf{147b}\cdot\text{Fe}]^{3+}$, $K_a = 2.00 \cdot 10^{18} \text{ M}^{-1}$ and $[\mathbf{147c}\cdot\text{Fe}]^{3+}$, $K_a = 4.00 \cdot 10^{18} \text{ M}^{-1}$).

In order to assess the importance of the counterion, the titration for the best complexing agent, cyclotripeptoid **147a**, with an ethylene spacer, was also performed with $\text{Fe}(\text{ClO}_4)_3$ and $\text{Fe}(\text{NO}_3)_3$. In all three cases (comparing the results with FeCl_3), the binding affinity remained the same; moreover, we discovered that the cyclopeptoid scaffold can host up to two equivalents of iron(III).

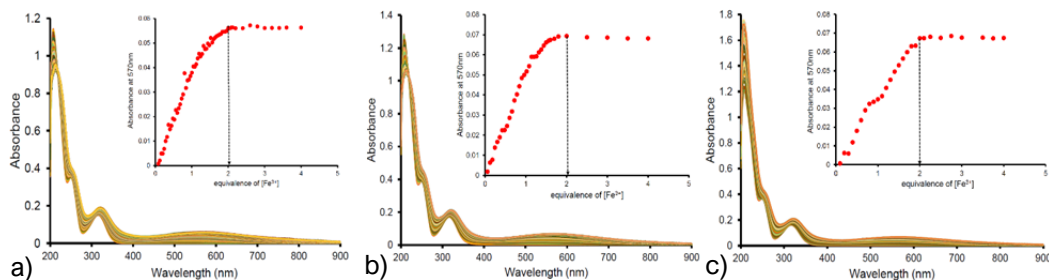


Figure 4.10. UV-Vis **147a** titration and complex stoichiometry determination in the presence of a) FeCl_3 , b) $\text{Fe}(\text{ClO}_4)_3$, c) $\text{Fe}(\text{NO}_3)_3$; concentration: $17 \mu\text{M}$, solvent: methanol.

Crystallization trials of the $[\mathbf{147a}\cdot\text{Fe}]^{3+}$ complex for X-ray measurements were not successful. We are currently running DFT calculations investigating the possible structure of the complex.

Our last investigation is concerning the selectivity of our hosts towards Fe^{3+} , since the biological systems contain several transition metal cations. Ligands **147a-c** will be subjected to competition experiments, in which increasing quantities of a 1:1 $\text{Fe}^{3+}:\text{M}^{2+}$ (where M is Co^{2+} , Cu^{2+} , Ni^{2+} or Zn^{2+}) are added to a methanol solution of the free host before acquiring the UV-Vis spectra.

Preliminary results are showing a selectivity of our hosts towards Fe^{3+} , in the presence of other metal cations; however, the assessment will be completed after several experiments comprising the use of different stoichiometry ratios between the metallic guests.

4.2.2 Conclusions

In this study, we proposed three cyclotripeptoids as archetype for iron(III) complexation. Resembling natural effectors, our molecules showed strong potential as synthetic Fe³⁺ chelators.

Most interestingly, we are assessing the selectivity towards ferric ion through competition experiments in the presence of several transition metal cations. The overall substitution of the macrolactone scaffold with a peptoid one seems to be not detrimental to the metal selectivity towards iron(III).

4.2.3 Experimental section

4.2.3.1 General methods

Refer to Paragraph 2.2.3.1.

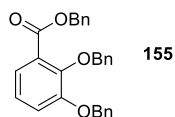
Additional NMR solvent used in this work: CD₂HOD, δ = 3.31; ¹³CD₃OD, δ = 49.00.

For the VT NMR experiments, refer to Paragraph 2.2.3.7.

UV-Vis titrations and competition experiments were performed by prof. G. Maayan research group, Schulich Faculty of Chemistry, Israel Institute of Technology (Technion), Haifa, Israel.

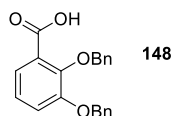
4.2.3.2 Synthesis of 2,3-bis(benzyloxy)benzoic acid (148)

2,3-dihydroxybenzoic acid (1.85 g, 12.0 mmol) was dissolved in dry DMF (12.0 mL); subsequently, K₂CO₃ (3.3 eq., 5.47 g, 40.0 mmol) and benzyl bromide (3.2 eq., 4.57 mL, 38.4 mmol) were added, and the reaction was stirred at room temperature overnight. After 24 hours, 8.00 mL of H₂O:brine 1:1 were added to quench the reaction, followed by 38.0 mL of DMF (to solubilize the resulting precipitate) and 76.0 mL of H₂O. The resulting aqueous phase was extracted three times with 80.0 mL of ethyl acetate. The organic phase was washed with 120 mL of NH₄Cl sat. aq. and 120 mL of brine, then anhydriified on Na₂SO₄; the solvent was evaporated to obtain the intermediate 2,3-bis(benzyloxy)benzoic acid benzyl ester.



2,3-bis(benzyloxy)benzoic acid benzyl ester (**155**): white amorphous solid, 5.09 g, 100% (crude). $^1\text{H-NMR}$ (400 MHz, CDCl_3) δ : 7.32-7.06 (13H, overlapping signals, Ar-*H* and CH_2 -Ph-*H*), 5.32 (2H, s, COOCH_3), 5.14 (2H, s, *o*-O- CH_2 -Ph), 5.07 (2H, s, *m*-O- CH_2 -Ph). ES-MS: 425.3 m/z [$\text{M}+\text{H}^+$].

2,3-bis(benzyloxy)benzoic acid benzyl ester (5.09 g, 12.0 mmol) was dissolved in 16.0 mL of methanol, then 16.0 mL of 2 M NaOH were added. The reaction was refluxed under stirring for 23 hours, then brought to room temperature. The methanol was evaporated, and 16.0 mL of H_2O were added; the resulting aqueous phase was extracted two times with 64.0 mL of diethyl ether. The resulting aqueous phase was acidified with 3 M HCl to $\text{pH} < 2$ to induce precipitation. The white precipitate was filtrated and washed with cold H_2O , then further dried to gain 2,3-bis(benzyloxy)benzoic acid.



2,3-bis(benzyloxy)benzoic acid (**148**): white amorphous solid, 4.00 g, 100% (crude). $^1\text{H-NMR}$ (400 MHz, CDCl_3) δ : 11.37 (1H, br s, COOH), 7.74 (1H, dd, J 7.9, 1.7 Hz, *o*-Ar-*H*), 7.49-7.17 (12H, overlapping signals, CH_2 -Ph-*H*, *m*-Ar-*H* and *p*-Ar-*H*), 5.26 (2H, s, *o*-O- CH_2 -Ph), 5.20 (2H, s, *m*-O- CH_2 -Ph). ES-MS: 335.3 m/z [$\text{M}+\text{H}^+$].

4.2.3.3 Synthesis of *tert*-butyl (2-aminoethyl)carbamate (**149a**)

Ethylenediamine (0.840 mL, 12.5 mmol) was dissolved in CHCl_3 (13.0 mL) under stirring. A solution of di-*tert*-butyl dicarbonate (0.3 eq., 0.818 g, 3.75 mmol) in CHCl_3 (20.0 mL), was added dropwise over the course of 1 hour to the amine solution. The reaction was stirred at room temperature for 23 hours, after which the resulting solution was washed three times with 21.0 mL of H_2O . The resulting organic phase was dried over anhydrous MgSO_4 and the solvent was evaporated to gain the oily product.



tert-butyl (2-aminoethyl)carbamate (**149a**): white oil, 1.76 g, 88% (crude). $^1\text{H-NMR}$ (400 MHz, CDCl_3) δ : 4.88 (1H, br s, *NH*-Boc), 3.17 (2H, q, J 5.9 Hz, CH_2 -*NH*-Boc), 2.79 (2H, t, J 6.0 Hz, $\text{H}_2\text{N-CH}_2$), 1.44 (9H, s, $\text{COO}(\text{CH}_3)_3$).

4.2.3.4 General methods for the preparation of the amines **152a-c**

Synthesis of derivatives **150a-c**

2,3-bis(benzyloxy)benzoic acid **148** (4.00 g, 12.0 mmol) was dissolved in dry dichloromethane (48.0 mL), under nitrogen atmosphere. A catalytic amount of dry dimethylformamide was added, followed by oxalyl chloride, dropwise (1.5 eq., 1.52 mL, 18.0 mmol). The mixture was stirred for 1 h under nitrogen atmosphere, then the solvent was evaporated. The desired *N*-Boc-diamine (11.0 mol) was dissolved in 46 mL of dry dichloromethane, then dry triethylamine (1.7 eq., 2.84 mL, 0.0200 mol) was added. The crude residue 2,3-bis(benzyloxy)benzoyl chloride was dissolved in further 46.0 mL of dry dichloromethane and added dropwise to the amine solution. The mixture was stirred at room temperature overnight. CH_2Cl_2 was removed *in vacuo* to yield a light yellow solid residue. The crudes were purified on flash silica gel: conditions: 100% – 95% A (A: dichloromethane; B: methanol).

N-(*N*-Boc-ethylenediamine)-2,3-bis(benzyloxy)benzamide (**150a**): light yellow amorphous solid, 3.77 g, 72%. $^1\text{H-NMR}$ (400 MHz, CDCl_3) δ : 7.98 (1H, br s, *N-H*), 7.62 (1H, d, J 2.4 Hz, *o*-*Ar-H*), 7.38-7.17 (11H, br signals, overlapping, *m*-*Ar-H* and CH_2 -*Ph-H*), 7.06 (1H, d, J 1.8 Hz, *p*-*Ar-H*), 5.07 (2H, s, CH_2 -*Ph*), 5.01 (2H, s, CH_2 -*Ph*), 3.27 (2H, m, C=O-NH-CH_2), 3.08 (2H, m, C=OOtBu-NH-CH_2), 1.32 (9H, s, $\text{C=OO}(\text{CH}_3)_3$). ES-MS: m/z ; 477.3 [$\text{M} + \text{H}$] $^+$.

N-(*N*-Boc-butanediamine)-2,3-bis(benzyloxy)benzamide (**150b**): light yellow amorphous solid, 5.10 g, 92%. $^1\text{H-NMR}$ (400 MHz, CDCl_3) δ : 7.93 (1H, br s, *N-H*), 7.74 (1H, br dd, J 5.1, 3.7 Hz, *o*-*Ar-H*), 7.48-7.29 (11H, br signals, overlapping, *m*-*Ar-H* and CH_2 -*Ph-H*), 7.15 (1H, br dd, J 4.2 Hz, *p*-*Ar-H*), 5.16 (2H, s, CH_2 -*Ph*), 5.09 (2H, s, CH_2 -*Ph*), 3.27 (2H, m, C=O-NH-CH_2), 3.03 (2H, m, C=OOtBu-NH-CH_2), 1.58 (4H, br signals, overlapping, $\text{NH-CH}_2\text{-CH}_2\text{-CH}_2$), 1.44 (9H, s, $\text{C=OO}(\text{CH}_3)_3$). ES-MS: m/z ; 505.2 [$\text{M} + \text{H}$] $^+$.

N-(*N*-Boc-hexamethylenediamine)-2,3-bis(benzyloxy)benzamide (**150c**): light yellow amorphous solid, 5.86 g, 100%. $^1\text{H-NMR}$ (600 MHz, CDCl_3) δ : 7.90 (1H, m, *N-H*), 7.74 (1H, br dd, J 6.2, 3.4 Hz, *o*-*Ar-H*), 7.40-7.30 (11H, br signals, overlapping, *m*-*Ar-H* and

CH₂-Ph-*H*), 7.15 (1H, br dd, *p*-Ar-*H*), 5.16 (2H, s, CH₂-Ph), 5.08 (2H, s, CH₂-Ph), 3.25 (2H, m, C=O-NH-CH₂), 3.07 (2H, m, C=OO^tBu-NH-CH₂), 1.44 (9H, s, C=OO(CH₃)₃, 1.42-1.22 (8H, br signals, overlapping, NH-CH₂-CH₂-CH₂-CH₂-CH₂). ES-MS: *m/z*; 533.6 [M + H]⁺.

Synthesis of derivatives **151a-c**

The *N*-Boc protected *N'*-2,3-bis(benzyloxy)benzamides (0.0100 mmol) were dissolved in dry dichloromethane (77.0 mL), then brought to 0 °C in an ice bath. A solution of trifluoroacetic acid in dry dichloromethane (20% v/v, 77.0 mL) was added dropwise to the benzamide solution. The reaction mixture was stirred at room temperature for 3 hours, then the completion of the reaction was assessed *via* TLC. The solution was then concentrated *in vacuo* and the crude oil dissolved in 5.00 mL of hot ethanol, then added dropwise to 200 mL of a cold 50/50 solution of diethyl ether/petroleum ether to induce the precipitation of the trifluoroacetate salt.

N-(aminoethyl)-2,3-bis(benzyloxy)benzamide, TFA salt (**151a**): white amorphous solid, 3.33 g, 68%. ¹H-NMR (400 MHz, CDCl₃) δ: 8.48 (1H, br s, *N*-*H*), 7.61 (1H, d, *J* 7.5 Hz, *o*-Ar-*H*), 7.41-7.13 (12H, br signals, overlapping, *m*-Ar-*H*, *p*-Ar-*H* and CH₂-Ph-*H*), 5.17 (2H, s, CH₂-Ph), 5.13 (2H, s, CH₂-Ph), 3.33 (2H, m, C=O-NH-CH₂), 2.96 (2H, m, CH₂-CH₂-NH₃⁺). ES-MS: *m/z*; 377.3 [M + H]⁺.

N-(aminobutyl)-2,3-bis(benzyloxy)benzamide, TFA salt (**151b**): white amorphous solid, 3.63 g, 70%. ¹H-NMR (400 MHz, CDCl₃) δ: 8.16 (3H, br s, ⁺NH₃), 8.10 (1H, br s, *N*-*H*), 7.58 (1H, d, *J* 6.8 Hz, *o*-Ar-*H*), 7.46-7.12 (12H, br signals, overlapping, *m*-Ar-*H*, *p*-Ar-*H* and CH₂-Ph-*H*), 5.13 (2H, s, CH₂-Ph), 5.08 (2H, s, CH₂-Ph), 3.17 (2H, m, C=O-NH-CH₂), 1.59 (2H, m, CH₂-CH₂-NH₃⁺), 1.36 (4H, m, C=O-NH-CH₂-CH₂-CH₂). ES-MS: *m/z*; 405.0 [M + H]⁺.

N-(*N*-Boc-hexamethylenediamine)-2,3-bis(benzyloxy)benzamide, TFA salt (**151c**): white amorphous solid, 2.84 g, 52%. ¹H-NMR (400 MHz, CDCl₃) δ: 8.04 (3H, br s, ⁺NH₃), 7.99 (1H, m, *N*-*H*), 7.57 (1H, dd, *J* 6.2, 3.1 Hz, *o*-Ar-*H*), 7.40-7.07 (11H, br signals, overlapping, *m*-Ar-*H* and CH₂-Ph-*H*), 7.07 (1H, br dd, *p*-Ar-*H*), 5.08 (2H, s, CH₂-Ph), 5.01 (2H, s, CH₂-Ph), 3.12 (2H, q, C=O-NH-CH₂), 2.85 (2H, m, CH₂-NH₃⁺), 1.55 (2H, m, CH₂-CH₂-NH₃⁺), 1.29-1.10 (6H, overlapping m, NH-CH₂-CH₂-CH₂-CH₂-CH₂-CH₂). ES-MS: *m/z*; 433.4 [M + H]⁺.

Synthesis of the derivatives *N*-(aminoethyl)-2,3-bis(benzyloxy)benzamide (**152a**),
N-(aminobutyl)-2,3-bis(benzyloxy)benzamide (**152b**), *N*-(aminohexyl)-2,3-
bis(benzyloxy)benzamide (**152c**)

The TFA salt derivatives (**151a-c**, 0.00600 mmol) were stirred for 30 minutes at room temperature with 25.0 mL of NaOH 1.25 M. The mixture was extracted three times with 50 mL of dichloromethane, then the organic phases were dried over anhydrous MgSO₄ and concentrated *in vacuo* to give the final product.

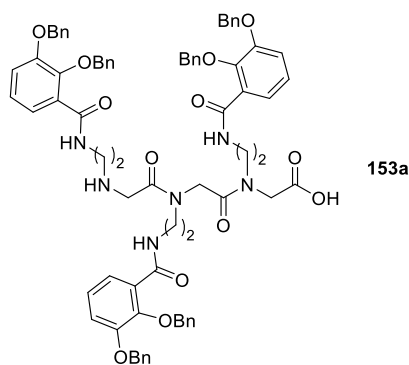
N-(2-aminoethyl)-2,3-bis(benzyloxy)benzamide (**152a**): light yellow oil, 2.10 g, 93%. ¹H-NMR (400 MHz, CDCl₃) δ: 8.10 (1H, br s, *N-H*), 7.71 (1H, t, *J* 4.7 Hz, *o*-Ar-*H*), 7.46-7.44 (11H, br signals, overlapping, *m*-Ar-*H* and CH₂-Ph-*H*), 7.12 (1H, d, *J* 4.7 Hz, *p*-Ar-*H*), 5.12 (2H, s, CH₂-Ph), 5.08 (2H, s, CH₂-Ph), 3.30 (2H, m, C=O-NH-CH₂), 2.65 (2H, t, *J* 6.1 Hz, CH₂-CH₂-NH₂), 0.85 (2H, br s, NH₂). ES-MS: *m/z*; 377.2 [M + H]⁺.

N-(aminobutyl)-2,3-bis(benzyloxy)benzamide (**152b**): light yellow oil, 2.40 g, 99%. ¹H-NMR (400 MHz, CDCl₃) δ: 7.96 (1H, br s, *N-H*), 7.74 (1H, dd, *J* 5.8, 3.7 Hz, *o*-Ar-*H*), 7.48-7.35 (11H, br signals, overlapping, *m*-Ar-*H* and CH₂-Ph-*H*), 7.15 (1H, d, *J* 3.7 Hz, *p*-Ar-*H*), 5.16 (2H, s, CH₂-Ph), 5.08 (2H, s, CH₂-Ph), 3.28 (2H, m, C=O-NH-CH₂), 2.60 (2H, t, *J* 6.3 Hz, CH₂-CH₂-NH₂), 1.35 (4H, m, C=O-NH-CH₂-CH₂-CH₂). ES-MS: *m/z*; 405.1 [M + H]⁺.

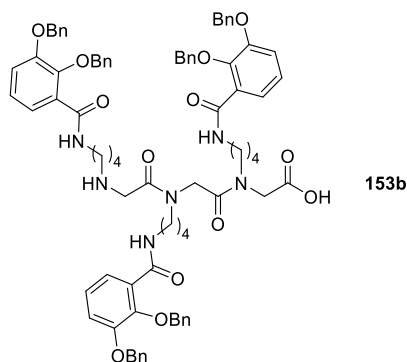
N-(aminohexyl)-2,3-bis(benzyloxy)benzamide (**152c**): light yellow oil, 2.54 g, 100%. ¹H-NMR (400 MHz, CDCl₃) δ: 7.84 (1H, m, *N-H*), 7.66 (1H, dd, *J* 6.0, 3.6 Hz, *o*-Ar-*H*), 7.40-7.26 (11H, br signals, overlapping, *m*-Ar-*H* and CH₂-Ph-*H*), 7.07 (1H, br dd, *p*-Ar-*H*), 5.08 (2H, s, CH₂-Ph), 4.99 (2H, s, CH₂-Ph), 3.20 (2H, q, C=O-NH-CH₂), 2.56 (2H, m, CH₂-NH₂), 1.28 (2H, m, CH₂-CH₂-NH₂), 1.16-1.14 (6H, overlapping m, NH-CH₂-CH₂-CH₂-CH₂-CH₂). ES-MS: *m/z*; 433.6 [M + H]⁺.

4.2.3.5 Synthesis of the linear peptoids **153a-c**

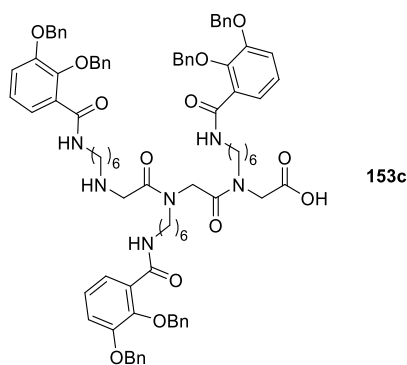
Refer to Paragraph 2.2.3.2. The synthesis was performed exploiting the sub-monomer protocol, on a 0.300 g 2-chlorotrytil chloride resin batch (1.47 mmol g⁻¹), using amines **152a-c**. Each elongation was performed using a solution of the chosen amine (2.20 mmol, 1.60 M in dry DMF), added to the bromoacetylated resin for 60 min at room temperature. Purity of the linear oligomers >80%.



153a: white amorphous solid, 0.558 g, 100%; t_R : 15.0 min. HRMS (MALDI-FTICR) m/z ; $[M + H]^+$ Calcd for $C_{75}H_{75}N_6O_{13}^+$ 1267.5387; Found 1267.5375.



153b: white amorphous solid, 0.578 g, 97%; t_R : 20.0 min. HRMS (MALDI-FTICR) m/z ; $[M + H]^+$ Calcd for $C_{81}H_{87}N_6O_{13}^+$ 1351.6326; Found 1351.6380.



153c: white amorphous solid, 0.531 g, 84%; t_R : 19.3 min. HRMS (MALDI-FTICR) m/z ; $[M + H]^+$ Calcd for $C_{87}H_{99}N_6O_{13}^+$ 1435.7265; Found 1435.7231.

4.2.3.6 Synthesis of the cyclic peptoids **154a-c**

Refer to Paragraph 2.2.3.3.

The cyclization reaction was performed on a 0.300 mmol scale of the linear oligomers, which were dissolved in 15.0 mL of dry DMF and added by a syringe pump in 6 hours to the reaction mixture. The crude cyclic peptoids were purified on flash silica gel; conditions: 50:50 petroleum ether:ethyl acetate, then 90:10 ethyl acetate:methanol. The cyclic peptoids were dissolved in 50% acetonitrile in HPLC grade water and analysed by RP-HPLC; purity >90%; conditions: 5% – 100% A in 30 min (A, 0.1% TFA in acetonitrile, B, 0.1% TFA in water); flow: 1 mL min⁻¹, 220 nm; subsequently characterized *via* ¹H-, ¹³C-NMR and HRMS (MALDI-FTICR).

154a: white amorphous solid, 0.0900 g, 24%; *t_R*: 20.2 min. ¹H-NMR (600 MHz, CDCl₃) δ: 7.85 (3H, br t, N-H), 7.60 (3H, dd, *J* 6.5, 2.9 Hz, *o*-Ar-H), 7.46-7.45 (6H, overlapping, *o*-CH₂-Ph-H), 7.40-7.30 (21H, overlapping, *m*-Ar-H and *m*-CH₂-Ph-H), 7.11-7.10 (9H, overlapping signals, *p*-Ar-H and *p*-CH₂-Ph-H), 5.13 (6H, s, CH₂-Ph), 5.07 (6H, s, CH₂-Ph), 4.17 (3H, d, *J* 15.6 Hz, C=O-CHH-N), 3.88 (3H, m, C=O-NH-CHH), 3.62 (3H, m, C=O-NH-CHH), 3.47 (3H, d, *J* 15.6 Hz, C=O-CHH-N), 3.27-3.23 (6H, overlapping m, N-CH₂-CH₂-NH). ¹³C-NMR (150 MHz, CDCl₃) δ: 167.7 x3 (C=O-N), 165.8 x3 (C=O-NH), 151.8 x3 (*m*-C-OBn), 146.7 x3 (*o*-C-OBn), 136.6 x3 (O-CH₂-C), 136.4 x3 (O-CH₂-C), 128.9 x3 (C-Ph), 128.6 x12 (C-Ph), 128.2 x3 (C-Ph), 127.6 x12 (C-Ph), 124.3 x3 (*m*-C-Ar), 122.8 x3 (*o*-C-Ar), 116.9 x3 (*p*-C-Ar), 76.2 x3 (O-CH₂-Ph), 71.2 x3 (O-CH₂-Ph), 48.7 x3 (C=O-CH₂-N), 46.1 x3 (C=O-NH-CH₂), 36.7 x3 (C=O-N-CH₂). HRMS (MALDI-FTICR) *m/z*; ([M + H]⁺ 49) Calcd for C₇₅H₇₃N₆O₁₂⁺ 1249.5281; Found 1249.5296; ([M + Na]⁺ 51) Calcd for C₇₅H₇₂N₆NaO₁₂⁺ 1271.5100; Found 1249.5113.

154b: white amorphous solid, 0.0960 g, 24%; *t_R*: 18.4 min. ¹H-NMR (600 MHz, CDCl₃) δ: 7.99 (3H, br t, N-H), 7.69 (3H, dd, *J* 7.6, 1.8 Hz, *o*-Ar-H), 7.46-7.45 (6H, overlapping, *o*-CH₂-Ph-H) 7.40-7.33 (21H, overlapping, *m*-Ar-H and *m*-CH₂-Ph-H), 7.13-7.08 (9H, overlapping signals, *p*-Ar-H and *p*-CH₂-Ph-H), 5.14 (6H, s, CH₂-Ph), 5.08 (6H, s, CH₂-Ph), 4.63 (3H, d, *J* 15.5 Hz, C=O-CHH-N), 3.76 (3H, m, C=O-NH-CHH), 3.54 (3H, d, *J* 15.5 Hz, C=O-CHH-N), 3.27-3.20 (9H, overlapping m, C=O-NH-CHH and N-CH₂-CH₂-CH₂-CH₂-NH), 1.47 (6H, m, N-CH₂-CH₂-CH₂-CH₂-NH), 1.27 (6H, m, N-CH₂-CH₂-CH₂-CH₂-NH). ¹³C-NMR (150 MHz, CDCl₃) δ: 167.2 x3 (C=O-N), 165.3 x3 (C=O-NH), 151.7 x3 (*m*-C-OBn), 146.8 x3 (*o*-C-OBn), 136.4 x6 (O-CH₂-C), 128.7 x3 (C-Ph), 128.2 x12 (C-Ph), 127.7 x3 (C-Ph), 127.2 x12 (C-Ph), 124.4 x3 (*m*-C-Ar), 123.2 x3 (*o*-C-Ar), 117.0 x3 (*p*-C-Ar), 76.4 x3 (O-CH₂-Ph), 71.3 x3 (O-CH₂-Ph), 48.9 x3 (C=O-CH₂-N), 46.5 x3 (C=O-NH-CH₂), 38.9 x3 (C=O-N-CH₂), 26.6

x3 (N-CH₂-CH₂-CH₂-CH₂-NH), 23.8 x3 (N-CH₂-CH₂-CH₂-CH₂-NH). HRMS (MALDI-FTICR) *m/z*; [M + H]⁺ Calcd for C₈₁H₈₅N₆O₁₂⁺ 1333.6220; Found 1333.6250.

154c: white amorphous solid, 0.0510 g, 12%; *t_R*: 22.1 min. ¹H-NMR (600 MHz, CDCl₃) δ: 7.90 (3H, br t, *N-H*), 7.72 (3H, dd, *J* 5.4, 4.2 Hz, *o-Ar-H*), 7.47-7.46 (6H, overlapping, *o-CH₂-Ph-H*), 7.41-7.33 (21H, overlapping, *m-Ar-H* and *m-CH₂-Ph-H*), 7.14-7.13 (9H, overlapping signals, *p-Ar-H* and *p-CH₂-Ph-H*), 5.15 (6H, s, *CH₂-Ph*), 5.07 (6H, s, *CH₂-Ph*), 4.66 (3H, d, *J* 15.3 Hz, C=O-*CHH-N*), 3.80 (3H, m, C=O-NH-*CHH*), 3.56 (3H, d, *J* 15.3 Hz, C=O-*CHH-N*), 3.26-3.19 (9H, overlapping m, C=O-NH-*CHH* and N-CH₂-CH₂-(CH₂)₂-CH₂-CH₂-NH), 1.47 (6H, m, N-CH₂-CH₂-(CH₂)₂-CH₂-CH₂-NH), 1.33-1.20 (18H, overlapping m, N-CH₂-CH₂-(CH₂)₂-CH₂-CH₂-NH). ¹³C-NMR (150 MHz, CDCl₃) δ: 167.0 x3 (C=O-N), 165.0 x3 (C=O-NH), 151.7 x3 (*m-C-OBn*), 146.8 x3 (*o-C-OBn*), 136.5 x6 (O-CH₂-C), 128.7 x15 (C-Ph), 127.7 x3 (C-Ph), 127.2 x12 (C-Ph), 124.4 x3 (*m-C-Ar*), 123.4 x3 (*o-C-Ar*), 117.0 x3 (*p-C-Ar*), 76.4 x3 (O-CH₂-Ph), 71.4 x3 (O-CH₂-Ph), 49.0 x3 (C=O-CH₂-N), 47.1 x3 (C=O-NH-CH₂), 39.4 x3 (C=O-N-CH₂), 29.1 x3 (N-CH₂-CH₂-(CH₂)₂-CH₂-CH₂-NH), 26.6 x3 (N-CH₂-CH₂-(CH₂)₂-CH₂-CH₂-NH), 26.4 x3 (N-CH₂-CH₂-(CH₂)₂-CH₂-CH₂-NH), 26.3 x3 (N-CH₂-CH₂-(CH₂)₂-CH₂-CH₂-NH). HRMS (MALDI-FTICR) *m/z*; [M + H]⁺ Calcd for C₈₇H₉₇N₆O₁₂⁺ 1417.7159; Found 1417.7190.

4.2.3.7 Catalytic hydrogenation procedure. Synthesis of the cyclic peptoids **147a-c**

To a solution of cyclic peptoids **154a-c** (0.0300 mmol), dissolved in ethyl acetate (0.430 mL), Pd 10% wt. on carbon was added (half of the weight respectively to the cyclic peptoid substrate). Three cycles of *vacuum*-hydrogen were performed, and the reaction was stirred for 5 hours. After 5 hours, 0.860 mL of ethanol were added, and three more *vacuum*-hydrogen cycles were performed. The reaction was stirred for additional 19 hours, then the completion of the reaction was assessed *via* TLC. The reaction mixture was filtered with ethanol through a Celite pad and extensively dried in *vacuo* to obtain the final products. The cyclic peptoids were dissolved in 50% acetonitrile in HPLC grade water and analysed by RP-HPLC; purity >90%; conditions: 5% – 100% A in 30 min (A, 0.1% TFA in acetonitrile, B, 0.1% TFA in water); flow: 1 mL min⁻¹, 220 nm; subsequently characterized *via* ¹H-, ¹³C-NMR and HRMS (MALDI-FTICR).

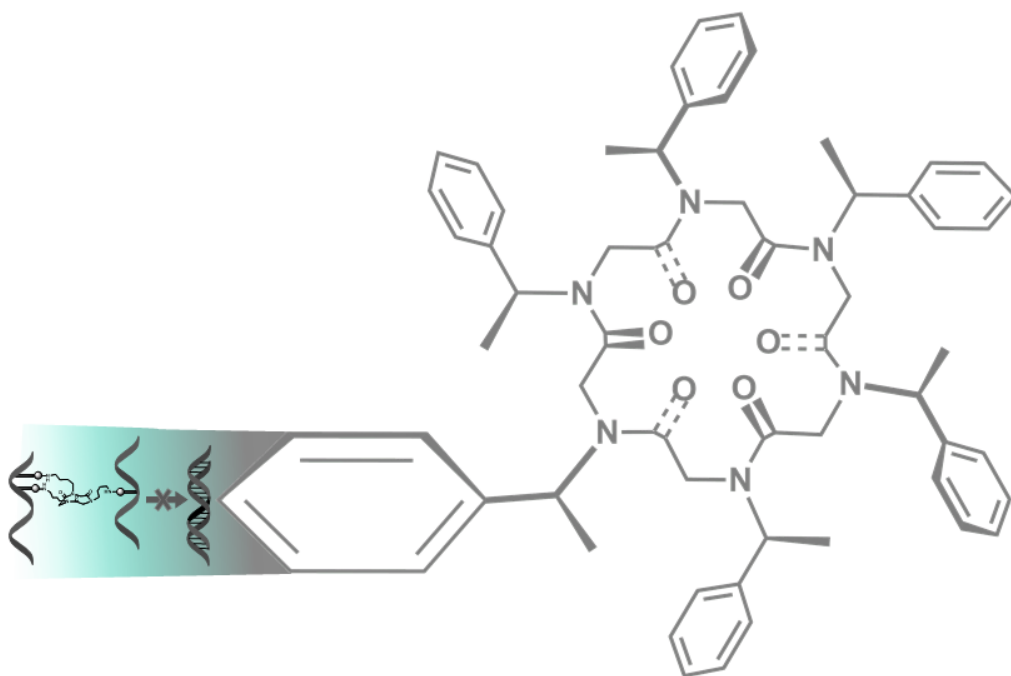
147a: white amorphous solid, 0.0210 g, 100%; *t_R*: 9.9 min. ¹H-NMR (600 MHz, CD₃OD) δ: 7.12 (3H, dd, *J* 8.2, 1.1 Hz, *o-Ar-H*), 6.90 (3H, dd, *J* 8.2, 1.1 Hz, *m-Ar-H*), 6.68 (3H, t, *J* 8.1 Hz, *p-Ar-H*), 5.13 (3H, d, *J* 15.8 Hz, C=O-*CHH-N*), 3.86 (3H, m, C=O-NH-*CHH*), 3.69

(3H, d, J 15.8 Hz, C=O-CHH-N), 3.61-3.57 (9H, overlapping m, C=O-NH-CHH and N-CH₂-CH₂-NH). ¹³C-NMR (150 MHz, CD₃OD) δ : 171.8 x3 (C=O-N), 170.7 x3 (C=O-NH), 150.4 x3 (*o*-C-OH), 147.3 x3 (*m*-C-OH), 119.7 x3 (*p*-C-Ar), 119.6 x3 (*m*-C-Ar), 118.7 x3 (*o*-C-Ar), 116.6 x3 (C=O-C-Ar), 51.0 x3 (C=O-CH₂-N), 48.3 x3 (C=O-NH-CH₂), 38.0 x3 (C=O-N-CH₂). HRMS (MALDI-FTICR) m/z ; [M + Na]⁺ Calcd for C₃₃H₃₆N₆NaO₁₂⁺ 731.2283; Found 731.2283.

147b: white amorphous solid, 0.0240 g, 100%; t_R : 11.5 min. ¹H-NMR (600 MHz, CD₃OD) δ : 7.21 (3H, dd, J 8.1, 1.1 Hz, *o*-Ar-*H*), 6.91 (3H, dd, J 8.1, 1.1 Hz, *m*-Ar-*H*), 6.70 (3H, t, J 8.0 Hz, *p*-Ar-*H*), 5.11 (3H, d, J 15.6 Hz, C=O-CHH-N), 3.65 (3H, m, C=O-NH-CHH), 3.62 (3H, d, J 15.6 Hz, C=O-CHH-N), 3.45-3.35 (9H, overlapping m, C=O-NH-CHH and N-CH₂-CH₂-CH₂-NH), 1.67-1.53 (12H, overlapping m, N-CH₂-CH₂-CH₂-CH₂-NH). ¹³C-NMR (150 MHz, CD₃OD) δ : 171.6 x3 (C=O-N), 170.1 x3 (C=O-NH), 150.3 x3 (*o*-C-OH), 147.3 x3 (*m*-C-OH), 119.6 x6 (*p*-C-Ar and *m*-C-Ar), 118.6 x3 (*o*-C-Ar), 116.8 x3 (C=O-C-Ar), 50.8 x3 (C=O-CH₂-N), 40.0 x3 (C=O-NH-CH₂), 27.6 x3 (C=O-N-CH₂), 25.1 x6 (N-CH₂-CH₂-CH₂-CH₂-NH). HRMS (MALDI-FTICR) m/z ; [M + H]⁺ Calcd for C₃₉H₄₉N₆O₁₂⁺ 793.3403; Found 793.3389.

147c: white amorphous solid, 0.0260 g, 100%; t_R : 14.0 min. ¹H-NMR (600 MHz, CD₃OD) δ : 7.21 (3H, d, J 7.8 Hz, *o*-Ar-*H*), 6.92 (3H, d, J 7.8 Hz, *m*-Ar-*H*), 6.70 (3H, t, J 7.8 Hz, *p*-Ar-*H*), 5.08 (3H, d, J 15.6 Hz, C=O-CHH-N), 3.65 (3H, m, C=O-NH-CHH), 3.58 (3H, d, J 15.6 Hz, C=O-CHH-N), 3.40-3.36 (9H, overlapping m, C=O-NH-CHH and N-CH₂-CH₂-(CH₂)₂-CH₂-CH₂-NH), 1.63-1.56 (12H, overlapping m, N-CH₂-CH₂-(CH₂)₂-CH₂-CH₂-NH and N-CH₂-CH₂-(CH₂)₂-CH₂-CH₂-NH), 1.42-1.29 (12H, overlapping m, N-CH₂-CH₂-(CH₂)₂-CH₂-CH₂-NH). ¹³C-NMR (150 MHz, CD₃OD) δ : 171.4 x3 (C=O-N), 170.1 x3 (C=O-NH), 150.3 x3 (*o*-C-OH), 147.3 x3 (*m*-C-OH), 119.6 x6 (*p*-C-Ar and *m*-C-Ar), 118.7 x3 (*o*-C-Ar), 116.9 x3 (C=O-C-Ar), 50.8 x3 (C=O-CH₂-N), 40.3 x3 (C=O-NH-CH₂), 30.2 x3 (C=O-N-CH₂), 27.6 x3 (N-CH₂-CH₂-(CH₂)₂-CH₂-CH₂-NH), 27.5 x3 (N-CH₂-CH₂-(CH₂)₂-CH₂-CH₂-NH), 27.4 x6 (N-CH₂-CH₂-(CH₂)₂-CH₂-CH₂-NH). HRMS (MALDI-FTICR) m/z ; [M + H]⁺ Calcd for C₄₅H₆₁N₆O₁₂⁺ 877.4342; Found 877.4353.

Chapter 5



5 Cyclic tripeptoids as mimics for natural DNA bis-intercalators

5.1 Introduction

5.1.1 Natural DNA bis-intercalators: a survey

Natural bis-intercalators constitute a vast class of secondary metabolites, produced by several fungi and bacteria strains, showing potent antitumor (and often antibacterial) activity. Echinomycin (**156**) was first isolated in 1957 from *Streptomyces echinatus* sp.;¹⁴⁶ this compound is constituted by a depsipeptide core, comprising four *N*-methylations and the presence of a dithiane bridge. Particularly, two residues of *N*-methyl-D-serine form an ester bond with Val, while their α -amino-groups are substituted, by means of an amide linkage, with 2-quinoxalinecarbonyl moieties.

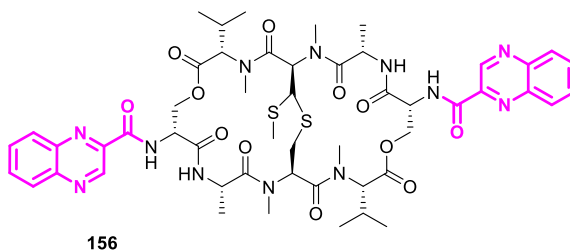


Figure 5.1. Echinomycin (**156**) schematic structure. Quinoxalinecarbonyl moieties depicted in magenta.

Quinomycins comprise a vast series of compounds, differentiated by dimension and monomers of the (bi)cyclic core; the two eteroaromatic units of quinoxaline-2-carboxylic acid constitute also triostins, isolated from S-2-210, a strain relative to *S. aureus*.^{147a} The aromatic unit is 3-hydroxyquinaldic acid for thiocoraline (**157**) and derivatives, sandramycins and quinaldopeptins; 6-methoxy-3-hydroxyquinaldic acid for the luzopeptins and 6-methoxyquinoxaline-2-carboxylic acid for the quinoxapeptins.^{147b,c}

¹⁴⁶ Yoshida T., Katagiri K., Yokozawa S., *J. Antibiot.* **1961**, *14*, 330-334.

¹⁴⁷ a) Dawson S., Malkinson J. P., Paumier D., Searcey M., *Nat. Prod. Rep.* **2007**, *24*, 109-126; b) Zolova O. E., Mady A. S. A., Garneau-Tsodikova S., *Biopolymers* **2010**, *93*, 9, 777-790; c) Fernández J., Marín L., Álvarez-Alonso R., Redondo S., Carvajal J., Villamizar G., Villar C. J., Lombó F., *Mar. Drugs* **2014**, *12*, 2668-2699.

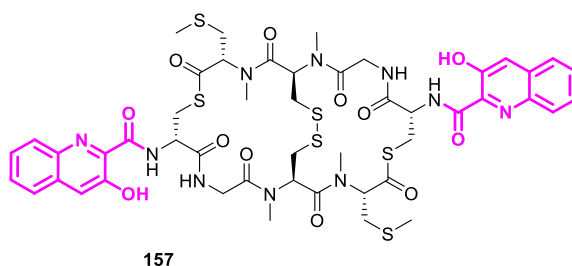


Figure 5.2. Thiocoraline (**157**) schematic structure. 3-Hydroxyquinaldoyl moieties depicted in magenta.

Structure elucidations evidenced the crucial role of *N*-methylation, the presence of a cyclic core, and the switch of amide linkages with ester or thioester; these features increase cell permeability and proteolytic resistance (*cf.* Paragraphs 1.1 and 1.2).¹⁵

It was proven, thanks to X-ray structures, theoretical studies and DNA footprinting, that the powerful action of these molecules is related to a phenomenon known as DNA bis-intercalation. DNA-drug interactions are classified in two main categories, covalent and non-covalent. Among the last ones, the three major modes are groove binding, electrostatic interactions and intercalative binding; often a combination of the last two is observed. Besides molecular docking, the main experimental techniques to study DNA-drug interactions are UV-Vis, fluorescence, and CD spectroscopy.¹⁴⁸

Intercalators bind DNA *via* insertion of a planar poly(hetero)aromatic unit between adjacent DNA base pairs; the main binding force is constituted by π stacking interactions between the polyaromatic unit of the dye and the heteroaromatic rings of the bases. This interaction can be co-adjuvated by ionic interactions, if the dye has a positively charged heteroatom (*i.e.* nitrogen), which interacts with the oxygen atom of the phosphodiester group of DNA.¹⁴⁹ The insertion of a portion of the intercalant into the major and/or the minor DNA groove enhances the binding, resulting in the so-called threaded intercalation (Figure 5.3 c)); the mode, kinetics and strength of the binding, determined by these factors, define the overall biological activity of the molecule.

¹⁴⁸ Rehman S. U., Sarwar T., Husain M. A., Ishqi H. M., Tabish M., *Arch. Biochem. Biophys.* **2015**, 576, 49-60.

¹⁴⁹ a) Nakamoto K., Tsuboi M., Strahan G. D., *Intercalating Drugs*, in: *Drug DNA Interactions*, John Wiley & Sons, **2008**, pp. 119-208; b) Strekowski L., Wilson B., *Mutat. Res.* **2007**, 623, 3-13.

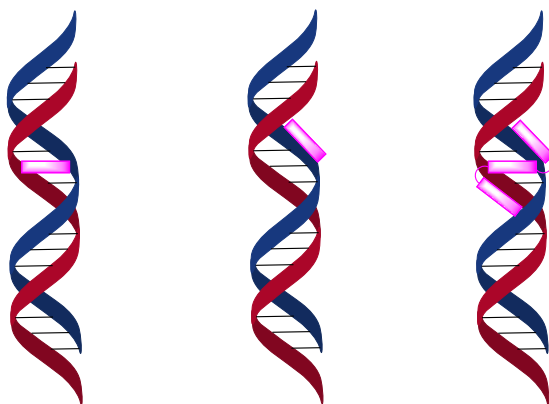


Figure 5.3. Pictorial representation of a) DNA intercalation; b) groove binding; c) threading intercalation. The intercalant is depicted in magenta.

The overall effect is a distortion of the typical DNA structure, which results in unwinding, stiffening, or lengthening of the DNA helix; in this way, DNA replication is interfered. DNA-targeted antitumor agents can display different sequence preferences, due to the binding mechanism; for example, echinomycin and thiocoraline bind selectively GC-rich sequences, while luzopeptin, sandramycins and triostins show preference for AT-rich sequences.^{147b} In any case, the natural bis-intercalator acts like a clamp, sandwiching the two polyaromatic units between the nucleotides; at the same time, the cyclic (depsi)peptide core is disposed parallel to the two DNA strands, interposed between the two (Figure 5.4).

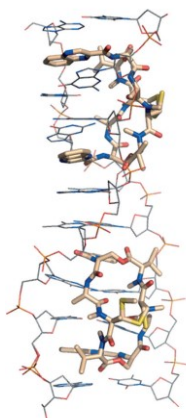


Figure 5.4. Stereomage of the co-crystal structure (PDB code: 3GO3)¹⁵⁰ of echinomycin (sticks) bound to a DNA d(ACGTACGT) duplex (lines).¹⁵

¹⁵⁰ Pfoh R., Cuesta-Seijo J. A., Sheldrick G. M., *Acta Cryst. F* **2009**, 65, 660-664.

The synthetic reproduction of such natural effectors, or their artificial analogues, proved to be quite challenging,¹⁴⁷ thus recent developments focus on the preparation of small organic DNA (bis)intercalators.

Classic intercalators include a polyaromatic unit with a positively charged heteroatom, typically a nitrogen, as in proflavin chloride (**158**) or ethidium bromide (**159**). If the molecule includes a bulky substituent, this can be located in the major or the minor groove of the DNA (*i.e.* **160** or **161**, ditercalinium), resulting in a threaded intercalation.

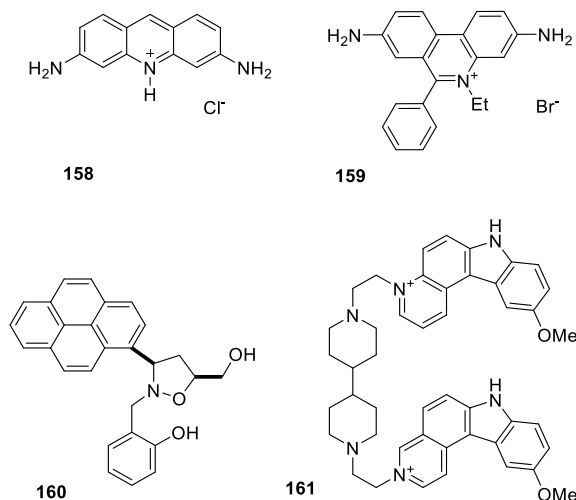


Figure 5.5. Classical DNA intercalants (**158**, **159**) and threading intercalants (**160**, **161**).

These molecules display strong cytotoxic activity against various human cancer cell lines; the binding extent is often evaluated *via* UV-Vis spectroscopy and, as expected, bis-intercalators display higher binding constants as well as a slower dissociation kinetics of the DNA complex.¹⁵¹

There are a few examples in the literature of intercalators bound to peptidomimetics; as mentioned, the auxiliary moiety increases the bioavailability as well as the proteolytic resistance, resulting in an overall enhanced activity. Quinoline linked triazole peptidomimetics (Figure 5.6, **162**), easily synthesized *via* click-chemistry, showed increased intercalating potential.

¹⁵¹ Rescifina A., Zagni C., Varrica M. G., Pistarà V., Corsaro A., *Eur. J. Med. Chem.* **2014**, *74*, 95-115.

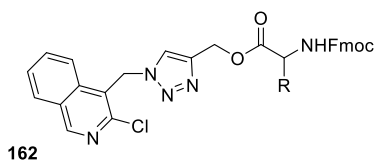


Figure 5.6. Quinoline linked triazole peptidomimetic **162**.

Besides efficiently bind DNA, compound **162** was able to cleave supercoiled DNA after only 1-2 hours, in a concentration dependent fashion.¹⁵² A small oligopeptide can also be conjugated to the intercalator component, by means of a bifunctional linker, retaining the DNA binding affinity while increasing the pharmacokinetic properties.¹⁵³

5.1.2 Purpose of the research

Considering the limited examples in the literature of peptidomimetic-intercalator conjugates, in this study we exploited a cyclotripeptoid framework as scaffold for the design of novel peptidomimetic-intercalant effectors. Particularly, we introduced five different polyaromatic units, and investigated both the length of the lateral spacer and the presence of a free primary amine moiety. The synthetic pathway and the conformational properties of these molecules will be discussed, as we aim to introduce them as cytotoxic agents against human cancer cell lines.

¹⁵² Aravinda T., Bhojya Naik H. S., Prakash Naik H. R., *Int. J. Pept. Res. Ther.* **2009**, *15*, 273-279.

¹⁵³ Howell L. A., Gulam R., Mueller A., O'Connell M. A., Searcey M., *Bioorg. Med. Chem. Lett.* **2010**, *20*, 6956-6959.

5.2 Results and discussion

5.2.1 Synthesis of the first generation of DNA-intercalators

The design of our cyclotripeptoids was meant to investigate the effect on the biological activity of a series of parameters; we devised a lead compound, **163**, whose cyclic scaffold was decorated with a tetramethylene spacer and three quinaldoyl moieties, known in the literature as strongly interacting with DNA bases (*cf.* Paragraph 5.1.1). Two polyaromatic units are sufficient to obtain bis-intercalation; however, we aimed to generate a statistic increase of the non-covalent interactions (*i.e.* a multivalent effect) with the addition of a third polyheteroaromatic unit.

As modification of such molecule, we designed **164**, bearing two intercalating functionalities, plus a free primary amine, as it is known that a synergic interaction between a positively charged nitrogen atom and the phosphodiester group of the nucleoside can enhance the binding activity.

Lastly, we sought to determine the impact of the spacer on the overall efficiency; a longer spacer (*i.e.* hexamethylene, compound **165**) could improve the conformational mobility and the steric availability of the intercalating units. As negative control, we also prepared chloride salt **166**, bearing three free ammonium groups, necessary for the following evaluation of the cytotoxic activities.

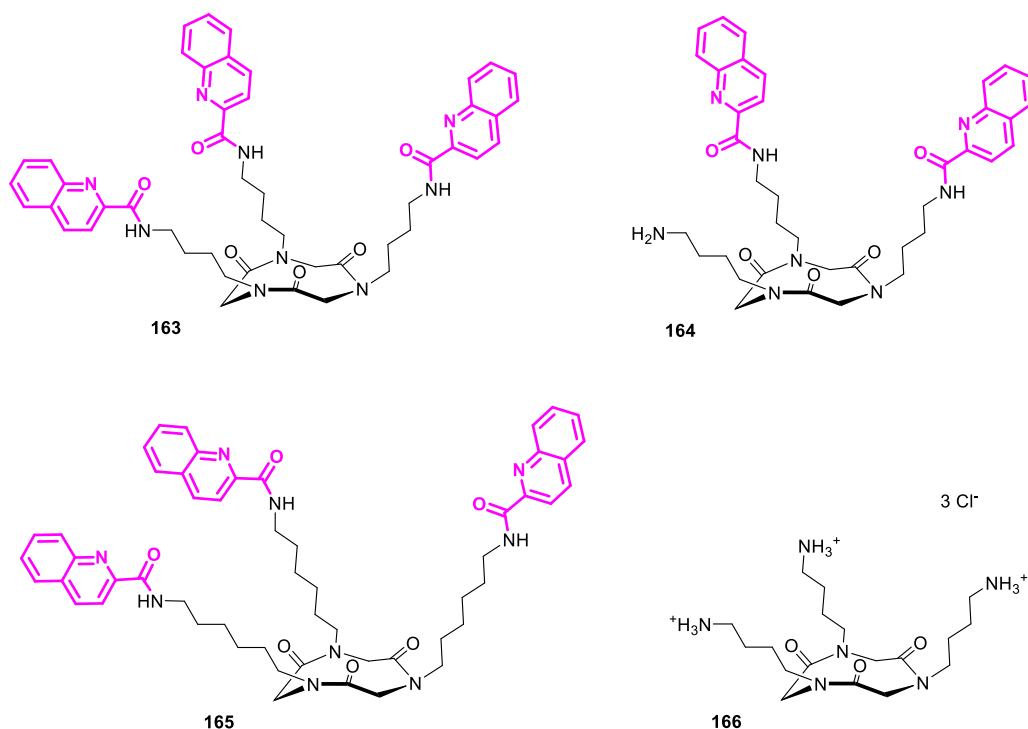
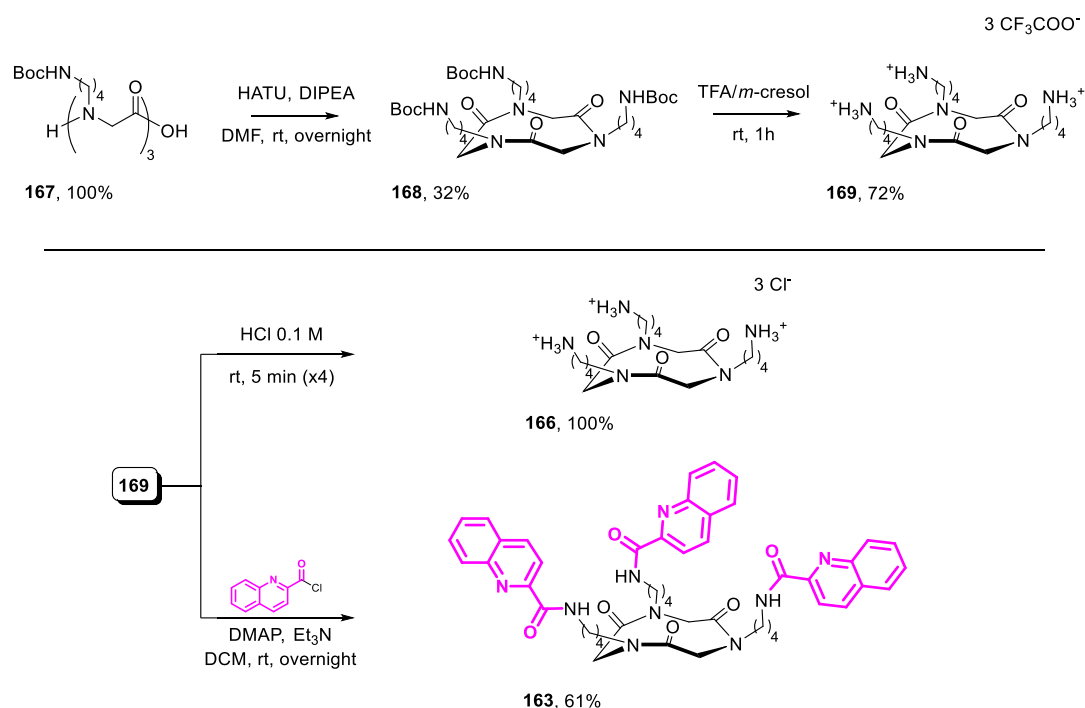


Figure 5.7. First generation of intercalating cyclotripeptides. Intercalating quinaldoyl units depicted in magenta.

Lead compound **163** and the derivative **166** were conveniently obtained from the same peptoid precursor; the sub-monomeric oligomerization, using commercially available *N*-Boc-1,4-butanediamine, led to trimeric **167** in good yield. This was subjected to the cyclization reaction with our standard procedure, and lastly to Boc-deprotection to afford the triple trifluoroacetate ammonium salt **169**.³⁵

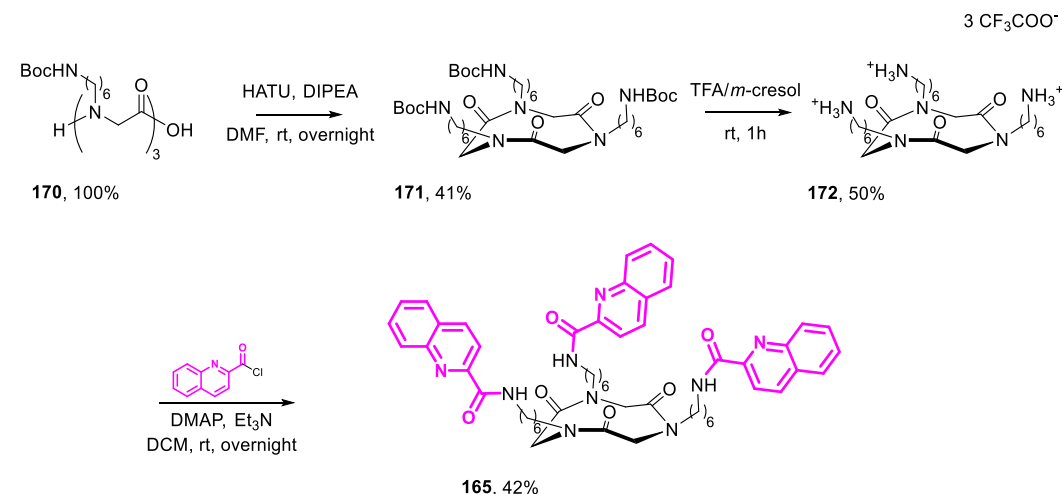
This intermediate was treated with 0.1 M HCl to afford the chloride salt **166**;¹⁵⁴ the same **169** was coupled with quinaldoyl chloride under standard amidation conditions to gain final product **163**.¹⁵³

¹⁵⁴ Sikora K., Neubauer D., Jaśkiewicz M., Kamysz W., *Int. J. Pept. Res. Ther.* **2018**, *24*, 265-270.



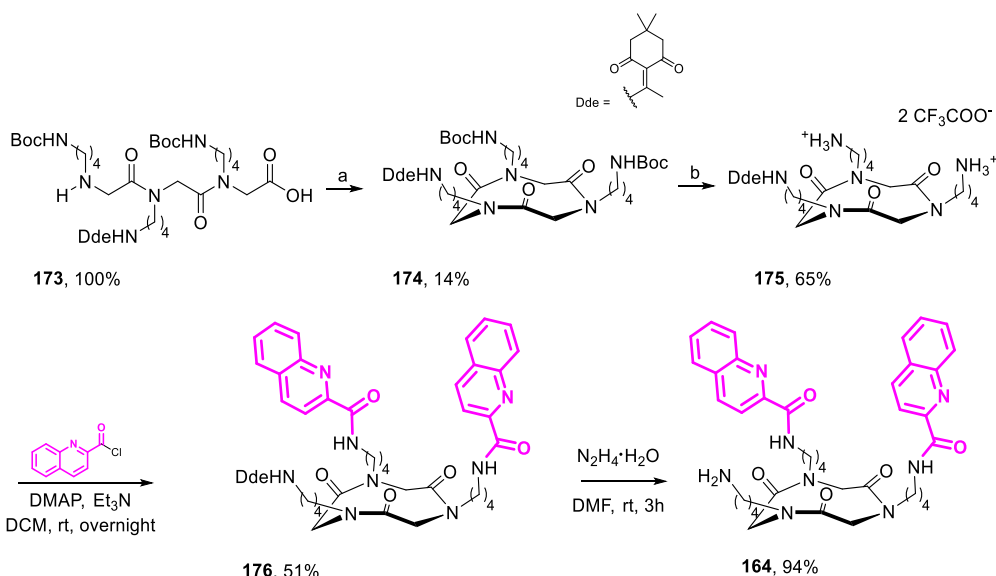
Scheme 5.1. Synthesis of cyclotripeptides **163** and **166**. Quinaldoyl moieties depicted in magenta.

Derivative **165**, comprising an hexamethylene spacer, was prepared following the same reactions pattern of **163**, starting with commercially available *N*-Boc-1,6-hexanediamine (Scheme 5.2). Both the cyclotripeptides showed a rigid “crown” all-*cis* conformation in the solution state (¹H-NMR analysis).



Scheme 5.2. Synthesis of cyclotripeptide **165**. Quinaldoyl moieties depicted in magenta.

Lastly, cyclotripeptoid **164** was prepared exploiting orthogonal protection of the three amine groups; the linear oligomer (**173**, Scheme 5.3) was prepared using two residues of *N*-Boc-1,4-butanediamine and one residue of 1,4-butanediamine, conveniently protected on-bead at the peripheral moiety using 2-Acetyl-5,5-dimethyl-1,3-cyclohexanedione (Dde).¹⁵⁵ This protecting group can be removed on-bead or in solution using hydrazine, and is stable under basic or acidic conditions. The head-to-tail coupling of **173** led to the cyclic analogue **174**, which was selectively Boc-deprotected to obtain two free amine moieties, subsequently coupled with quinaldoyl chloride using the standard procedure. Finally, the intermediate was deprotected by Dde to free the third amine group.



Scheme 5.3. Synthesis of cyclotripeptoid **164**. Quinaldoyl moieties depicted in magenta. Reagents and conditions: a) HATU, DIPEA, DMF, rt, overnight; b) TFA/*m*-cresol, rt, 1h.

5.2.2 Synthesis of the second generation of DNA-intercalators

Starting from lead compound **163**, we prepared a second generation of intercalators, this time focusing on the poly(hetero)aromatic unit rather than the length of the methylene spacer or the substitution at the amine moiety.

Taking account of the dye molecules incorporated in natural effectors or synthetic intercalators reported in the literature (*cf.* Paragraph 5.1.1 and references cited therein), we prepared four novel cyclotripeptoids, reported in Figure 5.8.

¹⁵⁵ Bolt H. L., Cobb S. L., *Org. Biomol. Chem.* **2016**, *14*, 1211-1215.

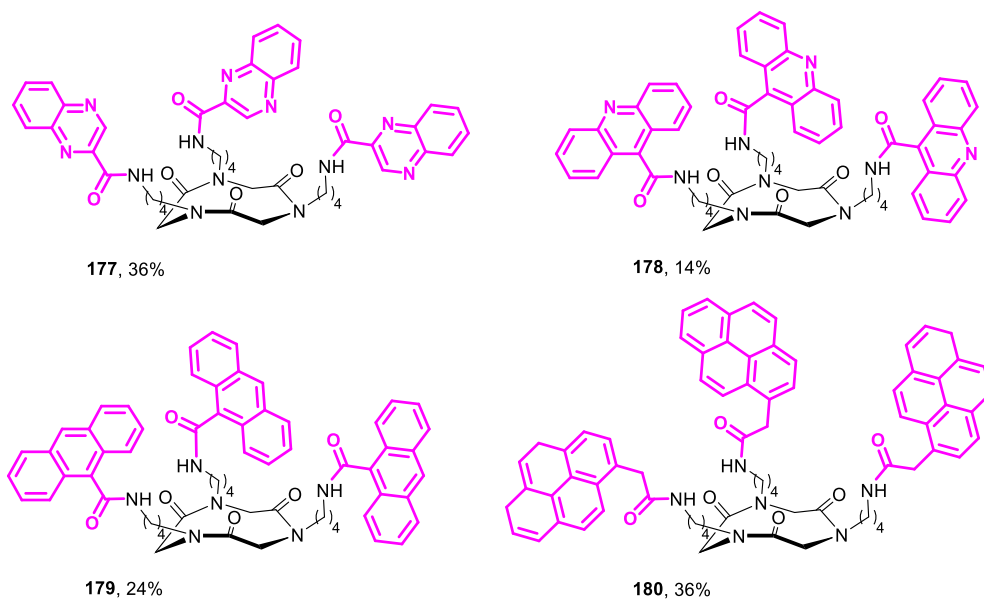
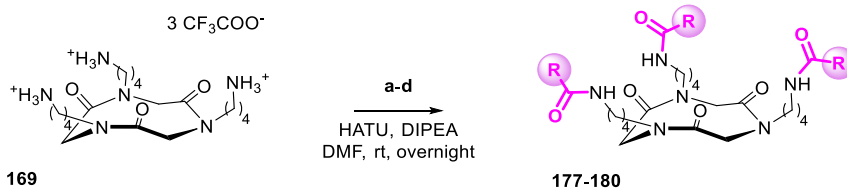


Figure 5.8. Second generation of intercalating cyclotripeptides. Intercalating units depicted in magenta.

The syntheses were conveniently performed starting from triple trifluoroacetate salt **169**, which was coupled with the commercially available polyaromatic carboxylic acids under standard amidation conditions (Scheme 5.4), leading to further four all-*cis* “crown” cyclotripeptides with intercalative pending moieties.¹⁵⁶



Scheme 5.4. Synthesis of cyclotripeptides **177-180**. Intercalating moieties depicted in bold magenta. Reagents: a) 2-quinoxalinecarboxylic acid; b) 9-acridinecarboxylic acid; c) 9-anthracenecarboxylic acid; d) 1-pyreneacetic acid.

5.2.3 Conclusions

In this study, we prepared a small library of cyclic tripeptides, functionalized with poly(hetero)aromatic moieties, potentially able to intercalate or bis-intercalate DNA. These compounds will be tested for cytotoxic activity against human cancer cell lines, in order to assess their biological activity.

¹⁵⁶ Graffion J., Dems D., Demirelli M., Coradin T., Delsuc N., Aimé C., *Eur. J. Inorg. Chem.* **2017**, 5047-5051.

5.2.4 Experimental section

5.2.4.1 General methods

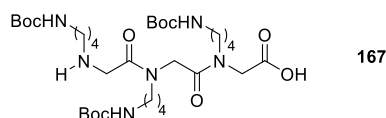
Refer to Paragraph 2.2.3.1.

Additional NMR solvent used in this work: CD₂HOD, δ = 3.31; ¹³CD₃OD, δ = 49.00.

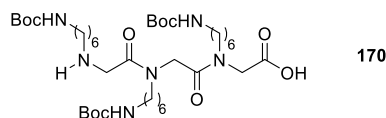
5.2.4.2 Synthesis of the linear peptoids **167**, **170**, **173**

*Synthesis of linear oligomers **167** and **170***

Refer to Paragraph 2.2.3.2. The synthesis was performed exploiting the sub-monomer protocol, on a 0.300 g 2-chlorotrytil chloride resin batch (1.47 mmol g⁻¹), using commercially available *N*-Boc-1,4-butanediamine or *N*-Boc-1,6-hexanediamine. Each elongation was performed using a solution of the chosen amine (1.6 M in dry DMF), added to the bromoacetylated resin for 30 min at room temperature. Purity of the linear oligomers >80%.



167: white amorphous solid, 0.310 g, 100%; t_R : 8.3 min. HRMS (MALDI-FTICR) m/z ; [M + H]⁺ Calcd for C₃₃H₆₃N₆O₁₀⁺ 703.4600; Found 703.4597.

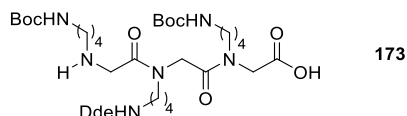


170: white amorphous solid, 0.347 g, 100%; t_R : 9.7 min. HRMS (MALDI-FTICR) m/z ; [M + H]⁺ Calcd for C₃₉H₇₅N₆O₁₀⁺ 787.5539; Found 787.5560.

*Synthesis of linear oligomer **173***

Refer to Paragraph 2.2.3.2. The synthesis was performed exploiting the sub-monomer protocol, on a 0.300 g 2-chlorotrytil chloride resin batch (1.47 mmol g⁻¹), using commercially available *N*-Boc-1,4-butanediamine for the first and the third monomer. As for the second monomer, after the bromoacetylation, performed according to the usual procedure, a 1.6 M solution of 1,4-diaminobutane in dry DMF was added to the resin for 30 minutes, after which the resin was filtered and washed in the usual manner. At this point, a solution of 2-(1-Hydroxyethylidene)-5,5-dimethylcyclohexane-1,3-dione in dry DMF (1.6 M) was added for additional 60 minutes, after which the reactive solution was

filtered away and the resin washed. The synthesis was then completed according to the described protocol, and the linear trimer was finally detached from the resin. Purity of the linear oligomer >80%.



173: white amorphous solid, 0.338 g, 100%; t_R : 10.7 min. HRMS (MALDI-FTICR) m/z ; $[M + H]^+$ Calcd for $C_{38}H_{67}N_6O_{10}^+$ 767.4913; Found 767.4901.

5.2.4.3 Synthesis of the cyclic peptoids **168**, **171**, **174**

Refer to Paragraph 2.2.3.3.

The cyclization reaction was performed on a 0.300 mmol scale of the linear oligomers, which were dissolved in 15.0 mL of dry DMF and added by a syringe pump in 6 hours to the reaction mixture. The crude cyclic peptoids were purified on flash silica gel; conditions: 20:80 petroleum ether:ethyl acetate, to 50:50 ethyl acetate:methanol. The cyclic peptoids were dissolved in 50% acetonitrile in HPLC grade water and analysed by RP-HPLC; purity >90%; conditions: 5% – 100% A in 30 min (A, 0.1% TFA in acetonitrile, B, 0.1% TFA in water); flow: 1 mL min^{-1} , 220 nm; subsequently characterized *via* NMR, HPLC and HRMS (MALDI-FTICR).

168: white amorphous solid, 0.0660 g, 32%; t_R : 10.8 min. $^1\text{H-NMR}$ (400 MHz, CDCl_3) δ : 4.73 (3H, d, J 15.2 Hz, C=O-CHH-N), 3.79 (3H, m, C=O-NH-CHH), 3.68 (3H, d, J 15.2 Hz, C=O-CHH-N), 3.37 (3H, m, C=O-NH-CHH), 3.12 (6H, m, N-CH₂-CH₂-CH₂-CH₂-NH), 1.56 (6H, m, N-CH₂-CH₂-CH₂-CH₂-NH), 1.48-1.44 (33H, overlapping signals, N-CH₂-CH₂-CH₂-CH₂-NH and C=O-O-(CH₃)₃). HRMS (MALDI-FTICR) m/z ; $[M + H]^+$ Calcd for $C_{33}H_{61}N_6O_9^+$ 685.4495; Found 685.4490.

171: white amorphous solid, 0.0950 g, 41%; t_R : 12.7 min. $^1\text{H-NMR}$ (400 MHz, CDCl_3) δ : 4.75 (3H, d, J 15.3 Hz, C=O-CHH-N), 3.80 (3H, m, C=O-NH-CHH), 3.70 (3H, d, J 15.3 Hz, C=O-CHH-N), 3.29 (3H, m, C=O-NH-CHH), 3.07 (6H, m, N-CH₂-CH₂-CH₂-CH₂-CH₂-CH₂-NH), 1.55 (6H, m, N-CH₂-CH₂-CH₂-CH₂-CH₂-CH₂-NH), 1.44 (27H, br s, C=O-O-(CH₃)₃), 1.34-2.25 (18H, overlapping m, N-CH₂-CH₂-CH₂-CH₂-CH₂-CH₂-NH). HRMS (MALDI-FTICR) m/z ; $[M + H]^+$ Calcd for $C_{39}H_{73}N_6O_9^+$ 769.5434; Found 769.5460.

174: white amorphous solid, 0.0310 g, 14%; t_R : 13.0 min. $^1\text{H-NMR}$ (400 MHz, CDCl_3) δ : 4.73 (3H, d, J 15.2 Hz, C=O-CHH-N), 3.79 (3H, m, C=O-NH-CHH), 3.66 (3H, d, J 15.2 Hz,

C=O-CHH-N), 3.34 (3H, m, C=O-NH-CHH), 3.12 (6H, m, N-CH₂-CH₂-CH₂-CH₂-NH), 2.54 (3H, s, NH-C-CH₃), 2.35 (4H, s, C=C-CH₂), 1.66 (6H, m, N-CH₂-CH₂-CH₂-CH₂-NH), 1.58 (6H, m, N-CH₂-CH₂-CH₂-CH₂-NH), 1.48-1.44 (24H, overlapping s, C-(CH₃)₂ and C=O-O-(CH₃)₃). HRMS (MALDI-FTICR) *m/z*; [M + H]⁺ Calcd for C₃₈H₆₅N₆O₉⁺ 749.4808; Found 749.4791.

5.2.4.4 *t*-Butoxycarbonyl deprotection procedure. Synthesis of the cyclic peptoids, trifluoroacetate salts **169**, **172**, **175**

The *N*-Boc protected cyclic tripeptoids **168**, **171**, **174** (0.0300 mmol) were dissolved in a solution of trifluoroacetic acid/*m*-cresol (95% v/v, 0.750 mL), added dropwise. The reaction mixture was stirred at room temperature for 1 hour, then the solution was then concentrated *in vacuo* and the crude oil dissolved in 0.5 mL of hot ethanol and added dropwise to 15.0 mL of a cold 50/50 solution of diethyl ether/petroleum ether to induce the precipitation of the trifluoroacetate salt.

169, TFA salt: white amorphous solid, 0.0160 g, 72%; *t_R*: 3.5 min. ¹H-NMR (600 MHz, CD₃OD) δ: 7.86 (3H, br s, NH₃⁺), 5.26 (3H, d, *J* 15.6 Hz, C=O-CHH-N), 3.75 (3H, m, CHH-NH₃⁺), 3.66 (3H, d, *J* 15.6 Hz, C=O-CHH-N), 3.37 (3H, m, CHH-NH₃⁺), 2.97 (12H, overlapping m, N-CH₂-CH₂-CH₂-CH₂-NH₃⁺ and N-CH₂-CH₂-CH₂-CH₂-NH₃⁺), 1.76-1.65 (6H, overlapping signals, N-CH₂-CH₂-CH₂-CH₂-NH₃⁺). HRMS (MALDI-FTICR) *m/z*; [M + H]⁺ Calcd for C₁₈H₃₇N₆O₃⁺ 385.2922; Found 385.2911.

172, TFA salt: white amorphous solid, 0.0120 g, 50%; *t_R*: 4.1 min. ¹H-NMR (400 MHz, CD₃OD) δ: 7.87 (3H, br s, NH₃⁺), 5.15 (3H, d, *J* 15.5 Hz, C=O-CHH-N), 3.70 (3H, m, CHH-NH₃⁺), 3.62 (3H, d, *J* 15.5 Hz, C=O-CHH-N), 3.35 (3H, m, CHH-NH₃⁺), 2.92 (6H, t, *J* 7.1 Hz, N-CH₂-CH₂-CH₂-CH₂-CH₂-CH₂-NH₃⁺), 1.64 (6H, m, N-CH₂-CH₂-CH₂-CH₂-CH₂-CH₂-NH₃⁺), 1.43-1.31 (18H, overlapping m, N-CH₂-CH₂-CH₂-CH₂-CH₂-CH₂-NH₃⁺). HRMS (MALDI-FTICR) *m/z*; [M + H]⁺ Calcd for C₂₄H₄₉N₆O₃⁺ 469.3861; Found 469.3849.

175: white amorphous solid, 0.0150 g, 65%; *t_R*: 5.8 min. ¹H-NMR (400 MHz, CD₃OD) δ: 5.17 (3H, d, *J* 15.7 Hz, C=O-CHH-N), 3.72 (2H, m, CHH-NH₃⁺), 3.65 (3H, d, *J* 15.7 Hz, C=O-CHH-N), 3.53 (2H, t, *J* 5.4 Hz, CH₂-NH), 3.40 (2H, m, CHH-NH₃⁺), 2.96 (6H, br t, N-CH₂), 2.56 (3H, s, NH-C-CH₃), 2.37 (4H, s, C=C-CH₂), 1.73-1.61 (18H, overlapping signals, C-(CH₃)₂ and N-CH₂-CH₂-CH₂). HRMS (MALDI-FTICR) *m/z*; [M + H]⁺ Calcd for C₂₈H₄₉N₆O₅⁺ 549.3759; Found 549.3770.

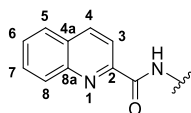
5.2.4.5 Anion exchange procedure. Synthesis of the cyclic peptoid, chloride salt **166**

Cyclic derivative **169** (0.0160 g, 0.0220 mmol) was agitated for five minutes with 0.1 M HCl (1.10 mL). The resulting solution was then lyophilised; this process was repeated four times. The resulting solid was dried extensively *in vacuo* to obtain the chloride salt.

166, chloride salt: white amorphous solid, 0.0110 g, 100%; t_R : 3.5 min. $^1\text{H-NMR}$ (600 MHz, CD_3OD) δ : 7.86 (3H, br s, NH_3^+), 5.26 (3H, d, J 15.6 Hz, C=O-CHH-N), 3.75 (3H, m, CHH- NH_3^+), 3.66 (3H, d, J 15.6 Hz, C=O-CHH-N), 3.37 (3H, m, CHH- NH_3^+), 2.97 (12H, overlapping m, N- CH_2 - CH_2 - CH_2 - CH_2 - NH_3^+ and N- CH_2 - CH_2 -CH₂- CH_2 - NH_3^+), 1.76-1.65 (6H, overlapping signals, N- CH_2 -CH₂- CH_2 - CH_2 - NH_3^+). $^{13}\text{C-NMR}$ (150 MHz, CD_3OD) δ : 170.3 x3 (C=O-N), 50.6 x3 (C=O- CH_2 -N), 47.8 x3 (NH_3^+ - CH_2), 40.3 x3 (C=O-N- CH_2), 25.7 x3 (CH_2 - CH_2 - NH_3^+), 24.5 x3 (N- CH_2 - CH_2). HRMS (MALDI-FTICR) m/z ; $[\text{M} + \text{H}]^+$ Calcd for $\text{C}_{18}\text{H}_{37}\text{N}_6\text{O}_3^+$ 385.2922; Found 385.2936.

5.2.4.6 General procedure for the acylation with quinaldoyl chloride. Synthesis of cyclic peptoids **163**, **165**, **176**

The cyclic peptoid (**169**, **172** or **175**) (0.0150 mmol) was dissolved in dry dichloromethane (0.400 mL), under nitrogen atmosphere; a catalytic amount (5% mol) of DMAP and triethylamine (0.0190 mL, 0.135 mmol) were added. Quinaldoyl chloride (0.0170 g, 0.090 mmol) was weighed under nitrogen atmosphere and dissolved in further 0.400 mL of dry dichloromethane. The acyl chloride solution was added dropwise, under stirring, to the cyclopeptoid solution. The mixture was stirred for 24 hours, then quenched with 5.00 mL of H_2O . The organic phase was diluted with DCM to 20.0 mL total, then subsequently extracted with 5.00 mL of 1 M HCl and 10.0 mL of sat. aq. Na_2CO_3 . The organic phase was dried over anhydrous MgSO_4 and the solvent was evaporated to gain the crude products. The crude cyclic peptoids were purified on flash silica gel; conditions: 20:80 petroleum ether:ethyl acetate, to 70:30 ethyl acetate:methanol. The cyclic peptoids were dissolved in 50% acetonitrile in HPLC grade water and analysed by RP-HPLC; purity >90%; conditions: 5% – 100% A in 30 min (A, 0.1% TFA in acetonitrile, B, 0.1% TFA in water); flow: 1 mL min^{-1} , 220 nm; subsequently characterized *via* NMR, HPLC and HRMS (MALDI-FTICR).



163: white amorphous solid, 0.0080 g, 61%; t_R : 13.6 min. $^1\text{H-NMR}$ (600 MHz, CDCl_3) δ : 8.32 (3H, t, J 5.7 Hz, NH), 8.28 (6H, s, H -5 and H -8), 8.10 (3H, d, J 8.3 Hz, H -4), 7.85 (3H, dd, J 8.3, 0.8 Hz, H -3), 7.74 (3H, ddd, J 8.7, 7.0, 1.4 Hz, H -7), 7.59 (3H, ddd, J 8.7, 7.0, 1.4 Hz, H -6), 4.74 (3H, d, J 15.3 Hz, C=O-CHH-N), 3.88 (3H, m, C=O-NH-CHH), 3.68 (3H, d, J 15.3 Hz, C=O-CHH-N), 3.53 (6H, m, N-CH₂-CH₂-CH₂-CH₂-NH), 3.39 (3H, m, C=O-NH-CHH), 1.70-1.63 (12H, m, N-CH₂-CH₂-CH₂-CH₂-NH). $^{13}\text{C-NMR}$ (150 MHz, CDCl_3) δ : 167.1 x3 (N-C=O), 164.6 x3 (NH-C=O), 149.8 x3 (C-2), 146.5 x3 (C-8a), 137.4 x3 (C-8), 130.0 x3 (C-7), 129.7 x3 (C-4), 129.3 x3 (C-4a), 127.8 x3 (C-6), 127.7 x3 (C-3), 118.8 x3 (C-5), 49.2 x3 (C=O-CH₂), 47.0 x3 (N-CH₂-CH₂-CH₂-CH₂-NH), 39.2 x3 (N-CH₂-CH₂-CH₂-CH₂-NH), 27.1 x3 (N-CH₂-CH₂-CH₂-CH₂-NH), 24.2 x3 (N-CH₂-CH₂-CH₂-CH₂-NH). HRMS (MALDI-FTICR) m/z ; $[\text{M} + \text{H}]^+$ Calcd for $\text{C}_{48}\text{H}_{52}\text{N}_9\text{O}_6^+$ 850.4035; Found 850.4033.

165: white amorphous solid, 0.0060 g, 42%; t_R : 15.2 min. $^1\text{H-NMR}$ (600 MHz, CDCl_3) δ : 8.29 (6H, s, H -5 and H -8), 8.28 (3H, br t, NH), 8.11 (3H, d, J 8.3 Hz, H -4), 7.86 (3H, dd, J 8.3, 0.9 Hz, H -3), 7.75 (3H, ddd, J 8.8, 6.8, 1.4 Hz, H -7), 7.60 (3H, ddd, J 8.8, 6.8, 1.4 Hz, H -6), 4.73 (3H, d, J 15.3 Hz, C=O-CHH-N), 3.82 (3H, m, C=O-NH-CHH), 3.64 (3H, d, J 15.3 Hz, C=O-CHH-N), 3.50 (6H, m, N-CH₂-CH₂-CH₂-CH₂-CH₂-NH), 3.31 (3H, m, C=O-NH-CHH), 1.68 (6H, m, N-CH₂-CH₂-CH₂-CH₂-CH₂-NH), 1.58 (6H, m, N-CH₂-CH₂-CH₂-CH₂-CH₂-NH), 1.44 (6H, m, N-CH₂-CH₂-CH₂-CH₂-CH₂-NH), 1.35 (6H, m, N-CH₂-CH₂-CH₂-CH₂-CH₂-NH). $^{13}\text{C-NMR}$ (150 MHz, CDCl_3) δ : 166.9 x3 (N-C=O), 164.4 x3 (NH-C=O), 149.9 x3 (C-2), 146.5 x3 (C-8a), 137.4 x3 (C-8), 130.0 x3 (C-7), 129.6 x3 (C-4), 129.3 x3 (C-4a), 127.8 x3 (C-6), 127.7 x3 (C-3), 118.8 x3 (C-5), 49.2 x3 (C=O-CH₂), 47.3 x3 (N-CH₂-CH₂-CH₂-CH₂-CH₂-NH), 39.4 x3 (N-CH₂-CH₂-CH₂-CH₂-CH₂-NH), 29.6 x3 (N-CH₂-CH₂-CH₂-CH₂-CH₂-NH), 26.6 x3 (N-CH₂-CH₂-CH₂-CH₂-CH₂-NH), 26.5 x3 (N-CH₂-CH₂-CH₂-CH₂-CH₂-NH), 26.4 x3 (N-CH₂-CH₂-CH₂-CH₂-CH₂-NH). HRMS (MALDI-FTICR) m/z ; $[\text{M} + \text{H}]^+$ Calcd for $\text{C}_{54}\text{H}_{64}\text{N}_9\text{O}_6^+$ 934.4974; Found 934.4976.

176: white amorphous solid, 0.0060 g, 51%; t_R : 14.8 min. $^1\text{H-NMR}$ (400 MHz, CDCl_3) δ : 8.34 (2H, br t, C=O-NH), 8.28 (4H, s, H -5 and H -8), 8.09 (2H, d, J 8.4 Hz, H -4), 7.86 (2H, d, J 8.4 Hz, H -3), 7.75 (2H, t, J 7.4 Hz, H -7), 7.60 (2H, t, J 7.4 Hz, H -6), 4.75 (3H, d, J 16.0 Hz, C=O-CHH-N), 3.88 (3H, m, C=O-NH-CHH), 3.68 (3H, d, J 16.0 Hz, C=O-CHH-N), 3.54 (3H, br m, C=O-NH-CHH), 3.37 (6H, m, N-CH₂-CH₂-CH₂-CH₂-NH), 2.51 (3H, s, NH-C-CH₃), 2.33

(4H, s, C=C-CH₂), 1.68-1.61 (12H, overlapping signals, N-CH₂-CH₂-CH₂-CH₂-NH), 1.00 (6H, s, C-(CH₃)₂). HRMS (MALDI-FTICR) *m/z*; [M + H]⁺ Calcd for C₄₈H₅₉N₈O₇⁺ 859.4501; Found 859.4530.

5.2.4.7 Dde deprotection procedure. Synthesis of the cyclic peptoid **164**

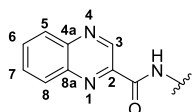
Cyclic derivative **176** (0.0060 g, 0.0080 mmol) was dissolved in 2.0 mL of dry DMF; hydrazine monohydrate (0.24 mL, 12% v/v) was added and the mixture was stirred for 3 hours. The solution was then concentrated *in vacuo* and the crude oil dissolved in 0.50 mL of hot ethanol and added dropwise to 15 mL of a cold 50/50 solution of diethyl ether/petroleum ether to induce the precipitation of the product.

164: white amorphous solid, 0.0050 g, 94%; *t_R*: 12.6 min. ¹H-NMR (600 MHz, CD₃OD) δ: 8.45 (2H, d, *J* 8.4 Hz, *H*-8), 8.18-8.15 (4H, overlapping signals, *H*-4 and *H*-5), 7.96 (2H, d, *J* 8.0 Hz, *H*-3), 7.81 (2H, t, *J* 7.5 Hz, *H*-7), 7.64 (2H, t, *J* 7.5 Hz, *H*-6), 5.15 (3H, d, *J* 15.7 Hz, C=O-CHH-N), 3.64 (3H, d, *J* 15.7 Hz, C=O-CHH-N), 3.54 (6H, m, N-CH₂-CH₂-CH₂-CH₂-NH), 3.19 (3H, br m, C=O-NH-CHH), 2.94 (3H, br m, C=O-NH-CHH), 1.64-1.56 (6H, m, N-CH₂-CH₂-CH₂-CH₂-NH), 1.33-1.30 (6H, m, N-CH₂-CH₂-CH₂-CH₂-NH). ¹³C-NMR (150 MHz, CD₃OD) δ: 170.1 x3 (N-C=O), 166.8.6 x2 (NH-C=O), 151.1 x2 (C-2), 148.0 x2 (C-8a), 138.9 x2 (C-8), 131.5 x2 (C-7), 130.7 x4 (C-4 and C-4a), 129.3 x2 (C-6), 129.0 x2 (C-3), 119.6 x2 (C-5), 51.1 x3 (C=O-CH₂), 50.9 x3 (N-CH₂-CH₂-CH₂-CH₂-NH), 40.3 (N-CH₂-CH₂-CH₂-CH₂-NH₂), 40.2 x2 (N-CH₂-CH₂-CH₂-CH₂-NH), 27.9 x3 (N-CH₂-CH₂-CH₂-CH₂-NH), 25.2 x3 (N-CH₂-CH₂-CH₂-CH₂-NH). HRMS (MALDI-FTICR) *m/z*; [M + H]⁺ Calcd for C₃₈H₄₇N₈O₅⁺ 695.3664; Found 695.3670.

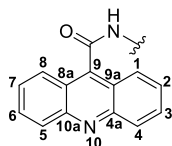
5.2.4.8 General procedure for the acylation with carboxylic acids. Synthesis of cyclic peptoids **177-180**

Cyclic peptoid **169** (0.0140 g, 0.0200 mmol) was dissolved in dry dimethylformamide (0.0700 mL), under nitrogen atmosphere; DIPEA (0.0240 mL, 0.140 mmol) was added under stirring. The chosen poly(hetero)aromatic carboxylic acid (0.0700 mmol) and HATU (0.0270 g, 0.0700 mmol) were weighted under nitrogen atmosphere and dissolved in further 0.0700 mL of dry dimethylformamide. This solution was added dropwise, under stirring, to the cyclopeptoid solution. The mixture was stirred for 24 hours, then the solvent was removed *in vacuo*. The crude was dissolved in 20.0 mL of ethyl acetate and washed three times with brine (10.0 mL each). The organic phase was

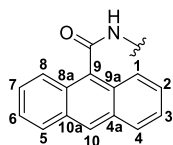
dried over anhydrous MgSO_4 and the solvent was evaporated to gain the crude products. The crude cyclic peptoids were purified on flash silica gel; conditions: 20:80 petroleum ether:ethyl acetate, to 70:30 ethyl acetate:methanol. The cyclic peptoids were dissolved in 50% acetonitrile in HPLC grade water and analysed by RP-HPLC; purity >90%; conditions: 5% – 100% A in 30 min (A, 0.1% TFA in acetonitrile, B, 0.1% TFA in water); flow: 1 mL min^{-1} , 220 nm; subsequently characterized *via* NMR, HPLC and HRMS (MALDI-FTICR).



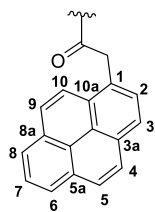
177: white amorphous solid, 0.0060 g, 36%; t_R : 14.0 min. $^1\text{H-NMR}$ (600 MHz, CDCl_3) δ : 9.64 (3H, s, H -3), 8.17 (3H, d, J 7.7 Hz, H -5), 8.10 (3H, dd, J 7.7, 1.3 Hz, H -8), 8.06 (3H, t, J 5.7 Hz, NH), 7.76 (6H, m, H -6 and H -7), 4.75 (3H, d, J 15.3 Hz, $\text{C}=\text{O}-\text{CHH}-\text{N}$), 3.86 (3H, m, $\text{C}=\text{O}-\text{NH}-\text{CHH}$), 3.69 (3H, d, J 15.3 Hz, $\text{C}=\text{O}-\text{CHH}-\text{N}$), 3.55 (6H, m, $\text{N}-\text{CH}_2-\text{CH}_2-\text{CH}_2-\text{CH}_2-\text{NH}$), 3.40 (3H, m, $\text{C}=\text{O}-\text{NH}-\text{CHH}$), 1.71-1.64 (12H, m, $\text{N}-\text{CH}_2-\text{CH}_2-\text{CH}_2-\text{CH}_2-\text{NH}$). $^{13}\text{C-NMR}$ (150 MHz, CDCl_3) δ : 167.0 x3 ($\text{N}-\text{C}=\text{O}$), 163.4 x3 ($\text{NH}-\text{C}=\text{O}$), 143.9 x6 ($\text{C}-2$ and $\text{C}-3$), 143.5 x3 ($\text{C}-4\text{a}$), 140.2 x3 ($\text{C}-8\text{a}$), 131.5 x3 ($\text{C}-5$), 130.8 x3 ($\text{C}-8$), 129.6 x3 ($\text{C}-6$), 129.5 x3 ($\text{C}-7$), 49.3 x3 ($\text{C}=\text{O}-\text{CH}_2$), 47.1 x3 ($\text{N}-\text{CH}_2-\text{CH}_2-\text{CH}_2-\text{CH}_2-\text{NH}$), 39.1 x3 ($\text{N}-\text{CH}_2-\text{CH}_2-\text{CH}_2-\text{CH}_2-\text{NH}$), 26.7 x3 ($\text{N}-\text{CH}_2-\text{CH}_2-\text{CH}_2-\text{CH}_2-\text{NH}$), 24.1 x3 ($\text{N}-\text{CH}_2-\text{CH}_2-\text{CH}_2-\text{CH}_2-\text{NH}$). HRMS (MALDI-FTICR) m/z ; $[\text{M} + \text{H}]^+$ Calcd for $\text{C}_{45}\text{H}_{49}\text{N}_{12}\text{O}_6^+$ 853.3893; Found 853.3976.



178: white amorphous solid, 0.0030 g, 14%; t_R : 10.8 min. $^1\text{H-NMR}$ (600 MHz, CDCl_3) δ : 8.07 (6H, d, J 8.5 Hz, H -4 and H -5), 7.92 (6H, d, J 8.5 Hz, H -1 and H -8), 7.70 (6H, t, J 7.5 Hz, H -3 and H -6), 7.51 (6H, t, J 7.5 Hz, H -2 and H -7), 4.81 (3H, d, J 15.2 Hz, $\text{C}=\text{O}-\text{CHH}-\text{N}$), 3.63 (6H, m, $\text{N}-\text{CH}_2-\text{CH}_2-\text{CH}_2-\text{CH}_2-\text{NH}$), 3.53 (3H, m, $\text{C}=\text{O}-\text{NH}-\text{CHH}$), 3.48 (3H, d, J 15.2 Hz, $\text{C}=\text{O}-\text{CHH}-\text{N}$), 3.39 (3H, m, $\text{C}=\text{O}-\text{NH}-\text{CHH}$), 1.43-1.42 (12H, m, $\text{N}-\text{CH}_2-\text{CH}_2-\text{CH}_2-\text{CH}_2-\text{NH}$). $^{13}\text{C-NMR}$ (150 MHz, CDCl_3) δ : 167.3 x3 ($\text{N}-\text{C}=\text{O}$), 167.0 x3 ($\text{NH}-\text{C}=\text{O}$), 148.5 x6 ($\text{C}-10\text{a}$ and $\text{C}-4\text{a}$), 141.5 x3 ($\text{C}-9$), 130.4 x6 ($\text{C}-4$ and $\text{C}-5$), 129.4 x6 ($\text{C}-1$ and $\text{C}-8$), 126.8 x6 ($\text{C}-3$ and $\text{C}-6$), 125.4 x6 ($\text{C}-2$ and $\text{C}-7$), 122.3 x6 ($\text{C}-8\text{a}$ and $\text{C}-9\text{a}$), 53.6 x3 ($\text{C}=\text{O}-\text{CH}_2$), 41.9 x3 ($\text{N}-\text{CH}_2-\text{CH}_2-\text{CH}_2-\text{CH}_2-\text{NH}$), 38.9 x3 ($\text{N}-\text{CH}_2-\text{CH}_2-\text{CH}_2-\text{CH}_2-\text{NH}$), 29.7 x3 ($\text{N}-\text{CH}_2-\text{CH}_2-\text{CH}_2-\text{CH}_2-\text{NH}$), 18.6 x3 ($\text{N}-\text{CH}_2-\text{CH}_2-\text{CH}_2-\text{CH}_2-\text{NH}$). HRMS (MALDI-FTICR) m/z ; $[\text{M} + \text{H}]^+$ Calcd for $\text{C}_{60}\text{H}_{58}\text{N}_9\text{O}_6^+$ 1000.4505; Found 1000.4504.

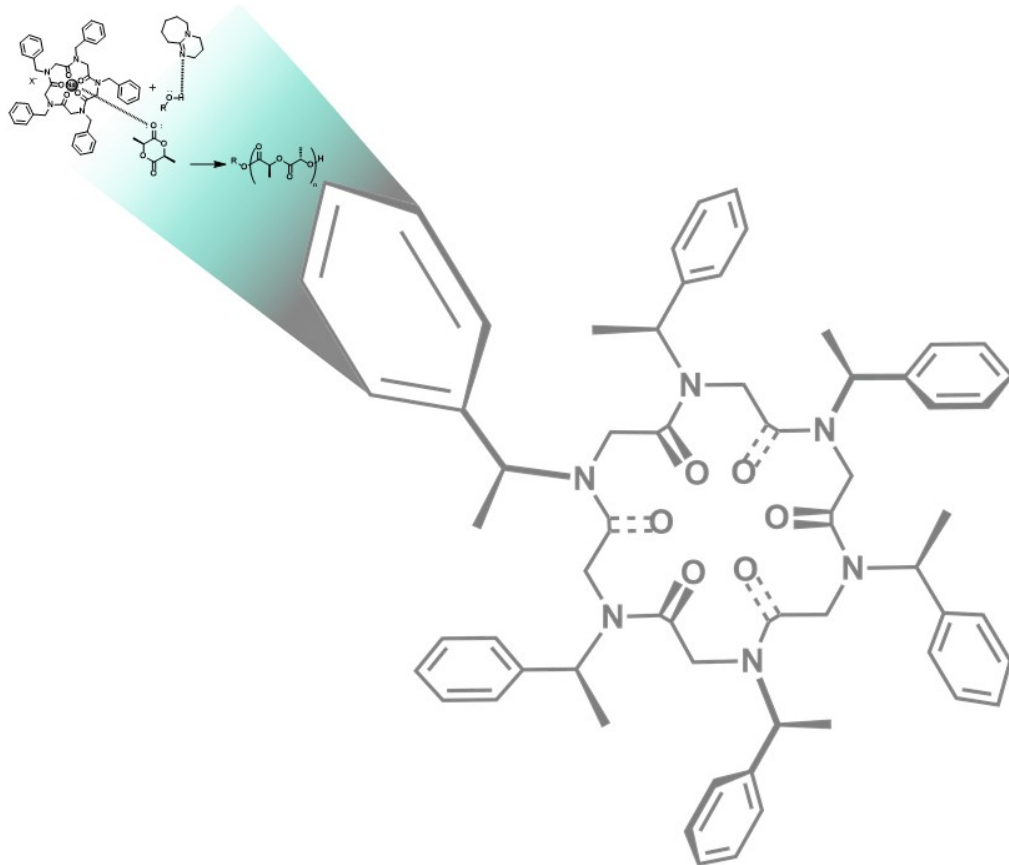


179: white amorphous solid, 0.0050 g, 24%; t_R : 17.5 min. $^1\text{H-NMR}$ (600 MHz, CDCl_3) δ : 8.35 (3H, s, H -10), 7.94-7.88 (12H, overlapping signals, H -1, H -4, H -5, H -8), 7.47-7.40 (12H, overlapping signals, H -2, H -3, H -6, H -7), 6.45 (3H, t, J 6.1 Hz, $\text{C}=\text{O-NH}$), 4.64 (3H, d, J 15.2 Hz, $\text{C}=\text{O-CHH-N}$), 3.54 (3H, m, $\text{C}=\text{O-NH-CHH}$), 3.44 (3H, d, J 15.2 Hz, $\text{C}=\text{O-CHH-N}$), 3.41-3.35 (9H, overlapping signals, $\text{C}=\text{O-NH-CHH}$ and $\text{N-CH}_2\text{-CH}_2\text{-CH}_2\text{-CH}_2\text{-NH}$), 1.52-1.46 (12H, m, $\text{N-CH}_2\text{-CH}_2\text{-CH}_2\text{-CH}_2\text{-NH}$). $^{13}\text{C-NMR}$ (150 MHz, CDCl_3) δ : 169.5 x3 ($\text{N-C}=\text{O}$), 167.1 x3 ($\text{NH-C}=\text{O}$), 132.1 x3 (C-9), 131.0 x6 (C-4a and C-10a), 128.4 x6 (C-4 and C-5), 127.9 x6 (C-2 and C-7), 126.7 x6 (C-8a and C-9a), 125.5 x9 (C-3 , C-6 , C-10), 125.1 x6 (C-1 and C-8), 50.0 x3 ($\text{C}=\text{O-CH}_2$), 47.5 x3 ($\text{N-CH}_2\text{-CH}_2\text{-CH}_2\text{-CH}_2\text{-NH}$), 39.2 x3 ($\text{N-CH}_2\text{-CH}_2\text{-CH}_2\text{-CH}_2\text{-NH}$), 29.7 x3 ($\text{N-CH}_2\text{-CH}_2\text{-CH}_2\text{-CH}_2\text{-NH}$), 24.0 x3 ($\text{N-CH}_2\text{-CH}_2\text{-CH}_2\text{-CH}_2\text{-NH}$). HRMS (MALDI-FTICR) m/z ; $[\text{M} + \text{H}]^+$ Calcd for $\text{C}_{63}\text{H}_{61}\text{N}_6\text{O}_6^+$ 997.4647; Found 997.4652.



180: white amorphous solid, 0.0080 g, 36%. $^1\text{H-NMR}$ (600 MHz, CDCl_3) δ : 8.17 (3H, d, J 9.0 Hz, H -10), 8.14 (3H, d, J 7.5, Hz, H -2), 8.13 (3H, d, J 7.5, Hz, H -6), 8.11 (3H, d, J 7.5 Hz, Hz, H -8), 8.09 (3H, d, J 7.5, Hz, H -9), 8.01 (6H, br d, H -4 and H -3), 7.98 (3H, d, J 7.5 Hz, H -7), 7.88 (3H, d, J 7.5 Hz, H -5), 5.54 (3H, t, J 5.8 Hz, $\text{C}=\text{O-NH}$), 4.26 (6H, s, $\text{C}=\text{O-CH}_2\text{-Pyr}$), 3.49 (3H, d, J 15.5 Hz, $\text{C}=\text{O-CHH-N}$), 3.32 (3H, m, $\text{C}=\text{O-NH-CHH}$), 3.11 (6H, m, $\text{N-CH}_2\text{-CH}_2\text{-CH}_2\text{-CH}_2\text{-NH}$), 2.85 (3H, m, $\text{C}=\text{O-NH-CHH}$), 2.72 (3H, d, J 15.5 Hz, $\text{C}=\text{O-CHH-N}$), 1.21-1.16 (12H, m, $\text{N-CH}_2\text{-CH}_2\text{-CH}_2\text{-CH}_2\text{-NH}$). $^{13}\text{C-NMR}$ (150 MHz, CDCl_3) δ : 171.0 x3 ($\text{N-C}=\text{O}$), 166.4 x3 ($\text{NH-C}=\text{O}$), 131.3 x3, 130.9 x3, 130.8 x3, 129.6 x3, 128.8 x3, 128.6 x4, 128.3 x4, 127.4 x6, 126.2 x4, 125.4 x4, 125.2 x3, 124.6 x4, 123.2 x4, 48.2 x3 ($\text{C}=\text{O-CH}_2$), 46.2 x3 ($\text{N-CH}_2\text{-CH}_2\text{-CH}_2\text{-CH}_2\text{-NH}$), 42.1 x3 ($\text{N-CH}_2\text{-CH}_2\text{-CH}_2\text{-CH}_2\text{-NH}$), 38.8 x3 ($\text{C}=\text{O-CH}_2\text{-Pyr}$), 29.7 x3 ($\text{N-CH}_2\text{-CH}_2\text{-CH}_2\text{-CH}_2\text{-NH}$), 23.3 x3 ($\text{N-CH}_2\text{-CH}_2\text{-CH}_2\text{-CH}_2\text{-NH}$). HRMS (MALDI-FTICR) m/z ; $[\text{M} + \text{H}]^+$ Calcd for $\text{C}_{72}\text{H}_{71}\text{N}_6\text{O}_6^+$ 1115.5430; Found 1115.5470. Note: chromatogram not reported due to the severe insolubility of the compound in the HPLC solvents.

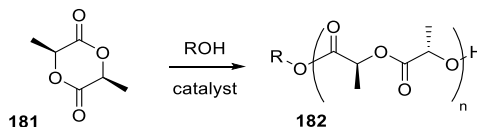
Appendix



Appendix. Cyclopeptoids as catalysts for ROP (Ring Opening Polymerization)

A.1 Introduction: route to sustainable polymers

Implementation of sustainable processes, starting with recycled materials and ending up with novel class of biodegradable polymers, has been a recent focus of polymer science. Among the starting materials, L-lactide (L-LA, **181**, the cyclic ester of L-lactic acid, Scheme A.1) is considered one of the most remunerative monomers, as it is derived from biomasses, and the resulting polymer, the polylactide (PLA, **182**, Scheme A.1) is ranked as the top polymer according to the green design metrics.¹⁵⁷



Scheme A.1. Polymerization of L-lactide (**181**) to polylactide (**182**).

The polymerization processes exclude the use of transition metal-free catalytic systems (a crucial aspect for biomedical applications), utilize straightforward synthetic methodologies, and take advantage of sustainable starting and final materials.¹⁵⁸

In the past few years, the attention has been focused on the use of alkali or earth alkali metal organic complexes,¹⁵⁹ and macrocyclic hosts are excellent chelating compounds.

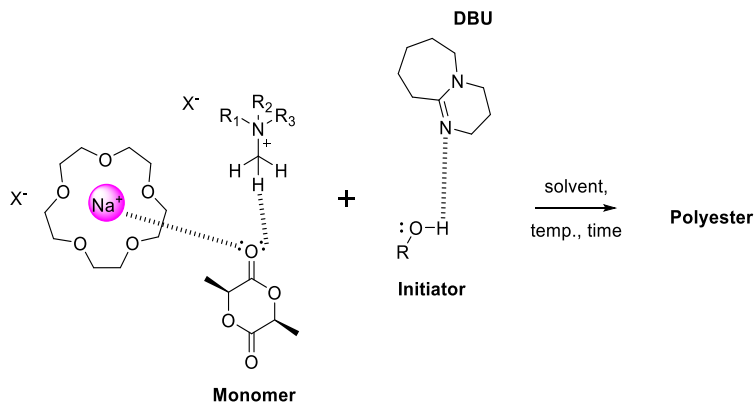
The polymerization is initiated by an alcohol (isopropanol, *i*PrOH and benzyl alcohol, are among the most common), and proceeds through ring-opening polymerization of the lactide. This process is favoured by addition of H-bond acceptor catalysts (usually DBU, DMAP or their derivatives), increasing the nucleophilicity of the alcohol (Scheme A.2) and by a supramolecular complex of an alkali metal or a quaternary ammonium salt, which activate the reacting monomer.

¹⁵⁷ Tabone M. D., Cregg J. J., Beckman E. J., Landis A., *Environ. Sci. Technol.* **2010**, *44*, 8264-8269.

¹⁵⁸ Zhang X., Fevre M., Jones G. O., Waymouth R. M., *Chem. Rev.* **2018**, *118*, 839-885.

¹⁵⁹ a) Lu W.-Yi, Hsiao M.-W., Hsu S. C. N., Peng W.-T., Chang Y.-J., Tsou Y.-C., Wu T.-Y., Lai Y.-C., Chen Y., Chen H.-Y., *Dalton Trans.* **2012**, *41*, 3659-3667; b) Zhang J., Jian C., Gao Y., Wang L., Tang N., Wu J., *Inorg. Chem.* **2012**, *51*, 13380-13389; c) Chen H.-Y., Mialon L., Abboud K. A., Miller S. A., *Organometallics* **2012**, *31*, 5252-5261; d) Alhashmialameer D., Ikpo N., Collins J., Dawe L. N., Hattenhauer K., Kerton F. M., *Dalton Trans.* **2015**, *44*, 20216-20231; e) Garcia-Valle F. M., Estivill R., Gallegos C., Cuenca T., Mosquera M. E. G., Tabernero V., Cano J., *Organometallics* **2015**, *34*, 477-487.

In this regard, crown ethers alkali metal complexes, such as 15-crown-5 (**183**) sodium complex, or 18-crown-6 (**184**) potassium complexes were well studied, and it was proven that such derivatives can influence not only the rate of polymerization, but also the *iso*-selectivity in the case of *rac*-lactide used as monomer.¹⁶⁰



Scheme A.2. Initiation of L-lactide ROP in the presence of a dual catalytic system.

Sodium and potassium-cyclopeptoid complexes are well-known catalytic systems in phase-transfer catalysis (PTC); particularly, in our research group their ability to activate alkylation processes, even in a stereoselective fashion, was well assessed.^{59,161}

Our aim was the investigation of the capability of cyclopeptoid-sodium complexes to catalyse the L-lactide polymerization. For this application, we analysed the importance of the macroring's dimension, using a pentameric, an hexameric, and an octameric scaffold; moreover, in the case of the last two, we also took account of the relative cyclopeptoid-sodium stoichiometry ratio, preparing both the monometallic and the bimetallic systems (Figure A.1). In all cases, we exploited TFPB⁻ as counter-anion, as extensively described in Chapters 2 and 3. The use of a superweak anion, such as tetrakis[3,5-bis(trifluoromethyl)phenyl]borate,⁷⁰ is crucial to exalt Lewis acid character of the catalytic complexes. We chose the benzyl group as the side-chain of the cyclic oligoamides.

¹⁶⁰ a) Thomas C., Milet A., Peruch F., Bibal B., *Polym. Chem.* **2013**, *4*, 3491-3498; b) Dai Z., Sun Y., Xiong J., Pan X., Wu J., *ACS Macro Lett.* **2015**, *4*, 556-560.

¹⁶¹ a) Schettini R., Nardone B., De Riccardis F., Della Sala G., Izzo I., *Eur. J. Org. Chem.* **2014**, 7793-7797; b) Schettini R., De Riccardis F., Della Sala G., Izzo I., *J. Org. Chem.* **2016**, *81*, 2494-2505; c) Schettini R., D'Amato A., De Riccardis F., Della Sala G., Izzo I., *Synthesis* **2017**, *49*, 6, 1319-1326.

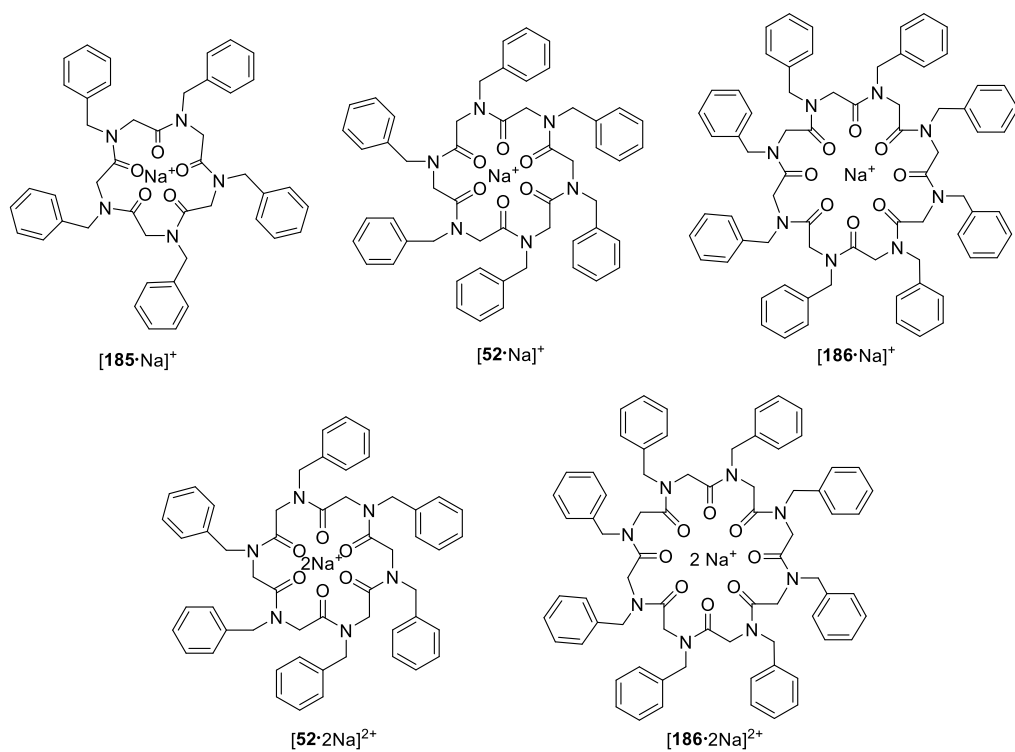


Figure A.1. Cyclic peptoid sodium complexes examined in this work. First row: monometallic complexes; second row: bimetallic complexes.

A.2 Results and discussion: Cyclopeptoid Na⁺ complexes as catalysts for L-lactide ROP¹⁶²

A.2.1 Synthesis of the cyclic peptoids **185-186** and their complexes

The linear precursors, pentamer *per*-benzyl (**187**) and octamer *per*-benzyl (**188**) were efficiently prepared *via* solid-phase synthesis according to our usual protocols, and subsequently cyclized to obtain the cyclic derivatives **185**^{100b,163} and **186**; compound **52**³² was already available in our research laboratory and was described in Chapter 2. While, as already reported, cyclopentapeptoid **185**, as free host, showed multiple species in slow equilibrium on the NMR time scale in the solution state, cyclooctamer **186** displayed a single *ccttcctt* C₂-symmetric conformational isomer (¹H-NMR, CDCl₃). The addition of a single equivalent of NaTFPB resulted, as expected, in a single all-*trans* species for [**185**·Na]⁺ and [**52**·Na]⁺ (described in Paragraph 2.2.1.3), while for the larger **186**, in the formation of a complex mixture of chelates. In particular, the small cavity of the pentameric host hampered the tight inclusion of a single sodium ion equivalent, resulting in a 1:2 complex stoichiometry (log *K*_a = 4.6, -Δ*G*⁰ = 6.3 kcal/mol).

The addition of a second equivalent of sodium resulted for cyclooctamer **186** in the formation of an all-*trans* [**186**·2Na]²⁺ species (log *K*_a = 6.4, -Δ*G*⁰ = 8.8 kcal/mol), as already observed elsewhere for this cavity dimension;^{80,113,123} complex [**52**·2Na]²⁺ was described in Paragraph 2.2.3.5.

Once prepared the necessary catalytic complexes, these were employed in the trial polymerization of L-LA, in the presence of DBU as co-catalyst, and *i*PrOH as initiator.¹⁶⁴ Table A.1 reports the data on the polymerization runs in the presence of the various cyclopeptoid complexes.

Run ^a	Active system	L-LA:active system	Time	Yield (%)
1	[185 ·Na] ⁺ :DBU: <i>i</i> PrOH	100:1:1:1	6 min	18
2	[185 ·Na] ⁺ :DBU: <i>i</i> PrOH	100:1:1:1	22 h	38
3	[52 ·Na] ⁺ :DBU: <i>i</i> PrOH	100:1:1:1	10 min	14
4	[52 ·Na] ⁺ :DBU: <i>i</i> PrOH	100:1:1:1	24 h	16

¹⁶² D'Amato A., Schettini R., Izzo I., Grisi F., De Riccardis F., Costabile C., **Na⁺ Complexes of Cyclic Peptoids as Initiators of L-Lactide Polymerization: Sustainable Catalysts for Sustainable Polymers**, manuscript in preparation.

¹⁶³ Schettini R., D'Amato A., Pierri G., Tedesco C., Della Sala G., Motta O., Izzo I., De Riccardis F., *Org. Lett.* **2019**, *21*, 7365-7369.

¹⁶⁴ Polymerization runs were performed by prof. C. Costabile, DCB Univ. of Salerno.

5	[52·2Na] ²⁺ :DBU; <i>i</i> PrOH	100:1:1:1	24 h	0
6	[186·1Na] ⁺ :DBU; <i>i</i> PrOH	100:1:1:1	6 min	12
7	[186·1Na] ⁺ :DBU; <i>i</i> PrOH	100:1:1:1	24 h	14
8	[186·2Na] ²⁺ :DBU; <i>i</i> PrOH	100:1:1:1	24 h	0
9	DBU; <i>i</i> PrOH	100:1:1	72 h	6
10	DBU	100:1	72 h	0

^a Polymerization runs conducted in an NMR Schlenk tube, CD₂Cl₂, T = 20 °C, L-LA concentration 0.5 M.

Table A.1. Polyesterification runs in the presence of the cyclopeptoid-sodium complexes.

Each complex was tested in the presence of a 0.5 M concentration of the L-LA monomer, in a 100:1 monomer:sodiated active species ratio; moreover, the results were compared with the behaviour of the active species generated only by the presence of DBU/*i*PrOH (Run 9) and by the presence of DBU alone (Run 10). These experimental conditions gave poor to no conversion, respectively, in longer reaction times (72 h).

The best catalytic system resulted the monometallic [185·Na]⁺, while both the bimetallic complexes gave no polymerization at all in 24 hours runs. The polymerization were then conducted at a higher concentration of the metallic complex (20:1 monomer:active species ratio); these conditions boosted the activity of our best catalyst, obtaining a quantitative yield after just five minutes and a good PDI (polydispersity index, 1.72) (Run 1, Table A.2). For comparison, one of the two bis-sodium systems, [52·2Na]²⁺, was tested in the optimized conditions, showing again worse results in longer reaction times (Run 2 and 3, Table A.2). At the same time extent, five minutes, the DBU/*i*PrOH system led to 83% yield (Run 4, Table A.2).

Run ^a	Active system	L-LA:active system	Time	Yield (%)	<i>M_n</i> ^b (kDa)	<i>M_n</i> th (kDa)	PDI
1	[185·Na] ⁺ :DBU; <i>i</i> PrOH	20:1:1:1	5 min	>99	4.881	2.883 ^c	1.72
2	[52·2Na] ²⁺ :DBU; <i>i</i> PrOH	20:1:1:1	20 min	91			
3	[52·2Na] ²⁺ :DBU; <i>i</i> PrOH	20:1:1:1	1 h	96	2.292	2.767 ^c	1.16
4	DBU; <i>i</i> PrOH	20:1:1	5 min	83			
5	DBU; <i>i</i> PrOH	20:1:1	20 min	97	3.190	2.796 ^d	1.22

M_n: number average molecular weight; *M_n*th: theoretical average molecular weight.

^a Polymerization runs conducted in an NMR Schlenk tube, CD₂Cl₂, T = 20 °C, L-LA concentration 0.5 M.

^b Experimental *M_n* (corrected using the factor of 0.58) and PDI values were determined by GPC analysis in THF using polystyrene standards.

^c Calculated *M_n* of PLA (in gmol⁻¹) = *MM*_{L-LA} × ([L-LA]/[Na⁺]) × conversion of L-LA.

^d Calculated *M_n* of PLA (in gmol⁻¹) = *MM*_{L-LA} × ([L-LA]/[DBU]) × conversion of L-LA.

Table A.2. Polyesterification runs in the presence of the cyclopeptoid-sodium complexes in optimized reaction conditions.

DFT calculations are currently ongoing with the aim to elucidate the activation mechanism; this was the first case of employment of cyclopeptoid metal complexes as catalysts for a polymerization reaction.

A.2.2 Experimental section

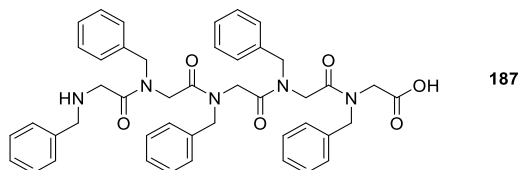
A.2.2.1 General methods

Refer to Paragraph 2.2.3.1.

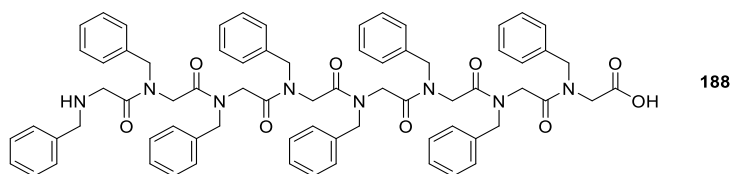
Polymerization runs were performed by prof. C. Costabile, Dpt. of Chemistry and Biology "A. Zambelli", Univ. of Salerno.

A.2.2.2 Synthesis of the linear peptoids **187** and **188**

Refer to Paragraph 2.2.3.2. The synthesis was performed exploiting the sub-monomer protocol, on a 0.300 g 2-chlorotrytil chloride resin batch (1.63 mmol g⁻¹), using commercially available benzylamine. Purity of the linear oligomer (**187**) >80%. Note: **188** chromatogram not reported due to the severe insolubility of the compound in the HPLC solvents.



187: white amorphous solid, 0.221 g, 100%; t_R : 11.3 min. HRMS (MALDI): m/z [M + H]⁺ Calcd for C₄₅H₄₈N₅O₆⁺ 754.3599; Found 754.3611.



188: white amorphous solid, 0.584 g, 100%. HRMS (MALDI): m/z [M + H]⁺ Calcd for C₇₂H₇₅N₈O₉⁺ 1195.5652; Found 1195.5700. Anal. Calcd for C₇₂H₇₄N₈O₉: C, 72.34; H, 6.24; N, 9.37; O, 12.05; Found C, 73.43; H, 6.23; N, 9.40; O, 12.03.

A.2.2.3 Synthesis of the cyclic peptoids **185** and **186**

Refer to Paragraph 2.2.3.3.

The cyclization reaction was performed on a 0.150 mmol scale of the linear oligomers, which were dissolved in 5.0 mL of dry DMF and added by a syringe pump in 3 hours to the reaction mixture. The crude cyclic peptoids were dissolved in hot acetonitrile and precipitated by slowly cooling the acetonitrile solution. The cyclic peptoids were dissolved in 50% acetonitrile in HPLC grade water and analysed by RP-HPLC; purity >90%; conditions: 5% – 100% A in 30 min (A, 0.1% TFA in acetonitrile, B, 0.1% TFA in water); flow: 1 mL min⁻¹, 220 nm; subsequently characterized *via* ¹H-, ¹³C-NMR and HRMS (MALDI-FTICR). Note: chromatograms not reported due to the severe insolubility of the compounds in the HPLC solvents.

Note: in the ¹H-NMR assignment, N_c stand for *cis* amide bond, N_t stands for *trans* amide bond.

cyclo-[Npm]₅ (**185**): white amorphous solid, 0.0810 g, 42%. ¹H-NMR (400 MHz, CDCl₃) δ: 7.44-7.04 (25H, *m*), 5.73 (1H, *d*, *J* 15.2 Hz), 5.54 (1H, *d*, *J* 14.8 Hz), 5.45 (1H, *d*, *J* 14.0 Hz), 5.41 (1H, *d*, *J* 14.7 Hz), 4.69 (1H, *d*, *J* 17.1 Hz), 4.65 (1H, *d*, *J* 16.2 Hz), 4.62 (1H, *d*, *J* 14.9 Hz), 4.45 (1H, *d*, *J* 16.2 Hz), 4.36 (1H, *d*, *J* 18.1 Hz), 4.33 (1H, *d*, *J* 17.1 Hz), 4.28 (1H, *d*, *J* 14.8 Hz), 4.04 (1H, *d*, *J* 18.2 Hz), 4.02 (1H, *d*, *J* 15.2 Hz), 3.93 (1H, *d*, *J* 18.0 Hz), 3.85 (1H, *d*, *J* 18.1 Hz), 3.72 (1H, *d*, *J* 14.9 Hz), 3.64 (1H, *d*, *J* 18.2 Hz), 3.59 (1H, *d*, *J* 18.0 Hz), 3.50 (1H, *d*, *J* 14.0 Hz), 2.95 (1H, *d*, *J* 14.9 Hz). HRMS (MALDI): *m/z* [M + H]⁺ Calcd for C₄₅H₄₆N₅O₅⁺ 736.3493; Found 736.3483. Anal. Calcd for C₄₅H₄₅N₅O₅: C, 73.45; H, 6.16; N, 9.52; Found C, 73.44; H, 6.16; N, 9.53.

cyclo-[Npm]₈ (**186**): white amorphous solid, 0.0560 g, 32%. ¹H-NMR (600 MHz, CDCl₃) δ: 7.35-7.23 (32H, *br* signals, overlapping, *Ar-H*), 7.04 (8H, *br t*, *Ar-H*), 5.50 (2H, *d*, *J* 15.4 Hz, N_c-CHH-Ph), 5.28 (2H, *d*, *J* 14.8 Hz, N_c-CHH-Ph), 5.04 (2H, *d*, *J* 17.3 Hz, O=C-CHH-N_t-Bn), 4.65 (2H, *d*, *J* 17.4 Hz, O=C-CHH-N_t-Bn), 4.59 (2H, *d*, *J* 16.7 Hz, N_t-CHH-Ph), 4.54 (2H, *d*, *J* 16.1 Hz, N_t-CHH-Ph), 4.30 (2H, *d*, *J* 16.9 Hz, O=C-CHH-N_c-Bn), 4.28 (2H, *d*, *J* 16.7 Hz, N_t-CHH-Ph), 4.20 (2H, *d*, *J* 16.1 Hz, N_t-CHH-Ph), 4.04 (2H, *d*, *J* 15.4 Hz, N_c-CHH-Ph), 4.01 (2H, *d*, *J* 19.2 Hz, O=C-CHH-N_c-Bn), 3.62 (2H, *d*, *J* 17.4 Hz, O=C-CHH-N_t-Bn), 3.58 (4H, *br d*, overlapping, O=C-CHH-N_c-Bn and O=C-CHH-N_c-Bn), 3.52 (2H, *d*, *J* 14.8 Hz, N_c-CHH-Ph), 3.48 (2H, *d*, *J* 17.3 Hz, O=C-CHH-N_t-Bn). ¹³C-NMR (150 MHz, CDCl₃) δ: 169.6 x2 (C=O), 169.4 x2 (C=O), 168.4 x2 (C=O), 167.6 x2 (C=O), 136.6 x2 (C-Ar), 136.4 x2 (C-Ar), 135.9 x2 (C-Ar), 135.7 x2 (C-Ar), 129.0 x4 (CH-Ar), 128.8 x8 (CH-Ar), 128.6 x8 (CH-Ar), 128.0 x4 (CH-Ar), 127.6 x4 (CH-Ar), 127.4 x4 (CH-Ar), 127.2 x4 (CH-Ar), 126.8 x4 (CH-Ar), 52.3 x2 (N_t-CH₂-Ph), 51.5 x2 (N_t-CH₂-Ph), 50.5 x2 (N_c-CH₂-Ph), 50.2 x2 (N_c-CH₂-Ph), 49.6

x2 (C=O-CH₂-N_r-Bn), 48.4 x2 (C=O-CH₂-N_r-Bn), 47.0 x4 (C=O-CH₂-N_c-Bn). HRMS (ESI/FTICR) *m/z*; [M + H]⁺ Calcd for C₇₂H₇₃N₈O₈⁺ 1177.5546; Found 1177.5656. Anal. Calcd for C₇₂H₇₂N₈O₈: C, 73.45; H, 6.16; N, 9.52; O, 10.87; Found C, 73.51; H, 6.17; N, 9.49; O, 10.89.

A.2.2.4 General procedure for the formation of complexes [185-186Na]⁺[TFPB]⁻ and [185-186·2Na]²⁺2[TFPB]⁻

Preparation of the complexes. 3.00 mM solutions of cyclopeptoid hosts were prepared dissolving **185-186** (0.00150 mmol) in CDCl₃ (0.45 mL) and adding to the solutions: 1.0 equivalent of NaTFPB (0.00150 mmol, 1.33 mg, for the monometallic complexes), or 2.0 equivalent of NaTFPB (0.00300 mmol, 2.66 mg, for the bimetallic complex of **186**), dissolved in CD₃CN (0.05 mL). After the addition the mixtures were sonicated for 5 minutes in a r.t. bath (25 °C); the resulting mixtures were concentrated under a nitrogen flux and dried under *vacuum*, then the complexes were dissolved in CDCl₃ (0.50 mL) and the NMR spectra were acquired.

K_a evaluation. The solution of compound **185**, adding 1.0 equivalent of NaTFPB, was used for the evaluation of the apparent *K_{a2}*, resulting in a 1:2 stoichiometry. The addition of further equivalents of NaTFPB induced precipitation of higher order complexes and made the evaluation of the *K_{a2}* impossible. The H·G₂ complex concentration, at the equilibrium – [H·G₂]_{eq} – was evaluated by integration of the ¹H-NMR complex signals (2.5-6.5 range) versus the total integration of the free host plus complexed molecules at 298 K. With the addition of 1.0 equivalent of guest, NaTFPB is complexed in a 1:2 host:guest stoichiometry, according to equation (2.6), leaving part of the cyclopeptoid as free host. Thus, following the relations (2.7-2.9), the evaluation of the apparent *K_{a2}* resulted in equation (A.1):

$$K_{a2} = \frac{[H \cdot G_2]_{eq}}{[H]_{eq} \times [G]_{eq}^2} \quad (A.1)$$

For the evaluation of apparent *K_{aTOT}* for complex [186·2Na]²⁺2[TFPB]⁻, refer to Paragraph 2.3.3.5. Apparent *K_{a1}* of known complex [52·Na]⁺[TFPB]⁻ is reported in Paragraph 2.2.1.3.

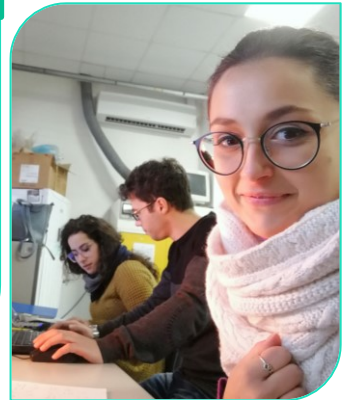
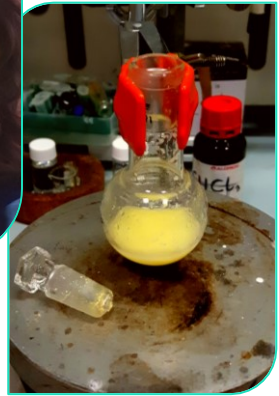
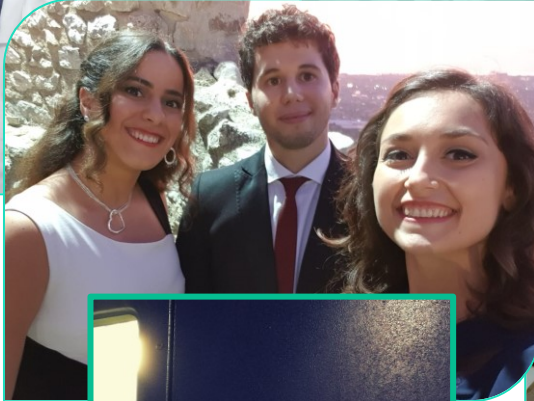
Note: it was not possible to calculate the apparent *K_{a1}* in [186Na]⁺[TFPB]⁻ due to the presence of a mixture of conformational isomers.

[**185**·2Na]²⁺2[TFPB]: yellow amorphous solid. ¹H-NMR (600 MHz, CDCl₃) δ: 7.71 (16H, s, TFPB-*o*-H), 7.50 (8H, s, TFPB-*p*-H), 7.27-7.26 (15H, br signals, overlapping, Ar-H), 7.02 (10H, d, *J* 6.7 Hz, *o*-Ar-H), 7.82 (10H, s, N-CH₂-Ph), 4.03 (10H, s, C=O-CH₂-N-Bn). ¹³C-NMR (150 MHz, CDCl₃) δ: 170.6 x5 (C=O), 161.6 (q, *J* 50 Hz, C-1), 137.6 x5 (C-Ar), 134.7 (C-2), 129.5 x10 (CH-Ar), 128.8 (q, *J* 30 Hz, C-3), 126.5 x15 (CH-Ar), 124.6 (q, *J* 270 Hz, C-5), 117.5 (C-4), 53.4 x5 (N-CH₂-Ph), 48.2 x5 (C=O-CH₂-N-Bn). HRMS (ESI/FTICR) *m/z*; [M + Na]⁺ Calcd C₄₅H₄₅N₅NaO₅⁺ 758.3313; Found 758.3358.

[**186**·Na]⁺[TFPB]: yellow amorphous solid. ¹H-NMR (400 MHz, CDCl₃, complex mixture of rotamers) δ: 7.71 (8H, s, TFPB-*o*-H), 7.50 (4H, s, TFPB-*p*-H), 7.28-6.94 (40H, br signals, overlapping, Ar-H), 4.68-3.45 (32H, br signals, overlapping, N-CH₂-Ph and C=O-CH₂-N-Bn). ¹³C-NMR (150 MHz, CDCl₃, complex mixture of rotamers) δ: 169.6, 169.3, 169.0, 161.7 (q, *J* 50 Hz, C-1), 134.8 (C-2), 129.2, 128.9, 128.7, 128.7 (q, *J* 30 Hz, C-3), 127.2, 126.9, 126.6, 124.6 (q, *J* 270 Hz, C-5), 117.4 (C-4), 54.0, 53.3, 53.0, 52.2, 52.0, 51.6, 51.3, 51.0, 50.4, 50.2. HRMS (ESI/FTICR) *m/z*; [M + Na]⁺ Calcd C₇₂H₇₂N₈NaO₈⁺ 1199.5365; Found 1199.5301.

[**186**·2Na]²⁺2[TFPB]: yellow amorphous solid. ¹H-NMR (400 MHz, CDCl₃) δ: 7.73 (16H, s, TFPB-*o*-H), 7.53 (8H, s, TFPB-*p*-H), 7.27 (24H, m, Ar-*m*-H and Ar-*p*-H), 6.89 (16H, d, *J* 6.8 Hz, Ar-*o*-H), 4.96 (8H, d, *J* 17.0 Hz, O=C-CHH-N-Bn), 4.58 (8H, d, *J* 16.2 Hz, N-CHH-Ph), 4.12 (8H, d, *J* 16.2 Hz, N-CHH-Ph), 3.64 (8H, d, *J* 17.0 Hz, O=C-CHH-N-Bn). ¹³C-NMR (150 MHz, CDCl₃) δ: 169.4 x8 (C=O), 161.6 (q, *J* 50 Hz, C-1), 134.8 (C-2), 132.7 x8 (C-Ar), 129.4 x16 (CH-Ar), 129.0 x8 (CH-Ar), 128.8 (q, *J* 30 Hz, C-3), 126.8 x16 (CH-Ar), 124.7 (q, *J* 270 Hz, C-5), 117.5 (C-4), 51.7 x8 (N-CH₂-Ph), 47.5 x8 (C=O-CH₂-N-Bn). HRMS (ESI/FTICR) *m/z*; [M + 2Na]²⁺ Calcd C₇₂H₇₂N₈Na₂O₈²⁺ 612.2707; Found 612.2696.

Spectral data of complexes [**52**·Na]⁺[TFPB] and [**52**·2Na]²⁺2[TFPB] are reported in Paragraph 2.2.3.4.



Questo piccolo libro, che poi tanto piccolo non è, potrebbe sembrare apparentemente un decalogo infinito di tutti i peptoidi che posso aver sintetizzato in questi tre anni (garantisco che ce ne sono molti, molti di più). Solo i lettori più attenti, che mi conoscono a fondo, sapranno che qui si racconta invece un po' la mia storia. Potrei usare centinaia di parole per cercare lontanamente di esprimere cosa hanno significato questi tre anni per me, ma delle tante una sola riesce a dare l'idea di quello che provo, ed è gratitudine. Ogni momento, ogni esperienza, sono andati oltre, ben oltre i miei desideri e le mie aspettative, e so che gran parte del merito stavolta è mio e del mio incaponimento (che sempre mi compenserà l'assenza di serendipity), ma anche di chi ho avuto accanto.

Francesco, non avrei potuto immaginare per me un mentore più adeguato, pronto a darmi le dritte giuste al momento giusto e a lasciarmi sola nelle mie decisioni e responsabilità quando è stato necessario, per farmi crescere umanamente a professionalmente. Irene e Giorgio, solo grazie: avete sempre avuto una parola od un consiglio per me, pensati con l'affetto di sempre.

Ai miei studenti ed i miei tesisti, siete stato quanto di più prezioso io abbia avuto; avete dato più lezioni di vita voi a me che di chimica organica io a voi. Mi avete riempita di amore e di entusiasmo per questo lavoro, mostrandomi la strada da seguire. Alle mie amiche di sempre: mi siete state vicine anche se ora siamo un po' più distanti; la felicità sarà sempre in cinque. Alle nuove amiche, mi avete regalato sorrisi ogni giorno.

Ogni singolo giorno ed ogni singola avventura mi hanno reso la persona che sono oggi; c'è stata tanta fatica, a volte anche tante lacrime, ma sono state sempre compensate da sorrisi e risate a non finire. Ros, le risate le ho sempre condivise con te, durante un numero immenso di colonne e di incombenze e di avventure fuori porta; oggi più che mai posso dire con certezza che per me sei la compagna di lavoro e l'amica di vita per eccellenza, lo sei stata sempre e sempre lo sarai. Givi, io per te non avrò mai parole a sufficienza; non so come sei arrivato dal nulla proprio nel momento in cui avevo più bisogno e mi hai sempre saputo risollevare nel modo giusto. Non avrei potuto immaginare un amico più fidato di te per condividere tutti questi momenti; diciamo che ti sei fatto perdonare! Se potessi esprimere un singolo desiderio, vorrei che noi tre restassimo sempre uniti come lo siamo oggi. Siete la mia forza più di chiunque altro, mi avete riempita di gioia e di affetto ogni singolo giorno, e per questo ho solo un immenso grazie.

Concludere non è mai stato il mio forte... Spero solo, in questi tre anni, di essere stata in grado di donare un po' dell'amore che ho ricevuto ed ho cercato di racchiudere in questo libricino così speciale per me.



